PhD degree in Systems Medicine (curriculum Molecular Oncology)

European School of Molecular Medicine (SEMM),

University of Milan and University of Naples "Federico II"

Settore disciplinare: BIO/11

The role of the m^{6}A methyltransferase METTL3 in an

in vitro model of antigen-selected germinal center B cells

Federica Greco

IFOM, FIRC Institute of Molecular Oncology, Milan, Italy

Tutor: Dr. Stefano Casola

IFOM, FIRC Institute of Molecular Oncology, Milan, Italy

PhD Coordinator: Prof. Giuseppe Viale

Anno accademico 2019-2020

Table of contents

List of abbreviations

AID	Activation Induced Deaminase
ALKBH5	Alk B homolog 5
APE1	Apurinic-apyrimidinic endonucleases 1
APRIL	A proliferation inducing ligand
ATF6	Activating Transcription Factor 6
BAFF	B-cell Activating Factor
BAFF-R	BAFF Receptor
Bcl-2	B Cell CLL/Lymphoma 2
Bcl-6	B Cell CLL/Lymphoma 6
BCMA	B-Cell Maturation Antigen
BCR	B Cell Receptor
BER	Base Excision Repair
BL	Burkitt lymphomas
BM	Bone Marrow
bp	Base Pair
BrdU	BromodeoxyUridine
C-term	Carboxy terminus
C9	Cas9
carRNA	Chromatin-associated regulatory RNA
Cbx	Chromobox homolog
CD40L	CD40-ligand
CDK	Cyclin-Dependent Kinase
cDNA	Complementary DNA
ChIP	Chromatin Immunoprecipitation
cIAP1 - 2	Cellular inhibitor of apoptosis 1 - 2
CLP	Common Lymphoid Progenitor
CSR	Class Switch Recombination
CXCR4	C-X-C chemokine receptor type 4
CXCR5	C-X-C chemokine receptor type 5
DEG	Differentially Expressed Gene
DEPTO	DEP domain containing mTOR interacting protein
DLBCL	Diffuse Large B cell lymphomas
DMEM	Dulbecco's Modified Eagle Medium
DNA	Deoxyribonucleic Acid
DNMT	DNA methyltransferases
dNTP	Deoxynucleoside triphosphate
DZ	Dark zone
EBF1	Early B-cell factor 1
EIF3H	Eukaryotic Initiation Factor 3H
ER	Endoplasmic Reticulum
ESC	Embryonic Stem Cell
FACS	Fluorescence Activated Cell Sorting
FDC	Follicular Dendritic Cell
FDR	False Discovery Rate
FL	Follicular lymphomas
Flt3	Fms-related tyrosine kinase 3

Flt3l	Flt3-ligand
FMR1	Fragile X Mental Retardation 1
FO	Follicular
FTO	Fat mass and obesity-associated protein
Fw	Forward
g	Relative centrifugal force expressed in units of gravity
GC	Germinal Center
GLTs	Germ-line transcripts
GSEA	Gene Set Enrichment Analysis
Gy	Gray
H	Histone
H3K27me3	Tri-methylated Histone H3 at Lysine 27
H3K36me3	Tri-methylated Histone H3 at Lysine 36
H3K4me3	Tri-methylated Histone H3 at Lysine 4
H3K9me3	Tri-methylated Histone H3 at Lysine 9
H8	Hoxb8
H8-HPCs	Hoxb8-immortalized hematopoetic progenitor cells
Hi	High
HIF	Hypoxia-inducible factor
HNRNP	Heterogenoeus nuclear ribonucleoprotein
Hox	Homeotic
HPCs	Hematopoietic progenitor cells
HSC	Hematopoietic Stem Cell
HSP	Heat shock protein
Ig	Immunoglobulin
iGB	*In vitro*-induced germinal center like B cells
IGF2BP	Insulin-like Growth Factor 2 mRNA-Binding Proteins
IgH	Immunoglobulin Heavy chain
IgL	Immunoglobulin Light chain
iKB	Inhibitor of the NF-kB
IL	Interleukin
IL-7R	IL-7 Receptor
Irf4	Interferon regulatory factor 4
ITAM	Immunoreceptor Tyrosine-based Activation Motifs
kb	Kilobase
KH	K homology
LMPP	Lymphoid-primed multipotent progenitors
LN	Lymph Node
lncRNA	Long non-coding RNA
Lo	Low
LZ	Light zone
m^1A	N^1-methyladenosine
m^3C	3-methylcytidine
m^5C	5-methylcytosine
m^6A	N^6-methyladenosine
m^6A-REF-seq	m^6A-sensitive RNA-Endoribonuclease-Facilitated sequencing
m^6Am	N^6,2'-O-dimethyladenosine
m^7G	N^7-methylguanosine

MACS	Magnetic-Activated Cell Sorting
MALT	Mucosa-associated lymphoid tissues
MAPK	Mitogen-activated protein kinases
mCD40L	Membrane-bound CD40-ligand
MCL-1	Myeloid leukemia cell differentiation protein 1
METTL14	Methyltransferase-like 14
METTL3	Methyltransferase-like 3
MHC	Major Histocompatibility Complex
miRNA	Micro RNA
mLST8	Mammalian Lethal with SEC13 protein 8
MMR	Mismatch Repair
MPP	Multipotent Progenitor
mRNA	Messenger RNA
MTA-3	Metastasis-Associated 1 family member 3
mTORC1	Mammalian Target Of Rapamycin Complex 1
MZ	Marginal Zone
MZF1	Myeloid Zinc Finger 1
ncRNA	Non-coding RNA
NIK	NF-κB-inducing kinase
Nm	2'-O-ribose-methylation
NXF1	Nuclear RNA export Factor 1
PAM	Protospacer adjacent motif
Pax5	Paired box 5
PB	Plasma blast
PBS	Phosphate Buffered Saline
PC	Plasma Cell
PCIF1	Phosphorylated C-terminal domain-interacting Factor 1
PCR	Polymerase Chain Reaction
PI3K	PhosphoInositide 3-Kinase
PIP$_2$	Phosphatidylinositol-4,5-bisphospate
PLCγ2	Phospholipase Cγ2
PRAS40	Proline-Rich AKT Substrate of 40 kDa
Prdm1	Positive regulatory domain containing 1
PRR	Pattern recognition receptor
PTP	Protein Tyrosine Phosphatase
RAG	Recombination Activation Genes
RAPTOR	Regulatory Protein Associated with mTOR
RARA	Retinoic Acid Receptor Alpha
RBC	Red Blood Cell
RBD	RNA binding domain
RBM15	RNA-Binding Motif protein 15
RBP	RNA binding protein
RGG	Arginine-glycine-rich
RIP	RNA immunoprecipitation
RNA	Ribonucleic Acid
rpm	Rotations per minute (centrifugal force)
rRNA	Ribosomal RNA
RT	Room temperature
RT-PCR	Reverse Transcriptase PCR

RT-qPCR	Real-time quantitative PCR
Rv	Reverse
S6K1	S6 kinase 1
SAM	S-adenosyl-methionine
Sca1	Stem cell antigen-1; Ly-6A/E
SD	Standard Deviation
Seq	Sequencing
SHM	Somatic Hypermutation
SHP-1	Src homology domain-containing phosphatase 1
SLO	Secondary lymphoid organ
snoRNA	Small nucleolar RNA
snRNA	Small nuclear RNA
SOCS	Suppressor of cytokine signaling
SPL	Spleen
SRSF3	Serine and arginine Rich Splicing Factor 3
T-D	T-dependent
T-I	T-indipendent
T-reg	T regulatory cells
TCR	T-cell receptor
TF	Transcription Factor
TFH	T-Follicular Helper cell
TLR	Toll-Like Receptor
TNF	Tumor necrosis factor
TNFR	Tumor necrosis factor receptor
TRAF	TNF Receptor Associated Factor
tRNA	Transfer RNA
TSS	Transcriptional Start Sites
UNG	Uracil-DNA glycosylase
UPR	Unfolded Protein Response
UTR	Untranslated region
VIRMA	Vir Like m^6A Methyltransferase associated
WTAP	Wilms Tumor 1-associated protein
Xbp1	X-box binding protein 1
Xbp1-S	X-box binding protein 1 spliced
YTHDF	YTH domain family
ZC3H13	Zinc finger CCCH-Type containing 13
ZCCHC4	CCHC zinc-finger-containing protein

Figures Index

13

Tables Index

Abstract

N^6-methyladenosine (m^{6}A) represents the most abundant modification introduced into messenger RNA. In mammals, m^{6}A regulates gene expression by controlling different facets of mRNA metabolism including splicing, translation and stability. Emerging evidences have assigned to m^{6}A a critical role in the regulation of cellular and humoral immunity.

To date, the function of m^{6}A in mature B cells, especially those recruited into T-cell dependent immune responses, remains unexplored. Here, we show that the *Mettl3* gene, encoding for the catalytic subunit of the m^{6}A methyltransferase complex, is expressed at relatively stable levels throughout B-cell development and increases in mature B cells activated in response to the engagement of the CD40 receptor. Given the crucial role played during a T-cell dependent immune response by CD40 signaling in sustaining the transient expansion of antigen-selected B cells in the light zone of the germinal center (GC) and, together with Interleukin-21 (IL-21), their terminal differentiation into antibody-secreting plasma cells (PCs), we asked to which extent these processes are under m^{6}A methylation control. To answer these questions, we disrupted by CRISPR/Cas9 technology the *Mettl3* gene in primary *in vitro*-induced germinal center-like B (iGB) cells, which were stimulated for 8-to-13 days with membrane-bound CD40-ligand (mCD40L). Efficient targeting of the *Mettl3* gene in iGB cells exerted distinct phenotypes on CD40-activated B cells starting from the fourth day of the culture, when IL-4 was replaced with IL-21 in the culture medium. Using two independent sgRNAs to disrupt the *Mettl3* gene, we observed a consistent significant growth delay of *Mettl3*-mutant iGB cells, which was restricted to the first 48 hours of mCD40L + IL-21 stimulation. The proliferation defect of *Mettl3*-mutant iGB cells caused their rapid counter selection when placed in competition with *Mettl3*-proficient counterparts.

The growth impairment of CD40-activated *Mettl3*-mutant iGB cells was associated with limited upregulation of c-MYC expression, a defect in cell-cycle progression at the G_1-to-S transition, due to reduced expression of E2F family members, and defective activation of the nutrient-sensitive mTORC1 signaling pathway. During the first 48 hours of mCD40L + IL-21 stimulation, *Mettl3*-mutant cultures suffered also from a significant defect in the transcriptional activation of genes encoding for master regulators of PC differentiation,

including *Irf4*, *Blimp1*, *Pou2af1* and *Xbp1*. The growth and developmental defects of *Mettl3*-mutant iGB cultures were normalized in the following 48 hours, due to the exhaustion of the proliferative burst of control B cells, while mutant ones completed the missing cell divisions, prior to undergoing terminal differentiation and/or senescence.

Sequencing of the *Mettl3* gene, retrieved from day-8 *Mettl3*-mutant iGB cultures, indicated a strong counter selection of iGB cells carrying loss-of-function alleles. This result was confirmed in terminally differentiated CD138^{+} plasmablasts isolated from day-13 in *Mettl3*-mutant iGB cultures, which displayed METTL3 protein levels comparable to those of wild-type cells. Altogether, these results establish for the first time a strict requirement for a full complement of METTL3 molecules, for optimal mitogenic B cell response to CD40 engagement, for initiating PC differentiation and for PCs persistence. In light of these results, our work assigns to METTL3 a crucial supportive function in B cells for the processes of clonal selection and antibody affinity maturation occurring in the GC during T-cell dependent immune responses.

To shed further light on the importance of METTL3 function in developmental decision-making processes, we employed an *in vitro* model of reversible immortalization of multipotent murine hematopoietic progenitor cells (HPCs), by expression of an estradiol-inducible form of the HoxB8 (H8) transcription factor. Application of CRISPR/Cas9 technology to H8-HPCs ensured efficient *Mettl3* gene targeting in these cells. We could show that interference with *Mettl3* expression led to the counter selection of highly proliferating *Mettl3*-mutant H8-HPCs. Moreover, *Mettl3*-targeted H8-HPCs expressed prematurely the myeloid-associated marker CD11b and displayed accelerated myeloid differentiation upon estradiol withdrawal from the culture medium. Altogether, these results support a view whereby METTL3 sustains self-renewal of multipotent HPCs and prevents inappropriate and premature differentiation of these cells into the myeloid lineage.

1. Introduction

1.1. Insights into N^6-methyladenosine regulation of gene expression

1.1.1. Epigenetics: genetic information above the DNA sequence

In multicellular organisms, the chromatin structure defines the state in which the DNA is compacted within the cell. Chromatin accessibility to transcription factors regulates gene expression and is controlled by a series of modifications affecting the DNA or histones, the structural components of chromatin. Such modifications are all referred as epigenetic modifications. By inducing conformational changes, epigenetic modifications favor chromatin compaction or alternatively, relaxation, thus leading to transcriptional repression or activation, respectively. Epigenetic processes are reversible, often heritable events, that influence gene expression without altering the DNA sequence (Goldberg, Allis, and Bernstein 2007; Berger et al. 2009).

One of the best studied epigenetic modifications is 5-methylcytosine (5-mC), catalyzed by DNA methyltransferases (DNMT). In mammals, DNA methylation is enriched at symmetric CpG islands (Jones 2012), where it exerts a repressive function on the activity of promoters and enhancer regions. Instead, deposition of 5-mC within the gene body is recurrently linked to active transcription (Jones 2012; Breiling and Lyko 2015).

The *N*-terminus of nucleosomal histone proteins are subjected to a variety of post-translational modifications, including acetylation, methylation, phosphorylation and ubiquitination (Lawrence, Daujat, and Schneider 2016). Each type of histone modification has a distinct distribution pattern and is associated with a specific transcriptional state of the chromatin. For instance, acetylation of histone H3 on lysine-9 (H3K9ac), or lysine-27 (H3K27ac), at enhancer and promoter regions, is associated with active gene transcription by loosening chromatin. Other histone marks associated with active transcription include trimethylation of histone H3 on lysine-4 (H3K4me3), which is deposited at promoters, and trimethylation of histone H3 on lysine-36 (H3K36me3), which is mainly localized within the gene body. By contrast, trimethylation of histone H3 on lysine-27 (H3K27me3) or lysine-9 (H3K9me3) at promoter regions is commonly associated to target gene silencing (Lawrence, Daujat, and Schneider 2016).

Altogether, epigenetic modifications generate a complex and combinatorial code which is essential for the development of multicellular organisms and for the maintenance of tissue-specific gene expression patterns. Disruption of epigenetic events can lead to altered gene functions which are responsible of a variety of inherited and acquired diseases, such as cancer (Kurdistani 2007; Feinberg 2018; Nebbioso et al. 2018).

1.1.2. The epitranscriptome: an additional layer of gene expression regulation

RNA molecules are also targets of chemical modifications, which serve as an additional layer of epigenetic regulation of gene expression in mammalian cells (Frye et al. 2018).

To date, more than 170 chemical post-transcriptional modifications have been associated with various RNA species, including messenger RNA (mRNA), transfer RNA (tRNA), ribosomal RNA (rRNA), small nuclear RNA (snRNA), small nucleolar RNA (snoRNA) and long non-coding RNA (lncRNA) (Frye et al. 2018; Pan 2018; Sloan et al. 2017; Roundtree and He 2016). Although some of these modifications have been known for decades, the interest towards the biological function of RNA modifications has emerged only recently, thanks to the optimization of protocols and availability of molecular tools ensuring antibody-based high-throughput sequencing methods. Such technologies have been instrumental to quantify and map at genome-wide level post-transcriptional modifications of low-abundant RNA species, including mRNA, thereby contributing to a better understanding of the epitranscriptome of both embryonal as well as somatic specialized cell-types (Roundtree and He 2016; Frye et al. 2018; Dominissini et al. 2012; Linder et al. 2015; Liu, Li, et al. 2020).

1.1.3. N^6-methyladenosine of mRNA

N^6-methyladenosine (m6A) is the most abundant and well-characterized mRNA modification. It consists in the addition of a methyl group to the nitrogenous base at the sixth position of the adenine residue incorporated into the RNA molecule (Figure 1). It has been estimated that 20% to 40% of nascent mRNAs carry at least one m6A modification (Frye et al. 2018). Transcriptome-wide m6A-mapping profiles have revealed that m6A deposition preferentially occurs within the DRACH (where D = A, G or U; R = G or A; H = A, C or U) consensus sequence, which is commonly located in long intragenic exons and 3' untranslated regions (3'UTR), near stop codons (Dominissini et al. 2012; Linder et al. 2015). Besides N^6-methyladenosine (m6A), mRNA modifications include N^7-methylguanosine (m7G), 2'-O-ribose-methylation (Nm), 5-methylcytosine (m5C), N^1-methyladenosine (m1A) and 5-methylcytidine (m5C). The function of these modifications remains largely unexplored (Figure 1) (Zaccara, Ries, and Jaffrey 2019; Karthiya and Khandelia 2020).

Karthiya, R., and P. Khandelia, *Mol Biotechnol* 2020
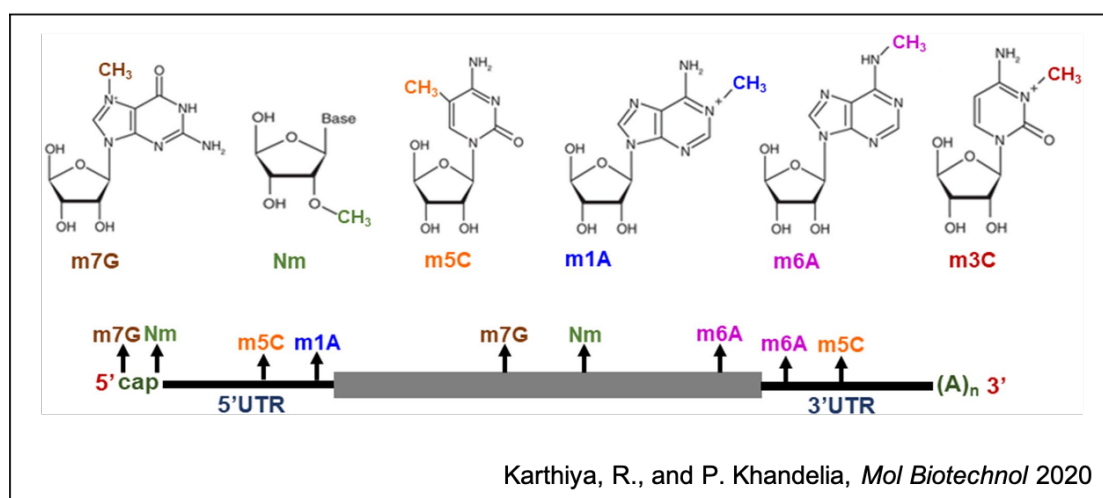
Figure 1. Spectrum of the most abundant mRNA modifications.

Top panel depicts the chemical structure of the modified nucleosides. The bottom panel displays modified nucleotides distribution pattern in 5' and 3' untranslated regions (UTR) and coding region of mRNA. m7G: N^7-methylguanosine; Nm: 2'-O-ribose-methylation; m5C: 5-methylcytosine; m1A: N^1-methyladenosine; m6A: N^6-methyladenosine; m3C: 3-methylcytidine.

1.1.4. m⁶A players: from writing to interpreting

The biological functions linked to N^6-methyladenosine deposition at target transcripts is the result of a complex equilibrium between m⁶A writers, readers and erasers (Figure 2) (Zaccara, Ries, and Jaffrey 2019; Shi, Wei, and He 2019). Although the past few years have witnessed a rapid advancement in elucidating the functions of modulators of m⁶A deposition, our understanding on how m⁶A regulates gene expression is far from being complete.
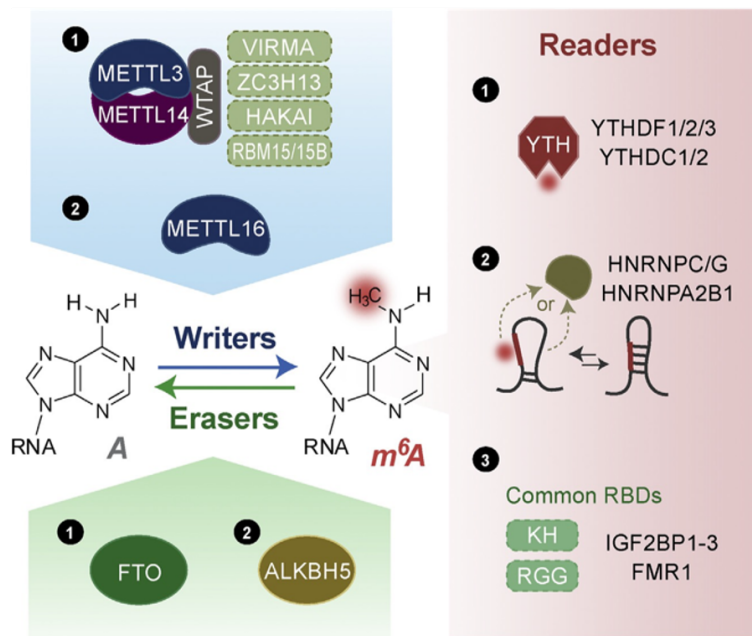
Shi, H., J. Wei et al., *Mol Cell* 2019

Figure 2. m⁶A players.

The majority of m⁶A methylation events are performed by the writer complex composed of the catalytic subunit METTL3 and several other regulatory subunits (1); the other known m⁶A writer, METTL16 (2), is involved in m⁶A deposition on the *Mat2a* transcript and on small nuclear RNAs. m⁶A mark can be eventually removed by specific erasers, including the demethylases FTO (1) and ALKBH5 (2). m⁶A functions are finally exerted by several classes of reader proteins: YTH domain family proteins (1), heterogeneous nuclear ribonucleoproteins (HNRNPs) (2), which preferentially bind to methylated transcripts thanks to their increased accessibility, and proteins that carry RNA-binding domains (RBD) (3), including the KH and RGG domains.

1.1.4.1. m⁶A writers

m^{6}A deposition is catalyzed by a methyltransferase complex composed of the METTL3-METTL14 (Methyltransferase-like 3 or 14) heterodimer, and a growing set of regulatory subunits, including WTAP (Wilms Tumor 1-Associated Protein), RBM15 (RNA-Binding Motif protein 15), VIRMA (Vir like m^{6}A Methyltransferase Associated, also known as KIAA1429), and ZC3H13 (Zinc finger CCCH-type containing 13) (Shi, Wei, and He 2019; Zaccara, Ries, and Jaffrey 2019). Within the m^{6}A methyltransferase complex, METTL3 is the sole catalytic subunit, whereas METTL14 serves as RNA-binding platform (Zaccara, Ries, and Jaffrey 2019; Wang et al. 2016; Liu et al. 2014; Sledz and Jinek 2016). Indeed, structural studies have revealed that METTL14 lacks specific amino acid residues that allow the binding of donor and acceptor substrates (Wang et al. 2016; Liu et al. 2014; Sledz and Jinek 2016). The presence of both METTL3 and METTL14 is essential to guarantee the activity of the complex, as knock-out of either of the two factors in mouse embryonic stem cells (ESCs) results in complete lack of m^{6}A mark of target mRNAs (Geula et al. 2015).

METTL3 *C*-terminus region carries the MTA-70 domain which contains the S-adenosyl-methionine (SAM) binding site (Bujnicki et al. 2002), whereas the *N*-terminus portion contains two zing finger motifs predicted to interact with the regulatory subunit WTAP, that ultimately guides the methyltransferase complex onto the target mRNA (Ping et al. 2014) (Figure 3). Given the crucial roles exerted by both domains in ensuring m^{6}A methylation onto target transcripts, disruption of either the *C*- or *N*-terminus region of METTL3 leads to a strong reduction in methyltransferase activity (Sledz and Jinek 2016).
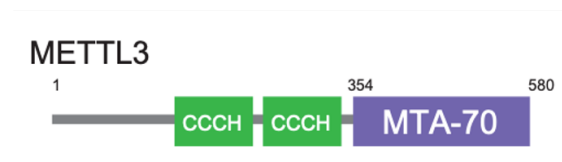
Sledz, P., and M. Jinek, *Elife* 2016

Figure 3. Schematic view of the domain composition of METTL3 protein.

The *N*-terminal region of the METTL3 protein carries two CCCH zing finger motifs (shown in green), whereas the *C*-terminal region contains the MTA-70 methyltransferase domain (residues 354 – 580, highlighted in violet).

The regulatory subunits RBM15 and VIRMA have been suggested to improve mRNA targeting specificity of the methyltransferase complex (Yue et al. 2018), whereas ZC3H13 ensures its nuclear localization (Wen et al. 2018), where m^6A deposition takes place. Recently, it was shown that H3K36me3 guides the methyltransferase complex onto nascent mRNAs, indicating that m^6A modification is added co-transcriptionally (Huang et al. 2019). Mechanistically, Huang and colleagues have shown that METTL14 recognizes H3K36me3 and binds to the nascent mRNA, leading to the recruitment of the other subunits of the complex, including METTL3, which ultimately catalyzes m^6A deposition when encountering stalling RNA polymerase II (Huang et al. 2019). In agreement with the scenario whereby H3K36me3 guides the METTL3/METTL14 complex to nascent target transcripts (Figure 4a), knockdown of the H3K36 methyltransferase *Setd2*, caused a substantial loss (~ 40%) in m^6A levels at polyadenylated mRNAs (Huang et al. 2019).

Mechanisms responsible for METTL3 targeting onto specific targets have been matters of intense investigation. In particular, molecular determinants controlling transcription elongation have been proposed as crucial regulators of m^6A deposition onto target transcripts (Figure 4b). In this context, recent work has reported the interaction between METTL3 and RNA polymerase II, suggesting that the polymerase itself may contribute to the recruitment of the m^6A methyltransferase complex onto their targets (Figure 4c). In support of the latter hypothesis, slowing RNA polymerase II, by expression of RNA Polymerase II mutants, or through inhibitors of transcription elongation, increased the recruitment of METTL3 on the target mRNAs as well as m^6A levels (Slobodin et al. 2017). Moreover, RNA-binding proteins (RBPs) have been proposed to guarantee the target specificity of the methyltransferase complex, by favoring its recruitment onto the target mRNA (Figure 4d) (Zaccara, Ries, and Jaffrey 2019).

In addition to the canonical METTL3/METTL14 catalytic complex, other enzymes with m^6A methyltransferase activity have been recently identified. For instance, METTL16 catalyzes m^6A modification of the *Mat2a* transcript, which encodes for the SAM synthetase, to promote its splicing and stability (Pendleton et al. 2017).
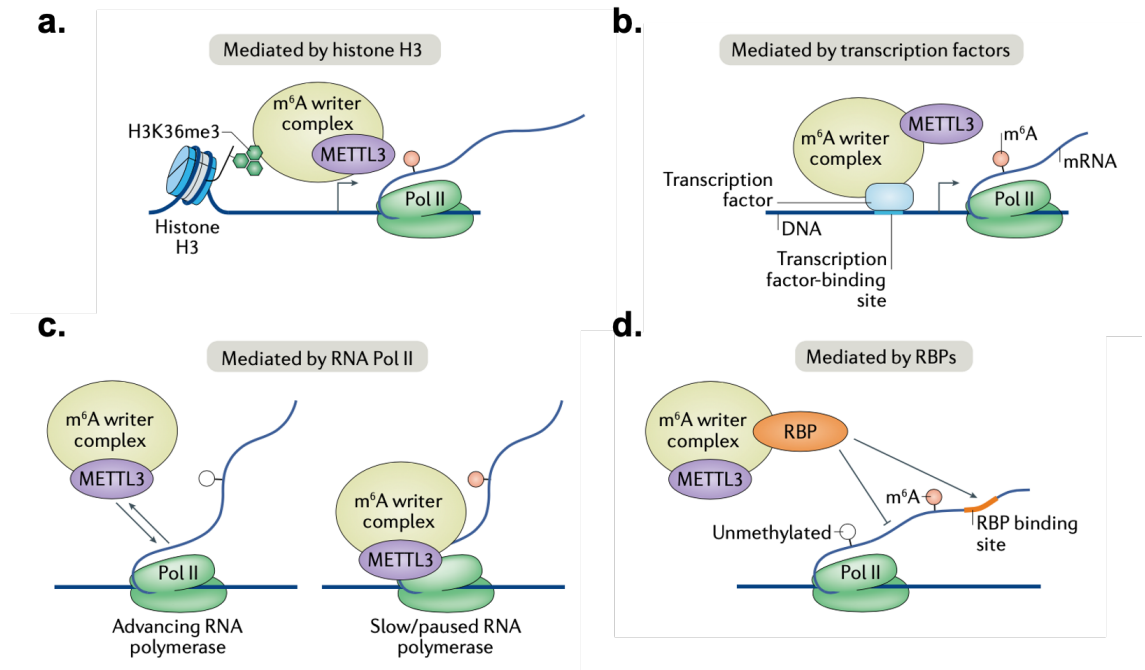
Figure 4. Mechanisms for target and m⁶A site specificity in m⁶A writing.

Specificity in m^6A writing can be mediated by players of the transcriptional machine, including histone modifications, such as histone H3 trimethylation on lysine-36 (**a**) and transcription factors (**b**). Additionally, site specificity can be mediated by RNA polymerase II, whose stalling on the mRNA during transcription may facilitate the recruitment of the methyltransferase complex on the target mRNA (**c**). Finally, target specificity can be ensured by the activity of RNA-binding proteins (RBPs) which bring the m^6A methyltransferase complex in close proximity to specific sites on the target mRNA (**d**).

The latter mechanism is particularly relevant and establishes a negative feedback loop to ensure SAM homeostasis, as it was shown that METTL16 catalyzes m^6A deposition on the *Mat2a* transcript when SAM levels become limiting (Pendleton et al. 2017). Additionally, METTL16 catalyzes m^6A deposition onto U6 small nuclear RNAs and other non-coding RNAs (Pendleton et al. 2017).

More recently, two new methyltransferases have been identified: ZCCHC4 (CCHC Zinc-finger-containing protein) and METTL5 methyltransferases, which catalyze m^6A onto 28S and 18S ribosomal RNAs, respectively (Ma et al. 2019; van Tran et al. 2019).

Finally, PCIF1 (Phosphorylated *C*-terminal domain-Interacting Factor 1) has been recently shown to add another methyl group to 2'-O-methylated adenosine, which is present at the transcription start site of 7-methylguanosine (m^7G)-capped mRNAs, thus giving rise to $N^6,2'$-

O-dimethyladenosine (m^6Am) (Sendinc et al. 2019). Transcripts marked at the transcription start site (TSS) by N^6,2'-O-dimethyladenosine (m^6Am) were shown to display enhanced stability (Liu, Li, et al. 2020; Engel et al. 2018; Mauer et al. 2017).

1.1.4.2. m^6A erasers

N^6-methyladenosine present into mRNA molecules can be recognized and removed by specific demethylases, thus rendering m^6A a reversible and dynamic mark (Zaccara, Ries, and Jaffrey 2019). Fat mass and obesity-associated protein (FTO) has been the first described m^6A demethylase. In 2011, it was shown that *Fto* gene deletion *in vivo* resulted in increased m^6A levels on total mRNA (Jia et al. 2011). Subsequently, several reports have shown that FTO preferentially contributes to demethylation of m^6Am, present at the 5' UTR of transcripts (Liu, Li, et al. 2020; Mauer et al. 2019; Wei et al. 2018). FTO is an iron (II) and α-ketoglutarate dependent dioxygenase, which has been associated with obesity and increased body mass in humans (Frayling et al. 2007). In mammals, FTO modulates several biological processes in a m^6A-dependent manner, including adipogenesis, triglyceride metabolism and circadian rhythms (Jiao et al. 2016; Wang, Shie, Wen, et al. 2015; Wang, Shie, Hsieh, et al. 2015). In addition, FTO indirectly influences mRNA splicing, by modulating the biogenesis of small nuclear RNAs (Mauer et al. 2019).

In 2013, a second demethylase enzyme, the α-ketoglutarate dependent dioxygenase ALKBH5 (Alk B homolog 5), was discovered (Zheng et al. 2013). Several studies linked deregulated expression of ALKBH5 with defects in the reproductive system (Zheng et al. 2013; Tang et al. 2018). *Alkbh5*-deficient male mice showed increased m^6A levels on total mRNA, and compromised spermatogenesis due to alterations in mRNA export and metabolism (Tang et al. 2018). Interestingly, expression of ALKBH5 is induced under hypoxic conditions, in a hypoxia-inducible factor (HIF)-dependent manner (Thalhammer et al. 2011).

1.1.4.3. m^{6}A readers

The major mechanism by which m^{6}A exerts its function, is through m^{6}A-reader proteins, which recognize and bind to methylated transcripts, ultimately influencing several aspects of mRNA metabolism (Zaccara, Ries, and Jaffrey 2019). Although it is unclear how readers achieve specificity towards selected mRNA targets, it is thought that the binding to specific transcripts may depend on several factors, including the density of m^{6}A sites, the sequence of m^{6}A sites and the cytoplasmic localization of mRNA targets (Zaccara and Jaffrey 2020; Shi, Wei, and He 2019).

One major class of m^{6}A readers is composed of proteins containing the YT521-B homology (YTH) domain, including YTH domain containing 1-2 (YTHDC1-2) and YTH domain family 1-3 (YTHDF1-3) proteins. The YTH domain is directly involved in the binding to the m^{6}A-modified transcript, by forming a tryptophan cage comprising two or three tryptophan residues around the methyl group (Zaccara and Jaffrey 2020). YTHDC1 localizes in the nucleus, where it stabilizes the m^{6}A-marked lncRNA X-inactive specific transcript (*Xist*), thus promoting X-chromosome inactivation (Patil et al. 2016). In addition, YTHDC1 is involved in the nuclear export of m^{6}A-modified mRNAs, by interacting with Serine and arginine Rich Splicing Factor 3 (SRSF3) and Nuclear RNA export Factor 1 (NXF1) (Roundtree et al. 2017; Lesbirel et al. 2018). YTHDC2 regulates both mRNA stability and translation and, through these functions, important biological processes, such as spermatogenesis (Hsu et al. 2017). Most of the downstream effects of m^{6}A modification have been linked to the function of YTH domain family proteins (YTHDF1-3). Several studies have assigned opposing functions to the YTHDF1 and YTHDF2 proteins, with the former promoting translation of m^{6}A-marked mRNAs (Wang, Zhao, et al. 2015), while the latter facilitating their degradation (Wang et al. 2014) (Figure 5). Instead, YTHDF3 enhanced both functions (Li, Chen, et al. 2017; Shi et al. 2017). On the other hand, emerging evidences indicate that different YTHDF family members share similar functions (Shi, Wei, and He 2019; Zaccara and Jaffrey 2020; Lasman et al. 2020).

Another family of m^{6}A readers achieves preferential binding of m^{6}A-modified mRNAs through defined RNA Binding Domains (RBDs), such as the RNA Recognition Motifs (RRM) domains and the Arginine/Glycine-Rich (RGG) or K Homology (KH) domains. For instance, FMR1 (Fragile X Mental Retardation 1) contains three KH domains and one RGG domain and was shown to bind to m^{6}A-modified targets, impacting on both RNA translation and stability. IGF2BP1 – 3 (Insulin-like Growth Factor 2 mRNA-Binding Proteins 1 – 3) contain KH domains and have been reported to stabilize m^{6}A-modified targets (Figure 5).

Several other RBPs, including Heterogeneous Nuclear Ribonucleoproteins (HNRNPs), preferentially bind to m^{6}A-modified mRNAs as a consequence of increased binding accessibility. Indeed, it was shown that m^{6}A modifications greatly reduce the property of mRNAs to form secondary structures. It remains unclear whether the binding of these reader proteins to RNA is a consequence of intrinsic high accessibility of the modified RNA molecules or, instead, specifically depends on the deposition of the m^{6}A mark (Shi, Wei, and He 2019; Zaccara and Jaffrey 2020).
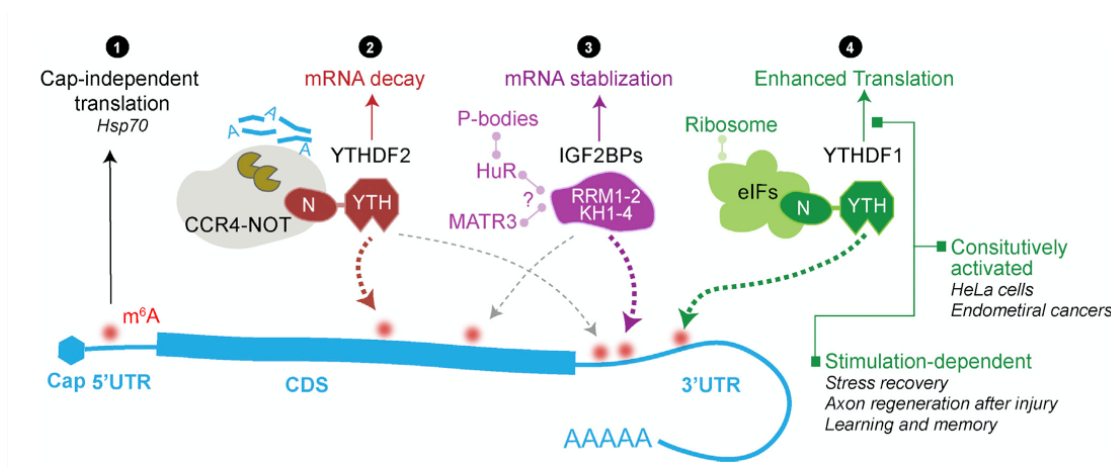
Shi, H., J. Wei et al., *Mol Cell* 2019

Figure 5. Functions of m^{6}A modification.

m^{6}A modification at the 5' UTR of transcript promotes cap-independent translation during stress responses (1). m^{6}A modification on the coding region of the mRNA triggers YTHDF2-mediated degradation (2). In addition, m^{6}A modification on the coding region can recruit RNA-binding proteins to the transcript, thus preventing mRNA degradation (3). Finally, m^{6}A mark at the 3' UTR can be linked to increased translation efficiency, thanks to the interaction of the reader YTHDF1 to members of the translational machinery, such as eIF proteins (4).

1.1.5. m⁶A-mediated effects on mRNA metabolism

Given the fact that m⁶A deposition occurs co-transcriptionally in the nucleus (Huang et al. 2019), it is thought that the m⁶A mark dictates the fate and half-life of the transcript, once it translocates to the cytosol. One of the most well-characterized functions of m⁶A is mRNA decay, which is usually associated with YTHDF2 activity. Mechanistically, upon target recognition, YTHDF2 recruits the endoribonuclease RNAse P/MRP, thus leading to mRNA decay (Park et al. 2019). This function renders m⁶A particularly important during cell fate transitions, as it enables the cells to properly switch a selected subset of their transcriptome to ensure the onset of new functions and the loss of others (Frye et al. 2018; Batista et al. 2014). Another established function of m⁶A is to increase mRNA stability, thanks to the binding of RNA-binding proteins which prevent mRNA degradation (Wang et al. 2014). Deposition of m⁶A can also enhance the translation efficiency of target transcripts, through three different mechanisms. (Wang, Zhao, et al. 2015). The first involves YTHDF1, which binds to the m⁶A-modified transcript and recruits the translation elongation factor eIF3, ultimately leading to the recruitment of all the other components of the translation machinery (Wang, Zhao, et al. 2015). The second mechanism, independent of YTHDF1, involves eIF3, which recognizes the m⁶A deposited at the 5' UTR of selected transcripts, leading to cap-independent translation (Meyer et al. 2015). The latter mechanism is particularly relevant for the synthesis of heat shock proteins (HSPs) during stress conditions, when cap-dependent translation is repressed (Meyer et al. 2015; Zhou et al. 2018). The third mechanism involves directly METTL3 and is particularly common in several cancer types. Specifically, METTL3 remains bound to the 3' UTR of m⁶A-modified proto-oncogene encoding transcripts and translocates with its target to the cytoplasm, where it promotes translation by favoring mRNA looping for ribosome recycling through interaction with eIF3h (Lin et al. 2016; Choe et al. 2018). Recent studies have suggested that m⁶A also marks Chromosome-Associated Regulatory RNAs (carRNAs), triggering their decay. Disruption of m⁶A modification increases the abundance of carRNAs, which ultimately promote gene transcription by increasing chromatin accessibility (Liu, Dou, et al. 2020).

1.1.6. Biological processes regulated by m^{6}A

1.1.6.1. m^{6}A regulation of stem cell fate

A major contribution to the understanding of m^{6}A functions comes from the extensive work performed on embryonic stem cells (ESCs) (Geula et al. 2015; Batista et al. 2014; Yang et al. 2018). In ESCs, the balance between self-renewal and lineage commitment is finely orchestrated by the levels of expression of a core set of pluripotency transcription factors, thus rendering this *in vitro* model highly suitable to study mechanisms of self-renewal and lineage differentiation.

In 2014, Batista and colleagues characterized for the first time the m^{6}A methylome of murine and human ESCs and found that they were largely overlapping, suggesting a conserved role for m^{6}A in ESCs across the species (Batista et al. 2014). Depletion of mouse and human METTL3 resulted in increased half-life of pluripotency-associated transcripts, including *Nanog* and *Sox2* mRNAs, thus preventing cell differentiation (Batista et al. 2014; Geula et al. 2015). These studies establish the importance of m^{6}A in ESCs in ensuring the rapid turnover of pluripotency transcription factors upon onset of differentiation (Batista et al. 2014). Other studies showed that in ESCs, the activation of the TGFβ-signaling pathway promotes cell differentiation by activating the SMAD2/3 transcription factors, which recruit the m^{6}A methyltransferase complex onto transcripts encoding for pluripotency factors, thereby favoring their degradation (Bertero et al. 2018).

During embryogenesis, m^{6}A plays a crucial role in the generation of hematopoietic stem cells (HSCs) (Lv et al. 2018), which derive from a subset of endothelial progenitor cells, known as hemogenic endothelial cells located in the ventral wall of the dorsal aorta. In the latter cells, the *Notch1* transcription factor sustains endothelial cell identity, whereas it is downregulated during the transition from endothelial cells to HSCs. In such transition, m^{6}A facilitates the generation of HSCs by ensuring YTHDF2-mediated recognition and degradation of m^{6}A-marked *Notch1* transcripts (Lv et al. 2018). In the last several years, many groups focused their studies on the role of m^{6}A in adult HSCs (Yao et al. 2018; Lee et al. 2019; Cheng et al. 2019).

Conditional *Mettl3* or *Mettl14* inactivation in HSCs, using the interferon-α inducible *Mx1*-cre transgene, resulted in the accumulation of HSCs in the bone marrow and impaired hematopoiesis (Yao et al. 2018). Two independent studies have shown that in HSCs, m[6]A increases the stability of the c-*Myc* transcript, which favors HSC differentiation through induction of symmetric commitment (Lee et al. 2019; Cheng et al. 2019). Interestingly, although *Mettl3*- or *Mettl14*-deleted HSCs showed downregulation of a c-MYC-controlled gene signature, the mutant cells failed to display decreased *c-Myc* transcript levels, favoring the alternative hypothesis that m[6]A regulates *c-Myc* translation (Lee et al. 2019). Inactivation of the YTHDF2 reader in HSCs, using the same experimental design, also showed accumulation of HSCs in the bone marrow. In this case, the increased self-renewal showed by HSCs was due to the impaired YTHDF2-mediated degradation of m[6]A marked transcripts including *Stat5*, *Gata2* and *Tal1*, which encode for transcription factors involved in the maintenance of stem cell state (Wang et al. 2018; Li et al. 2018).

A different outcome was obtained by Weng and colleagues, who studied the role of m[6]A in multipotent hematopoietic stem progenitor cells (HSPCs), triggered to differentiate towards the myeloid lineage *in vitro* (Weng et al. 2018). Indeed, in HSPCs, the stabilization of c-MYC and MYB proteins, exerted by METTL14, inhibited HSPC differentiation and supported the maintenance of the multipotent state. Instead, upon myeloid differentiation, upregulation of the transcription factor PU.1 triggered repression of *Mettl14* expression, thus leading to c-MYC and MYB destabilization (Weng et al. 2018).

1.1.6.2. m⁶A regulation of antiviral responses

Accumulating evidence assign to m⁶A and other mRNA modifications a key role in the regulation of immune responses, by sustaining the innate immune system to discriminate between self-transcripts and foreign molecules. Indeed, thanks to the nuclear deposition of the m⁶A mark on newly synthetized mRNAs, the immune system uses N^6-methyladenosine to discriminate and "tolerate" host mRNAs (Kariko et al. 2005). On the contrary, cytosolic RNA molecules lacking m⁶A are recognized as of foreign origin by several pattern-recognition receptors (PRRs), including the RIG-I-like receptors, RIG-I and MDA-5, and the Toll-like Receptors (TLR) 3, 7 and 8. This recognition triggers the activation of a type-I interferon response as part of a cellular immune response committed to eliminate host cells infected with viruses (Wu and Chen 2014). Recent studies have demonstrated that some viruses have acquired the ability to introduce m⁶A onto their transcripts in order to escape the innate immune response. Indeed, *in vitro* mutagenesis of such viruses, aimed to remove m⁶A deposition onto their transcripts, resulted in a stronger IFN-I response by infected cells (Lu et al. 2020). These data suggest that inhibitors of m⁶A may represent potent anti-viral agents.

1.1.6.3. m⁶A protection from T-cell mediated autoimmunity

The role of m⁶A modification in adaptive immune cells has only recently started to be unveiled. The first study addressing this point dealt with understanding the role of m⁶A in T-cell development (Li, Tong, et al. 2017). Combining the *Cd4*-cre transgene with conditional *Mettl3* knock-out alleles, authors reported minor effects on thymic T cell differentiation (Li, Tong, et al. 2017). However, upon adoptive transfer of *Cd4*-cre *Mettl3*^fl/fl T cells into RAG2-deficient mice, *Mettl3*-deficient CD4⁺ T-helper cells failed to homeostatically expand and differentiate into pathogenic effector T cells. This defect correlated with decreased m⁶A-dependent degradation of *Socs1*- (suppressor of cytokine signaling) and *Socs3*-specific transcripts, which encode for inhibitors of the IL-7/STAT5-signaling pathway (Li, Tong, et al. 2017) (Figure 6).

m6A methylation played a similar function in Regulatory T cells (Tregs), which are crucial to suppress autoimmune responses through the activation of IL-2 receptor α-chain and the induction of the downstream STAT5-signaling pathway (Tong et al. 2018; Shulman and Stern-Ginossar 2020). Indeed, selective inactivation of the *Mettl3* gene in *Foxp3*-expressing Tregs *in vivo*, led to the development of severe autoimmune diseases due to the accumulation of SOCS proteins which, in turn, inhibited the downstream activation of IL-2 receptor signaling (Tong et al. 2018; Shulman and Stern-Ginossar 2020) (Figure 6).
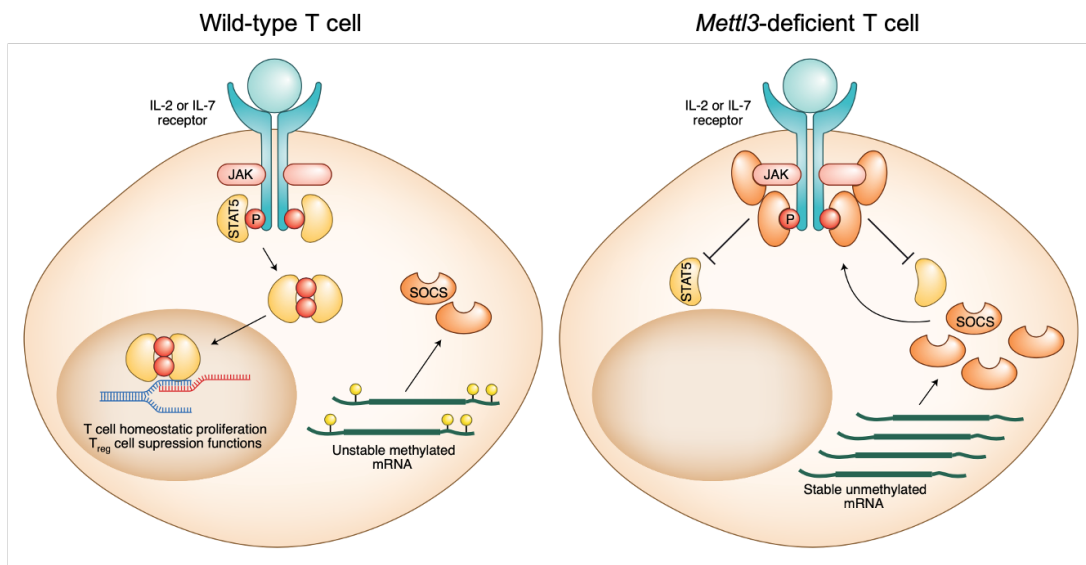
Adapted from Shulman, Z., and N. Stern-Ginossar, *Nat Immunol* 2020

Figure 6. Functions of m6A methylation in T cells.

In T cells, m6A marks the transcripts encoding for specific members of the SOCS protein family, which prevent the activation of the IL-7/STAT5 pathway in the unstimulated condition. Upon IL-7 signaling, m6A mark ensures the rapid degradation of the *Socs* transcripts, thus promoting the activation of the downstream STAT5-mediated pathway. *Mettl3*-deficient T cells show defect in IL-7 response, due to the accumulation of *Socs* transcripts.

1.1.6.4. m⁶A regulation of innate immune cell function

Deposition of m^{6}A onto target transcripts plays also an important role in innate immune cell maturation and function. Conditional deletion of the *Mettl3* gene in dendritic cells (DCs) resulted in impaired maturation of these cells in response to lipopolysaccharide (LPS) stimulation and reduced capacity to trigger T-cell responses (Wang et al. 2019). These defects correlated with reduced expression of the TLR4-adaptor protein TIRAP and the costimulatory molecules CD40 and CD80 (Wang et al. 2019). Similar observations were made analyzing DCs isolated from *Ythdf1*-knockout mice (Wang et al. 2019), thus indicating that m^{6}A sustains the translation of *Tirap*, *Cd40* and *Cd80* mRNAs in a YTHDF1-dependent manner (Figure 7). Recently, it was shown that *Ythdf1*-deficient DCs were more effective in antigen cross-presentation to CD8$^+$ T cells than wild-type cells, both *in vitro* and *in vivo* (Han et al. 2019). Mechanistically, YTHDF1 was found to enhance the translation of transcripts encoding for enzymes involved the phagosome and the lysosome pathways, which limit antigen cross-presentation through the degradation of antigens after uptake by DCs (Han et al. 2019) (Figure 7).
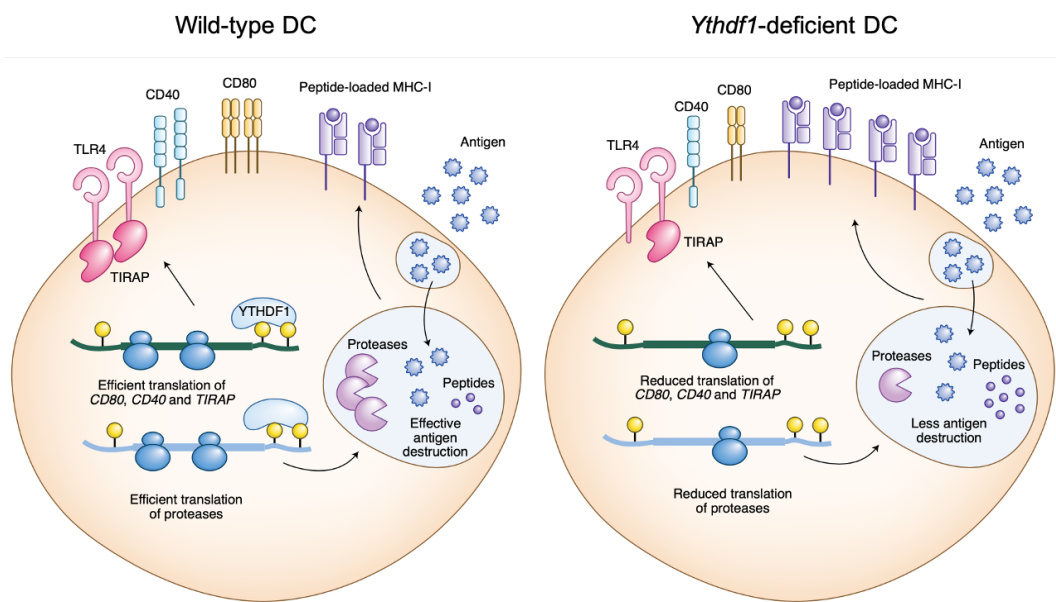
Adapted from Shulman, Z., and N. Stern-Ginossar, *Nat Immunol* 2020

Figure 7. Functions of m⁶A methylation in dendritic cells.

In dendritic cells, m^{6}A enhances, in a YTHDF1-dependent manner, the translation of transcripts encoding for the costimulatory molecules CD40 and CD80, for the TLR4-adaptor protein TIRAP and for antigen-degrading

proteases involved in the phagosome and lysosome pathways. In the absence of the m^{6}A reader YTHDF1, translation of proteases is less efficient and more peptides are available for antigen cross-presentation on surface MHC class I molecules. Lack of YTHDF1 or m^{6}A in LPS-stimulated DCs also leads to reduced expression of CD40, CD80 and TIRAP, due to inadequate translation of their corresponding transcripts.

1.1.6.5. m^{6}A as effector of stress responses

One of the mechanisms by which m^{6}A enhances mRNA translation is achieved through its deposition in the 5' UTR (Meyer et al. 2015). This process occurs commonly during stress responses when cap-dependent mRNA translation is transiently repressed, allowing the rapid translation of stress-induced transcripts, including those encoding for heat shock proteins (Meyer et al. 2015; Zhou et al. 2018). One study has shown that this process is regulated by the YTHDF2 reader protein, whose expression is rapidly induced 6 hours after heat shock stress *in vitro* (Yu et al. 2018). Under these conditions, YTHDF2 protected stress-induced transcripts marked by m^{6}A at the 5' UTR, preventing them from becoming substrate of the m^{6}A demethylase FTO (Yu et al. 2018). Emerging evidence suggest that, under stress conditions, YTHDF reader proteins also promote phase separation of m^{6}A-modified targets, thus facilitating partition of mRNAs into membrane-less compartments, including processing bodies (P-bodies), stress granules and neuronal RNA granules, where they are stored, degraded or transported to dendritic arbors in neurons (Ries et al. 2019; Liu, Feng, et al. 2020).

1.1.7. m^{6}A contribution to cancer pathogenesis

Dysregulation of the m^{6}A mRNA regulators have been found in many cancer types. One of the most studied m^{6}A alterations in cancer relates to the overexpression of METTL3, found in a variety of both hematological and solid malignancies (Barbieri et al. 2017; Vu et al. 2017; Yang et al. 2020). In acute myeloid leukemia (AML), overexpression of METTL3 sustains the survival of AML cells by increasing the m^{6}A deposition and thereby the stability and translation of transcripts encoding for proto-oncogenes, including c-MYC, MYB and BCL2 (Vu et al. 2017). In gastric cancer, METTL3 sustains cell proliferation and tumor invasion by directly promoting the expression of downstream targets of the MYC pathway (Yang et al. 2020). In hepatocellular carcinoma, the increased m^{6}A-methylation, catalyzed by METTL3 on tumor suppressor transcripts like *Socs*, leads to their instability and degradation (Chen et al. 2018)**.**

Deregulated expression of FTO has been linked to several cancer types, where it mediates up to 40% m^{6}A demethylation events on the total pool of mRNA molecules (Liu, Li, et al. 2020). In acute promyelocytic leukemia, FTO overexpression promotes leukemogenesis by downregulating the expression of the Retinoic Acid Receptor Alpha (RARA) (Li, Weng, et al. 2017). In lung squamous cell carcinoma, FTO upregulation sustains tumor cell growth and metastasis by overexpressing Myeloid Zinc Finger 1 (MZF1) transcription factor (Liu et al. 2018). In pancreatic cancer, FTO promotes tumor growth by upregulating the oncogene *c-Myc* (Tang et al. 2019). In breast cancer, overexpression of ALKBH5 sustains the self-renewal of tumor initiating cells by demethylating *Nanog* and *Klf4* transcription factors, thus increasing their stability (Zhang, Samanta, et al. 2016; Zhang, Zhi, et al. 2016).

Alterations in the expression of YTHDF2 reader protein have been detected in different cases of hepatocellular carcinoma (Zhong et al. 2019; Chen et al. 2018). Interestingly, in some cases, YTHDF2 behaves as tumor suppressor and its loss contributes to the establishment of the malignant phenotype (Zhong et al. 2019). In other instances, instead, the overexpression of YTHDF2 facilitates degradation of m^{6}A-marked *Socs2* transcripts, thereby reducing tumor suppressive activity (Chen et al. 2018).

Altogether, these results indicate that m^{6}A contribution to cancer pathogenesis, persistence and progression, is cell-type and context-specific. Therefore, dissecting the role of m^{6}A in individual cancer types represents a prerequisite to determine whether specific m^{6}A players can become targets of anti-tumor treatments.

1.1.8. Methods for m^{6}A detection

The study of the m^{6}A epitranscriptome requires the possibility to detect m^{6}A-marked transcripts at high resolution. A widely used method to map m^{6}A transcripts (called meRIP-seq) consists in the immunoprecipitation of fragmented m^{6}A-methylated transcripts by means of an anti-m^{6}A specific antibody, followed by deep sequencing (Figure 8) (Dominissini et al. 2013). However, this methodology lacks single-nucleotide resolution information. To overcome this limit, miCLIP-seq (m^{6}A Individual-nucleotide resolution Crosslinking and Immunoprecipitation combined with deep sequencing) was developed, which detects specific mutational signatures at m^{6}A residues induced by UV cross-linking of anti-m^{6}A antibodies bound to m^{6}A at target RNAs (Hsu and He 2019).

More recently, the *Escherichia coli* MazF RNA endoribonuclease was found to specifically cleave the unmethylated adenosine of an ACA m^{6}A consensus sequence, allowing for the first time single-base mapping of m^{6}A, employing an antibody-independent method called m^{6}A-sensitive RNA-Endoribonuclease-Facilitated sequencing (or m^{6}A-REF-seq) (Garcia-Campos et al. 2019; Zhang et al. 2019).
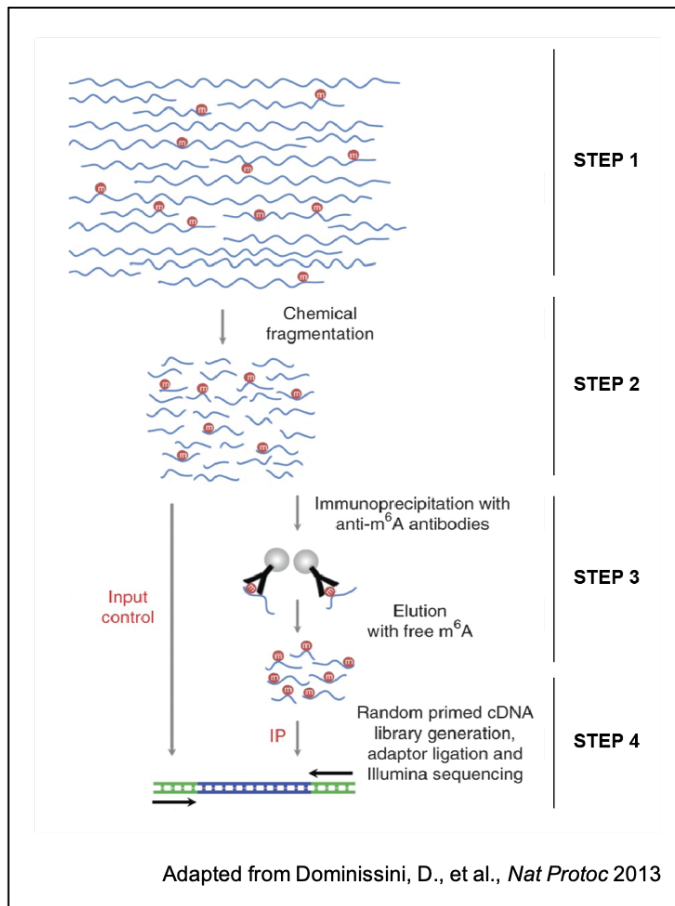
Figure 8. Schematic representation of meRIP-seq workflow.

mRNA is purified from total RNA to enrich for polyadenylated RNAs (step 1). Purified mRNA or total RNA is fragmented into 100-nucleotides long fragments by chemical fragmentation (step 2). m^6A-modified mRNA fragments are then immunoprecipitated using an anti-m^6A-specific antibody (step 3). Eluted m^6A-containing fragments (IP) and untreated input control are then converted by reverse transcriptase into cDNA using random hexamer primers, followed by adapter ligation and sequencing using next-generation-based sequencing methods (step 4).

1.2. B cell development

B lymphocytes originate from a small pool of multipotent HSCs, which undergo stepwise differentiation to ultimately express on the cell surface a broad spectrum of functional, non-autoreactive B cell receptors (BCRs). Thanks to the identification of selected surface markers specific for each stage of B cell development, research conducted over the past four decades has greatly contributed to shed light on the main molecular events underlying B cell lymphopoiesis, allowing a high-resolution assessment of B cell functions in different subsets of mature B cells.

1.2.1. Early steps of B cell development

In human and mouse post-natal life, B cell development starts in the bone marrow, as a result of a multistep differentiation process that leads HSCs to progressively become common lymphoid progenitor cells (CLPs). This process is triggered by enhanced response of lymphoid-primed multipotent progenitors (LMPPs) to Flt3-ligand (Flt3L) and IL-7, which is associated to the expression of the lymphoid-restricted transcription factor Early B-cell Factor 1 (EBF1) (Figure 9) (Kondo, Weissman, and Akashi 1997). CLPs are highly committed lymphoid progenitors co-expressing E2A and EBF1 transcription factors. Upon further stimulation through the IL-7 receptor (IL-7r) and EBF1 activation, restriction to the B-lineage is guaranteed by the expression of PAX5, the master transcription factor restricting B-cell identity (Nutt, Heavey, et al. 2015), which marks differentiation of CLPs into pro-B cells (Figure 9). PAX5 represses multipotency-associated genes, including those encoding for the receptor of Flt3L (*Flt3*) and Sca-1 surface marker, and simultaneously activates B-cell specific genes, such as components of the B cell receptor (BCR) signaling (Cobaleda et al. 2007). PAX5 is also crucial to ensure the process named Immunoglobulin V(D)J recombination (Tonegawa 1983), whereby a highly diversified repertoire of immunoglobulin (Ig) heavy and light chain variable region genes are consecutively assembled through rearrangements events catalyzed by the RAG-1 and RAG-2 proteins, which bring together, in a random fashion, variable (V), diversity (D) and joining (J) gene segments, respectively (Tonegawa 1983; McBlane et al. 1995; Schatz 1997).

The aim of this process is to generate a highly diversified repertoire of antigen binding sites which are assembled into IgH (heavy) and IgL (light) chain polypeptides, as part of single transcripts coding for both Ig variable and constant regions. V(D)J recombination is a temporally ordered process whereby V_H gene rearrangements precede V_L gene rearrangement, with the first taking place in pro-B cells, while the latter in pre-B cells (Figure 9). Productive V_H and V_L gene rearrangements ensure pre-B cells expressing paired IgH and IgL chains on the cell surface to receive appropriate signals from the BCR to stop further V(D)J recombination events and transit to the immature B cell stage (Figure 9) (Busslinger 2004).

HSC LMPP CLP Pro-B Pre-B Immature

FLT3

IL-7R

PAX5
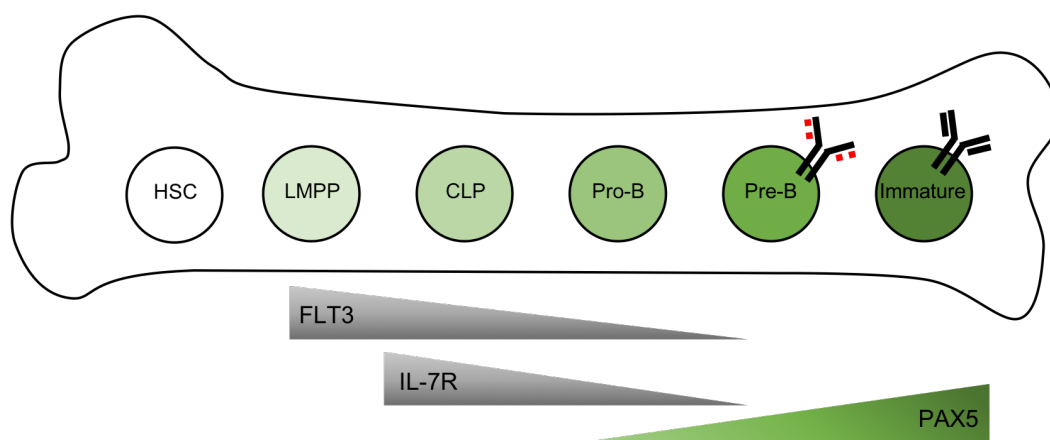
Figure 9. Schematic representation of early B cell development.

Early B cell development takes place in the bone marrow, where a hematopoietic stem cell (HSC) differentiates into a lymphoid-primed multipotent progenitor (LMPP). Stimulation through the Flt3 and IL-7 receptors progressively leads to the differentiation of a LMPP into a common-lymphoid progenitor (CLP). Expression of the transcription factor PAX5 marks the transition from CLP to pro-B cell. In pro-B cells, V(D)J recombination of the *IgH* locus takes place, leading to the expression of a pre-BCR where the rearranged heavy chain (in black) is assembled with a surrogate light chain (in red) and to the transition from the pro- to pre-B cell stage. In pre-B cells, *IgL* gene rearrangement occurs. Pairing of functional IgH and IgL chains leads to the generation of immature B cells expressing a functional BCR on their surface.

1.2.2. Peripheral B cell development

Transitional B cells. Bone marrow B cells which succeed to express a BCR on the surface are called immature B cells. These cells are characterized by the expression of IgM on the surface, while they still lack IgD expression. Immature B cells are screened in the bone marrow for BCR self-reactivity. This process is strictly influenced by the strength of the signal emanating from the BCR as a result of the putative recognition of self-antigens. B cells engaged in the recognition of autoantigens with high affinity are subjected to programmed cell death. BCR signals of intermediate strength trigger a process called receptor editing, which ensures self-reactive B cells to attempt a new round of IgL chain V gene rearrangements, accompanied by deletion of the previous one. Should the replacement of the IgL chain V gene lead to the formation of a BCR that no longer recognizes self-antigens, these B cells are rescued from apoptosis and allowed to exit the bone marrow to reach the spleen to continue their differentiation. Transitional non-autoreactive B cells can be classified into two main subsets, namely T1 ($B220^+CD93^+$ IgM^+ $CD23^-$) and T2 ($B220^+CD93^+$ IgM^+ $CD23^+$) B cells, with the latter ones deriving from the former (Loder et al. 1999; Allman et al. 2001). Both bone marrow and splenic transitional B cells are characterized by a short life span of around three days. Only a small fraction of transitional T2 cells successfully differentiates to become mature B-2 B cells in the spleen, which include follicular and marginal zone B cells.

Mature B cell subsets. Only 5% to 10% of transitional B cells succeeds every day to continue their differentiation pathway in the spleen to become either follicular (Fo) or marginal zone (MZ) B cells (Figure 10). The entry of short-lived immature/transitional B cells into the pool of long-lived mature B cells strongly depends on molecular signals generated through the BAFF receptor (BAFF-R) and the BCR. Binding of immature B cells through BAFF-R to soluble BlyS/BAFF, produced by follicular dendritic cells (FDCs) residing within primary B cell follicles in the white pulp of the spleen, is crucial to sustain and extend the survival of these cells. In addition, BAFF/BAFF-R signals are integrated by others emanating from the BCR expressed by immature B cells (Mackay and Browning 2002).

Specifically, transitional B cells receiving through their BCR a continuous relatively strong signaling mainly differentiate into Fo B cells, whereas weak BCR signaling favors the development of MZ B cells (Pillai and Cariappa 2009) (Figure 10).

Fo B cells represent by-and-large the major population of mature B cells in both human and mice and primarily reside in primary follicles of the spleen and other secondary lymphoid organs (SLOs), including lymph nodes and mucosa-associated lymphoid tissues (MALT). Fo B cells express on the surface two types of BCRs, namely IgM and IgD. MZ B cells, instead, express only IgM on the surface and are preferentially residing in the spleen, positioning themselves outside of primary B cell follicles, juxtaposing the marginal sinus. Based on their proximity to the blood stream, flowing through the marginal sinus, MZ B cells are preferentially recruited into immune responses triggered by blood-borne pathogens.

In addition to the strength of BCR signaling, MZ B cell development also depends on the activation of the NOTCH2 receptor as a result of the binding to NOTCH ligands presented to the B cells by local endothelial cells, MZ macrophages and fibroblastic stromal cells (Casola et al. 2004; Pillai and Cariappa 2009; Hampel et al. 2011; Fasnacht et al. 2014).

A substantial difference between Fo and MZ B cells is the ability of the latter to self-renew, while the former require a constant input of immature B cells from the bone marrow to sustain their number (Hao and Rajewsky 2001).

B-1 B cells represents the third population of mature B cells and reside in body-cavity sierosa, including the peritoneum, the pleura and the pericardium. B-1 B cells are mainly generated during fetal life, deriving from progenitor B cells that are different from those giving rise to B-2 B cells. As MZ B cells, B-1 B cells express exclusively IgM on the surface, are self-replenishing and participate mainly to innate immune B cell responses. B-1 B cells express a rather restricted repertoire of BCRs which reacts against recurrent components of microorganisms such as polysaccharides or phospholipids, rendering them commonly cross-reactive with self-antigens. Together with MZ, B-1 B cells predominantly participate to T-cell independent B cell responses, giving rise to short-lived plasma cells expressing low affinity antibodies (Figure 10).

Instead, Fo B cells represent the main mature B cell subset recruited into adaptive, T-cell dependent immune responses, which generate long-lived antibody secreting plasma cells (PCs) and memory B cells expressing affinity-matured BCRs as a result of their participation to the germinal center (GC) reaction (Figure 10).
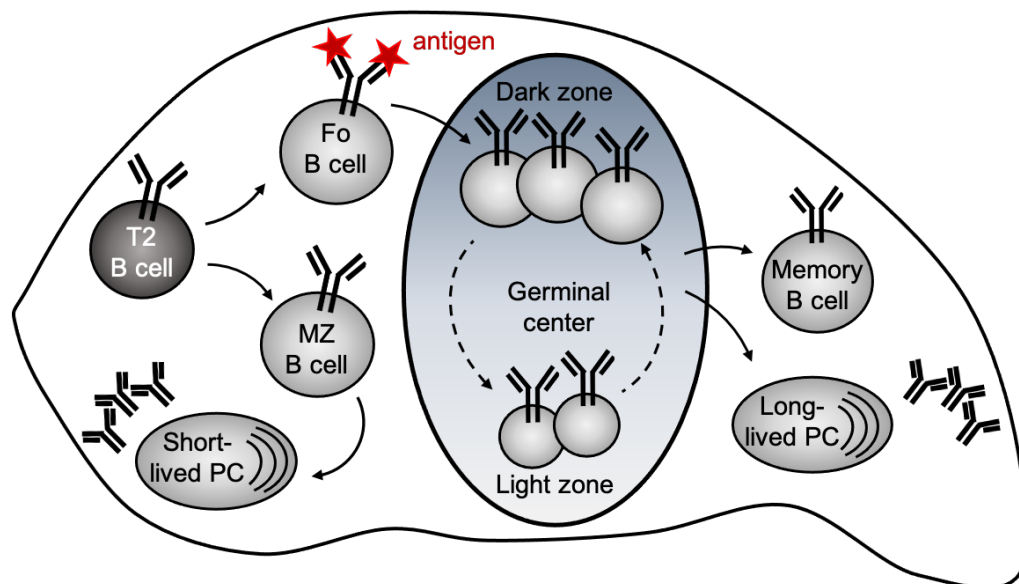
Figure 10. Peripheral B cell development.

Once immature B cells express a functional BCR on the cell surface, they leave the BM and arrive to the spleen. Here, immature B cells can mature further, through transient transitional (T1 and T2) B cell stages, into either follicular (Fo) or marginal zone (MZ) B cells. MZ B cells participate to T-cell independent immune responses, giving rise to short-lived plasma cells (PCs), secreting low-affinity antibodies. Fo B cells, instead, represent the main population involved in T-cell dependent immune responses. In particular, upon antigen encountering, antigen-specific B cells are recruited into the germinal center reaction, where they undergo cycles of proliferation, mutations in their Ig genes, and selection on the basis of their affinity towards the antigen. High-affinity germinal center B cells ultimately differentiate into high-affinity Ig expressing memory B cells and PCs, secreting high-affinity antibodies for the encountered antigen.

1.2.3. B cell immunity

Depending on the requirement for T-cell help in antibody production, B cell responses can be of two major types: T-cell independent (T-I) or T-cell dependent (T-D). The element in common between the two types of immune responses is the generation of terminally differentiated PCs, which secrete antibodies directed against foreign antigens expressed by the invading pathogens. However, the affinity and class of antibodies released during T-I and T-D immune responses are very different, with the former being of low-affinity and primarily of the IgM or IgG3 isotype, while the latter ones are of high-affinity and predominantly of the IgG1, IgG2 and IgA isotypes (Castro-Dopico and Clatworthy 2019). Given the relevance for my thesis project of T-D B cell responses, I will mainly focus on them in the following paragraphs.

1.2.3.1. T-cell dependent immune responses

Antigens that induce T-cell help to orchestrate the production of high-affinity antibodies are called T-dependent antigens. Successful T-cell dependent immune responses require primary and secondary signals, which derive from B and T cell interactions. A primary signal is the binding of cognate antigen to the T and B cell receptor (respectively TCR and BCR), whereas secondary signals involve the engagement of costimulatory molecules, expressed by T and B lymphocytes, with their respective ligands.

During T-cell dependent immune responses, antigens are presented to naïve Fo B cells in the form of immune complexes, often exposed on the surface of FDCs. Upon antigen recognition through the BCR, B cells internalize the antigen, process it into short peptides and ultimately load them onto MHC-class II molecules. Activation via the BCR rapidly induces changes in the expression of chemokine receptors, in order to favor the migration of B cells towards the T-cell area (Pereira, Kelly, and Cyster 2010). Once arrived to the T-B border, B cells present the antigen to CD4$^+$ T-helper cells. MHC-class-II/TCR pairing, in the presence of costimulatory signals, promotes the full activation of antigen-specific B cells. Costimulatory signals derive from the binding of CD40 receptor, expressed on the surface of B cells, with CD40-ligand (CD40L, also called CD154), expressed by activated T cells,

as well as from the binding of the B cell costimulatory molecules CD80 and CD86 with their corresponding ligand CD28, expressed by T cells (Zotos and Tarlinton 2012).

In addition to cell-cell interaction, CD4^{+} T cells provide help by secreting cytokines, such as IL-4 and IL-21, which are crucial for full activation, survival and differentiation of B cells (Zotos and Tarlinton 2012). After having received T-cell help, antigen-specific B cells can undergo two possible fates: they can migrate to the extrafollicular area, where they differentiate into short-lived low-affinity antibody-secreting PCs (Smith et al. 1996); otherwise, they can return to the B-cell zone in the primary follicle to be recruited into the germinal center (GC) reaction, where they will undergo cycles of proliferation, mutations at their Ig genes and selection on the basis of their affinity towards the antigen, ultimately leading to their terminal differentiation into either long-lived antibody secreting PCs or memory B cells (Kosco-Vilbois and Scheidegger 1995).

1.2.3.2. Regulation of the germinal center reaction

Once received cognate CD4$^+$ T-cell help at the T-B border, antigen-activated B cells migrate to the center of the follicle, where they proliferate extensively and give rise to specialized structures named germinal centers (GCs) (Figure 11) (Victora and Nussenzweig 2012; Zhang, Garcia-Ibanez, and Toellner 2016; Mesin, Ersching, and Victora 2016; Zotos and Tarlinton 2012). Consequently, naïve B cells which originally resided in the follicle are pushed in the periphery, forming a compartment which surrounds the GC reaction, named B cell mantle (Victora and Nussenzweig 2012). Morphologically, GCs can be divided into two distinct compartments: a dark zone (DZ), which is proximal to the T-cell zone, and a light zone (LZ), which is distal to the T-cell area and proximal to the lymph-node capsule. The identification of surface markers which can clearly distinguish these two populations by flow cytometry greatly helped in understanding the molecular mechanisms underlying the GC reaction. The first contribution came from the Cyster laboratory, showing that the chemokine receptor CXCR4 is responsible for retaining a population of GC B cells in the DZ (Allen et al. 2004). Some years later, the Nussenzweig laboratory used *in situ* photoactivation to label DZ and LZ cell populations directly within the GC, showing that they could be clearly distinguished according to the expression of the surface markers CD83 and CD86, when used in combination with CXCR4 (Victora et al. 2010). Indeed, whereas DZ B cells show a low expression of the two markers (CXCR4^{hi} CD83^{lo} CD86^{lo}), B cells transiting to the LZ upregulate CD86 and CD83 expression (CXCR4^{lo} CD83^{hi} CD86^{hi}) (Figure 11) (Victora et al. 2010). Within the DZ, GC B cells, named centroblasts, undergo cycles of intense proliferation and diversify their immunoglobulin genes through a process called Ig somatic hypermutation (SHM) (Jacob et al. 1991), which leads to single nucleotide substitutions, preferentially within the portion of the V gene encoding for the hypervariable region (also called Complementarity Determining Region or CDR) of the BCR, which is directly involved in the binding to the antigen. The process of SHM depends on the activity of the Activation-Induced cytidine Deaminase (AID) enzyme, encoded by the *Aicda* gene, whose expression is induced in GC B cells (Muramatsu et al. 2000). As a result of SHM, clonally-related GC B cells express BCRs with different affinity (Berek, Berger, and Apel

1991). Centroblasts upregulate several genes associated with cell proliferation, while silencing negative regulators of the cell cycle (Victora et al. 2012). Moreover, DZ B cells are also highly prone to undergo apoptosis, as a result of the downregulation of anti-apoptotic proteins, including members of the BCL2 protein family, and the upregulation of pro-apoptotic proteins, including CD95/FAS (Victora and Nussenzweig 2012; Victora et al. 2012; Klein et al. 2003a; Saito et al. 2009). The latter feature is extremely relevant, as it ensures the clearance of B cells displaying low-affinity BCRs as a result of Ig SHM.

Within the LZ, thanks to the tight contact with FDCs and T-follicular helper (Tfh) cells, GC B cells, also called centrocytes, undergo a multi-step process of selection, based on their improved affinity for the antigen (Schwickert et al. 2007; Allen, Okada, and Cyster 2007). The first step of this selection consists in the ability of B cells to recognize and bind to the antigen: only B cells expressing newly mutated BCRs, which exhibit the highest affinity, succeed in capturing and internalizing the antigen, presented by FDCs.

The second step of the selection consists in the capacity of B cells to present the processed antigen in the form of peptides, expressed on their surface, to Tfh cells, which will provide costimulatory signals that are essential to survive (Shulman et al. 2014; De Silva and Klein 2015). This process is called positive selection and ultimately leads to the survival of high-affinity BCR-expressing B cells, which received both primary and secondary signals. Mechanistically, it was shown that BCR and CD40 signaling synergize and cooperate together to upregulate the proto-oncogene *c-Myc*, whose expression is a key determinant of positive selection (Calado et al. 2012; Dominguez-Sola et al. 2012; Luo, Weisel, and Shlomchik 2018). Positively selected B cells in the LZ can undergo two different fates: they can either leave the GC reaction and differentiate into terminally differentiated B cells, including antibody-secreting PCs or memory B cells, or they can re-enter the DZ, where they undergo clonal expansion and further increase their affinity for the antigen by performing additional rounds of SHM, thus ensuring affinity maturation (Figure 11) (Victora and Nussenzweig 2012).
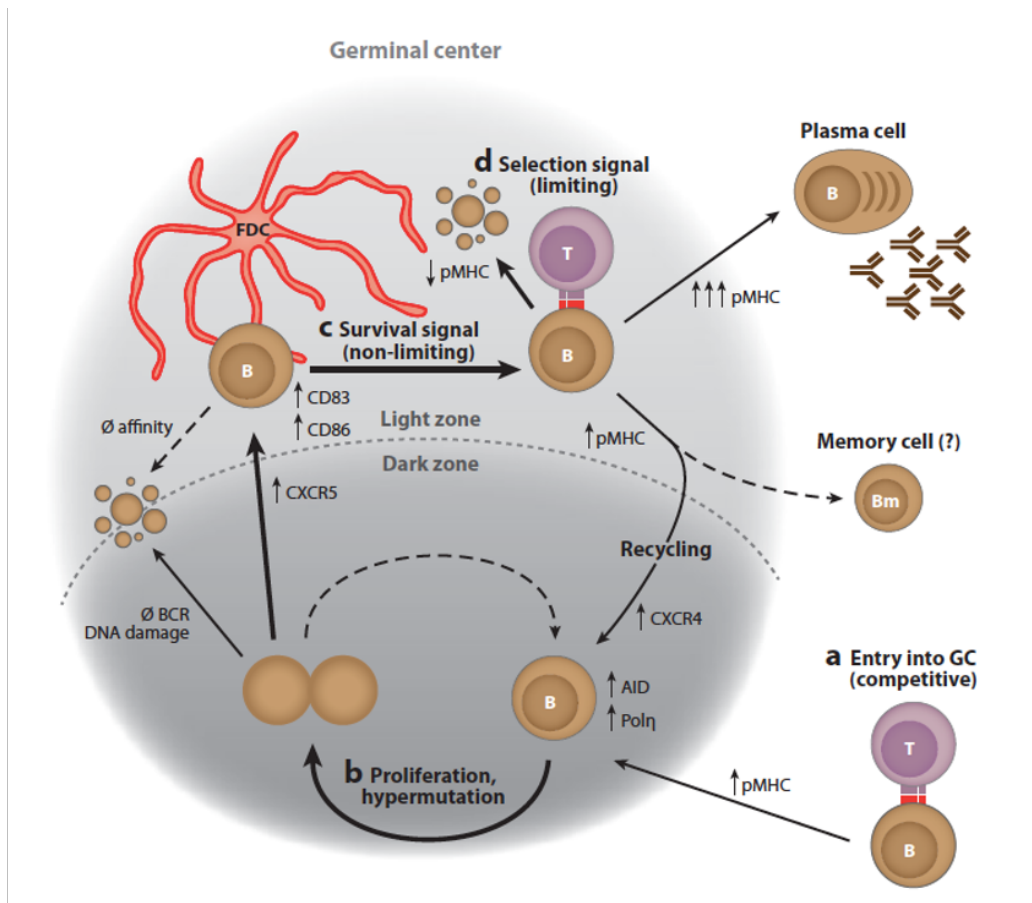
Adapted from Victora, G. D., and M. C. Nussenzweig, *Annu Rev Immunol* 2012

Figure 11. The germinal center reaction.

Upon antigen encountering, antigen-specific B cells receive T-cell help at the T-B border (a). After receiving T-cell help, B cells are recruited into the germinal center (GC) reaction and undergo cycles of proliferation and somatic hypermutation (SHM) in the dark zone (b). Here, cells are called centroblasts and are characterized by high CXCR4 and AID expression. Autoreactive B cells generated by chance through SHM are immediately killed. GC B cells then migrate to the light zone and upregulate CD83 and CD86, two costimulatory molecules (c). Here, B cells are called centrocytes and compete for the binding to the antigen, presented by follicular dendritic cells (FDCs) (c). B cells expressing BCR exhibiting the highest affinity for the antigen will succeed in internalizing the antigen and presenting it to the few T-follicular helper (Tfh) cells. At this point, B cells with higher MHCs preferentially interact with Tfh cells, thus preventing the interaction of the latter cells with lower-affinity B cells, in a competitive fashion (d). Positively selected B cells can now undertake two possible fates: they can either leave the GC to differentiate into PCs or memory B cells, or they can re-enter in the dark zone and undergo additional rounds of proliferation and SHM, to further increase their affinity towards the antigen.

Kennedy and colleagues have recently contributed to shed light on the molecular events downstream the re-entry in the DZ of positively selected GC B cells (Kennedy et al. 2020). They demonstrated that proliferation and SHM occur in two distinct microenvironments in the DZ, arbitrarily called DZp (proliferation) and DZd (differentiation), respectively (Kennedy et al. 2020). The DZp contains actively dividing cells, organized into clusters, that can be distinguished thanks to higher expression of cell-cycle associated genes, including *Ccnb1*, encoding for cyclin B1 (Kennedy et al. 2020). The DZd contains cells that are undergoing SHM at the Ig genes, which can be distinguished thanks to high levels of *Aicda* transcript, and other genes associated with DNA damage and stress response (Kennedy et al. 2020). This work proposes a scenario whereby cell division and SHM are physically and temporally distinct, in order to guarantee genomic stability and prevent malignant transformation.

Additionally, mutations generated through SHM in the DZ can accidentally lead to the expression of autoreactive BCRs. The latter cells are quickly eliminated in the GC through a process called negative selection, which is defective in several autoimmune diseases. Negative selection is mainly achieved through apoptosis of self-reactive B cells, thanks to the high expression of pro-apoptotic factors which characterizes GC B cells (Chan et al. 2012; Yau et al. 2013). Although initially it was thought that negative selection only occurred in the GC reaction, it was recently shown that self-reactive B cells, which manage to escape negative selection in the GC, can be eliminated in post-GC compartments, such as the PC or the memory B cell compartments (Mayer et al. 2020).

1.2.3.2.1. Transcriptional regulation of the GC reaction

BCL6. The transcription factor BCL6 is a critical regulator of the GC reaction and mice lacking its expression are incapable of forming GCs (Ye et al. 1997; Shaffer et al. 2000; Basso and Dalla-Favera 2010). BCL6 belongs to POZ/BTB-zinc finger protein family and is highly expressed in B cells recruited in the GC reaction, where it sustains the maintenance of GC B-cell identity by repressing the expression of selected genes. Specifically, BCL6 can exert the repressive function either by directly binding to the promoter region of its targets or by recruiting histone deacetylases and co-repressor complexes (Basso and Dalla-Favera 2010). In B cells, *Bcl6* expression is regulated at multiple levels. In naïve B cells, *Bcl6* is expressed at the transcript level but not at the protein level. In GC B cells, *Bcl6* expression is rapidly incremented thanks to increased gene transcription as well as to post-translational modifications that increase BCL6 stability at the protein level (Cattoretti et al. 1995; Allman et al. 1996). In the GC reaction, BCL6 contributes to the maintenance of GC B-cell identity by exerting the following functions: i) it ensures the pro-apoptotic state of GC B cells, by repressing genes encoding for anti-apoptotic factors, including members of the BCL2 protein family, thus making GC B cells prone to undergo apoptosis, should they express low affinity or autoreactive BCRs as a result of SHM (Saito et al. 2009; Cattoretti et al. 1995; Ci et al. 2009); ii) it inhibits terminal differentiation, by silencing the *Prdm1* gene (Shaffer et al. 2000), encoding for BLIMP1, the master regulator of PC identity; iii) it downregulates the expression of mediators of BCR and CD40 signaling (Shaffer et al. 2000; Basso and Dalla-Favera 2010), which are, instead, crucial for positive selection in the LZ; iv) it allows GC B cells to tolerate DNA damage, induced by AID activity, by repressing genes encoding for determinants of DNA damage response, including Trp53, ATR, CHEK1 and cell-cycle inhibitors, such as p19 and p21 (Phan and Dalla-Favera 2004; Ranuncolo et al. 2007; Ranuncolo, Polo, and Melnick 2008; Phan et al. 2007; Liang et al. 2014; Phan et al. 2005). On the other hand, BCL6 levels are tightly controlled by the degree of DNA damage accumulated in the cell: over certain thresholds of accumulated DNA lesions, ATM indirectly promotes the phosphorylation, followed by ubiquitin-mediated degradation of BCL6 (Phan et al. 2007).

The latter mechanism ensures the death of GC B cells which accumulate excess of DNA lesions that cannot be further repaired, in order to prevent malignant transformation. Upon transition to the LZ, centroblasts progressively downregulate *Bcl6* expression. This downregulation is the result of the BCR-dependent antigen recognition and of the interaction with Tfh cells via CD40/CD40L (Alinikula et al. 2011). Specifically, the BCR signaling pathway promotes BCL6 phosphorylation by mitogen-activated protein kinases (MAPK), followed by polyubiquitination and subsequent proteasomal degradation (Niu, Ye, and Dalla-Favera 1998). CD40 signaling pathway, instead, indirectly downregulates *Bcl6* expression (Allman et al. 1996), by triggering NF-κB-mediated upregulation of IRF4 that, at higher doses, promotes the repression of *Bcl6* gene transcription, thus favoring terminal differentiation (Saito et al. 2007). Indeed, upon further differentiation into long-lived PCs or memory B cells, *Bcl6* expression must be repressed. This is achieved thanks to specific transcriptional regulators of PCs, including IRF4 and BLIMP1, that cooperate to repress *Bcl6* gene transcription (Saito et al. 2007).

BACH2. BACH2 is a transcriptional repressor that is expressed in mature B cells until the GC stage, whereas it is silenced in antibody-secreting PCs. In mature B cells, *Bach2* gene transcription is positively regulated by the B-cell identity master regulator PAX5 and further incremented upon B cell activation (Schebesta et al. 2007). As a repressor, a major target of BACH2 is the *Prdm1* gene, encoding for the PC master regulator BLIMP1 (Ochiai et al. 2006; Muto et al. 2010). Mice lacking the *Bach2* gene selectively in B cells are incapable of forming GCs due to the premature upregulation of BLIMP1 that leads to the downregulation of *Pax5* and, hence, of the *Aicda* gene. Specifically, it was found that BACH2 ensures the time-window required for AID expression in GC B cells in order to sustain affinity maturation through SHM and class switch recombination (CSR) (Muto et al. 2004), a process whereby B cells are able to express immunoglobulins with a different constant region of the heavy chain, without affecting the variable region directly involved in the binding to the antigen. Indeed, *Bach2*-deficient B cells prematurely express BLIMP1 and differentiate into IgM-expressing PCs (Muto et al. 2010).

Recently, it was suggested that *Bach2* levels may dictate the fate of positively selected GC B cells to differentiate either into PCs or memory B cells. Specifically, high levels of *Bach2* expression are mainly associated with differentiation of positively selected LZ B cells into the memory B cell fate (Inoue et al. 2021).

IRF4/IRF8 axis. In GC B cells, IRF4 and IRF8 follow a reciprocal expression pattern (Cattoretti et al. 2006). *Irf8* is highly expressed in DZ B cells, which are negative for *Irf4* expression. By contrast, LZ B cells undergoing PC differentiation upregulate *Irf4* gene transcription (Cattoretti et al. 2006). Recent studies showed that IRF8 is dispensable for GC formation, as mice lacking IRF8 specifically in B cells were still able to form GCs (Feng et al. 2011). By contrast, the transcription factor IRF4 is essential for GC biology, where it exerts its role in a dose-dependent manner (Klein et al. 2006; Ochiai et al. 2013; Sciammas et al. 2006). Before GC formation, IRF4 is upregulated in CD40-activated B cells, and its expression levels dictate the further steps of antigen-specific B cells: high amounts of IRF4 protein favor differentiation into short-lived PCs in the extrafollicular area, whereas low IRF4 levels favor the recruitment into the GC reaction (Zotos and Tarlinton 2012). In GC B cells, low IRF4 levels sustain the GC program by favoring *Bcl6*, *Pou2af1* and *Aicda* gene transcription, whereas high levels of IRF4 favor the expression of the *Prdm1* gene, encoding for the PC master regulator BLIMP1 (Klein et al. 2006), which will lead to the silencing of *Bcl6*, thus promoting the repression of GC B-cell identity and the establishment of the PC transcriptional program (Saito et al. 2007).

OCT2 and OBF1. Octamer-binding protein 2 (OCT2) is a B-cell specific transcription factor, encoded by the *Pou2f2* gene. It belongs to the POU domain family of transcription factors that uses a POU-specific domain to bind to DNA. Specifically, the binding of OCT2 to the octamer DNA motif 5' – ATGCAAAT – 3' (Staudt et al. 1988), induces a conformational change in the POU-domain which allows the recruitment of the coactivator OBF1, encoded by the *Pou2af1* gene, whose expression is also B-cell specific (Sauter and Matthias 1998; Chasman et al. 1999; Luo et al. 1992; Luo and Roeder 1995; Strubin, Newell, and Matthias

1995; Gstaiger et al. 1995). Constitutive *Pou2f2* knock-out mice die shortly after birth (Corcoran et al. 1993), whereas conditional deletion of the *Pou2f2* gene in mature B cells led to reduced B cell proliferation and Ig secretion when stimulated *in vitro* (Corcoran et al. 1993; Corcoran and Karvelas 1994). Additional studies have revealed that OCT2 directly binds to *c-Myc* and specific PC-associated genes, including *Stat3* and *Xbp1*, to positively regulate their expression (Hodson et al. 2016). Indeed, whereas STAT3 promotes the expression of the PC master regulator BLIMP1, the induction of the transcription factor XBP1 is required in PCs to ensure the establishment of a potent Ig production and secretion machinery to fulfil their protective functions.

Constitutive knock-out mice for the *Pou2af1* gene, encoding for the coactivator OBF1, show normal peripheral B-cell development, although they are unable to form GCs upon immunization (Kim et al. 1996; Nielsen et al. 1996; Schubart et al. 1996; Schubart et al. 2001; Hess et al. 2001; Samardzic et al. 2002). *In vitro* stimulation of *Pou2af1*-deficient B cells with T-cell mediated signals, such as CD40L and IL-4, resulted in reduced BLIMP1 induction, whereas *c-Myc* and *Xbp1* gene transcription was not affected (Corcoran et al. 2005). As a result of reduced levels of BLIMP1 transcription factor, differentiating *Pou2af1*-deficient B cells also displayed reduced expression of genes encoding for PC-associated factors, including J chain, a mediator of polymeric IgM and IgA transport, and IRF4, whose upregulation is required to efficiently trigger differentiation into PCs (Corcoran et al. 2005). Moreover, as a result of the reduced repression activity exerted by BLIMP1, *Pou2af1*-deficient B cells displayed high levels of B-cell and GC B-cell specific genes, including *Bcl6*, *Pax5* and *Pou2f2*, whose expression need to be silenced in plasmablasts (Corcoran et al. 2005). In addition, Kim and colleagues revealed that OCT2 and OBF1 support CSR in GC B cells, by binding to the 3' IgH enhancer of the Ig genes, thus sustaining transcription of the switched forms of *IgH* genes (Kim et al. 1996). The latter mechanism can explain the reduced humoral responses observed in *Pou2af1*-deficient mice, which was particularly evident for the Ig of the switched isotype (Kim et al. 1996).

1.2.3.2.2. Molecular determinants of the GC reaction

<u>CD40 signaling.</u> B and T cell interaction via CD40/CD40L represents a key determinant of T-cell dependent immune responses. CD40, a member of the Tumor Necrosis Factor Receptor (TNFR) family, is a transmembrane protein expressed by a variety of hematopoietic cells, including mature B cells, dendritic cells, monocytes, platelets and macrophages (Banchereau et al. 1995; Bourgeois, Rocha, and Tanchot 2002). The ligand of CD40 is a transmembrane protein, called CD40-ligand (CD40L) or CD154, which belongs to the TNF superfamily. CD40L is predominantly expressed by activated CD4$^+$ T-helper cells and, during inflammation, by monocytes, mast cells, natural killer (NK) cells and basophils (Carbone et al. 1997). In B cells, CD40 signaling promotes B cell survival, activation, proliferation and upregulation of surface molecules involved in antigen presentation, thus playing a crucial role for the initiation and the progression of the GC reaction (Elgueta et al. 2009; Homig-Holzel et al. 2008; Shulman et al. 2014).

The binding of CD40L to CD40 promotes the clustering of the receptors into lipid rafts, followed by the recruitment of adapter proteins, known as TNFR-associated factors (TRAFs), that lack intrinsic catalytic activity (Bishop et al. 2007). Upon CD40 engagement, TRAFs are recruited to the cytoplasmic tails of the receptor and activate downstream pathways including the phosphoinositide 3-kinase (PI3K) and phospholipase Cγ (PLCγ), as well as the mitogen-activated protein kinases (MAPK) signaling pathways (Elgueta et al. 2009). Moreover, CD40 signaling can lead to phosphorylation and activation of JAK3 kinase independently of TRAF proteins (Elgueta et al. 2009).

CD40 engagement in B cells also triggers both the canonical and non-canonical NF-κB signaling pathways (Berberich, Shu, and Clark 1994; Coope et al. 2002). In mammals, the NF-κB family is composed of five genes which encode for the transcription factors NF-κB1 (p105/p50), NF-κB2 (p100/p52), RelA (p65), RelB and c-Rel. In the unstimulated condition, the activity of NF-κB transcription factors is prevented thanks to the binding of proteins of the inhibitor of the NF-κB (IκB) family, which retain the NF-κB dimers in their inactive form in the cytoplasm.

Specifically, the non-canonical NF-κB pathway is induced when the protein kinase NF-κB-inducing kinase (NIK) activates IKKα, leading to the proteolysis of p100 and the release of p52, which associates with RelB and translocates to the nucleus (Bonizzi and Karin 2004; Bonizzi et al. 2004; Derudder et al. 2003). In the unstimulated condition, TRAF2 and TRAF3 cooperate with the cellular inhibitor of apoptosis 1 and 2 (cIAP1 and cIAP2) to mediate the degradation of NIK, thus preventing p100 proteolysis (Vallabhapurapu et al. 2008; Zarnegar et al. 2008). Upon CD40/CD40L engagement, the recruitment of TRAF2 and TRAF3 to the cytoplasmic tail of the receptor results in the release of NIK, thus leading to the activation of the non-canonical NF-κB pathway (Figure 12) (Vallabhapurapu et al. 2008; Zarnegar et al. 2008).

In the canonical NF-κB pathway, the heterodimers p50/p65 and p50/c-Rel are inhibited by IκB. CD40 engagement results in the formation of the inhibitor of IκB kinase (IKK) complex, containing the catalytic subunits IKKα, IKKβ, IKKγ and NEMO, which triggers the ubiquitination and proteasomal-dependent degradation of IκB molecule, thus leading to the translocation of the p50/p65 and p50/c-Rel heterodimers into the nucleus (Bonizzi and Karin 2004). Activation of the canonical NF-κB signaling pathway upon CD40 engagement plays a crucial role in the LZ, where it cooperates with the BCR signaling, triggered upon antigen recognition, to induce the transcription factor c-MYC, whose expression is essential to promote the positive selection of high-affinity B cells (Calado et al. 2012; Dominguez-Sola et al. 2012; Luo, Weisel, and Shlomchik 2018). Moreover, the intensity of T-cell help received in the LZ via CD40L/CD40 and other T-cell derived signals, dictates the number of cell division that GC B cells will undergo once re-entered in the DZ (Mesin, Ersching, and Victora 2016). Given these crucial roles, the loss of CD40 prevents GC formation (Kawabe et al. 1994; Xu et al. 1994). On the other hand, constitutive CD40 signaling has been shown to promote malignant B cell transformation (Homig-Holzel et al. 2008; Furman et al. 2000; Baxendale et al. 2005; Challa et al. 2002).
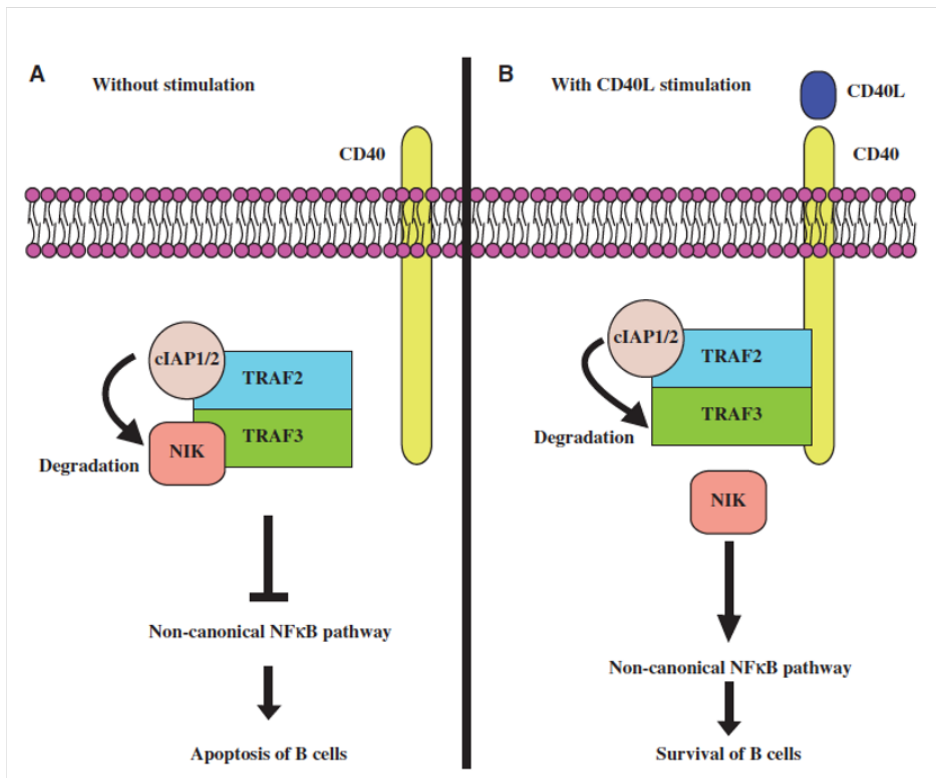
Figure 12. Role of TRAF-2 and -3 in the regulation of the non-canonical NF-κB signaling pathway.

In unstimulated cells, TRAF2 and TRAF3 form a complex with cellular inhibitor of apoptosis 1 and 2 (cIAP1-2), thus sequestering NF-κB-inducing kinase (NIK). Upon CD40 engagement, TRAF2 and TRAF3 are recruited into the cytoplasmic tail of CD40 receptor, thus leading to the release of NIK in the cytoplasm and the consequent activation of the non-canonical pathway.

IL-4 and IL-21. IL-4 and IL-21 are type 1 cytokines, a family that also includes IL-2, IL-7, IL-9 and IL-15. Type 1 cytokines bind to receptors made of two subunits: the common cytokine receptor γ chain and the other subunit which is specific to the cytokine (Leonard 2001). The binding of IL-4 and IL-21 to their specific receptors leads to the activation of JAK1 and JAK3 that, in turn, phosphorylate members of the STAT protein family, thus promoting their dimerization and translocation into the nucleus, where they bind to DNA and modulate gene expression (Schindler, Levy, and Decker 2007). IL-4 signaling pathway relies on STAT5 and STAT6 (Hou et al. 1994), whereas IL-21 predominantly uses STAT3 and, to a lesser extent, STAT1 and STAT5 (Asao et al. 2001).

IL-4 is produced by CD4^{+} T cells, including Tfh cells, and plays an important role both in T and B lymphocytes (Ben-Sasson et al. 1990). In B cells, IL-4 influences the magnitude of the GC reaction by promoting B-cell proliferation and, above all, by enhancing CSR to IgG1, which is the dominant isotype of humoral responses (Finkelman et al. 1990; Kuhn, Rajewsky, and Muller 1991). IL-4 is also required for IgE CSR, as IL-4-deficient mice display reduced serum titers of IgG1 and undetectable IgE both in the naïve state and upon immunization (Kuhn, Rajewsky, and Muller 1991).

IL-21 is produced by NK cells and CD4^{+} T cells, with the Tfh cells being one of the highest producers (Chtanova et al. 2004). The IL-21 receptor (IL-21R) is expressed by a variety of immune cells. Among these, B cells display the highest expression, which further increases upon activation (Good, Bryant, and Tangye 2006). *In vivo* and *in vitro* experiments have revealed that IL-21 can exert both positive and negative effects on B-cell proliferation, differentiation and apoptosis, depending on the activation signals and co-stimulation (Jin et al. 2004). In association with CD40L, IL-21 enhances B cell proliferation; by contrast, when B cells are activated through TLRs, IL-21 promotes apoptosis by downregulating the expression of anti-apoptotic proteins (Jin et al. 2004). During T-D immune responses, IL-21 positively regulates both the expression of the GC master regulator BCL6 and of the PC master regulator BLIMP1 (Jin et al. 2004), thus sustaining both affinity maturation and terminal differentiation. Indeed, in IL-21- and IL-21R-deficient mice, memory B cells, generated upon immunization, display reduced SHM at the V genes (Zotos et al. 2010).

Activation Induced cytidine Deaminase. Accumulation of somatic mutations at Ig V genes through SHM is the pre-requisite for Ig affinity maturation, a process whereby GC B cells are selected on the basis of the affinity of their mutated BCR for cognate antigen (Berek, Berger, and Apel 1991). The process of SHM relies on the expression of the *Aicda* gene, which encodes for Activation Induced cytidine Deaminase (AID), identified for the first time by the Honjo group, which catalyzes the deamination of cytidine residues, leading to their transition into uridine (Muramatsu et al. 2000). In addition to SHM, AID is responsible for the CSR process.

Experiments of *in situ* mutagenesis revealed that the *C*-terminus of AID is absolutely required for CSR but seems dispensable for SHM (Barreto et al. 2003; Shinkura et al. 2004). To exert its functions, AID acts as a homo-, di- or multimeric complex and cooperate with several cofactors (Ta et al. 2003), including the single-strand-DNA-binding protein RPA and the protein kinase Ar1α. Specifically, RPA stabilizes the binding of AID to the DNA during the process of SHM (Chaudhuri, Khuong, and Alt 2004), whereas both RPA and the kinase Ar1α participate to CSR by directly binding to the DNA (Nambu et al. 2003). In GC B cells, *Aicda* gene transcription is induced thanks to the cooperation of E2A and PAX5 transcription factors (Xu et al. 2007). Upon CD40 and IL-21 signaling, the *Hoxc4* transcription factor promotes AID expression (Park et al. 2009). By contrast, *Aicda* gene transcription is repressed upon terminal differentiation into PCs thanks to the activity of the PC master regulator BLIMP1.

Immunoglobulin Class-Switch Recombination. Class-switch recombination (CSR) is an intrachromosomal DNA rearrangement of the immunoglobulin *IgH* locus. As a result of CSR, IgM$^+$ and IgD$^+$ mature B cells are able to express immunoglobulins of the IgA, IgG or IgE classes, which differ only for the constant region, whereas the variable region is unaltered (Stavnezer, Guikema, and Schrader 2008). Besides to AID, the process of CSR requires the uracil-DNA glycosylase (UNG) and the apurinic-apyrimidinic endonucleases 1 (APE1), which act in concert and introduce DNA breaks at the levels of intronic areas of the *IgH* locus named switch (S) regions (Guikema et al. 2007; Begum et al. 2004). The repair of DNA breaks promotes the recombination of the variable heavy-chain (VDJ) segment, with a different constant heavy chain (CH) gene, called isotype (Stavnezer, Guikema, and Schrader 2008). In the course of the immune response, cytokines and T-cell help trigger CSR of specific isotypes, leading to the generation of germ-line transcripts (GLTs), non-coding RNA that are transcribed from specific promoters located upstream of each set of S regions (except for IgD) before the onset of CSR (Stavnezer 1996). Given the high levels of AID in GC B cells, CSR was thought to occur in the course of the GC reaction. However, a recent study demonstrated that CSR can be triggered already in activated B cells, prior to

their recruitment into GCs, as the expression of GLTs and APE1 is strongly downregulated at the peak of the GC reaction, by BCL6-mediated repression (Roco et al. 2019).

Immunoglobulin Somatic Hypermutation. Somatic hypermutation (SHM) is a process whereby single nucleotide substitutions are introduced in the V(D)J of Ig genes, at rates that are about 10^6-fold higher than the background mutation rates observed in other genes (McKean et al. 1984; Berek and Milstein 1987). Mutations tend to accumulate in the CDRs of the antibody V genes, which directly bind to the antigen (McKean et al. 1984). SHM process relies on the activity of AID. Specifically, AID-mediated cytidine to uracil deamination generates an U:G mismatch. Upon DNA replication, in the absence of mismatch repair, the product of AID activity results mainly in C to T transitions. Other types of nucleotide substitutions, observed at sites of SHM, result from recognition of U:G lesions by proteins involved in either base excision (BER) or mismatch repair (MMR) pathways (Di Noia and Neuberger 2007; Rada, Di Noia, and Neuberger 2004). Upon recognition and repair of the mismatch, the DNA strand is re-synthetized by low-fidelity DNA polymerases introducing mutations (Di Noia and Neuberger 2007), thus leading to the generation of a large repertoire of Ig with different affinities for the same antigen.

1.2.3.2.3. Regulators of positive selection of B cells in the GC reaction

c-MYC. c-MYC transcription factor, encoded by the proto-oncogene *c-Myc*, regulates the expression of thousands of genes (Conacci-Sorrell, McFerrin, and Eisenman 2014). In mammals, c-MYC has a crucial role in regulating cell proliferation, apoptosis and cell differentiation (Conacci-Sorrell, McFerrin, and Eisenman 2014). During cell-cycle progression, c-MYC favors the transition from G_0-G_1 to S phase through the activation of genes which encode for the cyclin-dependent kinase (CDK) complex, as well as by the repression of CDK inhibitors (Perez-Roger et al. 1999; Bouchard et al. 1999). Moreover, c-MYC can promote cell proliferation, by directly targeting the *E2f* gene, thus leading to the activation of the *E2f* downstream targets (Leung et al. 2008). In naïve resting B cells, *c-Myc* is barely undetectable, both at the transcript and at the protein level (de Alboran et al. 2001; Klein et al. 2003b). Interestingly, despite their massive proliferation, the bulk of GC B cells expresses comparable levels of c-MYC protein with that measured in resting B cells (Calado et al. 2012). These observations initially led to the conclusion that c-MYC was a dispensable factor for the GC reaction. By contrast, recent studies showed the importance of *c-Myc* expression for GC initiation, maintenance and affinity maturation (Calado et al. 2012; Dominguez-Sola et al. 2012; Luo, Weisel, and Shlomchik 2018). Specifically, c-MYC is expressed at high levels in antigen-specific B cells which have received T-cell help at the T-B border and that migrate to the center of the follicle in order to enter in the DZ (Calado et al. 2012). The loss of c-MYC at this early stage, prevents further GC development (Calado et al. 2012). In mature GCs, c-MYC is highly expressed by centrocytes which have been positively selected and that are ready to re-enter in the DZ in order to undergo further cycles of SHM and proliferation (Calado et al. 2012). Recent work by the Shlomchik group demonstrated that the CD40 signaling cooperates with the BCR signaling to induce *c-Myc*, whose expression is required for positive selection (Luo, Weisel, and Shlomchik 2018). Except for these two important moments, GC B cells do not express *c-Myc*, due to the repression imposed by BCL6 transcription factor. In the latter cells, BCL6 promotes cell-cycle progression through MYC-independent pathways (Phan et al. 2005).

Mechanistically, it has been shown that BCL6 also suppresses CDK inhibitors through the recruitment of a known partner of c-MYC, MIZ1 (Phan et al. 2005).

BCR signaling. Surface expression of BCR and its constant tonic signal are necessary to sustain naïve B cells survival. The BCR expressed on the surface of B lymphocytes is composed of immunoglobulins (IgH and IgL) associated with the Igα (CD79a)/Igβ (CD79b) heterodimer (Reth 1989). BCR engagement results in the tyrosine phosphorylation of the intracellular Ig$\alpha\beta$ immunoreceptor tyrosine activation motifs (ITAMs) by Src-family kinases like LYN, which leads, in turn, to the activation of the kinase SYK (Dal Porto et al. 2004; DeFranco 1997; Kurosaki and Kurosaki 1997; Reth and Wienands 1997), followed by the induction of a complex signalosome made of different cascades, including the activation of Bruton's tyrosine kinase (BTK), phosphoinositide 3-kinase (PI3K) and of phospholipase γ-2 (PLCγ2) (Dal Porto et al. 2004; Kurosaki 1999). In the GC, the BCR signaling is a key determinant for positive selection of LZ B cells, where it cooperates with the CD40 signaling pathway to induce the expression of the *c-Myc* gene (Luo, Weisel, and Shlomchik 2018).

FOXO1. FOXO proteins belong to the Fox-O family of transcription factors, characterized by the presence of a forkhead DNA binding domain (Eijkelenboom and Burgering 2013). Forkhead proteins are subdivided in different families, alphabetically named from FOXA to FOXR. FOXO family comprises four proteins: FOXO1, FOXO3A, FOXO4 and FOXO6 (Eijkelenboom and Burgering 2013). Among the FOXOs, FOXO1 is the most abundantly expressed in B cells and plays a crucial role in the formation and maintenance of the GC DZ (Inoue et al. 2017; Dominguez-Sola et al. 2015; Sander et al. 2015). In DZ B cells, FOXO1 positively regulates BCL6 and CXCR4 expression, sustains AID-mediated CSR (Dominguez-Sola et al. 2015; Sander et al. 2015) and, together with BCL6, represses the expression of genes involved in DNA damage response, thus supporting affinity maturation (Dominguez-Sola et al. 2015). Ablation of FOXO1 in GC B cells led to the formation of GCs which lacked DZ (Inoue et al. 2017; Dominguez-Sola et al. 2015; Sander et al. 2015).

Moreover, although SHM was unperturbed, the processes of CSR and selection of high-affinity clones were both impaired in GCs of *Foxo1*-deficient mice (Sander et al. 2015). FOXO1 activity is then repressed in LZ B cells by PI3K signaling pathway, triggered upon BCR engagement, which leads to AKT-mediated phosphorylation of FOXO1 in the nucleus, and to the subsequent export of the protein to the cytoplasm, thus preventing it to act as transcription factor (Yusuf et al. 2004). Despite the majority of LZ B cells do not express FOXO1 due to the repression exerted by PI3K signaling pathway, FOXO1 activity has been reported in the small population of c-MYC-expressing B cells that are candidates for DZ re-entry (Calado et al. 2012; Dominguez-Sola et al. 2015; Sander et al. 2015). In addition, *Foxo1*-deficient GC LZ B cells also displayed reduced capacity to respond to T-cell help provided by Tfh, thus indicating that FOXO1 also plays a crucial role in promoting LZ-to-DZ switch (Inoue et al. 2017).

The mTOR pathway. The mechanistic target of rapamycin (mTOR) is a serine/threonine kinase which forms the catalytic subunit of two distinct complexes: mTOR Complex 1 (mTORC1) and mTOR Complex 2 (mTORC2) (Saxton and Sabatini 2017). mTORC1 is made of three core components: mTOR, RAPTOR (Regulatory Protein Associated with mTOR), and mLST8 (mammalian Lethal with SEC13 protein 8). Of these, RAPTOR and mLST8 are involved in the recruitment of the target and in stabilizing its association to the complex. In addition, mTORC1 contains two inhibitory subunits, PRAS40 (Proline-Rich AKT Substrate of 40 kDa) and DEPTO (DEP domain containing mTOR interacting protein) (Saxton and Sabatini 2017). mTOR activity is stimulated by PI3K, whose levels increase in the cytoplasm upon engagement of several receptors with the corresponding ligands. In mammalian cells, mTOR controls the balance between anabolism and catabolism in response to environmental conditions. Several biological processes are regulated by mTORC1, including protein, nucleotide and lipid synthesis as well as glucose metabolism. In addition, mTORC1 sustains protein turnover, by promoting proteasome-mediated degradation and mediates lysosome biogenesis (Saxton and Sabatini 2017; Laplante and Sabatini 2012). Hence, mTOR is crucial to regulate cell growth.

In GC B cells, mTORC1 sustains the expression of *Bcl6* and *Aicda*, thereby favoring GC B cell maintenance and affinity maturation (Raybuck et al. 2018; Jones et al. 2016; Keating et al. 2013). In addition, together with c-MYC, mTORC1 is induced in positively selected LZ B cells upon T-cell help, where it ensures the anabolic cell growth that is essential in order to sustain the massive proliferation once they will re-enter in the DZ. Specifically, because the strength of T-cell help defines the extent of the B cell proliferative burst, it is believed that the magnitude of c-MYC and mTORC1 activation that B cells receive in the LZ may be proportional to the number of cell division they will undergo in the DZ (Mesin, Ersching, and Victora 2016). In the context of the anabolic support, a recent study has revealed a novel role exerted by mTORC1 signaling in plasmablasts (Gaudette et al. 2020). In details, Gaudette and colleagues have shown that plasmablasts rely on mTORC1 signaling pathway to implement specialized pathways aimed to support Ig production and secretion, including the unfolded protein response (UPR), prior to the establishment of the PC program orchestrated by BLIMP1 (Gaudette et al. 2020).

1.2.3.3. Cellular output of the germinal center reaction

In addition to cyclic re-entry in the DZ, positively selected GC B cells can eventually leave the GC reaction as antibody-secreting PCs, or long-lived memory B cells (Zotos and Tarlinton 2012) (Figure 13).

1.2.3.3.1. High-affinity, long-lived antibody-secreting plasma cells

Antibody-secreting PCs are terminally differentiated B cells and final effectors of humoral immune responses (Nutt, Hodgkin, et al. 2015). Contrary to those developing from the MZ or B1-B cells upon T-cell independent immune responses, PCs differentiated from GC B cells provide persistent production of high affinity antibodies. PC maturation is a multi-step process which is dictated, on one hand, by the progressive upregulation of PC master regulators, including BLIMP1, IRF4 and XBP1 (Klein et al. 2006; Ochiai et al. 2013; Sciammas et al. 2006; Angelin-Duclos et al. 2000; Shaffer et al. 2002; Shaffer et al. 2004), and, on the other hand, by the downregulation of the B-cell and GC-B-cell specific transcriptional programs, controlled by PAX5 and BCL6, respectively (Delogu et al. 2006; Kwon et al. 2008; Saito et al. 2007) (Figure 13). PC differentiation associates with the loss of B-cell specific markers such as CD19, CD21, CD23, MHC-Class-II, CXCR5, CD79a.

In contrast, PC-specific markers including Syndecan1/CD138, CD43 and CXCR4 are expressed on the surface of B cells undergoing terminal differentiation into PCs. Although long-lived PCs exist in different lymphoid organs, the majority of them resides in the BM, due to the upregulation of CXCR4 chemokine receptor which guide them to the CXCL12-expressing niche in the BM (Kabashima et al. 2006). Here, several factors promote the survival of PCs, such as IL-6, tumor necrosis factor (TNF) and APRIL (a proliferation inducing ligand) (Cassese et al. 2003; Kawano et al. 1995; Benson et al. 2008). In particular, by signaling through BCMA (B-cell maturation antigen), APRIL promotes the expression of the anti-apoptotic myeloid leukemia cell differentiation protein 1 (MCL-1), which is essential for PCs survival (Peperzak et al. 2013).
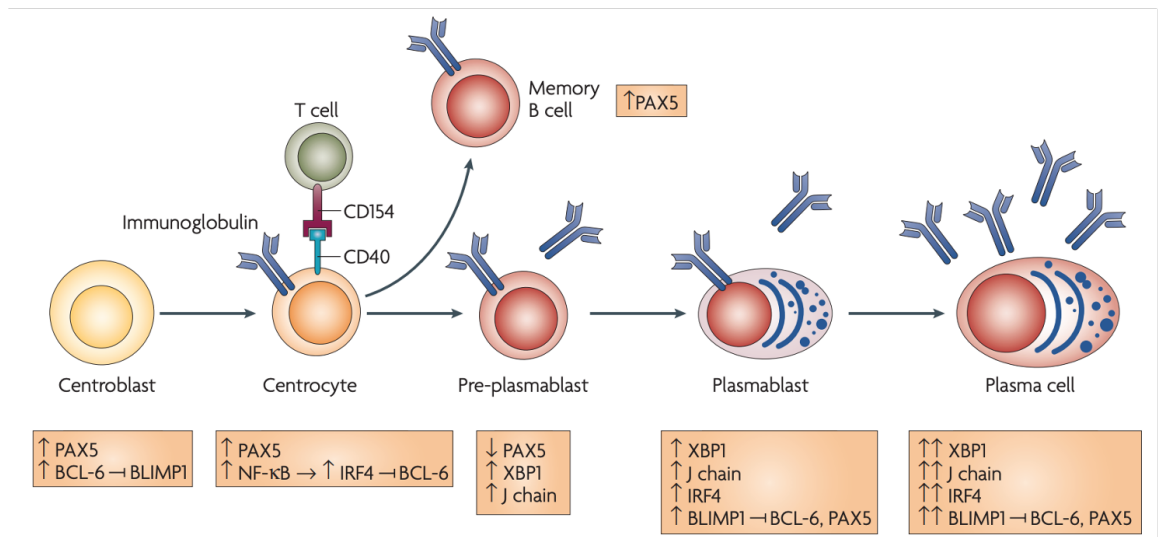
Klein, U., and R. Dalla-Favera, *Nat Rev Immunol* 2008

Figure 13. GC transcriptional regulation and post-GC B-cell terminal differentiation.

Centrocytes which received T-cell help and that are characterized by the expression of high-affinity BCR can exit the GC reaction to terminally differentiate into either memory B cells or plasma cells (PCs). PC commitment results in the downregulation of B-cell specific transcription factors, including PAX5, and in the upregulation of PC-associated factors, including the master regulators BLIMP1 and IRF4. XBP1 and J chain upregulation in PCs will sustain Ig production. BLIMP1 transcription factor contribute to maintain PC-identity by suppressing B-cell and GC-specific transcription factors, including PAX5 and BCL6, respectively.

1.2.3.3.2. High-affinity, long-lived memory B cells

Another essential output of the GC reaction consists of high-affinity antigen-selected Ig-switched memory B cells. The most important difference between the PC and the memory compartment is that, while PCs show the highest affinity towards the antigen, the memory B cells fraction retains lower-affinity B cells. Indeed, class-switched memory B cells cannot be distinguished from GC B cells in terms of affinity. This observation led to the hypothesis that memory B cells are generated by chance among the positively selected GC B cells, through differentiation of lower-affinity centrocytes which survive apoptosis, possibly thanks to an increased expression of anti-apoptotic factors like BCL2 (Victora and Nussenzweig 2012). In support of this hypothesis, mice over-expressing the *Bcl2* gene show increased number of IgG[+] GC/memory B cells after immunization, and display reduced efficiency of selection of both memory and GC B cells, but not of PCs (Smith et al. 1994).

On the other hand, there are several other signals that favor PC commitment, at the expense of the memory B cell compartment. For instance, mice lacking the IL-21 receptor show reduced number of PCs upon immunization and accumulation of memory B cells, suggesting that the T-cell-derived IL-21 cytokine mainly sustains terminal differentiation of GC B cells towards the PC fate (Zotos et al. 2010).

1.2.3.3.3. Transcriptional regulation of terminal differentiation

IRF4. Interferon-Regulatory-Factor 4 (IRF4) is essential for PC development (Klein et al. 2006; Sciammas et al. 2006). IRF4 levels increase in centrocytes as a result of CD40 signaling. In these cells, high amounts of IRF4, together with IL-21 signaling, contribute to activate *Prdm1* expression, encoding for the PC master regulator BLIMP1, which promotes the silencing of GC B-cell identity and the establishment of the PC transcriptional program. BLIMP1 can also induce *Irf4* expression (Sciammas et al. 2006), thereby generating a feed-forward positive loop that is needed to ensure repression of *Bcl6*. Dynamic and progressive increase in the levels of IRF4, from the beginning to the termination of the GC reaction, contributes to the progressive commitment of GC B cells towards the PC fate. IRF4 is also required to induce *Xbp1* expression, thereby sustaining Ig secretion in PCs (Sciammas et al. 2006). Coherently with its crucial role in sustaining PC differentiation when expressed at high levels, *Irf4*-deficient mice are unable to generate antibody-secreting PCs upon infection or immunization (Tellier et al. 2016).

BLIMP1. B-lymphocyte-induced maturation protein 1 (BLIMP1) is a transcription factor encoded by the *Prdm1* (Positive Regulatory Domain containing 1) gene. BLIMP1 is required for the formation of both short-lived and long-lived PCs, where it acts both as transcriptional repressor and activator (Angelin-Duclos et al. 2000; Shaffer et al. 2002). In addition to PCs, BLIMP1 is expressed at low levels in positively selected centrocytes which represent PC progenitors (Kallies et al. 2004). By contrast, *Prdm1* expression is repressed in GC B cells by the concerted actions of BCL6 and MTA3 protein (Metastasis-associated 1 family, member 3) (Shaffer et al. 2000).

In the context of *Prdm1* gene expression regulation, our group has demonstrated that EZH2, the catalytic subunit of the Polycomb Repressive Complex 2 (PRC2), limits BLIMP1 expression in GC B cells undergoing IL-21 stimulation, by catalyzing the deposition of H3K27me3 mark on the *Prdm1* locus, thereby favoring the persistence of B cells within the GC (Caganova et al. 2013). In late GC B cells, the induction of BLIMP1 relies on: i) IL-21 signaling, which induces the activation of the transcription factor STAT3 (Zotos et al. 2010); ii) CD40 signaling, leading to NF-κB-dependent IRF4-upregulation (Kwon et al. 2009). Together, STAT3 and IRF4 bind to an IL-21-responsive element, downstream the *Prdm1* gene, thus mediating its full expression (Kwon et al. 2009). In PCs, BLIMP1 ensures the maintenance of PC-identity by promoting the expression of PC-associated genes and by silencing B-cell- and GC-B-cell-specific genes. Specifically, BLIMP1 induces the expression of *Irf4*, *Xbp1*, *J chain*, *Ell2* and *Eaf2*, which further sustain the PC transcriptional program and promote Ig production and secretion (Shaffer et al. 2002; Angelin-Duclos et al. 2000; Shaffer et al. 2004). On the other hand, BLIMP1 is crucial for the repression of several genes including: i) B-cell- and GC-B-cell-specific genes, such as *Pax5* and *Bcl6*, respectively (Delogu et al. 2006; Saito et al. 2007); ii) genes responsible for BCR signaling, such as *Blnk*, *Lyn*, *Syk* (Delogu et al. 2006); iii) genes involved in SHM and CSR, such as *Aicda* (Shaffer et al. 2002) iv) genes that control cell-cycle progression, including *c-Myc* and *E2f* (Shaffer et al. 2002).

XBP1. The main function of PCs is to produce and secret large amounts of antibodies. For this purpose, B cells undergoing terminal differentiation significantly increase their protein synthesis and secretory apparatus. To prevent ER stress induced by high rate of protein synthesis, cell responds by coordinated enhancement of the unfolded protein response (UPR) machinery controlled by the X-box Binding Protein 1 (XBP1) transcription factor (Reimold et al. 1996; Reimold et al. 2001). Specifically, XBP1 target genes encode for factors that regulate organelle size, protein folding, degradation of mis-folded proteins, protein glycosylation, trafficking between ER and Golgi and exocytosis (Gass, Gifford, and Brewer 2002; Shaffer et al. 2004).

In PCs, *Xbp1* gene transcription is induced by BLIMP1, IL-4 and ATF6 (Activating Transcription Factor 6) (Calfon et al. 2002; Yoshida et al. 2000). *Xbp1* mRNA is then cleaved by the endonuclease IRE-1, resulting in the generation of the *Xbp1S* transcript, which encodes for the active version of the transcription factor (Calfon et al. 2002). Loss of XBP1 leads to impaired Ig secretion, thus resulting in failure to control infections (Reimold et al. 1996).

1.2.3.4. Germinal center-derived B-cell lymphomas

Dysregulations at the GC B cell stage are the main causes of B-cell neoplasms (Kuppers et al. 1999). Among these, non-Hodgkin lymphomas (B-NHL) comprise a heterogeneous set of genetically, biologically, and clinically distinct neoplasms which originate from the clonal expansion of GC B cells that underwent malignant transformation.

According on histological features, the majority of B-NHL are classified into Diffuse Large B cell lymphomas (DLBCL), Burkitt lymphomas (BL) and Follicular lymphomas (FL). Based on their transcriptomic prolife, DLBCL can be further divided into two subtypes, the GC B cell-like (GCB-) DLBCL, which resemble LZ B cells, and the activated B cell-like (ABC-) DLBCL, which is most similar to PBs; BL can resemble both DZ or LZ B cells, whereas FL is more similar to LZ B cells (Pasqualucci 2019). The genetic lesions that are always determinant for the onset of B-NHL are of two types: chromosomal translocations and aberrant SHM (ASHM), which are the result of mistakes in the process of CSR and of altered AID activity (Kuppers 2005). B-NHL-associated translocations are determined by the juxtaposition of regulatory sequences of heterologous chromosomes with the intact coding sequence of proto-oncogenes, thus leading to their constitutive expression in GC B cells. Therefore, the main events that are responsible of the malignant transformation include the transcriptional dysregulation of genes that regulate the GC reaction, or the ectopic expression of genes that are normally expressed in specific stages of the B cell development.

Translocations involving the *IgH* locus and the *Bcl2* proto-oncogene are characteristic of follicular lymphomas, leading to uncontrolled cell division and tumor growth (McDonnell and Korsmeyer 1991). Translocations of the proto-oncogene *c-Myc* into the immunoglobulin heavy chain or light chain loci are associated with 100% of Burkitt lymphoma cases and up to 10% of DLBCL cases (Klein and Dalla-Favera 2008).

BCL6 dysregulation is commonly associated to DLBCL and less frequently to Burkitt lymphomas. Chromosomal translocations involving *Bcl6* lead to aberrant *Bcl6* expression, thus preventing its silencing at the end of the GC response (Cattoretti et al. 2005).

1.3. The aim of the study

The importance of m^{6}A methylation in T-cell dependent B cell immune responses remains largely unexplored. Our preliminary observations indicate a reproducible increase in *Mettl3* expression in mature B cells upon activation through the CD40 receptor. This result raises the hypothesis that m^{6}A methylation influences B cell selection in GCs, which strictly depends on the entity of cross-talk between LZ GC B cells and Tfh cells, operated through the CD40/CD40L axis. To address this question, we chose an *in vitro* model of antigen-selected LZ GC B cells, also called *in vitro*-induced germinal center-like B (iGB) cells, where cells are subjected to stimulation with membrane-bound CD40L and IL-21 (Nojima et al. 2011). To achieve this goal, we optimized a protocol to genetically modify, through CRISPR/Cas9 technology, primary mature murine B cells, obtaining high efficiency targeting of the *Mettl3* gene (Chu, Graf, et al. 2016).

The focus of my investigations was to determine the impact of *Mettl3* gene disruption on the capacity of CD40-activated B cells to proliferate, compete in mixed cultures with *Mettl3*-proficient counterparts and ultimately to differentiate into CD138-expressing PBs upon co-stimulation with IL-21. A combination of flow cytometric immunophenotyping and cell-cycle distribution analyses, *Mettl3* gene sequencing, METTL3 protein quantification, whole transcriptome performed at multiple timepoints of stimulation with membrane-bound CD40L together with IL-21, allowed us to obtain for the first time a comprehensive molecular picture of the impact of *Mettl3* gene disruption on CD40-activated B cells and on their PCs derivatives.

In a parallel set of experiments, we employed a different *in vitro* differentiation model to monitor the effects of *Mettl3* gene disruption, achieved by CRISPR/Cas9 technology, on the ability of conditionally immortalized multipotent murine hematopoietic progenitor cells (HPCs) to sustain their self-renewal and capacity to undergo Flt3L-driven differentiation into myeloid committed progenitors (Redecke et al. 2013). Close monitoring by flow cytometric analyses of *Mettl3*-mutant bulk HPC cultures and clonal variants, assessed in their multipotent state, or at different days after triggering myeloid differentiation, was coupled to determination of *Mettl3* gene functional integrity and to METTL3 protein levels.

Altogether, this project applies CRISPR/Cas9 gene targeting technology to primary murine *in vitro* cultures of CD40-activated B cells and multipotent HPCs to monitor, both at the cellular and molecular level, how reduced m^6A methylation affects the proliferative potential and the developmental trajectories of *Mettl3*-mutant cells.

2. Materials and methods

2.1. Mice

2.1.1. Mouse strains

C57BL/6J and Ly5.1 (B6.SJL-*Ptprc^{a}Pepc^b*/BoyCrl) mice were purchased from Charles River. Rosa26-Cas9iGFP (*Gt(ROSA)26Sor$^{em1.1(CAG-cas9*,-EGFP)Rsky}$*) mice were previously described (Chu, Weber, et al. 2016) and purchased from the Jackson Laboratory. Mice were housed and bred in animal facility at the IFOM-IEO Campus Institute, Milan, Italy. Experimentations were performed under the protocol numbers 728/2017 and 707/2018, approved by the Italian Ministry of Health and the IFOM OPBA Committee.

2.1.2. Genomic DNA extraction from tail biopsy

Lysis Buffer:

100 mM Tris-HCl pH 8.5

5 mM EDTA

200 mM NaCl

0.2% SDS

0.5 cm of a tail biopsy was incubated in 400 µl of lysis buffer with Proteinase K (100 µg/ml) at 56°C, shaking at 850 rpm, overnight in the thermomixer compact. The lysate was transferred into a new tube and 1 ml of isopropanol was added, mixed by inverting and centrifuged at maximum speed of 16.000 rpm for 1 minute. DNA pellet was dissolved in 300 µl of milliQ water by incubation at 60°C for 20 minutes.

2.1.3. Genotyping strategy

The genotypes of Rosa26-Cas9iGFP mice were analyzed by polymerase chain reaction (PCR) amplification performed on genomic DNA extracted from tail. For amplification, primers summarized in Table 1 and PCR reagents in Table 2 were used. PCR conditions are shown in Table 3. PCR reactions were run in automatic thermocycler GeneAmp PCR System9700 (Applied Biosystems).

Table 1. **Primers used for genotyping and annealing temperatures.**

PCR product	Primer ID	Sequence	T$_A$
Amplicon size: Wild-type 200 bp Knock-in 120 bp	RTR26 Forward	5'-GCCTCCTGGCTTCTGAGGACCG-3'	60°C
	SACas9 Reverse 1	5'-CCTGGACTACTGCGCCCTACAGA-3'	
	RTR26 Reverse 2	5'-TCTGTGGGAAGTCTTGTCCCTCC-3'	

Table 2. Master mix used for genotyping.

Component	Final volume (µl)
5x Flexi buffer	5
MgCl$_2$ solution, 25 mM	2.5
PCR Nucleotide Mix, 2.5 mM each	2.5
Forward primer, 50 µM	0.25
Reverse primer1, 50 µM	0.25
Reverse primer2, 50 µM	0.25
GoTaq® DNA Polymerase (5U/µl)	0.25
Template DNA	3
Nuclease-Free Water	11
Total	25

Table 3. Genotyping PCR conditions.

Temperature (°C)	Time (min:sec)	
98	3:00	
95	0:20	
T$_A$	0:20	x 40 cycles
72	0:30	
72	3:00	
4	hold	

2.1.4.   Mice immunization

For FACS sorting of GC B cells, 6 to 8 weeks old mice were immunized with 2 x 10^8 sheep red blood cells (SRBCs) (Thermo Fisher Scientific) and sacrificed 8 days later.

2.2. Cell culture techniques

2.2.1. B cell purification

Erythrocyte lysis buffer:

- o   solution A   0.17 M Tris pH 7.65
- o   solution B   0.83% NH_4Cl
- o   working solution   9 parts B + 1 part A

iGB cell medium: RPMI 1640

                          10% FBS

                          2 mM glutamine

                          200 U/ml pen/strep

                          1 mM Sodium Pyruvate

                          50 µM β-mercaptoethanol

                          2 mM HEPES

MACS Buffer   1x PBS

                          0.5% BSA

                          2 mM EDTA

Spleen was collected and smashed for single cell suspension. Erythrocyte lysis was performed by incubating cell suspension with Erythrocyte lysis Buffer for 3 minutes on ice. Reaction was stopped by adding 10 ml of B cell medium. Live cells were counted using Erythrosine dye (Sigma-Aldrich) to distinguish live and dead cells. All centrifugation steps were performed for 5 minutes at 1200 rpm at 4°C. After counting, cell suspensions were labeled with a cocktail of biotin-conjugated antibodies against CD43, CD11b, CD11c, Ter119, CD4, CD8 and CD3 (Table 4), followed by incubation with anti-biotin magnetic MicroBeads (Miltenyi Biotec). B cells were purified after loading antibody-labelled cell suspensions onto LS columns (Miltenyi Biotec), following the manufacturer's protocol. This procedure allows the isolation of untouched resting B cells from single-cell suspensions in lymphoid tissues.

B cells purity was assessed by measuring the expression of the pan-B cell marker CD19 (monoclonal rat anti-mouse CD19, Cy7PE, clone 1D3, eBioscience, 1/400) and the non-B cell marker TCRβ (monoclonal Armenian hamster anti-mouse TCRβ, APC, clone H57-597, eBioscience, 1/600) by flow cytometry. Cells were stained in FACS buffer and analyzed as described in paragraph 2.3.1.

Table 4. Antibodies used for B cell purification.

Antibody	Clone	Company	Dilution
Monoclonal rat anti-mouse CD43 biotin	S7	eBioscience	1/800
Monoclonal rat anti-mouse Ter119 biotin	TER-119	eBioscience	1/800
Monoclonal rat anti-mouse CD11b biotin	M1/171	eBioscience	1/800
Monoclonal Armenian hamster anti-mouse CD11c biotin	N418	eBioscience	1/800
Monoclonal rat anti-mouse CD4 biotin	GK1.5	eBioscience	1/400
Monoclonal rat anti-mouse CD8 biotin	53-6.7	eBioscience	1/400
Monoclonal Armenian hamster anti-mouse CD3 biotin	145-2C11	eBioscience	1/200

2.2.2. *In vitro*-induced germinal center B (iGB) cell culture

In the *in vitro*-induced germinal center B (iGB) cell culture system (Nojima et al. 2011), primary naïve B cells are plated onto previously irradiated 40LB feeder cells (BALB/c3T3), stably producing BAFF and membrane-bound CD40-ligand. 40LB cells were maintained in DMEM medium supplemented with 10% FBS and 2 mM L-glutamine. Before plating B cells, a confluent 10-cm tissue culture dish (containing 5×10^4 cells per centimeter) was irradiated with 15 Gy (CellRad). Naïve B cells were isolated from the spleen of 6-8 weeks old C57BL/6J, Ly5.1 or heterozygous (HE) Rosa26-Cas9iGFP mice. Purified B cells were plated at 1.25×10^4 cells per milliliter onto 40LB cells, in 40 ml of iGB cell medium containing murine recombinant IL-4 (1 ng/ml; Peprotech). After four days, iGB cells were re-plated (1.25×10^4 cells per milliliter) onto new 40LB feeder cells, in 40 ml of iGB medium containing murine recombinant IL-21 (10 ng/ml; Peprotech) and cultured for other 4 days. Cells were cultured at 37°C with 5% CO_2.

2.2.3. B cell activation prior infection

For the optimization of the CRISPR/Cas9-based protocol, purified B cells were cultured for two days at 2×10^5 cells per milliliter in 20 ml of iGB cell medium containing IL-4 (1 ng/ml; Peprotech) and α-CD40 antibody (Biolegend); otherwise, they were plated at 2×10^5 cells per milliliter in 20 ml of iGB cell medium containing IL-4 (1 ng/ml; Peprotech) onto previously irradiated 40LB cells, expressing membrane-bound CD40-ligand (mCD40L) for 2 days. In experiments performed applying the optimized version of the CRISPR/Cas9-based protocol in the iGB culture, naïve purified B cells were plated at 2×10^5 cells per milliliter in 20 ml of iGB cell medium onto previously irradiated 40LB cells for 2 days.

2.2.4. Retroviral production

Retroviral ECO-Phoenix cells were maintained in DMEM medium supplied with 10% FBS ad 2 mM L-glutamine. The day before transfection, 2×10^6 cells were seeded in 10 ml of medium into a 10-cm tissue culture dish. On the next day, ECO-Phoenix cells were transfected with 10 µg of plasmid DNA, together with 5 µg of ecotropic packaging vector pCL-ECO (Imgenex), using $CaCl_2$ transfection protocol. Twelve hours after transfection, supernatant was discarded, following the addition of 5.5 ml of fresh iGB cell medium into each dish. Two days after transfection, the retroviral supernatant was collected and filtered through 0.45 µm filter.

2.2.5. CRISPR/Cas9 gene targeting in the iGB culture

Cas9-expressing naïve B cells, purified from the spleen of a Rosa26-Cas9iGFP mouse (HE), were plated at 2×10^5 cells per milliliter in 20 mL of iGB medium onto previously irradiated 40LB cells. After 48 hours, activated B cells were harvested and resuspended 2 $\times 10^5$ cells per milliliter in iGB medium, supplemented with 8 µg/mL of Polybrene. A total of 500 µL cell suspension was transferred into each well of a 12-well-plate. Cells were spin transduced in two rounds, for a total of 90 minutes at 32°C. For each spin infection, 500 µl of retroviral supernatant was added. At the end of the second spin infection, transduced cells from 4 wells were harvested and transferred onto a new 40LB feeder layer (10-cm

tissue culture dish), in a final volume of 10 ml. On the next day, medium was replaced with fresh one supplemented with IL-4 (1 ng/ml; Peprotech). Two days after infection, puromycin was added to each dish (1.25 µg/ml). On day 4 after infection, transduced cells in suspension were collected. To harvest B cells bound to 40LB cell, 3 ml of MACS buffer was added into 10-cm tissue culture dish and cells incubated for 3 minutes at 37°C. B cells were then plated at 1.25 x 10^4 cells per milliliter in 40 ml of iGB medium onto a new 40LB feeder layer, in the presence of IL-21 (10 ng/ml; Peprotech) and puromycin. On day 6, cells were either harvested, counted and used for the downstream analyses, or refreshed with new medium, containing IL-21 and puromycin. On day 8, cells were harvested, counted and used for downstream analyses. Cells were plated at 1.25 x 10^4 cells per milliliter in 40 ml of medium onto new 40LB feeder layer, in the presence of IL-21 and puromycin and cultured until day 11. On day 11, the medium was replaced with fresh one, containing puromycin and IL-21. Starting from day 4 after infection, 40LB feeder layers were changed each four days.

2.2.6. Generation of stable Cas9-expressing NG108-15 clones

Lentiviral 293T packaging cells were maintained in DMEM medium supplied with 10% FBS ad 2 mM L-glutamine. The day before transfection, 2 x 10^6 cells were seeded in 10 ml of medium into a 10-cm tissue culture dish. One day later, 293T cells were transfected with 10 µg of Lenti-Cas9-2A-Blast (Addgene #73310, expressing the Cas9 nuclease and the blasticidin resistance gene), together with ENV, pMDL and REV lentiviral packaging vector, using the $CaCl_2$ method. Twelve hours after transfection, medium was aspirated and 5.5 ml of fresh medium was added to transfected cells. 48 hours after transfection, lentiviral supernatant was collected, filtered with 0.45 µm filter, supplemented with 8 µg/mL of Polybrene and transferred onto NG108-15 target cells. One day after infection, the medium was changed. Two days after infection, cells were subjected to blasticidin selection (15 µg/ml) for ten days. Blastidicin resistant NG108-15 cells were then plated at 3 cells per milliliter in 96-well-plates in the presence of blasticidin in order to establish Cas9-expressing clones.

2.2.7. *In vitro* assay to test sgRNAs efficiency in Cas9-expressing NG108-15 cells

Clones expressing an intermediate level of Cas9 nuclease and established from the infected pool of NG108-15 neuroblastoma cell line, were used to test the efficiency of 4 different sgRNAs previously designed and cloned into the MSCV-pU6-(BbsI)-Pgk-Puro-T2A-BFP vector (Addgene #86457). Cells were transfected either with the empty vector of with one of the four vectors expressing a different sgRNA targeting the *Mettl3* gene. Transfection mix consisted of 2 μg of DNA plus 12 μl of polyethylenimine (PEI), prepared in Optimem. After 10 minutes of incubation at room temperature (RT), the transfection mix was added to cells. One day later, medium was changed. Two days later, puromycin was added to cells (2 μg/ml) in order to start selection of cells expressing the vector and, consequently, the sgRNA. Cells were harvested after 5 days from puromycin selection and subjected to immunoblotting analysis for METTL3 protein.

2.2.8. Generation and cell culture of HoxB8-immortalized HPCs

Bone marrow cell suspension were obtained by flushing femurs of 4-8-week-old C57BL/6J or Rosa26-Cas9iGFP (HE) mice with 5 ml of RPMI-1640 supplemented with 10% FBS not heat inactivated, 2mM L-glutamine and 50 μM β-mercaptoethanol (RP-10 medium). Cells were then pelleted by centrifugation and then loaded on 3 ml of Ficoll-Paque (GE Healthcare) and separated by centrifugation at 450 g for 30 min. The entire supernatant was collected (discarding only 500 μl including the cell pellet), diluted with 45 ml of PBS containing 1% FBS and pelleted again at 800 g for 10 min. Cells were then resuspended in 10 mL of RP-10, centrifuged at 450 g for 5 min and finally resuspended 5 x 10^5 cells per milliliter in RP-10 containing recombinant mouse IL-3 (10 ng/mL; Peprotech), IL-6 (20 ng/mL; Peprotech) and murine stem cell factor (mSCF, R&D Systems; 250 ng/mL). After two days of culture, cells were collected, resuspended in progenitor outgrowth medium (POM), corresponding to RP-10 supplemented with 1 μM β-estradiol and cell culture supernatant from Flt3L-producing B16 melanoma cell line (5% final concentration). A total of 3 x 10^5 cells was resuspended in 1 ml of retroviral supernatant, transferred into a well of a 12-well-plate and spin transduced for 60 minutes at 1500 g, in the presence of

Lipofectamine (0,1% Invitrogen). After infection, cells were cultured by adding 1,5 ml of POM. On the next day, infected cells were centrifuged and resuspended in 2 ml of fresh new POM. During the following culture, cells were dispensed every 2 days in fresh medium and kept at concentrations between 1×10^5 and 2×10^5 cells per milliliter of POM.

2.2.9. *In vitro* B cell differentiation of HoxB8-immortalized HPCs

In vitro B cell differentiation of Hoxb8-immortalized HPCs (H8-HPCs) was performed as already described (Redecke et al. 2013). H8-HPCs were plated at 1.5×10^5 cells per milliliter in 20 ml of Optimem, supplemented with Fl3tL (30 ng/ml) and mouse recombinant IL-7 (10 ng/ml) and plated onto OP9 feeder cells (Pro-B cell medium). The latter, were previously maintained in IMDM medium, supplemented with 20% FBS and 2mM L-glutamine. Each two days, H8-HPCs undergoing pro-B cell differentiation were harvested, counted and re-plated onto new OP9 feeder cells in fresh medium, at 1.5×10^5 cells per milliliter. Starting from day 6, cells were plated at 2.5×10^5 cells per milliliter in 20 ml of pro-B cell medium and cultured until day 12.

2.2.10. *In vitro* myeloid differentiation of HoxB8-immortalized HPCs

To trigger myeloid differentiation, H8-HPCs were plated at 2×10^5 cells per milliliter in 20 ml of RPMI-1640 supplemented with 10% FBS not heat inactivated, 2mM L-glutamine, 50 μM β-mercaptoethanol and cell culture supernatant from Flt3L-producing B16 melanoma cell line (5% final concentration). Each two days, cells were harvested, counted and re-plated in fresh new medium until day 8.

2.2.11. *In vitro* culturing of λ-MYC B cell lymphomas

λ-MYC B cell lymphoma lines were previously established from λ-MYC transgenic mice (Varano et al. 2017; Kovalchuk et al. 2000). Cells were cultured in DMEM medium, supplemented with 10% FBS, 2 mM glutamine, 1 mM Sodium Pyruvate, non-essential amino acids (NEAA) and 50 μM β-mercaptoethanol. Cells were plated at 2×10^5 cells per milliliter each two days.

2.3. Imaging techniques

2.3.1. Immunostaining for flow cytometry and cell sorting

FACS buffer: 1x PBS

1% BSA

0.05% NaN3

For flow cytometric analysis, 10^6 cells were stained for 20 minutes on ice in 50 µl of FACS buffer containing the appropriate mixture of fluorescently labeled antibodies and subsequently washed twice in 150 µl of FACS buffer. Cells were either freshly acquired using FACSCanto (BD Biosciences) or fixed with 1% formaldehyde in PBS for later acquisition. Data were analyzed with FlowJo Software (Tree Star). For FACS-assisted cell sorting, cells were resuspended in FACS buffer at 10^8 cells per milliliter and stained for 15 minutes at 4°C on rotation in FACS buffer. Cells were then washed twice in 10 volumes of FACS buffer and resuspended in 1x PBS supplemented with 2% FBS, at 10^7 cells per milliliter. Cell sorting was performed using FACSAria Cell Sorter (BD Biosciences). Antibodies and working dilutions used for flow cytometric analysis and FACS sorting are listed in Table 5.

Table 5. List of antibodies used for surface staining.

Antibody	Company	Dilution
Monoclonal rat anti-mouse IgM (Alexa 488) (R33.24.12)	Home-made	1/400
Monoclonal rat anti-mouse CD23 (FITC)(B3B4)	Biolegend	1/100
Peanut Agglutinin	Vector Laboratories	1/150
Monoclonal hamster anti-mouse CD95/Fas (PE)	BD Biosciences	1/170
Monoclonal rat anti-mouse Sca-1 (PE) (D7)	eBioscience	1/100
Monoclonal rat anti-mouse CD11b (PE) (M1/70)	eBioscience	1/200
Monoclonal rat anti-mouse MHC-II (PE) (M5/114.15.2)	eBioscience	1/400
Monoclonal rat anti-mouse IgG1 (PE) (A85-1)	BD Biosciences	1/20
Monoclonal rat anti-mouse CD138 (PE) (281-2)	BD Biosciences	1/200
Polyclonal fragment goat anti-mouse IgM, F(ab')$_2$	Jackson ImmunoRes	1/1000
Monoclonal rat anti-mouse CD19 (Cy7PE) (1D3)	eBioscience	1/400
Monoclonal rat anti-mouse CD86 (Cy7PE) (GL1)	eBioscience	1/400
Monoclonal rat anti-mouse B220 (Cy7PE) (RA3-6B2)	eBioscience	1/400
Monoclonal mouse anti-CD45.1 (Cy7PE) (A20)	eBioscience	1/200
Streptavidin (Cy7PE)	eBioscience	1/400
Monoclonal rat anti-mouse CD45R/B220 (APC) (RA3-6B2)	eBioscience	1/600
Monoclonal rat anti-mouse IgG1 (APC) (M1-14D12)	eBioscience	1/200
Monoclonal mouse anti-CD45.2 (APC) (104)	eBioscience	1/200
Monoclonal rat anti-mouse CD117(c-Kit) (APC) (ACK2)	TONBO biosciences	1/200
Monoclonal rat anti-mouse IRF4 (Alexa 647) (3E4)	BioLegend	1/200
Monoclonal Armenian hamster anti-mouse CD80 (PerCP-eFluor710) (B7-1)	eBioscience	1/150
Monoclonal rat anti-mouse CD40 (PerCP-Cy5.5) (3/23)	BioLegend	1/50
Monoclonal rat anti-mouse MHC-II (biotin) (M5/114.15.2)	eBioscience	1/400
Monoclonal rat anti-mouse B220 (biotin) (RA3-6B2)	eBioscience	1/400
Monoclonal Armenian hamster anti-mouse CD3e (biotin) (145-2C11)	eBioscience	1/400
Monoclonal rat anti-mouse CD11b (biotin) (M1/70)	eBioscience	1/400
Monoclonal rat anti-mouse TER-119 (biotin)	eBioscience	1/400

2.3.2. Intracellular immunostaining for flow cytometry

Surface staining was performed as described above (paragraph 2.3.1). At the end of the last wash, cells were centrifuged for 3 minutes at 1300 rpm and then resuspended in BD Cytofix/Cytoperm™ buffer for 20 minutes at RT in U-bottom 96-well microplates, shaking. After that, cells were washed in Perm/Wash™ (P/W) buffer and stained with the appropriate fluorochrome-conjugated antibody for 1 hour, shaking, at RT. Cells were washed twice in P/W buffer and acquired using FACSCanto (BD Biosciences). For intracellular staining for METTL3, fixation in BD Cytofix/Cytoperm™ was followed by incubation in blocking buffer (5% donkey serum in P/W buffer) for 20 minutes on ice and staining with primary antibody (monoclonal rabbit anti-mouse METTL3, (Table 6) in P/W buffer for 1 hour, at RT, shaking. Two rounds of washing in P/W buffer were performed and cells stained with the secondary antibody (donkey anti-rabbit Alexa647, working dilution 1/200) in staining solution for 1 hour at RT, shaking. Cells were washed twice with P/W buffer and acquired using FACSCanto (BD Biosciences). All centrifugation steps were performed at 1300 rpm, for 3 minutes, 4°C. Antibodies used for intracellular staining and working dilutions are listed in Table 6.

Table 6. List of antibodies used for intracellular staining.

Antibody	Clone	Company	Dilution
Monoclonal rat anti-mouse IRF4 (Alexa647)	3E4	Biolegend	1/200
Monoclonal rat anti-mouse PAX5 (PE)	1H9	BD Biosciences	1/200
Monoclonal rabbit anti-mouse METTL3 (unconjugated)	EPR18810	Abcam	1/70

2.3.3. *In vitro* cell-cycle analysis

For this procedure, cells were treated with reagents of Fixation/Permeabilization Solution Kit (BD Biosciences). 1×10^6 of *in vitro* activated B cells were collected by centrifugation at 1500 rpm for 5 min, resuspended in 1 ml of medium supplemented with BrdU (33 µM, Sigma Aldrich) and incubated at 37°C and 5 % CO_2 for 1 hour. Cells were washed in 1x PBS, fixed in 100 µl of BD Cytofix/Cytoperm™ buffer for 20 min at RT and washed with Perm/Wash™ (P/W) buffer. Cells were resuspended in 70 µl of 10 % DMSO in FBS solution and incubated at RT for 10 minutes. After washing in P/W buffer, cells were re-fixed in 100 µl of C/C buffer at RT for 5 min and washed by P/W buffer again. Cells were resuspended in DNase solution (1x PBS, 300 µg/ml DNase) and incubated at 37°C for 1 hour. After washing with P/W solution, cells were stained in 50 µl of P/W buffer with anti-BrdU (monoclonal mouse anti-BrdU, clone Bu20A, eBioscience, dilution factor 1/20) at RT for 20 min. After washing with P/W buffer, for DNA staining cells were resuspended in 1 ml of cold propidium iodide (50 µg/ml) + RNase (250 µg/ml) and incubated at 4°C overnight. Samples were collected in doublet discrimination mode by FACSCanto (BD Biosciences) and analyzed using FlowJo software (Tree Star).

2.4. Molecular biology techniques

2.4.1. RNA and DNA extraction

For cell pellets containing more than 1×10^5 cells, RNA and DNA were extracted using AllPrep DNA/RNA mini kit (Qiagen), following the manufacturer's protocol. For FACS sorted cells with total cell number lower than 1×10^5 cells, RNA and DNA were extracted using the AllPrep DNA/RNA micro kit (Qiagen), following the manufacturer's protocol. Purified DNA and RNA were quantified by a microvolume UV spectrophotometer (NanoDrop ND-100).

2.4.2. cDNA synthesis

Complementary DNA (cDNA) was obtained by reverse transcription of total RNA (100 to 1000 ng), using SuperScript™ III Reverse Transcriptase Kit (Thermo Fisher Scientific), following the manufacturer's protocol. After an initial denaturation in the presence of random primers at 65°C for 5 minutes, RNA samples were retro-transcribed in 1x First Strand Buffer (50 mM Tris-HCl pH 8, 375 mM KCl, 3 mM $MgCl_2$), 5 mM Dithiothreitol (DTT), 0.5 mM dNTPs, 40 units of RNase OUT and 200 units of Super Script II (Thermo Fisher Scientific), for 5 minutes at 25°C, followed by 60 minutes at 50°C. Reaction was terminated by 15 minutes incubation at 72°C.

2.4.3. Real-Time quantitative PCR (RT-qPCR)

For gene expression analysis, real-time qPCR was performed using 1-25 ng of cDNA, 5 µl of primers mix (0.5 µM final concentration) and 10 µl of Takara Bio Green Premix Ex Taq™ II (Tli RNase H Plus) (Takara Bio) in a final volume of 20 µl per reaction in 96-well format. PCR conditions consisted of an initial denaturation step at 95°C for 10 minutes, followed by 45 cycles at 95°C for 10 seconds, 60°C for 10 seconds and 72°C for 10 seconds, followed by a final Taq polymerase elongation step of 10 minutes. Accumulation of fluorescent products was monitored using LightCycler® 96 software, provided along with the LightCycler® 96 Real-Time PCR Systems (Roche).

Specificity of the PCR reaction was controlled through the assessment of the melting temperature profiles of the final PCR products (dissociation curve). To normalize for DNA input, a segment of the *Rplp0* gene was amplified. Primers used are listed in Table 7.

Table 7. RT-qPCR primers.

Primer ID	Sequence	Target	Organism
Mettl3 forward	ATCCAGGCCCATAAGAAACAG	cDNA	Mouse
Mettl3 reverse	CTATCACTACGGAAGGTTGGG	cDNA	Mouse
Mettl14 forward	GGAGCGGCAGAAGTTACG	cDNA	Mouse
Mettl14 reverse	GCAGATGTATCATAGGAAGCCC	cDNA	Mouse
Fto forward	TCACAGCCTCGGTTTAGTTC	cDNA	Mouse
Fto reverse	GCAGGATCAAAGGATTTCAACG	cDNA	Mouse
Alkbh5 forward	AGTTCCAGTTCAAGCCCATC	cDNA	Mouse
Alkbh5 reverse	GGCGTTCCTTAATGTCCTGAG	cDNA	Mouse
Irf4 forward	CAATGTCCTGTGACGTTTGG	cDNA	Mouse
Irf4 reverse	GGCTTCAGCAGACCTTATGCT	cDNA	Mouse
Prdm1 forward	GACGGGGGTACTTCTGTTCA	cDNA	Mouse
Prdm1 reverse	GGCATTCTTGGGAACTGTGT	cDNA	Mouse
Xbp1 forward	AAGAACACGCTTGGGAATGG	cDNA	Mouse
Xbp1 reverse	ACTCCCCTTGGCCTCCAC	cDNA	Mouse
Xbp1-S forward	GAGTCCGCAGCAGGTC	cDNA	Mouse
Xbp1-S reverse	GTGTCAGAGTCCATGGGA	cDNA	Mouse
Rplp0 forward	TTCATTGTGGGAGCAGAC	cDNA	Mouse
Rplp0 reverse	CAGCAGTTTCTCCAGAGC	cDNA	Mouse

2.4.4. Design and cloning of sgRNAs

Four independent small guides RNA (sgRNA) targeting the *Mettl3* gene were designed using the CrispRGold database (https://crisprgold.mdc-berlin.de). sgRNAs targeting the Cd38 gene, used in the validation of the optimized protocol, have been previously published (Chu, Graf et al. 2016). Each sgRNA was then individually cloned into the MSCV-pU6-(BbsI)-Pgk-Puro-T2A-BFP vector (Addgene #86457). sgRNAs sequences are listed in Table 8.

Table 8. List of sgRNAs.

Gene	sgRNA ID	sgRNA forward sequence (5' – 3')
Mettl3	sgRNA#1	CACCGCACGGGACTATCACTACGGA
Mettl3	sgRNA#2	CACCGACGCCGTTTCTGCCCTGCGA
Mettl3	sgRNA#3	CACCGGACTATCACTACGGAAGGTT
Mettl3	sgRNA#4	CACCGGCGAGAGATTGCAGCGGCGA
Cd38	sgRNA#1	CACCGACCCACTCCGAGACCGATC
Cd38	sgRNA#2	CACCGTCCTGATCGCCTTGGTAGTA

2.4.5.   T7 endonuclease assay

Cas9-targeted regions of *Mettl3* locus on genomic DNA were amplified by PCR reaction using the Q5® High-Fidelity Taq DNA Polymerase (NEB). Primers, reagents and conditions used are summarized in Table 9, Table 10 and Table 11, respectively.

Table 9. Primers used to amplify the Cas9-targeted region of *Mettl3* locus.

Primer ID	Primer sequence 5' – 3'	T$_A$
Mettl3 forward	GATGCTGGACAGTTGAACCC	60°C
Mettl3 reverse	TGAACAAAAGCAAACTCGGG	

PCR products were then purified using the Wizard Purification Kit (Promega), according to manufacturer's protocol. 200 ng of purified PCR product was then subjected to the following denaturation and re-annealing program to facilitate the formation of mismatched fragments: 95°C from 10 minutes, ramping from 95°C to 85°C at 2°C/second, 85°C for 1 minute, ramping from 85°C to 75°C at 0.3°C /second, 75°C for 1 minute, ramping from 75°C to 65°C at 0.3°C/second, 65°C for 1 minute, ramping from 65°C to 55°C at 0.3°C/second, 55°C for 1 minute, ramping from 55°C to 45°C 0.3°C /second, 45°C for 1 minute, ramping from 45°C to 35°C at 0.3°C/second, 35°C for 1 minute, ramping from 35°C to 25°C at 0.3°C/second and 25°C for 1 minute. Next, re-annealed PCR products were incubated with 5 units of T7 Endonuclease 1 enzyme (NEB) at 37°C for 15 minutes. Products from T7 endonuclease assay were loaded on a 3% agarose gel and subjected to electrophoretic analysis.

Table 10. Reagents of PCR used to amplify the Cas9-targeted region of *Mettl3* locus.

Component	Final volume (µl)
5x Q5® buffer	10
dNTPs 10 mM	1
Mettl3 primer Reverse, 10 µM	2.5
Mettl3 primer Forward, 10 µM	2.5
Q5® Taq DNA Polymerase	0.5
Template DNA	200 ng
Nuclease-Free Water	up to 50

Table 11. PCR conditions to amplify the Cas9-targeted regions of *Mettl3* locus.

Temperature (°C)	Time (min:sec)	
98	3:00	
95	0:20	
60	0:20	x 35 cycles
72	0:30	
72	3:00	
4	hold	

2.4.6. Characterization of mutant alleles

2.4.6.1. PCR amplification of the Cas9-targeted region

Target regions on genomic DNA were amplified by PCR reaction using the Q5® High-Fidelity Taq DNA Polymerase (NEB) as described above (see paragraph 2.4.5. and Table 10-11). To amplify the region on the *Mettl3* or *Cd38* gene, targeted by Cas9-cleavage, primers used are listed in Table 12.

Table 12. Primers used to amplify the region on *Mettl3* and *Cd38* locus interested by Cas9-cleavage.

Primer ID	Primer sequence 5' – 3'	T$_A$
Mettl3 forward	GATGCTGGACAGTTGAACCC	60°C
Mettl3 reverse	TGAACAAAAGCAAACTCGGG	
Cd38 forward	CTCTTCCTGCCTAGCCTGG	60°C
Cd38 reverse	AAAAGTGCTTCGTGGTAGGC	

PCR products were purified using the Wizard Purification Kit (Promega), according to manufacturer's protocol. Subsequently, tailing reaction using reagents summarized in Table 13 was performed, in which Taq polymerase forms polyA overhangs at the 3' ends of the PCR products. Tailing reaction was performed using 500 ng of PCR product and consisted in an initial denaturation at 94°C for 2:30 minutes, followed by 10 minutes at 72°C. These polyA overhangs facilitate ligation into pGEM®-T easy Vector (Promega), containing 3'-T overhangs at the insertion site.

Table 13. Reagents for polyA overhangs formation.

Component	Quantity
GoTaq Buffer (5x)	4 µl
dNTPs 10 mM	1 µl
GoTaq Polymerase	1 µl
DNA template	500 ng
Nuclease-Free Water	up to 20 µl

2.4.6.2. Cloning and plasmid DNA extraction

PCR fragments were ligated with pGEM®-T easy Vector (Promega) (Figure 14) using the reagents listed in Table 14 and incubated for 1 hour at RT.
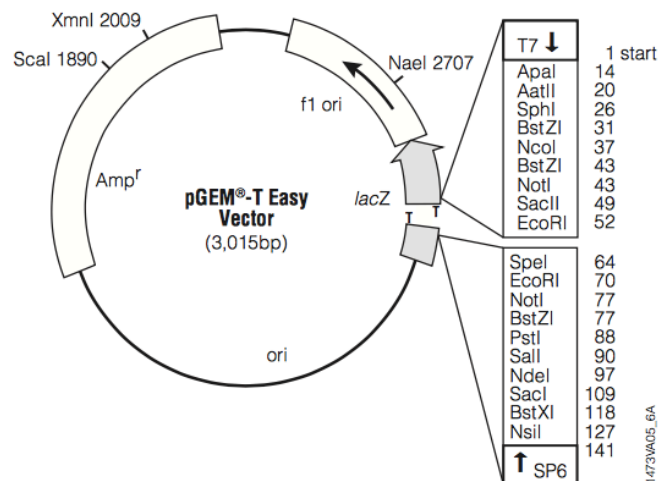
Figure 14. Map of pGEM®-T-easy Vector.

Table 14. T4 ligation conditions.

Reagent	Quantity
pGEM®-T easy buffer (2x)	2 µl
T4 DNA ligase	1 µl
pGEM®-T easy vector	50 ng
PolyA tailed PCR fragment	50 ng
Nuclease-Free Water	up to 50 µl

Bacterial TOP10 (home-made) were thawed on ice. 4 µl of ligation product was added to 50 µl of bacteria and incubated for 20 minutes on ice. Cells were heat shocked for 45 seconds at 42°C and immediately returned to ice for 2 minutes. 250 µl of SOC medium was added and cells were incubated in thermomixer for 60 minutes at 37°C shaking at 250 rpm. Cells were centrifuged for 3 minutes at 3000 rpm and 200 µl of supernatant was aspirated. Cells were resuspended in the remaining 100 µl of SOC medium and plated on ampicillin (50 µg/ml) containing agar-plates pre-treated with X-gal (20 mg/ml) and IPTG (1mM) and incubated overnight at 37°C. White colonies (containing cloned PCR fragment in the LacZ

gene) were picked into 3 ml of LB medium + ampicillin (50 μg/ml) and incubated overnight at 37°C. Cells were centrifuged for 5 minutes at 3000 rpm and plasmid DNA was extracted using the Wizard Plus Minipreps DNA purification System (Promega), according to manufacturer's protocol. Plasmid DNA was eluted in 100 μl of milliQ water.

2.4.6.3.   Screening of recombinant clones and sequencing

To make sure the purified plasmid DNA contained the cloned PCR fragment, 100-200 ng of extracted plasmid DNA was used to amplify by PCR the region on the vector covering the insertion site. PCR reaction was performed according to the conditions described in Table 2 and Table 3, using primers listed in Table 15.

Table 15. Primers used to amplify the insertion site of the pGEM®-T-easy Vector.

M13 Primer sequence 5' – 3'	T_A
Forward: GTTTTCCCAGTCACGAC	50°C
Reverse: CAGGAAACAGCTATGACC	

Samples that resulted positive for the cloned PCR by agarose gel electrophoretic analysis, and whose amplicon size corresponded to the expected one, were subjected to Sanger sequencing using M13-21 universal forward primer (5' -TGTAAAACGACGGCCAGT- 3'), annealing to the multiple cloning site of the pGEM®-T-easy vector, thus enabling the full-length sequencing of the cloned fragment.

2.5. Biochemical techniques

2.5.1. Immunoblot analysis

RIPA buffer: 50 mM Tris HCl pH 8

                                           150 mM NaCl,

                                           1% NP40

                                           0.2% Na deoxicolate

                                           0.1% SDS

Laemmli loading buffer: NuPAGE® (Invitrogen)

                                           2 mM DTT

Ponceau S: 0.1% Ponceau S

                                           5% acetic Acid

TBS-Tween: 20 mM Tris HCl pH 7.4

                                           500 mM NaCl

                                           0.1 % Tween

Blocking solution: 5% Milk in TBS-Tween

Cells were harvested by centrifugation for 5 min at 1200 rpm, at 4° C and washed in cold PBS. After that, cells were centrifuged for 5 minutes at 6000 rpm at 4° C and resuspended in RIPA buffer containing protease inhibitors (Millipore), PMSF (2 mM), Na vanadate (10 mM), Benzonase (Novagen) and incubated for 1 hour on ice. Sonication was performed for 10 cycles (30 sec ON/ 30 sec OFF) using Bioruptor™ Next Gen (Diagenode). Lysates were centrifuged at 15000 rpm for 10 min at 4°C and then transferred to a new tube. Lysates concentration was established using the Bio-Rad Protein Assay Dye Reagent concentrate. The appropriate volume of lysates was then mixed with Laemmli loading buffer. Samples and protein marker (NOVEX® Sharp PreStained protein standard – Invitrogen) were electrophoresed by 4-12 % SDS-PAGE (Invitrogen) in an XCell Surelock™ Mini-cell apparatus (Life Technologies) in NuPAGE MOPS or MES SDS running buffers (Thermo

Fisher Scientific). Separated proteins were transferred into Amersham™ Protran R nitrocellulose membranes and then stained with Ponceau S staining solution to verify equal loading and transfer. Membranes were briefly washed in distilled water and incubated in blocking solution at RT, shaking for 1 hour. After blocking, membranes were incubated with primary antibodies diluted in Blocking solution, at 4°C overnight. On the next day, after three washes of 5 minutes each in TBS-Tween (TBS-T), membranes were incubated with the horseradish peroxidase conjugated secondary antibody, diluted in Blocking solution for 1 hour at RT and then washed three times in TBS-T for 5 minutes each. Bound secondary antibody was revealed using the ECL (Enhanced Chemiluminescence) plus method (Amersham) or the SuperSignal™ West Pico PLUS chemiluminescent substrate (Thermo Fisher Scientific) and detected using the Chemidoc™ XRS + imaging System (Bio-Rad). Image analysis was performed using the Image Lab™ 5.2.1 software tool. Primary and secondary antibodies used for immunoblotting analysis are listed in Table 16.

Table 16. Antibodies used for immunoblot protein detection.

Primary antibody	Cat. #	Company	Dilution
Monoclonal rabbit anti-mouse METTL3 (EPR18810)	ab195352	eBioscience	1/1000
Polyclonal rabbit anti-mouse METTL14	HPA038002	BD Biosciences	1/200
Monoclonal mouse anti-FTO (5-2H10)	ab92821	Abcam	1/1000
Monoclonal rabbit anti-mouse c-MYC (Y69)	ab32072	Abcam	1/1000
Monoclonal rat anti-mouse IRF4 (3E4)	646402	Biolegend	1/50
Monoclonal mouse anti-CAS9 (7A9-3A3)	ab191468	Abcam	1/1000
Secondary antibody	Cat. #	Company	Dilution
Polyclonal goat anti-mouse Ig HRP-linked	7076S	Cell signaling	1/2000
Polyclonal goat anti-rabbit Ig HRP-linked	7074S	Cell signaling	1/2000
Polyclonal goat anti-rat Ig HRP-linked	7077S	Cell signaling	1/2000

2.5.2. Colorimetric quantification of m⁶A on total RNA

m^{6}A content on total RNA was measured by using the m^{6}A RNA Methylation colorimetric assay kit (Abcam, ab185912), following manufacturer's protocol. In details, 200 ng of total RNA from each sample were added into an assay strip well. In parallel, standard curve was performed, by diluting the positive control in order to have different concentrations, from 0.01 ng/µl to 0.5 ng/µl. Once added to the well, RNA was bound to the bottom of the well after incubation with RNA binding solution for 90 minutes, at 37°C. Next, samples were washed in 1x Wash Buffer, followed by incubation with the capture antibody, at RT, for 60 minutes, to favor the recognition and the binding of the antibody to m^{6}A. After that, excess of capture antibody was removed and samples washed in 1x Wash Buffer. Detection antibody was then added into each well, followed by incubation at RT for 30 minutes. At the end of this time, samples were washed in Wash Buffer and then incubated with Enhancer solution for 30 minutes, at RT, away from light. Next, Enhancer solution was replaced with Developer solution and samples incubated for 1 to 10 minutes, away from light. In the presence of sufficient m^{6}A, the Developer solution will turn blue. After having monitored that positive control turned blue, the reaction was stopped by adding Stop solution. Finally, the absorbance was measured within 2 to 10 minutes, at 450 nm. In order to build the standard curve, specific signal from diluted positive controls was obtained by subtracting the background signal, corresponding to the OD (optical density) of the negative control. Then, slope was determined by interpolation of the sample OD on the standard curve. Each sample was performed in duplicates. Amount and percentage of m^{6}A in the total RNA were calculated using the following formulae:

$$m^6A \ (ng) = \frac{Sample \ OD - NC \ OD}{Slope}$$

$$m^6A \ \% = \frac{m^6A \ (ng)}{S} \times 100 \ \%$$

S is the amount of input sample RNA in ng;

NC is Negative Control;

All reagents for the colorimetric quantification of m^6A content previously described (strip wells, positive and negative controls, capture and detection antibodies, Binding, Wash, Enhancer and Developer Solutions) were provided by the kit and used at the final concentration suggested by the manufacturer's protocol.

2.5.3. m^6A-RNA immunoprecipitation (meRIP)

2.5.3.1. RNA extraction

Total RNA was isolated from λ-MYC lymphoma cells using the Maxwell® RSC SimplyRNA tissue kit, according to the manufacturer's protocol. A DNase digestion step is included in the protocol to ensure the complete elimination of contaminant DNA.

2.5.3.2. mRNA purification

Total RNA was then subjected to mRNA purification using Oligo $d(T)_{25}$ Magnetic Beads (NEB). In details, 200 μl of Oligo $d(T)_{25}$ Magnetic Beads were mixed with 600 μg of RNA in Binding Buffer (1 M LiCl in 6.5 mM EDTA, 20 mM Tris-HCl pH 7.4, in ultra-pure H_2O). Samples were then transferred into the thermomixer and incubated for 2 minutes at 70°C, to favor denaturation of secondary structures of total RNA. Samples were then incubated for 30 seconds on ice and then at RT for 5 minutes, in order to favor the annealing of polyadenylated (polyA) mRNA to the oligo $d(T)_{25}$ Magnetic Beads. Next, tubes were exposed to a magnetic field fitting them to a magnet (Life Technologies) to wash off unbound RNA. The mixture of beads and RNA was then washed three times in Washing Buffer (150 mM LiCl in 1 mM EDTA, 10 mM Tris-HCl pH 7.4, in ultra-pure H_2O). After the last wash, beads were resuspended in ultra-pure H_2O and placed on the thermomixer at 70°C for 2 minutes, in order to favor the elution of the mRNA from the oligod$(T)_{25}$ bound to the beads. After that, samples were immediately exposed to the magnetic field by fitting them to the magnet, and the eluted mRNA was collected and transferred into a new tube.

The procedure was repeated in total twice, in order to recover the highest fraction of mRNA. Purified mRNA was quantified using UV spectrophotometer (NanoDrop ND-100).

2.5.3.3.   mRNA fragmentation

Purified mRNA was fragmented to ~100 nucleotide fragments with Ambion fragmentation reagent (6 minutes at 72°C). After that, fragmented mRNA was transferred on ice and 2 μl of EDTA 0.5 M was added to stop fragmentation. Size of fragments was checked by loading 200 ng of fragmented mRNA on a 3% agarose gel, followed by electrophoretic analysis.

2.5.3.4.   Immunoprecipitation of m^{6}A-modified mRNA

IP Buffer 5x   50 mM Tris-HCl pH 7.4

                                            750 mM NaCl

                                            0.5% Igepal CA-630

Elution buffer   IP Buffer 1x

                                            6.7 mM N^6-methyladenosine, 5'-monophosphate sodium salt (Sigma-Aldrich, cat. #M2780)

Buffers were freshly prepared in ultra-pure H$_2$O, as described above. Fragmented mRNA was added to 500 μl of IP mix containing the reagents listed in Table 17 and incubated for 2 hours at 4°C on rotation. A parallel reaction including the same amount of fragmented mRNA but without the antibody was set up, in order to assess background levels and efficiency of mRNA elution (beads-only control).

Table 17. Reagents m⁶A RIP mix.

Component	Volume (µl)	Final
Fragmented RNA	-	1 µg
RNasin (40 U/ µl)	5	200 U
RVC 200 mM	5	2 mM
IP Buffer 5x	100	1x
Anti-m⁶A antibody (1 µg/µl)	3	3 µg
Ultra-pure H_2O	up to 500	-

While samples were incubating, Dynabeads™ protein A and protein G (Thermo Fisher Scientific; 50 µl of magnetic dynabeads were used in 500 µl of IP mix) were exposed to a magnetic field by fitting them to a magnet (Life Technologies) and washed twice in IP buffer 1x. At the end of the last wash, Dynabeads were resupended in the same volume of IP buffer 1x containing BSA (0.5 mg/ml) and incubated for 2 hours at 4°C on rotation. After 2 hours of incubation, 50 µl of Dynabeads were added into each IP mix containing mRNA previously bound to anti-m⁶A polyclonal antibody (Synaptic System, cat. #202 003) and incubated for 2 hours at 4°C on rotation. After that, samples were exposed to the magnetic field by fitting them to the magnet to remove the unbound fraction.

Beads were then washed three times in IP Buffer 1x. At the end of the last wash, 100 µl of Elution Buffer was transferred into each tube and samples were incubated at 4°C for 45 minutes, shaking at 1100 rpm, in the thermomixer. Samples were then fitted to the magnet and the eluted m⁶A-modified mRNA was transferred into a new tube. For each tube, one-tenth volumes of 3 M sodium acetate (pH 5.2), 2.5 volumes of 100% ethanol and 1 µl of glycogen were added. Samples were mixed and incubated at - 80°C overnight. On the next day, RNA was precipitated by centrifugation at 4°C, for 25 minutes at 13.000 rpm and the pellet washed in ice-cold 75% ethanol. Samples were centrifuged, the ethanol aspirated and pellets resuspended in 15 µl of ultra-pure H_2O.

2.6. Next-generation sequencing (NGS) applications

2.6.1. RNA-sequencing

To perform transcriptome analysis of iGB cells, the quality of total RNA, previously purified from these cells using AllPrep DNA/RNA minikit, was assessed using the RNA 6000 Nano kit (Agilent Technologies) on a Bioanalyzer 2100 (Agilent Technologies) instrument. 100 ng of RNA was used for NGS library construction using TruSeq RNA Library Prep Kit v2, according to manufacturer's protocol. Samples were sequenced using single-end 75-nt cycles on an Illumina NextSeq™ 550 instrument. We sequenced at least 30 million reads per sample with an average of 35 million reads. Library construction and sequencing were performed with the support of the IFOM Genomic unit.

2.6.2. meRIP-sequencing

For meRIP-seq, libraries from input (fragmented mRNA) and m^{6}A-enriched IP samples were prepared using the TruSeq RNA Library Prep Kit v2. The step of mRNA purification was skipped. Specifically, input and IP-samples were directly incubated with the master mix containing random primers for cDNA synthesis at 65°C for 5 minutes. After that, libraries preparation was performed according to manufacturer's protocol. Samples were sequenced using paired-end 2 x 75-nt cycles on an Illumina NextSeq™ 550 instrument. We sequenced at least 30 million reads per sample with an average of 35 million reads. Library construction and sequencing were performed with the support of the IFOM Genomic unit.

2.7.   Bioinformatic Analysis

2.7.1. Bioinformatic analysis of RNA-seq data

Reads were aligned to the mm10 reference genome with STAR (Dobin and Gingeras 2015) with default parameters and setting the option *quantMode GeneCounts* in order to count the number of reads per gene while mapping. Reads normalization and differential gene expression analysis was performed with DESeq2 (Love, Huber, and Anders 2014).

Principal Component Analysis (PCA) was performed with DESeq2 considering the 500 genes with highest variance among samples. Genes with absolute log2FC > 0.58 and adjusted *p*-value < 0.05 were considered significantly deregulated. Heatmaps were generated with the Pheatmap R package on the 50 most significantly deregulated genes after ranking them according to their fold change.

2.7.1.1.   Gene Set Enrichment Analysis and intersections with c-MYC-targets

Gene Set Enrichment Analysis (GSEA) for gene sets of the GO Biological Process and MSigDB Hallmark collections was performed on the fold change rank ordered gene list with an *ad-hoc* script in R which made use of the FGSEA (Korotkevich et al. 2019, BioRvix depository) and Ggplot2 packages. Intersections between gene lists were performed with *ad-hoc* scripts in R which made use of the R package VennDiagram.

2.7.2. Bioinformatic analysis of meRIP-seq data

Reads were trimmed with Cutadapt (DOI:10.14806/ej.17.1.200) and mapped to the mm10 transcriptome with STAR (doi: 10.1093/bioinformatics/bts635) (Dobin and Gingeras 2015). Input reads were downsized in order to have a number of reads comparable to those of IP samples. Duplicates and reads mapping to multiple regions were removed prior peak calling with MACS2 (version 2.1.1) (Zhang et al. 2008) using default parameters and setting the "effective genome size" equal to the mouse transcriptome size (9.94×10^8 bp).

Peaks were intersected with mm10 RefSeqs coordinates using the IntersectBed tool (https://bedtools.readthedocs.io/en/latest/). Only peaks mapping into a RefSeq, with a with a fold enrichment $\geq$ 2.5 and a False Discovery Rate (FDR) $\leq$ 5% were kept. The DeepTools suite (Ramirez et al. 2016) was used to assess both the correlation between replicates and the reads distribution along the mm10 RefSeq transcripts. Both the analyses were performed on the BigWig files generated after filtering and duplicates removal of the reads mapped to the whole transcriptome. The Venn diagram showing the overlap between the target genes of the two replicates, was generated in R with an *ad-hoc* script which made use of the R package VennDiagram. Annotation of the peaks with respect to the genomic regions was performed with the Bioconductor package ChIPseeker (Yu, Wang, and He 2015) using the TxDb. Mmusculus.UCSC.mm10.knownGene annotation package.

2.7.2.1. m⁶A consensus site enrichment analysis

Motif enrichment analysis was performed with the MEME-ChIP tool (Machanick and Bailey 2011) of the MEME suite. Only peaks mapping into RefSeq regions with a *q*-value $< 10^{-12}$ and a fold enrichment > 4 in at least one replicate were considered for the analysis. A 100 bp transcript sequence around the center of each peak was extracted using the FastaFromBed utility of bedtools. MEME-ChIP was run on these sequences with the parameters -meme-minw 4 and -meme-maxw 6 in order to identify consensus binding sites of 4-6 bp length. Enrichment and pathways analyses for m⁶A targets were performed using the EnrichR tool (Kuleshov et al. 2016). The Gene lists provided by EnrichR were ranked based on the adjusted *p*-value.

2.7.2.2. Intersections of meRIP-seq and microarray data

Association of target genes identified in both replicates with expression data was performed with an *ad-hoc* script in R using Affymetrix microarray data of λ-MYC B cell lymphomas, previously generated in our laboratory (Varano et al. 2017). Statistical significance between the mean expression value of m^{6}A-marked genes and m^{6}A-negative genes was assessed with a two-tailed *t*-test.

2.8. Statistical analysis

Statistical analysis of normally distributed values (Gaussian) was performed with a two-tailed unpaired Student's *t*-test, using the GraphPad Prism version 9.0.1. In case of non-normal distribution, a two-sided unpaired Wilcoxon test was applied, using the R software. To establish the significance of enrichment between two lists of genes a Chi square test was performed using the R software. Differences were considered significant at *p*-value < 0.05.

3. Results

3.1.   The *Mettl3* gene is expressed throughout B cell development

To establish the expression pattern of the *Mettl3* gene throughout B cell lymphopoiesis, B cell subsets representative of both early and late stages of B cell development were purified by cell sorting from the bone marrow and the spleen of three wild-type C57BL/6J mice (Table 18).

Table 18. Table showing the gating strategy used to sort the indicated B cell subset.

B cell subset	Gating strategy
Pro-B cells	B220$^+$ c-Kit^{high}
Pre-B cells	B220$^+$ c-Kit^{low}
Immature B cells	B220^{low} IgM$^+$
Recirculating B cells	B220^{high} IgM$^+$
Follicular B cells	CD19$^+$ CD23$^+$ CD38^{low}
Marginal zone B cells	CD19$^+$ CD23^{low} CD38^{high}
Germinal center B cells	C1D9$^+$ CD95^{high} CD38^{low}

From these cells, total RNA was extracted, reverse transcribed into cDNA and ultimately subjected to quantitative RT-PCR (qRT-PCR) analysis using intron-spanning gene-specific primers. As shown in Figure 15, *Mettl3*-specific transcripts were detected throughout B cell development. In the bone marrow, *Mettl3* transcript levels were higher in immature B cells when compared to pro-B, pre-B or recirculating mature B cells (Figure 15). The main mature B cell subsets residing in the spleen, represented by Fo and MZ B cells continued to express *Mettl3*, with Fo B cells showing roughly twice as many transcripts as compared to MZ B cells (Figure 15). *Mettl3* expression was retained in GC B cells, isolated from the spleen of C57BL/6J mice immunized 8 days earlier with sheep red blood cells (SRBCs), yet at slightly lower level as compared to the Fo B cells precursors (Figure 15).

Altogether, these data reveal that the expression of the catalytic subunit of the methyltransferase complex responsible of m^{6}A mRNA methylation is retained throughout B cell development and remains expressed upon recruitment of mature B cells into GCs, during a T-cell dependent immune response. The oscillations in *Mettl3* expression seen in the transition through defined stages of B cell lymphopoiesis may hint to a specific requirement for this protein at distinct steps of such developmental trajectory.
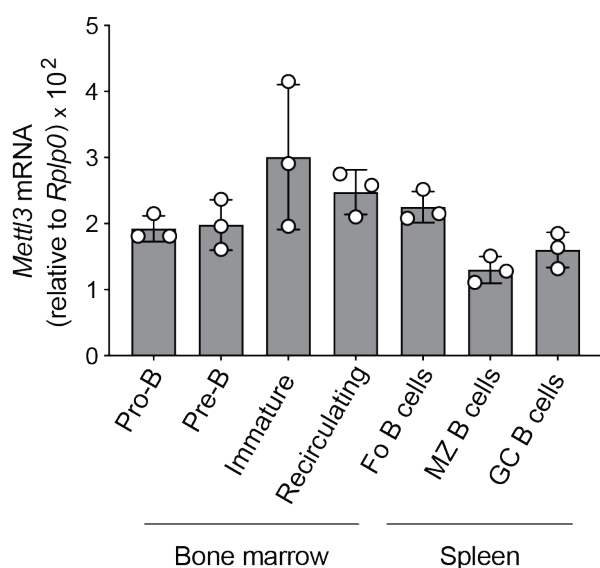
Figure 15. *Mettl3* expression pattern during B cell development.

Quantitative RT-PCR analysis of *Mettl3* transcript, respectively in pro-B and pre-B cells, immature, recirculating, follicular (Fo), marginal zone (MZ) and germinal center (GC) B cells, purified by cell sorting from 3 C57BL/6J mice. *Mettl3* transcript levels were normalized to the housekeeping gene *Rplp0*. Columns represent mean *Mettl3* transcript levels (n = 3), ± SD. White symbols indicate *Mettl3* transcript levels relative to *Rplp0*, measured into each mouse.

3.2. *Mettl3*/m^{6}A modulation in mature B cells in response to Tfh-derived signals

It has been recently shown that METTL3/m^{6}A methylation finely modulates IL-7 signaling to ultimately control T-lymphocyte proliferation and differentiation (Li, Tong, et al. 2017). We hypothesized that m^{6}A mRNA methylation could regulate analogous processes in B cells. In particular, we decided to focus our investigations on the study of mature B cells responding to CD40 ligation and IL-21 stimulation. The importance to study the role of m^{6}A mRNA methylation in B cells receiving costimulatory signals through the IL-21 and the CD40 receptors, resides in the crucial role of the interaction between CD40L/IL-21-expressing Tfh cells and antigen-selected B cells in the LZ of the GC reaction in the following processes: i) to favor B cell LZ to DZ re-entry, ii) to establish the DZ B cell proliferative potential (Gitlin et al. 2015) and iii) for controlling PC differentiation (Victora et al. 2010).

3.2.1. The iGB culture is a suitable system to study proliferative responses and developmental trajectories of antigen-selected light zone GC B cells

An *in vitro* experimental system that is suitable to genetic manipulation and which allows close monitoring of the response of primary B cells to Tfh-derived CD40L/IL-21 signals is represented by the so-called "*in vitro*-induced germinal center B (iGB) cell culture system". The iGB culture consists of *ex-vivo* isolated resting naïve murine B cells seeded for up to 13 days onto a BALB/c3T3 fibroblast feeder layer (also called 40LB cells) engineered to constitutively express the soluble B-cell survival factor BAFF, and membrane-bound CD40L (Figure 16a). Exposure of CD40-activated B cells, for the first four days of the culture to IL-4, sustains vigorous cell proliferation and triggers AID-dependent immunoglobulin CSR to IgG1 and IgE (Figure 16b and data not shown). Upon replacement on day-4 of the culture of IL-4 with IL-21, B cells undergo further five to six rounds of cell divisions before completing, in a fraction of cells, a developmental program that leads to the appearance of terminally differentiated plasmablasts (PBs). The latter are short-lived cells which express high levels of the transcription factor IRF4, in combination with the PC surface marker syndecan-1/CD138 (Figure 16b).
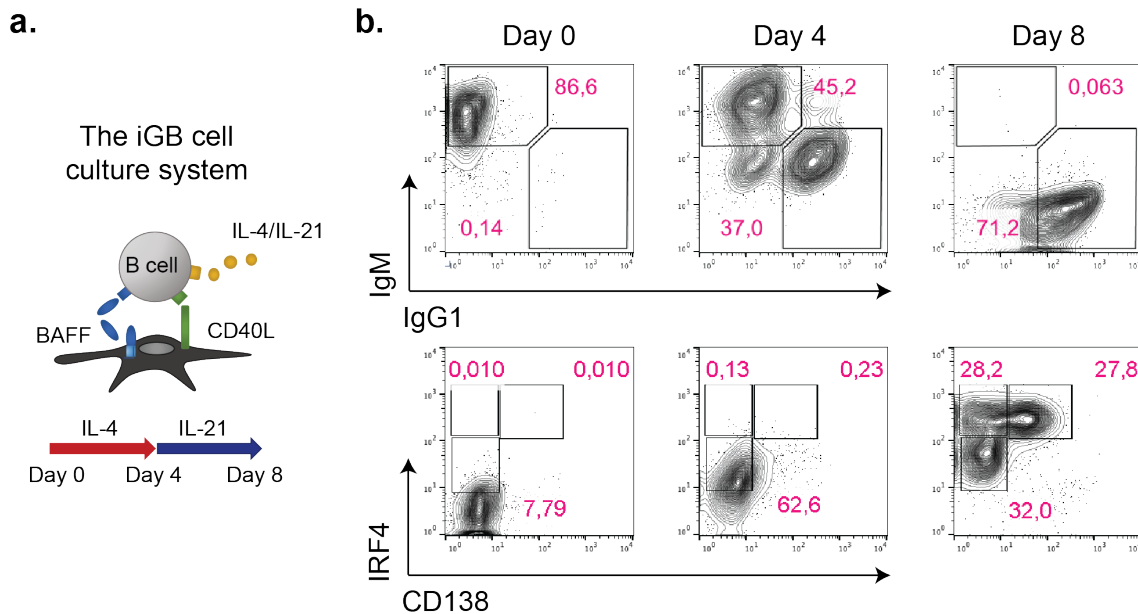
Figure 16. The *in vitro*-induced germinal center B cell culture system.

a. Schematic representation of the iGB culture, where naïve B cells are cultured on a feeder layer, engineered to express both BAFF and CD40L (named 40LB cells), in the presence of IL-4, for the first four days, and IL-21 for the last four days of culture. **b.** Flow cytometric analysis of control B cells isolated from a C57BL/6J mouse (day 0) and activated *in vitro* in the iGB culture (day 4 and day 8). FACS data refer to iGB cells analyzed at the indicated day of the culture, assessing for iGB cells undergoing IgG1 isotype class switching (top panel) or upregulating the plasma cell markers IRF4 and CD138 (bottom panel). A representative case of 5 independent experiments is shown.

A comprehensive immunophenotypic analysis of iGB cells at different days of the culture highlighted a remarkable similarity with LZ GC B cells, which have received T-cell help through the CD40L/CD40 axis. Similarly to GC B cells, iGB cells displayed heightened binding to peanut agglutinin (PNA) and responded to CD40 engagement by upregulating expression on the surface of MHC class II (MHC-II) molecules, the costimulatory receptors CD80 and CD86 and the pro-apoptotic receptor CD95/Fas (Figure 17a). Replacement of IL-4 with IL-21 at day-4 of the culture induced in iGB cells a further (modest) increase in PNA binding and in surface MHC-II and CD86 levels (Figure 17a). In contrast, expression of the CD95/Fas receptor showed a substantial downregulation by day-8, when compared to B cells at day-4 of the culture (Figure 17a).
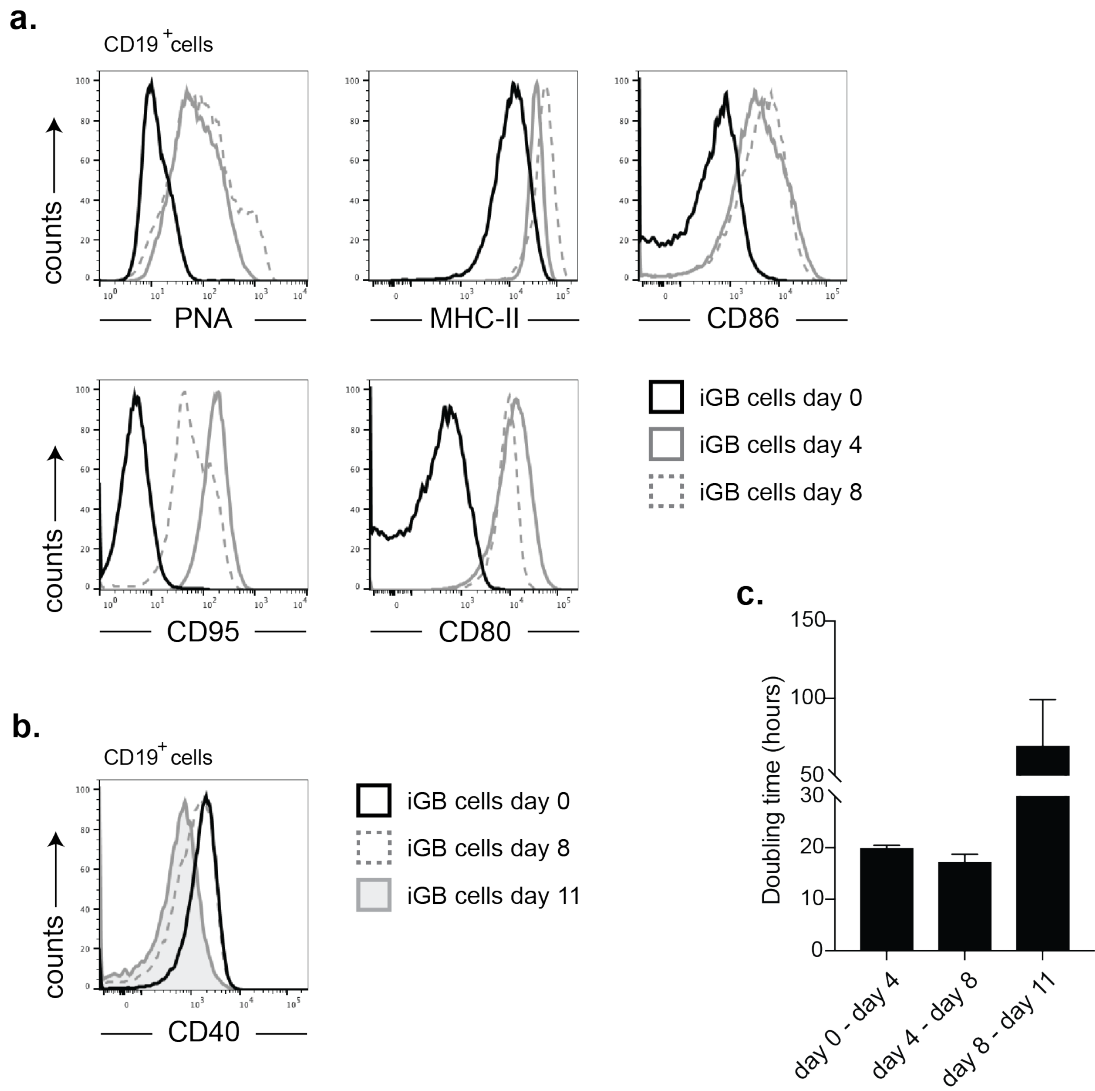
Figure 17. iGB cells reproduce immunophenotypic and proliferative responses of LZ GC B cells.

a. Flow cytometric analysis of PNA, MHC-II, CD86, CD95/Fas and CD80 expression in C57BL/6J splenic naïve B cells (iGB cells day 0, black not filled), iGB cells at day 4 (grey, not filled) and day 8 (grey, not filled, dashed line) of the iGB culture. Cells were pre-gated on CD19+ cells. A representative case of 3 independent experiments is shown. **b.** Flow cytometric analysis of CD40 expression in splenic naïve B cells (iGB cells day 0, black not filled), iGB cells at day 8 (grey, not filled, dashed line) and day 11 (grey, filled) of the iGB culture. Cells were pre-gated on CD19+ cells. A representative case of 3 independent experiments is shown. **c.** Doubling time (hours) of wild-type iGB cells measured in the following time-intervals: i) day 0 – day 4; ii) day 4 – day 8; iii) day 8 – day 11, respectively. Columns represent the mean (n = 4) values, ± SD.

This result is in agreement with the observation that expression of the CD40 receptor (which induces expression of the *Cd95/Fas* gene) is strongly downregulated in B cells at later timepoints of the iGB culture, in particular at day-11, when compared to unstimulated mature B cells (Figure 17b).

Based on growth curve analyses, iGB cells stimulated for the first four days through CD40 receptor in the presence of IL-4 displayed an average doubling time of 17 hours (Figure 17c). Replacement of IL-4 with IL-21 at day-4 of the culture, together with a refreshment of the 40LB feeder support, promoted a second phase of intense cell proliferation that gradually diminished and finally ceased by day-11 of the iGB culture, concomitantly with the loss of the CD40 receptor expression, and activation of terminal differentiation program (Figure 17c). Altogether, these data show that iGB cells reproduce, to a great extent, the complexity of the B cell immunophenotypic, proliferative and differentiation responses, featured by antigen-selected LZ GC B cells interacting with Tfh cells.

3.2.2. Components and activity of the m^{6}A methyltransferase complex are temporally modulated in the iGB culture

To start investigating the importance of m^{6}A mRNA methylation in B cells receiving T-cell help, we measured, by immunoblotting analysis, the expression of the main subunits of the m^{6}A methyltransferase complex, METTL3 and METTL14, in iGB cells. Upon engagement of the CD40 receptor, in the presence of BAFF and IL-4 for four days, iGB cells showed a reproducible increase in both METTL3 and METTL14 protein levels, which ranged between 0.5- and 1.5-fold, respectively, when compared to resting naïve B cells (Figure 18a). Replacement of IL-4 with IL-21, together with a new round of CD40L/BAFF stimulation, sustained the upregulation of the METTL3 and METTL14 protein levels in iGB cells, yet to a weaker extent than the one measured in the first four days of the culture (Figure 18a). Complementary to such analyses, I quantified by colorimetric assay the levels of m^{6}A mRNA methylation from total RNA samples extracted from iGB cells at different timepoints of the culture (Figure 18b).
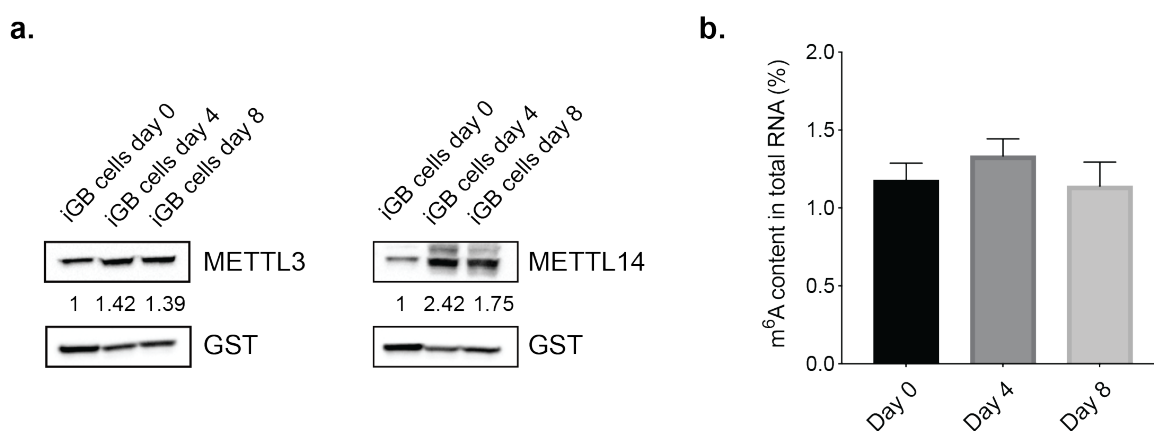
Figure 18. METTL3/METTL14 expression and m^{6}A levels at different timepoints of the iGB culture.

a. Immunoblotting analysis of METTL3 and METTL14 protein levels in control naïve B cells (day 0), and in iGB cells collected at day 4 and 8 of the iGB culture, respectively. Each lane contains the same number of cells. Numbers refer to METTL3/METTL14 protein levels shown as relative to those measured in naïve B cells (day 0). A representative case of at least 3 independent experiments is shown. **b.** Quantification by colorimetric assay of m^{6}A RNA methylation in total RNA extracted from control iGB cells at day 0, 4 and 8 of the culture. The frequency (%) of m^{6}A modification in total RNA extracted from iGB cells at the indicated timepoint is shown. Columns represent the mean (n = 3 independent iGB cultures) values, ± SD.

This analysis revealed an increase in the levels of m^{6}A-marked RNA molecules in iGB cells stimulated for the first four days with CD40L + BAFF + IL-4 (Figure 18b). Conversely, replacement, at day-4 of the culture, of IL-4 with IL-21, under conditions of persistent stimulation with CD40L + BAFF, caused a reduction in m^{6}A-marked transcripts in iGB cells analyzed at day-8 after the initial seeding of the cells (Figure 18b). These results indicate that CD40 engagement on B cells, in the presence of BAFF and IL-4, causes a transient upregulation of crucial components of the m^{6}A methyltransferase complex, which is linked to a transient increase in total m^{6}A RNA levels. Instead, exhaustion of the proliferative potential of CD40-activated B cells, accompanied by IL-21-induced terminal differentiation, is associated with a reduction in METTL3/METTL14 expression and lower m^{6}A deposition onto target transcripts. Altogether, these results establish a scenario whereby incremented m^{6}A-mediated mRNA tagging accompanies the proliferative phase of LZ GC B cells that have just received Tfh co-stimulation through the CD40/CD40L axis. Our data also suggest that induction of terminal differentiation imposed by IL-21 stimulation, and the consequent exit from cell-cycle, is accompanied by a reduction in m^{6}A mRNA methylation.

3.2.3. Opposite regulation on METTL3 expression by CD40L and IL-21 stimulation in iGB cells

To understand the individual contribution of IL-21 and CD40 signaling to the regulation of METTL3 expression, *ex vivo* isolated naïve B cells were cultured for four days onto CD40L-expressing 40LB cells in the presence of IL-4. After that, cells were diluted and freshly re-plated under different culture conditions as represented in the cartoon displayed in Figure 19a. Specifically, B cells received: 1) membrane-bound CD40L, expressed by 40LB cells, and soluble IL-21 (condition A); 2) membrane-bound CD40L (condition B); 3) soluble IL-21 (condition C); 4) membrane-bound CD40L and IL-21 for two days, followed by deprivation of all stimuli (condition D); 5) membrane-bound CD40L and IL-21 for two days, followed by soluble IL-21 stimulation only (condition E) (Figure 19a).

Measurements of the fold expansion of iGB cells stimulated under the different experimental conditions described above, revealed that B cells receiving individually CD40L or IL-21 stimuli (conditions B and C) proliferated sub-optimally between day-4 and day-8 of the culture, when compared to their counterparts receiving the combination of stimuli (conditions A, D and E) (Figure 19b). Moreover, flow cytometric analysis performed on day-8 of the culture to monitor the frequency of terminally differentiated IRF4^{hi}CD138^{+} PBs and their IRF4^{hi}CD138^{-} precursors (pPBs), revealed the highest PBs/pPBs ratio in those conditions in which two days of CD40L + IL-21 stimulation were followed by extinction of mitogenic signals imposed on the cells by continuous CD40 engagement (conditions D and E) (Figure 19c).
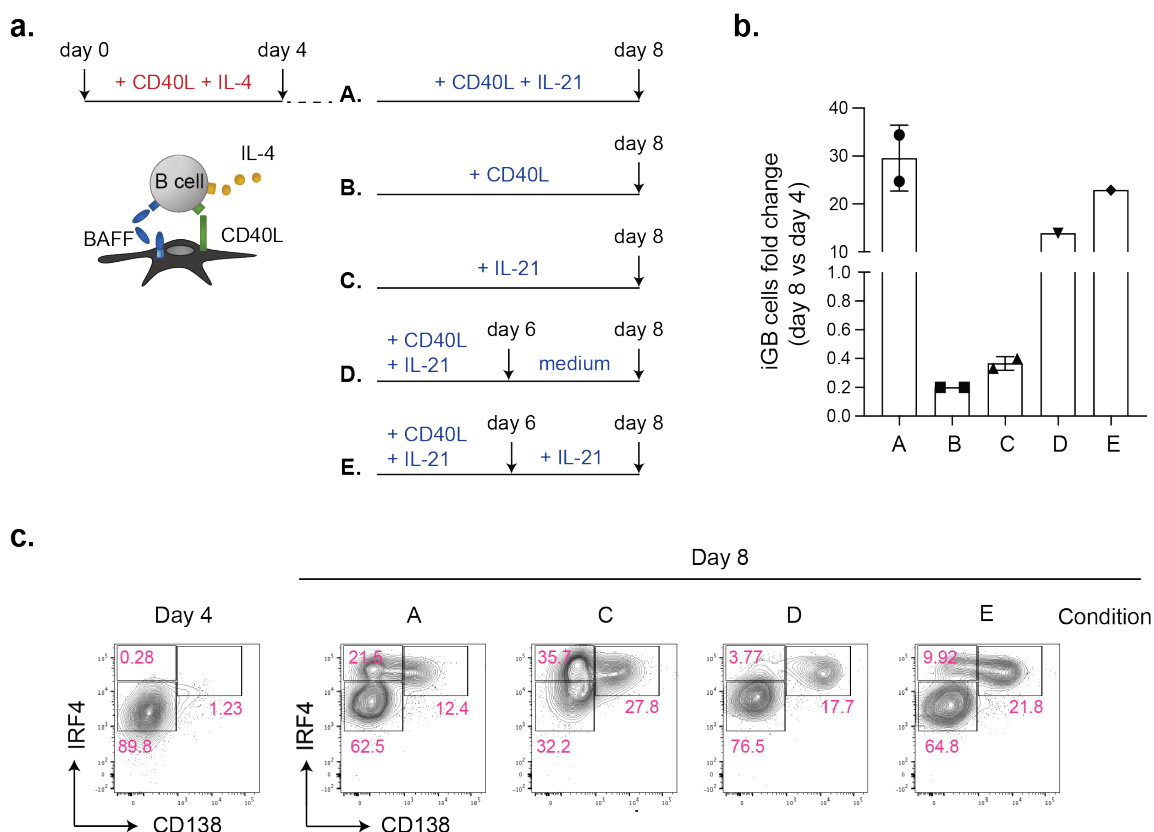
Figure 19. Stimulation settings used to test the contribution of CD40L and IL-21 on *Mettl3* expression.

a. Cartoon depicting the different stimulation settings used to test the contribution of CD40L and IL-21 on *Mettl3* expression in iGB cells. **b.** Fold increase of iGB cell numbers from day 4 to day 8 in cultures undergoing different stimulation conditions. For condition A, B, and C, columns represent the mean (*n* = 2) of technical replicates, ± SD. **c.** Flow cytometric analysis of PC-associated markers IRF4 and CD138 in iGB cells subjected to 4 different

stimulation conditions from day 4 to day 8. Day 4 was included in the analysis to confirm the absence of IRF4^{hi} CD138$^+$ plasmablasts prior to IL-21 stimulation. Numbers indicate percentage of cells in the corresponding quadrants. Data shown are representative of a single experiment.

Immunoblotting analysis of METTL3 protein levels in the bulk of iGB cells receiving the combination of CD40L and IL-21 stimulation in the last four days of the culture (condition A), showed an initial induction (i.e. compare day-4 to day-6 B cells) of the methyltransferase, followed by a subsequent downregulation (i.e. compare day-6 to day-8 B cells) (Figure 20). iGB cells stimulated for the last four days with only CD40L (condition B), displayed a steady upregulation of METTL3 levels (i.e. compare day-4 to day-8 B cells) (Figure 20).

By contrast, B cells cultured in the presence of only soluble IL-21 (condition C) for the last four days of the culture downregulated METTL3 expression at day-8 of the analysis (i.e. compare day-4 to day-8 B cells) (Figure 20). The same result was observed when IL-21 was given alone to iGB cells just for two days (i.e. between day-6 and day-8 of the culture-condition E) (Figure 20). Interestingly, METTL3 downregulation was prevented in iGB cells where abrogation of all stimuli was imposed between day-6 and day-8 of the iGB culture, after full stimulation of the cells for two days with CD40L and IL-21 (condition D) (Figure 20).

Figure 20. CD40L and IL-21 stimulation exert opposite regulation on *Mettl3* expression in iGB cells.

Immunoblotting analysis for METTL3 protein levels in iGB cells undergoing different settings of CD40L and IL-21 stimulation starting from day 4 to day 8. Numbers refer to METTL3 protein levels shown as relative to day 4. The same number of cells was loaded into each lane. Data shown are representative of a single experiment.

Altogether, these data indicate that CD40 ligation and stimulation by IL-21 play antagonistic roles in modulating METTL3 expression in activated B cells. Specifically, whereas the proliferative burst induced in B cells in response to CD40 engagement is accompanied by an induction of METTL3 expression, IL-21 stimulation counteracts this effect favoring the silencing of the m^{6}A mRNA methyltransferase. Overall, these results are compatible with a scenario whereby concomitant stimulation of B cells with CD40L and IL-21 favors an initial wave of robust proliferation, which is accompanied by *Mettl3* induction. Upon exhaustion of the proliferative burst of the iGB cells, which coincides with a downregulation of the CD40 receptor, IL-21-driven signals contribute to the silencing of *Mettl3* expression in cells that are committed to terminally differentiate into PCs.

3.2.4.   IL-21-stimulated iGB cells progressively downregulate *Mettl3* expression

iGB cells analyzed at day-8 of the iGB culture consist of two sub-populations that differ in the expression of the B cell marker CD19 and the PC-associated marker syndecan-1/CD138. Whereas the former represents activated B cells, the latter consists of B cells which have undergone terminal differentiation, becoming PC precursors (PBs).

To determine the relative contribution of the two subsets to the downregulation of METTL3 expression, we purified by cell sorting CD19$^+$ CD138$^{lo/mid}$ activated B cells, and CD19^{lo} CD138$^+$ PBs from day-8 iGB cultures (Figure 21a). In accordance with data shown in Figure 20, immunoblotting analyses revealed that both IRF4^{lo} activated B cells and IRF4^{hi} PBs expressed lower METTL3 levels than those detected in B cells retrieved at day-4/6 of the iGB culture (Figure 21b). Importantly, the lowest levels of *Mettl3* expression were observed in the PBs subset of day-8 iGB cells (Figure 21b). These data indicate that the reduction in METTL3 protein observed in the latest stages of the iGB cultures is mostly contributed by the appearance of terminally differentiated CD138$^+$ PBs.
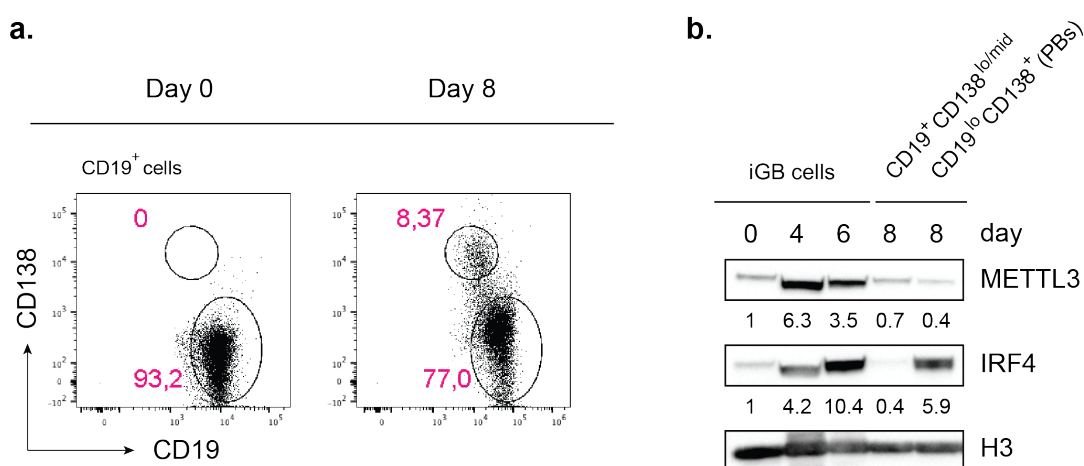
Figure 21. METTL3 expression in CD19$^+$ CD138$^{lo/mid}$ and CD19^{lo} CD138$^+$ iGB cells on day 8.

a. Gating strategy used to sort wild-type CD19$^+$ CD138$^{lo/mid}$ activated B cells and CD19^{lo} CD138$^+$ plasmablasts on day 8. **b.** Immunoblotting analysis of the m6A methyltransferase METTL3 and of the PC transcription factor IRF4, respectively in naïve B cells (day 0), in the bulk of iGB cells at day 4 and 6, and in FACS-sorted CD19$^+$ CD138$^{lo/mid}$ activated B cells and in CD19^{lo} CD138$^+$ plasmablasts (PBs) at day 8. Each lane contains the same number of cells. Numbers refer to METTL3 or IRF4 protein levels shown as relative to that measured at day 0. Data shown are representative of a single experiment.

3.3. Optimization of a CRISPR/Cas9 gene editing protocol to manipulate iGB cells

3.3.1. Activation through membrane-bound CD40L improves B cell infection efficiency

To investigate the role of METTL3 in CD40-activated primary B cells and in IL-21-induced terminal differentiation, we took advantage of a recently published protocol to genetically manipulate iGB cells (Chu, Graf, et al. 2016). The protocol is based on the manipulation of primary resting mature B cells from mice inheriting the Rosa26-Cas9iGFP knock-in allele. In the latter animals, the Cas9 transgene, together with the GFP reporter gene, are ubiquitously and continuously expressed under the control of the Rosa26 promoter (Chu, Weber, et al. 2016). According to the original protocol, *ex vivo* isolated Rosa26-Cas9iGFP splenic B cells are activated *in vitro* for two days, with soluble agonistic α-CD40 antibody plus IL-4, in order to ensure their infectivity with MSCV-based retroviral particles, expressing small guides RNAs (sgRNAs), targeting the gene of interest, together with the puromycin resistance (PuroR) and the blue fluorescent protein (BFP) genes (Chu, Graf, et al. 2016).

To improve the step of B cell activation, and thereby the infection efficiency, we compared the original protocol, based on the treatment of primary B cells with soluble α-CD40, to co-cultures of B cells and 40LB fibroblasts expressing membrane-bound trimeric CD40L. The rationale behind this change in the activation mode stands from previous observation indicating a significantly more potent activation of B cells upon binding of their CD40 receptors to membrane-bound CD40L (mCD40L) (Elmetwali et al. 2020).

Therefore, naïve B cells were activated in parallel for two days with IL-4 plus either soluble α-CD40 or mCD40L. Two days later, B cells were infected with GFP-expressing retroviral particles. Flow cytometric analysis performed 48 hours after infection revealed a substantially higher fraction of GFP-expressing B cells in cultures that had received mCD40L signals (Figure 22a). In addition, B cells infected with GFP-expressing retroviruses in cultures activated with mCD40L, displayed a higher mean fluorescent intensity for the fluorescent reporter, when compared to GFP$^+$ B cells that have been previously activated with soluble α-CD40 (Figure 22b). These results indicate that activation of B cells via mCD40L favors a higher infection rate/cell than when B cells are stimulated with agonistic α-CD40.

Based on these results, I decided to perform all the experiments listed in my thesis employing mCD40L to activate Rosa26-Cas9iGFP B cells, prior to their infection with retroviruses expressing sgRNAs targeting the gene of interest.
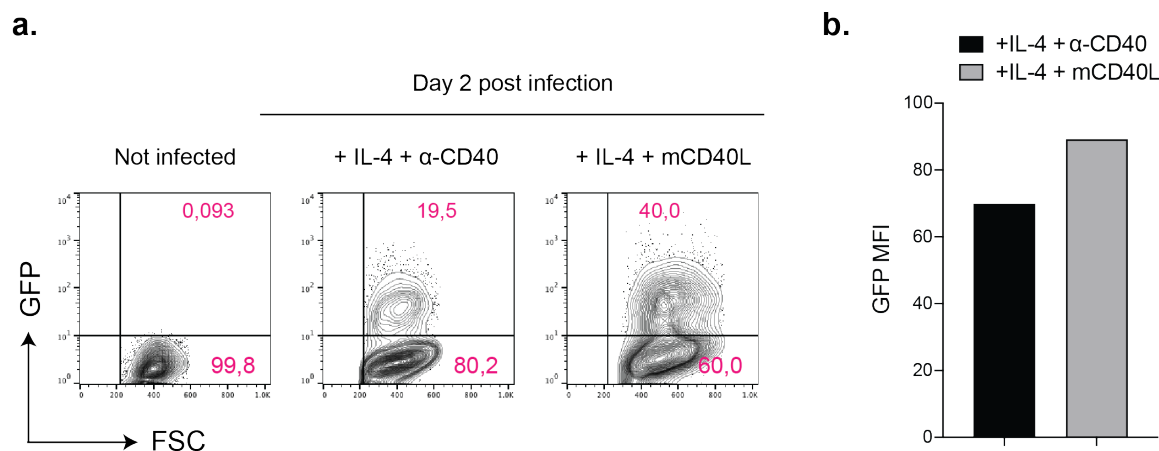
Figure 22. B cell activation through membrane-bound CD40L improves infection efficiency.

a. Flow cytometric analysis of GFP expression (Y axis) in primary B cells measured 2 days after infection with a GFP-expressing viral vector. Before infection, B cells have been activated for 48 hours with IL-4 and either soluble α-CD40 or membrane-bound CD40L (mCD40L), expressed by 40LB cells. Not infected primary B cells were used as negative control. Forward scatter (FSC) in the X axis allows to discriminate cells according on their size. Data shown are representative of a single experiment. **b.** Mean Fluorescent Intensity (MFI) of GFP expression measured in GFP+ B cells which have been infected, 2 days earlier, with a GFP-expressing viral vector. In black, MFI of GFP-expressing B cells which have been activated with IL-4 and soluble α-CD40 for 48 hours before infection; in grey, MFI of GFP-expressing B cells which have been activated with IL-4 and membrane-bound CD40L (mCD40L) for 48 hours before infection.

3.3.2. Optimization of the protocol to study the effect of gene knock-out on CSR

The infection protocol described by Chu et al. included the addition of IL-4 to the culture medium, containing soluble α-CD40, to activate primary B cells prior to infection. However, such experimental setting is expected to initiate AID expression and thereby Ig CSR. Such condition will preclude the possibility to study the effect of Cas9-mediated gene editing on processes linked to AID function, including Ig isotype switching. To overcome such limitation, we activated for two days *ex vivo* isolated splenic primary B cells with mCD40L, in the absence of IL-4.

Under such conditions, B cells retained IgM expression (Figure 23a), whereas B cells activated in the presence of IL-4 displayed a distinct subset of IgG1$^+$ class-switched B cells (Figure 23a). Importantly, the lack of IL-4 in the culture medium during the activation step did not preclude roughly 80% of the B cells from getting infected by a BFP-expressing retroviral vector (Figure 23b). We could also demonstrate that 2 volumes of fresh viral supernatant were sufficient to obtain the highest infection rate (Figure 23b-c) and number of BFP-expressing viral particles/cell (Figure 23b-c), achieved with our improved activation protocol.
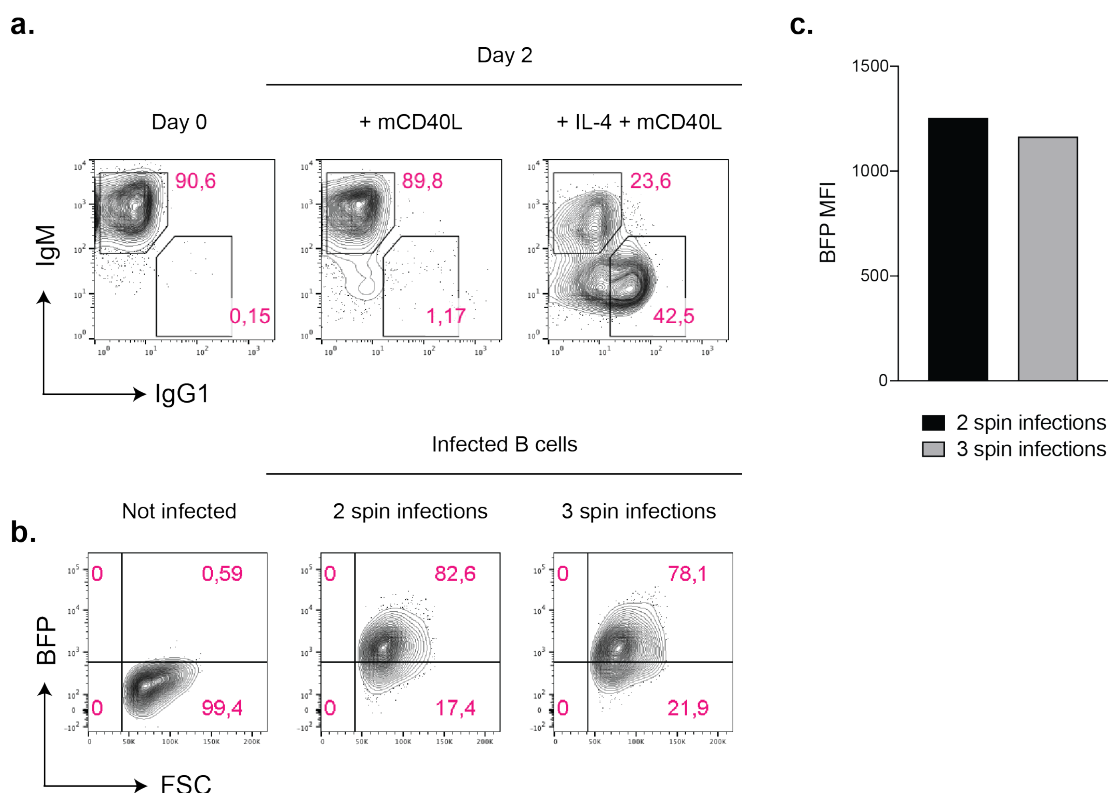
Figure 23. B cell activation in the absence of IL-4 prevents CSR without affecting infection efficiency.

a. Flow cytometric analysis of IgM and IgG1 expression in naïve B cells (day 0) and in B cells activated for two days either with membrane-bound CD40L (mCD40L) or with mCD40L plus IL-4, respectively. A representative case of 3 independent experiments is shown. **b.** Flow cytometric analysis of BFP expression (Y axis) in B cells infected with a BFP-expressing retroviral vector, through either 2 or 3 spin infections, and that had been previously activated for 48 hours in the presence of only mCD40L. Not infected B cells were used as negative control for BFP expression. A representative case of 2 independent experiments is shown. **c.** Mean Fluorescent Intensity (MFI) of BFP expression displayed by BFP$^+$ B cells infected either with 2 (in black) or 3 volumes (in grey) of fresh virus, 2 days after infection.

3.3.3. Validation of the optimized B cell infection protocol

To test the efficiency of Cas9-dependent gene disruption in iGB cells manipulated according to our improved protocol of B cell infection, we chose to disrupt the *Cd38* gene using two sgRNAs previously employed by Chu et al. The experimental scheme is outlined in Figure 24. Specifically, *ex vivo* isolated resting splenic B cells from Rosa26-Cas9iGFP mice were: 1) seeded on 40LB cells for 48 hours, 2) infected with an empty retroviral vector (EV), or with retroviruses expressing *Cd38*-specific sgRNAs, 3) cultured for the first four days onto 40LB cells with IL-4, and 4) for the last four days onto a new layer of 40LB cells with IL-21.
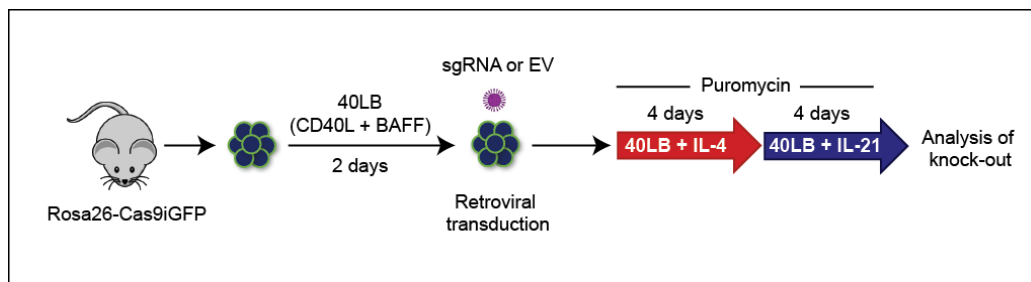
Figure 24. Optimized version of the CRISPR/Cas9-based protocol to genetically manipulate iGB cells.

B cells are purified from the spleen of a Rosa26-Cas9iGFP mouse and activated on 40LB cells for 2 days. Cells are then infected either with empty retroviral particles (EV) expressing the puromycin resistance and the BFP reporter genes or with retroviral vector expressing also the sgRNA targeting the candidate gene. After infection, B cells are activated in the iGB culture to study the effect of gene knock-out on IL-4-induced isotype class switch recombination (CSR) during the first four days, and on IL-21-induced terminal differentiation, during the last four days of culture. Puromycin is added two days after infection to kill all the not infected B cells.

Four days after infection, flow cytometric analysis of infected iGB cells revealed the appearance of respectively 67% (sgRNA #1) and 53% (sgRNA #2) of cells that had strongly downregulated/lost surface CD38 expression in response to Cas9-driven gene editing (Figure 25a). In contrast, all iGB cells infected with the empty vector and analyzed at the same timepoint retained surface CD38 expression.

To confirm Cas9-dependent *Cd38* gene disruption, genomic DNA from iGB cells infected with sgRNA#1-expressing retroviruses, harvested 8 days after infection, was used to amplify by PCR the *Cd38* gene segment targeted by the Cas9 nuclease. Amplicons were cloned and subjected to Sanger sequencing.

Analysis of sequencing results revealed that over 70% of the *Cd38* alleles carried nucleotide deletions (Figure 25b). Specifically, 64% of the alleles carried frameshift mutations, whereas 9% had suffered from in-frame deletions (Figure 25b-c). Altogether, these results indicated that our improved infection protocol was suitable to achieve highly efficient Cas9-dependent gene editing in iGB cells, under conditions preceding the onset of AID expression and function.
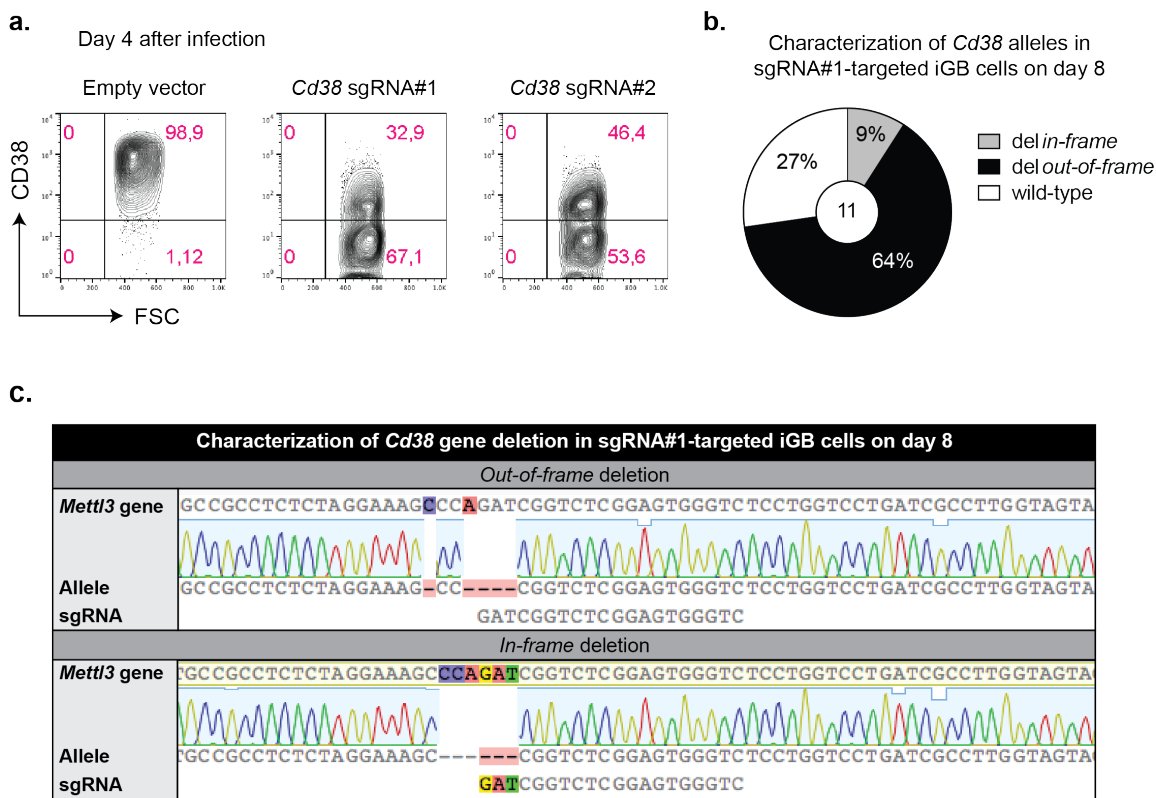
Figure 25. CRISPR/Cas9-mediated *Cd38* gene editing in the iGB culture.

a. Flow cytometric analysis of CD38 surface marker expression (Y axis) measured in Cas9-expressing iGB cells which had been infected, 4 days earlier, either with the empty vector or with one of two independent sgRNAs targeting the *Cd38* gene, respectively. A representative case of three independent experiments is shown. **b.** Pie chart displaying the frequency (among 11 sequences analyzed) of wild-type alleles, in-frame and out-of-frame mutated alleles, amplified from the region of the *Cd38* locus interested by the Cas9 cleavage in iGB cells infected with retroviral particles expressing the sgRNA#1 against the *Cd38* gene. DNA was extracted from iGB cells harvested 8 days after infection. Results from a representative case of two independent experiments are shown. **c.** Examples of Sanger sequencing results of one out-of-frame (top) and one in-frame (bottom) deletion from two representative *Cd38* mutant alleles amplified from the DNA of sgRNA#1-expressing iGB cells.

3.3.4. Establishment of a Cas9-expressing cell line to screen for the best sgRNAs

Despite the availability of a growing number of open source algorithms developed to select the best sgRNAs suitable for Cas9-driven gene editing, the yet limited knowledge of the molecular mechanisms controlling sgRNA-mediated Cas9-recruitment to target sites, hampers their predictive value. To overcome this, we decided to generate a Cas9-constitutively-expressing cell line with which we could rapidly compare the efficiency of Cas9-driven gene editing using different candidate sgRNAs targeting the gene of interest. For this, we chose the murine NG108-15 neuroblastoma cell line, based on the high transfection rate using the PEI method. Specifically, NG108-15 were infected with the Cas9-2A-Blast lentiviral vector, expressing the Cas9 nuclease together with the blasticidin resistance gene. Two days after infection, cells were subjected to blasticidin selection for 10 days, followed by cloning of the resistant cells using the limiting dilution assay (Figure 26a). With this approach we established six independent NG108-15 Cas9-expressing clones. Among the latter, clone #4 was chosen for testing of sgRNAs targeting performance, based on intermediate expression level of Cas9 protein in cells that retained normal proliferative potential (Figure 26a). In order to identify the two best sgRNAs targeting the *Mettl3* gene, we took advantage of the CrispRGold algorithm to select four sgRNAs targeting the first four exons of the gene (Figure 26b). These sgRNAs were individually cloned into retroviruses bearing BFP and puromycin resistance gene cassettes. NG108-15 clone #4 cells were transfected either with the empty vector or with plasmids expressing each one of the four *Mettl3*-targeting sgRNAs (Figure 26c). Two days after transfection, cells were selected with puromycin for four days prior to performing immunoblotting analysis for the METTL3 protein (Figure 26c). Quantification of the data revealed that sgRNA #1 and sgRNA #3 showed the strongest downregulation of METTL3 protein levels, reaching respectively 50% and 60% of the levels measured in control cells (Figure 26d).

a.

NG108-15 infected cells

Not infected / Infected pool / Clone 1 / Clone 2 / Clone 3 / Clone 4 / Clone 5 / Clone 6

CAS9

1   1,2   0,2   1   0,9   0,5   2,5

GAPDH

c.

day 0   day 2   day 5   day 7

Trasfection   Start   End of   Assessment of
               puromycin   puromycin   sgRNA-targeting
               selection   selection   efficiency

b.

CrispR Gold

Mettl3	exon	forward sequence (5' - 3')
sgRNA#1	2	CACCGCACGGGACTATCACTACGGA
sgRNA#2	3	CACCGACGCCGTTTCTGCCCTGCGA
sgRNA#3	2	CACCGGACTATCACTACGGAAGGTT
sgRNA#4	1	CACCGGCGAGAGATTGCAGCGGCGA

d.

Clone 4, day 7 after trasfection

CTRL #1 #2 #3 #4   sgRNA

CAS9

METTL3

1   0,5   0,9   0,4   0,8

GAPDH

Figure 26. Generation of a Cas9-expressing cell line to test sgRNAs efficiency.

a. Immunoblotting analysis of the Cas9 nuclease in the pool and in six established clones of NG108-15 cells infected with a lentiviral vector expressing both the Cas9 gene and the blasticidin resistance gene. Numbers refer to Cas9 protein levels normalized to GAPDH loading control and shown as relative to those measured in the infected pool. **b.** Selection of four sgRNAs designed with CrispRGold, targeting the murine *Mettl3* gene. **c.** Schematic representation of the experimental workflow applied to test the editing efficiency of the 4 sgRNAs targeting the *Mettl3* gene in Cas9-expressing NG108-15 clone 4 cells. **d.** Immunoblotting analysis of METTL3 protein measured in Cas9-expressing NG108-15 clone 4 cells transfected either with the empty vector (CTRL) or with vectors expressing one of the four *Mettl3*-targeting sgRNAs (#1, #2, #3 or #4), 7 days after transfection. Numbers refer to METTL3 protein levels normalized to GAPDH loading control and shown as relative to those measured in CTRL cells.

3.4. Assessment of *Mettl3* gene deletion in GC-like B cells *in vitro*

3.4.1. Disruption of the *Mettl3* gene in iGB cells by CRISPR/Cas9 technology

To study the role of *Mettl3* in CD40-driven B cell activation and IL-21-driven terminal differentiation, we applied the optimized primary B cell infection protocol and conducted iGB cultures as described in Figure 27.
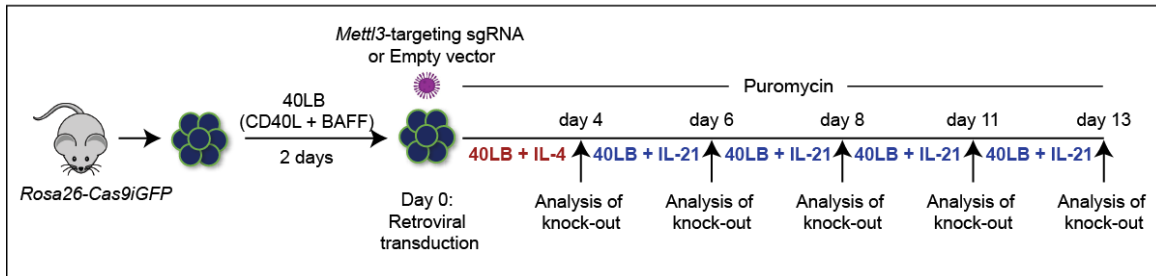
Figure 27. Experimental workflow of CRISPR/Cas9-mediated *Mettl3*-gene editing in iGB cells.

Splenic B cells isolated from Cas9 transgenic mice are activated for two days on 40LB feeder cells. Two days after activation, iGB cells are transduced either with the empty vector or with retroviral particles expressing one of two independent sgRNAs against the *Mettl3* gene, together with the puromycin resistance and the BFP reporter genes. At the end of infection, B cells are plated on a new 40LB feeder layer. IL-4 and puromycin are added one and two days later, respectively. Four days after infection, IL-4 is replaced with IL-21. Cells are then analyzed at different timepoints to study the effect of METTL3 loss on IL-21-induced terminal differentiation.

Specifically, splenic Cas9-expressing B cells were activated *in vitro* for two days by culturing them onto 40LB feeder cells expressing mCD40L and BAFF. Two days later, activated B cells were infected with retroviral particles expressing either of two sgRNAs (sgRNA #1 or #3) targeting exon-2 of the *Mettl3* gene, together with the BFP reporter and the puromycin resistance genes. As control of the experiment, iGB cells were infected in parallel with BFP-PuroR-expressing retroviral vectors lacking sgRNAs (hereafter called empty vector, EV). Infected B cells were plated onto new 40LB feeder cells and 24 hours after infection, IL-4 was added to the culture medium as previously described (Nojima et al. 2011). Puromycin was added to the medium one day later (i.e. 48 hours post-infection), in order to positively enrich for gene-edited B cells.

Four days after infection and two days after the start of puromycin selection, B cells were collected for the first timepoint to determine the extent of *Mettl3* gene disruption and the effects of putative METTL3 inactivation on Ig CSR. On day-4 of the culture, infected iGB cells were counted, diluted and seeded onto new 40LB cells replacing IL-4 with IL-21 in the culture medium. Depending on the purpose of the experiment, *Mettl3*-targeted iGB cells were collected at day-6, -8, -11 and -13 after the initial infection, as described in Figure 27.

3.4.2. Monitoring the efficiency of primary B cell infection with retroviral vectors expressing *Mettl3*-targeting sgRNAs

The availability of the BPF reporter gene allowed us to monitor at single-cell level, by flow cytometry, the percentage of B cells that successfully got infected with retroviral vectors expressing *Mettl3*-targeting sgRNAs. Four days after infection, including two days of puromycin selection, around 90% of the cells expressed the BFP reporter gene (Figure 28). Percentages of BFP-expressing cells increased on day-6 of the culture, reaching over 90% of infection rate, and remained then after stable (Figure 28). These results indicate that infection and selection of iGB cells, according to the improved protocol described in paragraph 3.3, allows the entire population of primary CD40-activated B cells to remain infected at least until day-8 of the iGB culture. Importantly, at day-8 after infection, we did not observe major differences in the frequency of BFP-expressing iGB cells between cultures infected with EV and those expressing sgRNAs targeting the *Mettl3* gene.
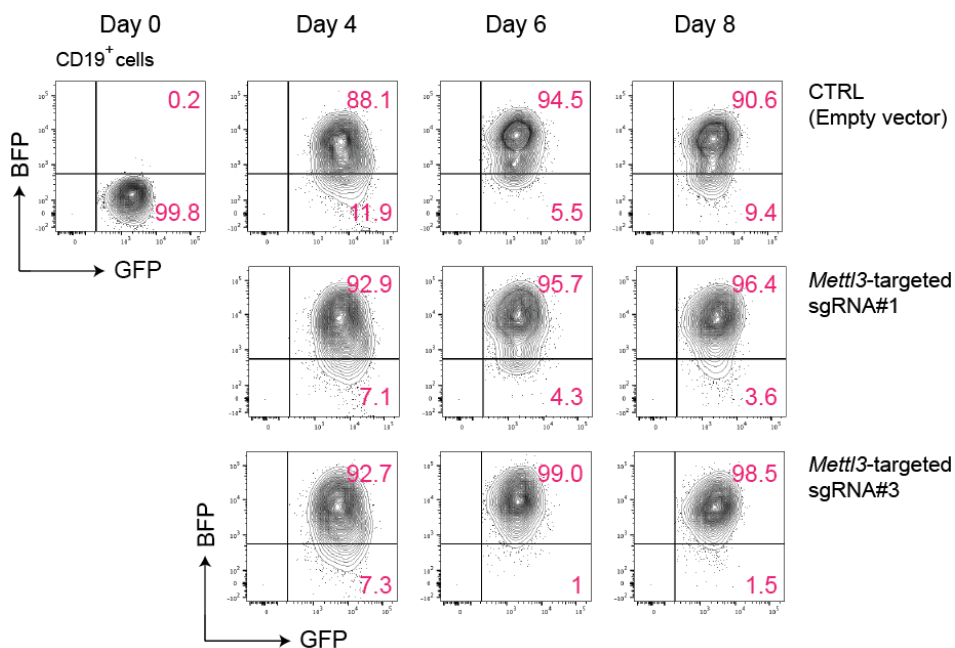
Figure 28. BFP expression in infected Cas9-expressing iGB cells over time.

Flow cytometric analysis of BFP (Y axis) reporter expression in Rosa26-Cas9iGFP iGB cells infected either with the empty vector (CTRL) or with retroviruses expressing one of the two independent sgRNAs targeting the *Mettl3* gene. BFP expression was measured at day 4, 6 and 8 after infection. Day 0 is shown as negative control for BFP expression. A representative case of 7 independent experiments is shown.

3.4.3. Determination of *Mettl3* gene disruption in iGB cultures

To determine the degree of *Mettl3* gene disruption in iGB cells expressing sgRNA#1 or #3, we performed the T7 endonuclease surveyor assay. Specifically, genomic DNA extracted from these cells at day 8 after infection, was subjected to PCR amplification using primers annealing, respectively, proximally and distally to the Cas9 cleavage onto the *Mettl3* gene (Figure 29). Heat denaturation of the amplicons was followed by renaturation of the double-stranded DNA molecules. Exposure of renatured DNA fragments to the T7 endonuclease enzyme led to the specific recognition and cleavage of heteroduplexes at mismatch(es) sites. Finally, PCR fragments were subjected to agarose gel electrophoresis to visualize the digested DNA products. As shown in Figure 29, the vast majority of the full-length PCR products, obtained from genomic DNA retrieved from iGB cells expressing sgRNA#1 and #3, which had been exposed to T7 endonuclease, was cleaved into smaller fragments. Instead, DNA retrieved from iGB control cultures (CTRL), which had been infected with the empty vector, gave rise to *Mettl3* amplicons that were fully resistant to T7-digestion.
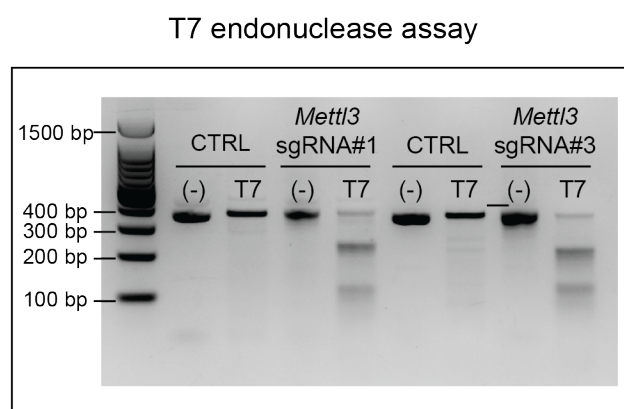
Figure 29. T7 endonuclease surveyor assay to assess *Mettl3* gene disruption in iGB cells.

PCR products amplifying the region of the *Mettl3* locus interested by the Cas9 cleavage and obtained from Cas9-expressing iGB cells, infected either with the empty vector (CTRL) or with retroviral particles expressing sgRNA#1 or sgRNA#3, were subjected to denaturation and renaturation steps, followed by incubation with the T7 endonuclease enzyme (T7). In the presence of mismatches, T7 enzyme will cut the amplicon at the site of mismatch, leading to the formation of two smaller fragments. Digested products were then analyzed by agarose gel electrophoresis. Aliquots of PCR products which were not digested with T7 (-) acted as negative controls. A representative case of at least 3 independent experiments is shown.

To characterize in more detail the nature of Cas9-driven mutations into the *Mettl3* gene in iGB cells, DNA extracted from iGB cells expressing sgRNA#1 and harvested 8 days after infection, was used as template to amplify the region of the *Mettl3* locus interested by the Cas9 cleavage (Figure 30a). PCR amplicons were cloned and subjected to Sanger sequencing. This analysis revealed that over 90% of the alleles carried insertions and/or deletions into exon-2 of the *Mettl3* gene (Figure 30b). Specifically, of the mutant alleles: 1) 27% carried small insertions/deletions (1 to 5 nucleotides); 2) 21% displayed mid-size deletions (between 6 and 20 nucleotides); 3) 45% carried large-size deletions (between 20 and 50 nucleotides) and 4) 6% had undergone deletions larger than 50 nucleotides (Figure 30c). Analysis of the open reading frame of the mutant alleles, revealed that in 44% of the cases, deletions and/or insertions caused a functional knock-out of the gene (Figure 30d). Instead, in the remaining 56% of the mutant alleles, the original reading frame of the *Mettl3* coding sequence was retained (Figure 30d). These results highlight the high efficiency with which the Cas9 nuclease targeted the *Mettl3* gene in iGB cells. At the same time, it is surprising to observe that over 50% of the mutant alleles (mostly represented by deletions of 50 or more nucleotides) retained the possibility to encode for (some form of) the METTL3 protein. To what extent the mutant METTL3 protein retains catalytic activity remains unknown. These results hypothesize that at least some METTL3 activity is required to ensure iGB cell proliferation and survival.
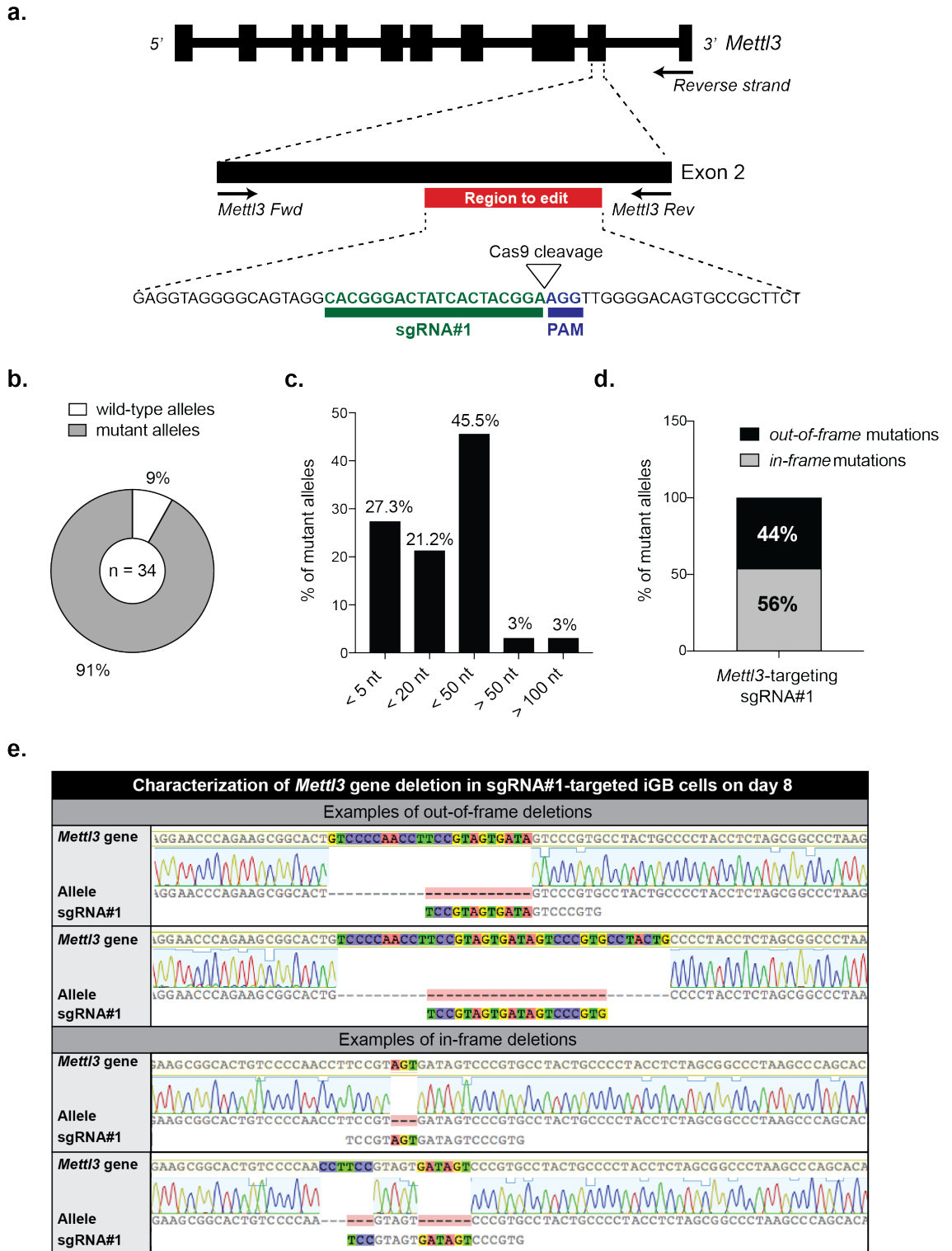
Figure 30. Characterization of *Mettl3* mutant alleles in the bulks of infected iGB cells.

a. Schematic view of the *Mettl3* gene and of the region (in red) in the second exon recognized by the sgRNA#1 and interested by the Cas9 cleavage. The region of the *Mettl3* gene recognized and bound by the sgRNA#1 is indicated in green. The protospacer adjacent motif (PAM), consisting in the three nucleotides downstream to the site interested by the Cas9 cleavage, is indicated in blue. **b.** Pie chart representation of *Mettl3* alleles status among the bulk of iGB cells expressing sgRNA#1. Cells were analyzed at day 8 after infection and 34 sequences

were analyzed. Results from a representative case of 3 independent experiments are shown. **c.** Histograms representing the percentages (%) of alleles carrying insertions and deletions classified according on their size, sequenced from Rosa26-Cas9iGFP iGB cells expressing sgRNA#1. Cells were analyzed at day 8 after infection. Results from a representative case of 3 independent experiments are shown. **d.** Histogram showing percentages (%) of out-of-frame and in-frame mutations on the total of mutant sequenced alleles from sgRNA#1-expressing iGB cells at day 8 after infection. Results from a representative case of 3 independent experiments are shown. **e.** Examples of two out-of-frame (top) and two in-frame (bottom) deletions at the *Mettl3* locus, identified among *Mettl3* mutant alleles, amplified from the bulk of iGB cells infected with retroviral particles expressing the sgRNA#1 and subjected to Sanger sequencing. Cells were analyzed at day 8 after infection. Examples retrieved from a representative case of 3 independent experiments are shown.

3.5. Effects of *Mettl3* gene disruption on mCD40L/BAFF/IL-4-stimulated iGB cells

We first studied the impact of *Mettl3* gene disruption on mCD40L/BAFF + IL-4 stimulation of B cells during the first four days of the iGB culture. To address this point, we determined whether *Mettl3* inactivation influenced the expression of a representative set of surface markers regulated by CD40 signaling, which are crucial for GC B cell survival and cross-talk with Tfh cells. As shown in Figure 31a, flow cytometric analysis revealed comparable expression levels of the surface markers Fas/CD95, CD80 and CD86 between *Mettl3*-control and gene-edited activated iGB cells. These results suggest that sgRNA-infected iGB cells respond normally to CD40 signaling. In agreement with this result, iGB cells expressing either sgRNA#1 or #3, proliferated comparably well to control iGB cells, as assessed by measuring the fold-increase in cell numbers comparing day-0 to day-4 cultures (Figure 31b).
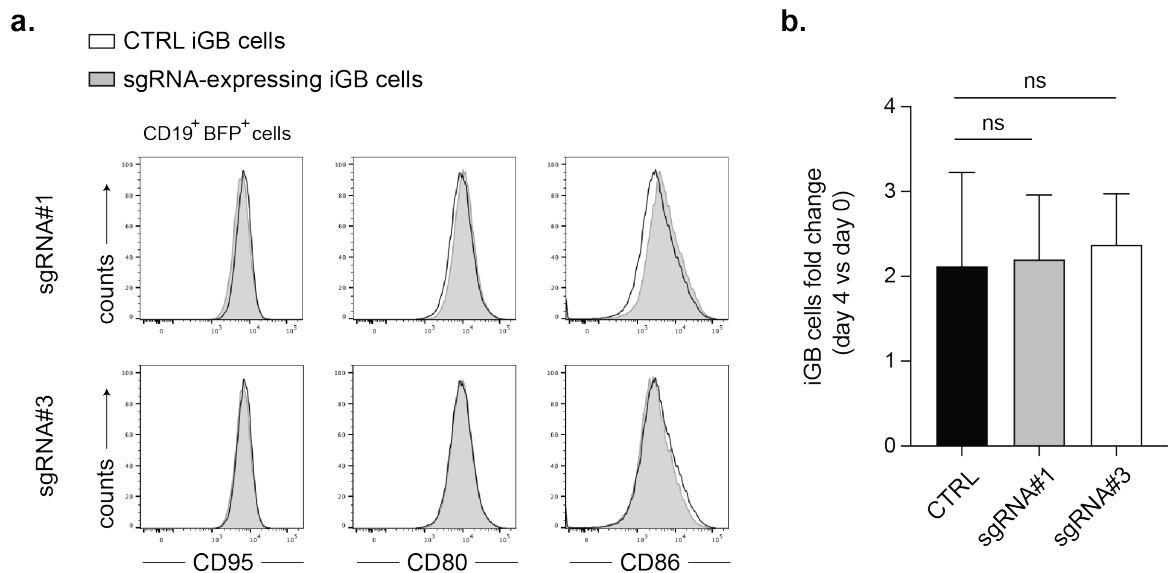
Figure 31. Effects of *Mettl3* gene deletion in mCD40L/IL-4-stimulated iGB cells 4 days after infection.

a. Flow cytometric analysis of CD95/Fas, CD80 and CD86 expression levels in *Mettl3*-deleted iGB cultures (filled grey line), expressing either sgRNA#1 (top) or sgRNA#3 (bottom), 4 days after infection. Comparison of *Mettl3*-deleted iGB cells with *Mettl3*-proficient ones (CTRL, black not filled), is shown. Cells were pre-gated on CD19+ BFP+ cells. A representative case of 5 independent experiments is shown. **b.** Fold change of iGB cell numbers from day 0 to day 4 after infection in iGB cultures infected with the empty vector (CTRL, black) or with retroviral particles expressing either sgRNA#1 (grey) or sgRNA#3 (white), respectively. Columns represent the mean (*n* = 5) values, ± SD. Unpaired Student's *t*-test: sgRNA#1 vs CTRL: ns, *P*-value = 0.9; sgRNA#3 vs CTRL: ns, *P*-value = 0.7.

To study the impact of *Mettl3* gene disruption on mCD40L/IL-4-induced IgG1 isotype switching, we measured by flow cytometry, the fraction of IgG1-expressing B cells four days after stimulation. Flow cytometric analyses revealed similar fractions of IgG1$^+$ B cells between control (CTRL) and *Mettl3*-mutant iGB cultures (Figure 32).
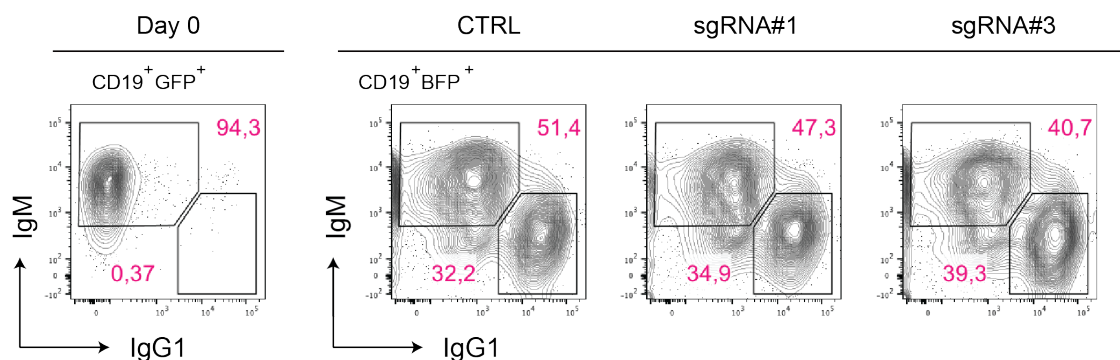
Figure 32. IgG1 isotype switching in *Mettl3*-mutant cultures 4 days after infection.

Flow cytometric analysis of IgM and IgG1 expression measured in the bulk of mCD40L/IL-4-stimulated Cas9-expressing iGB cells, infected either with the empty vector (CTRL) or with retroviral particles expressing one of the two sgRNAs targeting the *Mettl3* gene (sgRNA#1 and sgRNA#3), 4 days after infection, corresponding to 3 days of IL-4 stimulation (right panel). Flow cytometric analysis of iGB cells before infection (day 0, left panel) was included to confirm the absence of IgG1-expressing iGB cells, prior to IL-4 stimulation. Numbers refer to percentages of cells within the quadrant. A representative case of 7 independent experiments is shown.

To determine the degree of *Mettl3* inactivation, we compared, by immunoblotting analysis, METTL3 protein levels in protein extracts retrieved after four days of mCD40L/BAFF/IL-4 stimulation of control and *Mettl3*-mutant iGB cells. As shown in Figure 33, METTL3 protein levels were comparable (if not slightly higher) in the *Mettl3*-mutant iGB cultures, when compared to controls. Combined with the high frequency of *Mettl3* gene disruption events, observed at day-8 of the iGB culture, these results reveal that *Mettl3* mutant iGB cells failed to achieve appreciable downregulation of METTL3 protein levels by the end of the first four days of mCD40L/BAFF/IL-4 stimulation.

These results are compatible with a relatively long half-life of the METTL3 protein in iGB cells, thus preventing us from drawing any conclusion on the contribution of *Mettl3* and m^{6}A mRNA methylation on IL-4 signaling and IgG1 isotype switching.
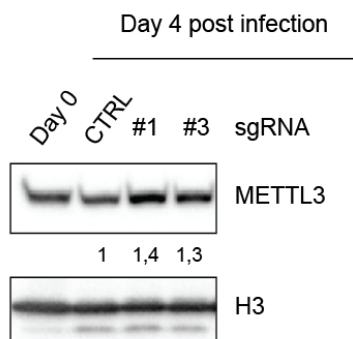
Figure 33. METTL3 protein levels in *Mettl3*-mutant iGB cultures 4 days after infection.

Immunoblotting analysis for METTL3 protein levels in Cas9-expressing iGB cells before infection (day 0), and in Cas9-expressing iGB cells infected either with the empty vector (CTRL) or with retroviral particles expressing one of the two sgRNAs targeting the *Mettl3* gene (sgRNA#1 and #3), 4 days after infection. Numbers refer to METTL3 protein levels normalized to the housekeeping gene H3 and shown as relative of those measured in CTRL cells at the same timepoint. A representative case of at least 3 independent experiments is shown.

3.6. Impact of *Mettl3* gene disruption on mCD40L/IL-21-induced B cell proliferation and terminal differentiation

We hypothesized that extended *in vitro*-culturing, accompanied by further rounds of cell division, would ultimately lead *Mettl3*-defective iGB cells to unravel phenotypic defects associated with the reduction/loss of METTL3 protein and, consequently, m^6A mRNA methylation. Upon replacement of IL-4 with IL-21 in the culture medium and refreshment of the 40LB feeder layer, diluted *Mettl3*-mutant iGB cultures (expressing either sgRNA#1 or #3), analyzed in 9 independent experiments, displayed a substantial contraction in B cell expansion, when compared to control cultures (Figure 34a-c). To prove that the reduced proliferative burst of *Mettl3*-mutant iGB cultures was associated to METTL3 downregulation, we performed immunoblotting analysis on protein extracts retrieved from *Mettl3*-proficient and -mutant cells at day-8 of the *in vitro* culture. Levels of METTL3 protein were consistently reduced in *Mettl3*-mutant iGB cultures, when compared to their proficient counterparts (Figure 34d). However, full extinction of the protein was never achieved, in agreement with the mutational analyses performed at day-8 after infection, shown in Figure 30d.
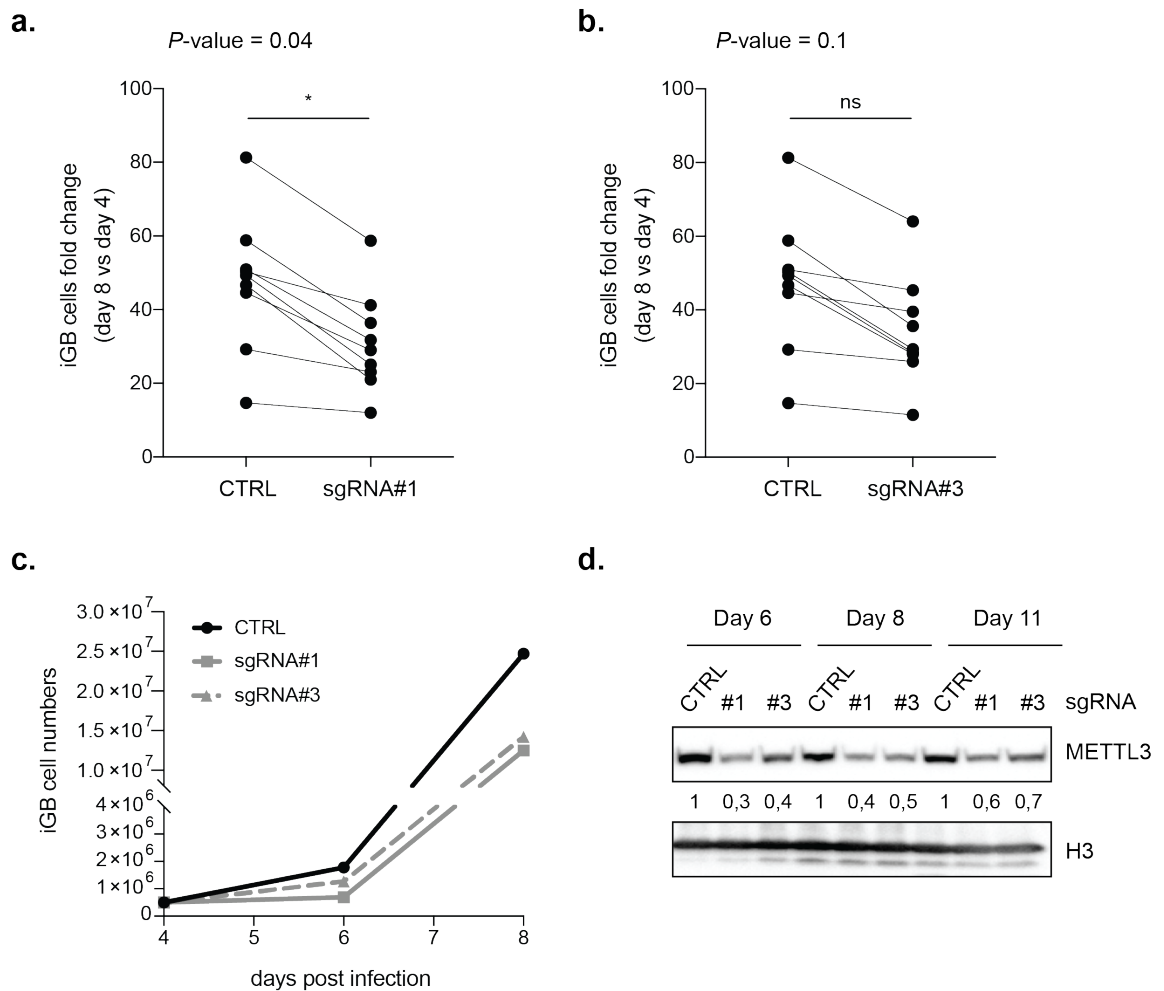
Figure 34. *Mettl3*-mutant iGB cells display reduced mCD40L/IL-21-induced proliferation.

a. Fold change of iGB cell numbers from day 4 to day 8 after infection in control (CTRL, infected with the EV) and sgRNA#1-expressing iGB cultures. Each line represents an independent experiment. Unpaired student's *t*-test: sgRNA#1 vs CTRL: *P-value = 0.04. **b.** Fold change of iGB cell numbers from day 4 to day 8 after infection in control (CTRL, infected with the EV) and sgRNA#3-expressing iGB cultures. Each line represents an independent experiment. Unpaired student's *t*-test: sgRNA#3 vs CTRL: ns, *P*-value = 0.1. **c.** Growth curve of Cas9-expressing iGB cells infected either with the EV (CTRL, in black) or with retroviral particles expressing the sgRNA#1 (in grey) or the sgRNA#3 (in grey, dashed line), analyzed from day 4 to day 8 after infection. A representative case of 7 independent experiments is shown. **d.** METTL3 immunoblotting analysis in Cas9-expressing iGB cells infected either with the EV (CTRL) or with retroviral particles expressing the sgRNA#1 or the sgRNA#3, performed 6, 8 and 11 days after infection, respectively. Numbers refer to METTL3 protein levels normalized to the housekeeping gene H3 and shown as relative to those measured in CTRL cells at the corresponding timepoint. A representative case of 3 independent experiments is shown.

A tighter monitoring of the growth behavior of *Mettl3*-mutant iGB cells within the day-4-to-8

interval of the iGB culture, revealed a striking delay in the growth properties of the mutant

B cells, which was restricted to the first two days of mCD40L + IL-21 stimulation. Indeed, a

significant contraction in the fold-expansion of both *Mettl3*-mutant cultures (sgRNA#1 and

#3), was selectively observed in the interval between day-4 and day-6 of the culture, when

compared to controls B cells (Figure 35a). The growth delay of *Mettl3*-mutant iGB cells was

reflected by a significative increase in the doubling time of the latter cells (Figure 35b).
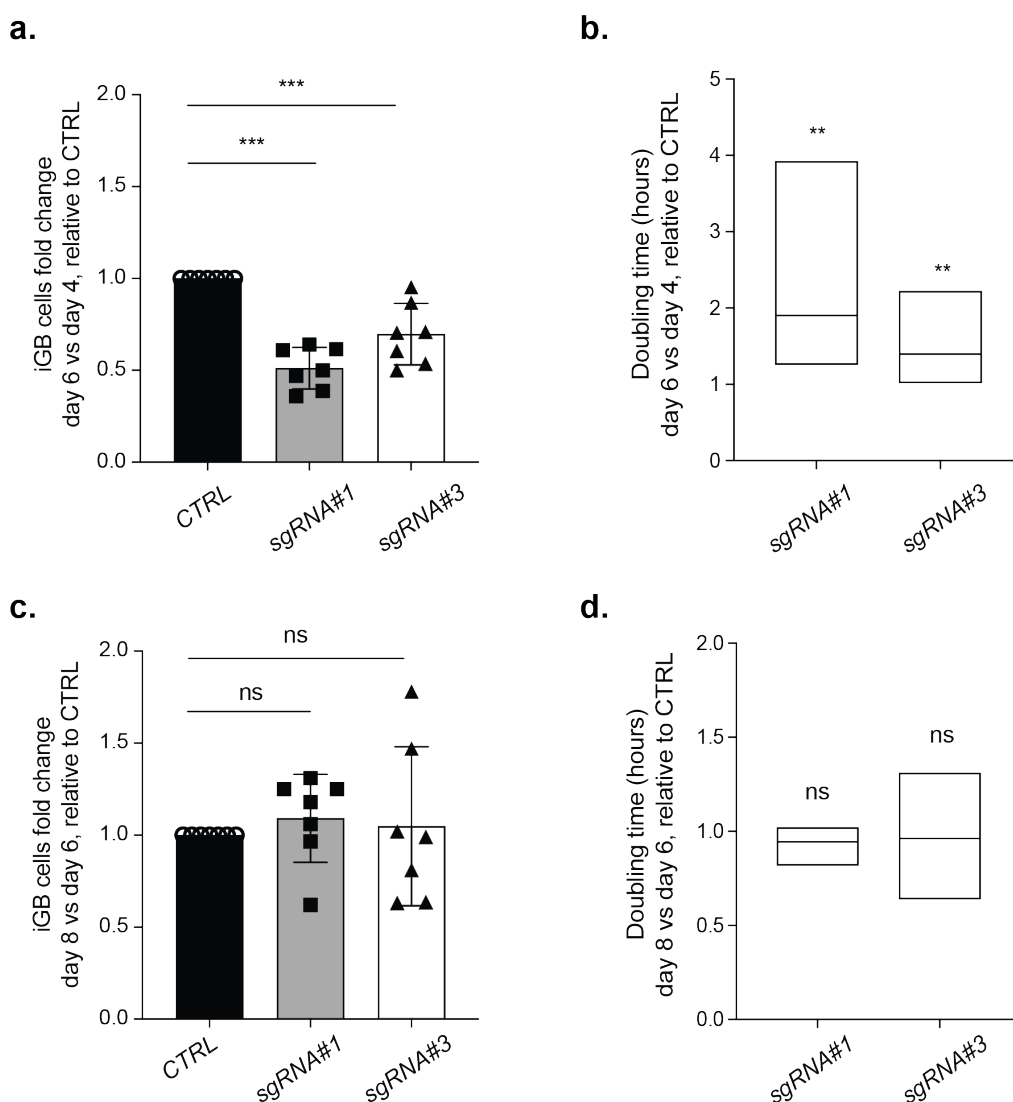
Figure 35. METTL3 knockdown delays the mCD40L/IL-21-induced proliferative burst of iGB cells.

a. Fold change of iGB cell numbers in *Mettl3*-mutant cultures, expressing either sgRNA#1 (in grey) or sgRNA#3

(in white), from day 4 to day 6 after infection, shown as relative to that observed in the corresponding control

culture of the same experiment (CTRL, in black). Columns represents the mean (*n* = 7) values, ± SD. Each

symbol in the column represents an independent experiment. Unpaired Wilcoxon test: sgRNA#1 vs CTRL: ***P-value = 0.001; sgRNA#3 vs CTRL: ***P-value = 0.001. **b.** Doubling time (hours) of *Mettl3*-mutant iGB cells measured from day 4 to day 6 after infection and shown as relative to that displayed by *Mettl3*-proficient cells (CTRL) of the same experiment, in the same time-interval. Extremities of the box indicate the maximum and the minimum values of the set (n = 5). The horizontal line inside each box indicates the mean. Unpaired Wilcoxon test: sgRNA#1 vs CTRL: **P-value = 0.008; sgRNA#3 vs CTRL: **P-value = 0.008. **c.** Fold change of iGB cell numbers in *Mettl3*-mutant cultures, expressing either sgRNA#1 (in grey) or sgRNA#3 (in white), from day 6 to day 8 after infection, shown as relative to that observed in the corresponding control culture of the same experiment (CTRL, in black). Columns represent the mean (n = 7) values, ± SD. Each symbol in the column represents an independent experiment. Unpaired Wilcoxon test: sgRNA#1 vs CTRL: ns, P-value = 0.17; sgRNA#3 vs CTRL: ns, P-value = 0.68. **d.** Doubling time (hours) of *Mettl3*-mutant iGB cells measured from day 6 to day 8 after infection and shown as relative to that displayed by *Mettl3*-proficient cells (CTRL) of the same experiment, in the same time-interval. Extremities of the box indicate the maximum and the minimum values of the set (n = 5). The horizontal line inside each box indicates the mean. Unpaired Wilcoxon test: sgRNA#1 vs CTRL: ns, P-value = 0.29; sgRNA#3 vs CTRL: ns, P-value = 0.66.

The growth delay observed in *Mettl3*-mutant iGB cultures was strikingly normalized in the subsequent two days of mCD40L + IL-21 stimulation (Figure 35c), which was confirmed by the comparable doubling times between *Mettl3*-proficient and -mutant iGB cells (Figure 35d). Altogether, these data establish the strict requirement for *Mettl3* full proficiency in the first 48 hours following B cell activation via CD40 signaling, in the presence of IL-21 stimulation, in order to execute the optimal proliferative program.

3.6.1. METTL3 knockdown delays the IL-21-induced proliferative burst of iGB cells

To establish the impact of METTL3 knockdown on cell-cycle progression, we performed *in vitro* cell-cycle distribution analyses on *Mettl3*-mutant and control iGB cells, respectively after two (day-6 after infection) and four (day-8 after infection) days of mCD40L + IL-21 stimulation (Figure 36a-c).

iGB cells expressing either sgRNA#1 or sgRNA#3, stimulated for 48 hours with mCD40L + IL-21, showed a delay in G_1-to-S transition, as compared to control B cells, in at least two independent experiments (Figure 36a-b). Furthermore, analyses of the Sub-G1 fraction, representative of cells undergoing apoptosis, revealed a higher fraction of the latter cells in *Mettl3*-mutant iGB cultures as compared to *Mettl3*-proficient ones, in three independent experiments (Figure 36d-e). Altogether, these data indicate that *Mettl3* downregulation prevents effective G_1-to-S transition in B cells stimulated for two days with CD40L + IL-21, while increasing at the same time the proportion of cells undergoing programmed cell death.

Cell-cycle distribution analyses on *Mettl3*-proficient and -mutant iGB cells, performed after four days of mCD40L + IL-21 stimulation, provided a strikingly different picture (Figure 36a;c). Indeed, whereas *Mettl3*-proficient B cells consisted of a relatively lower (as compared to day-6) fraction of cells transiting from the G_1-to the S-phase of the cell-cycle, *Mettl3*-mutant iGB cells recuperated the cell-cycle delay seen at day-6 of the culture, showing a larger proportion of S-phase cells (Figure 36a;c).

These results are coherent with a model whereby METTL3 plays a crucial role in the optimization of the initial proliferative burst imposed on cells by concomitant mCD40L + IL-21 stimulation. Upon METTL3 downregulation, mCD40L + IL-21-induced B cell proliferation is delayed, thus, requiring a longer time to complete a pre-defined number of cell divisions, which ultimately trigger cellular senescence or, in a fraction of cells, PC differentiation.
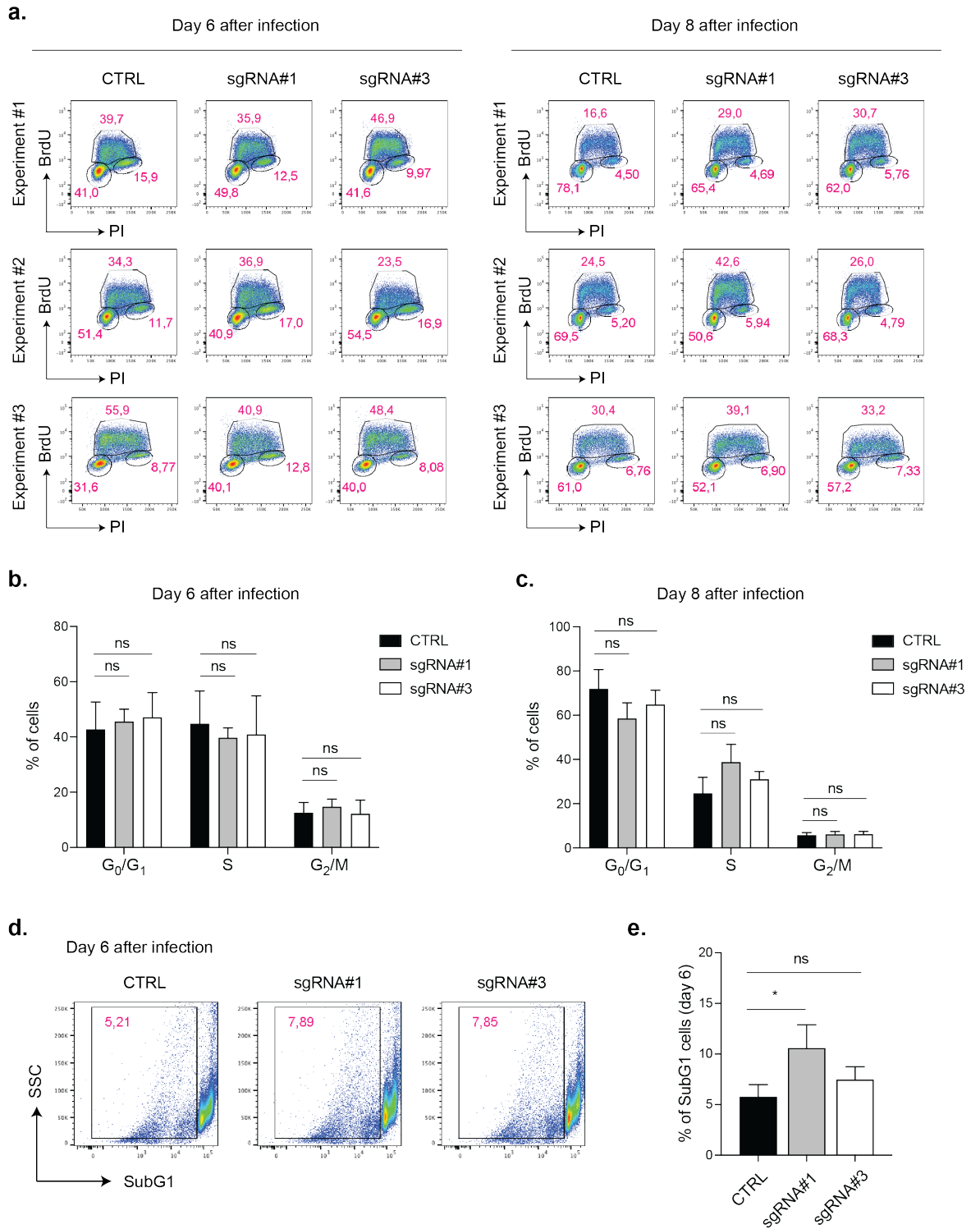
Figure 36. Cell cycle distribution analysis of *Mettl3*-mutant iGB cells.

a. Cell cycle distribution analyses of *Mettl3*-proficient (CTRL) and *Mettl3*-mutant (expressing either sgRNA#1 or sgRNA#3) iGB cells performed at day 6 (left panel) and day 8 (right panel) after infection, from three independent experiments. Cells were stained with propidium iodide (PI, X axis) and pulsed with BrdU (Y axis), 1 hour prior to analysis. Numbers indicate percentage of cells in G_0/G_1 (bottom left), S (top), and G_2/M (bottom right) phases of the cell cycle, respectively. **b.** Summary data on distribution of *Mettl3*-proficient (CTRL, in black) and -mutant iGB cultures, expressing either sgRNA#1 (in grey) or sgRNA#3 (in white), respectively in G_0/G_1, S and G_2/M

phases of the cell cycle, at day 6 after infection. Columns indicate mean (n = 3) values, ± SD. Unpaired student's t-test: sgRNA#1 vs CTRL: ns P-value = 0.7; ns P-value = 0.5; ns P-value = 0.5; sgRNA#3 vs CTRL: ns P-value = 0.6; ns P-value = 0.7; ns P-value = 0.9. **c.** Summary data on distribution of *Mettl3*-proficient (CTRL, in black) and -mutant iGB cultures, expressing either sgRNA#1 (in grey) or sgRNA#3 (in white), respectively in G_0/G_1, S and G_2/M phases of the cell cycle, at day 8 after infection. Columns indicate mean (n = 3) values, ± SD. Unpaired student's t-test: sgRNA#1 vs CTRL: ns P-value = 0.1; ns P-value = 0.09; ns P-value = 0.7; sgRNA#3 vs CTRL: ns P-value = 0.3; ns P-value = 0.2; ns P-value = 0.7. **d.** FACS plots showing the frequency of subG1 cells in *Mettl3*-proficient (CTRL) and *Mettl3*-mutant iGB cultures (expressing either sgRNA#1 or #3) at day 6 after infection. A representative case of 3 independent experiments is shown. **e.** Summary data on the frequency (%) of subG1 cells measured by flow cytometry in control (CTRL, in black) and *Mettl3*-mutant iGB cultures expressing either sgRNA#1 (in grey) or sgRNA#3 (in white), at day 6 after infection. Columns represent mean (n = 3) values, ± SD. Unpaired student's t-test: sgRNA#1 vs CTRL: *P-value = 0.03; sgRNA#3 vs CTRL: ns P-value = 0.2.

In line with this scenario, *Mettl3*-proficient and -hypomorphic day-8 iGB cells displayed similar, yet fairly limited growth, when cultured for further three days onto a new layer of 40LB cells, in the presence of IL-21 (Figure 37).
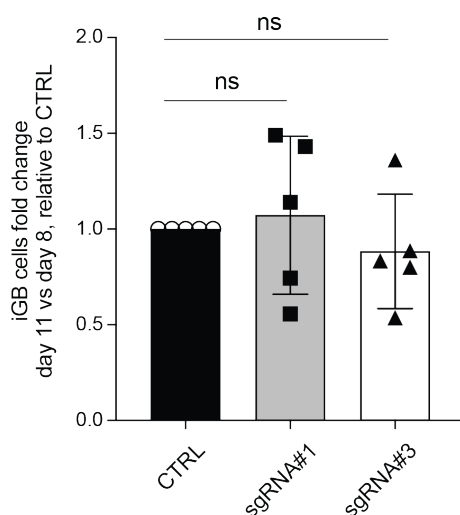
Figure 37. *Mettl3*-mutant iGB cells normalize their proliferative defect in the latest stage of the culture.

Fold change of iGB cell numbers in *Mettl3*-mutant cultures, expressing either sgRNA#1 (in grey) or sgRNA#3 (in white), from day 8 to day 11 after infection, shown as relative to that observed in the corresponding control culture of the same experiment (CTRL, in black). Columns represents the mean (n = 5) values, ± SD. Each symbol in the column represents an independent experiment. Unpaired Wilcoxon test: sgRNA#1 vs CTRL: ns, P-value = 0.6; sgRNA#3 vs CTRL: ns, P-value = 0.07.

3.6.2. *Mettl3*-deleted iGB cells show reduced fitness under competitive settings

We hypothesized that the growth retardation suffered by *Mettl3*-hypomorphic iGB cultures in the first two days of mCD40L + IL-21 stimulation, could exert a detrimental impact on the competitive fitness of the cells if placed in competition with *Mettl3*-proficient ones. This hypothesis has relevance in the context of the GC response, as competitive re-entry into the DZ of antigen-selected LZ GC B cells depends on the strength of the mitogenic signals imposed on B cells by CD40 engagement (Mesin, Ersching, and Victora 2016).

To address the role of *Mettl3* in the fitness of CD40-actived B cells, we performed co-culture experiments where Cas9-expressing naïve B cells (Ly5.2$^+$) were mixed in a 1:1 ratio with Cas9-negative Ly5.1$^+$ congenic B cells (Figure 38). Upon CD40 activation, Ly5.1$^+$/Ly5.2$^+$ B cell mixtures were transduced with retroviral particles expressing either one of two sgRNAs targeting the *Mettl3* locus, or with the empty vector (Figure 38). Transduced cells were cultured for three initial days onto 40LB cells in the presence of IL-4 and puromycin, followed by further four days in which mCD40L was combined to IL-21 stimulation (Figure 38).
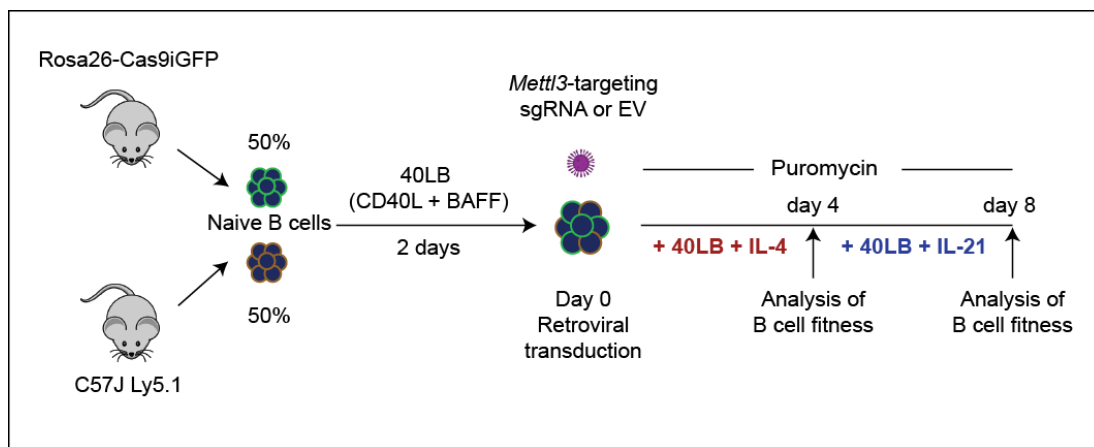
Figure 38. Experimental workflow to study the effect of METTL3 loss on B cell fitness.

Splenic B cells isolated from Rosa26-Cas9iGFP mice (Ly5.2$^+$) and from Ly5.1-expressing mice were mixed in a 1:1 ratio and plated on 40LB cells for two days. After 48 hours of activation, Ly5.2$^+$ and Ly5.1$^+$ cells were infected either with the empty vector or with retroviral particles expressing one of the two independent sgRNAs against the *Mettl3* gene. Further steps followed the previously described protocol. Cells were analyzed on day 4 and 8 after infection.

We took advantage of flow cytometric analyses to separately monitor, in the same culture, the frequency of *Mettl3*-proficient Ly5.1$^+$ B cells and that of their Ly5.2$^+$ *Mettl3*-mutant counterparts. Ly5.2$^+$ B cells infected with the empty vector (and thus representing *Mettl3*-proficient B cells) acted as internal control of the experiment. Comparison of flow cytometric data between day-4 and day-8 of the co-cultures revealed a reproducible roughly 50% reduction of Ly5.2$^+$ transduced B cells expressing either of two sgRNAs against the *Mettl3* gene. Instead, *Mettl3*-proficient Ly5.2$^+$ B cells (infected with the EV) remained equally represented, when comparing day-4 to day-8 co-cultures with *Mettl3*-proficient Ly5.1$^+$ B cells (Figure 39).
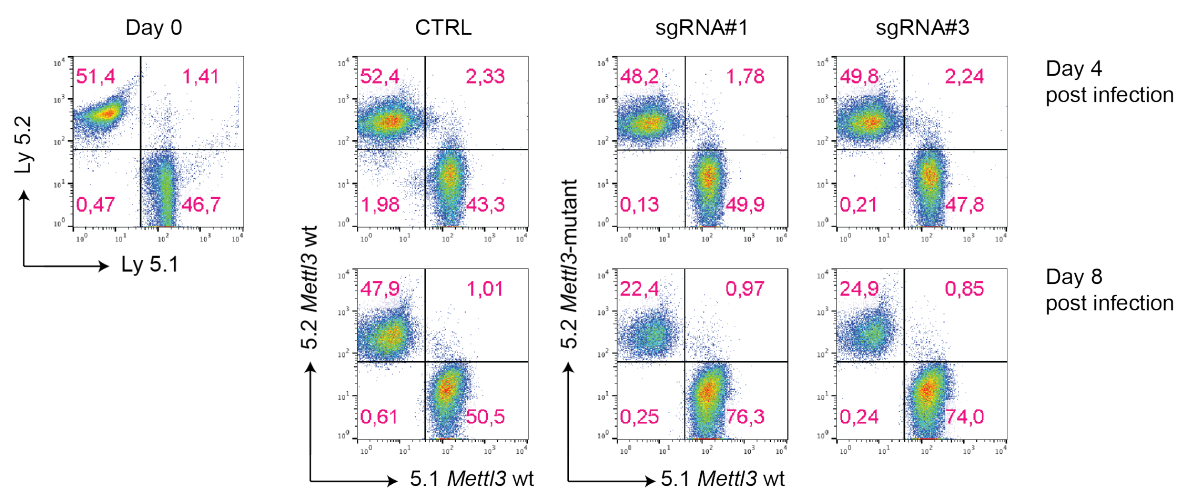
Figure 39. *Mettl3*-mutant iGB cells are counter selected when co-cultured with wild-type cells.

Flow cytometric analysis of Ly5.1$^+$ (X axis) and Ly5.2$^+$ (Y axis) B cells in iGB co-cultures, analyzed before infection (day 0, left panel), and 4 and 8 days later (right panel), respectively. On the right panel: frequency of Ly5.1$^+$ and Ly5.2$^+$ cells in co-cultures of iGB cells infected either with the empty vector (CTRL) or with retroviral particles expressing sgRNA#1 or sgRNA#3, analyzed 4 (top) and 8 (bottom) days after infection. Numbers indicate percentages of cells present within the quadrant. The genotype of the Cas9-expressing (Ly5.2$^+$) iGB cells is indicated on the Y-axis. A representative case of 2 independent experiments is shown.

To determine the status of the *Mettl3* gene, Ly5.1$^+$ and Ly5.2$^+$ iGB cells were FACS-sorted from co-cultures, 6 days after infection, and T7 endonuclease assay was performed on PCR amplicons spanning the portion of the *Mettl3* gene targeted by the sgRNAs. As shown in Figure 40a, T7-digested PCR fragments were solely derived from Ly5.2$^+$ B cells infected with sgRNA-expressing retroviruses. To assess *Mettl3* gene expression in sorted Ly5.1$^+$ and Ly.5.2$^+$ B cells from iGB co-cultures, we performed quantitative RT-PCR analysis (Figure 40b). A reproducible reduction in *Mettl3*-specific transcripts was selectively observed in Ly5.2$^+$ B cells sorted from mixed cultures transduced with retroviruses expressing *Mettl3*-targeting sgRNAs (Figure 40b). Altogether, these results strengthen the hypothesis that METTL3 exerts a crucial role in supporting the competitive growth of mature B cells receiving CD40 agonistic signals in combination with IL-21 stimulation.
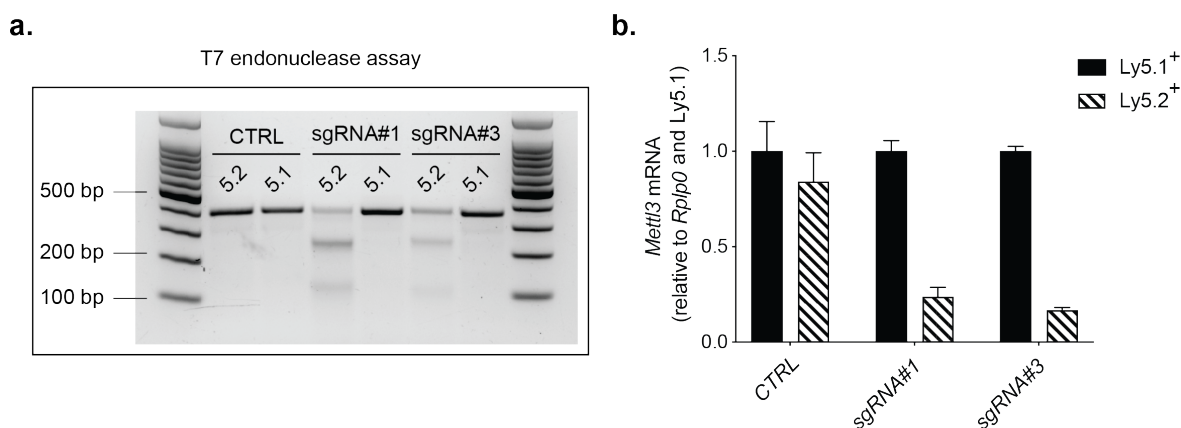
Figure 40. Assessment of *Mettl3* gene disruption in sgRNA-expressing Ly5.2$^+$ cells.

a. T7 endonuclease surveyor assay performed on PCR products covering the *Mettl3*-targeted region, amplified from day 6-FACS-sorted Ly5.1$^+$ and Ly5.2$^+$ iGB cells, respectively from iGB mixed cultures infected either with the empty vector (CTRL) or with retroviral particles expressing one of the two sgRNAs targeting the *Mettl3* gene (sgRNA#1 or sgRNA#3). In the presence of heteroduplexes, T7 enzyme will cut the amplicon at the site of mismatch, leading to the generation of two smaller fragments. **b.** Quantification of *Mettl3*-specific transcript in Ly5.1$^+$ and Ly5.2$^+$ iGB cells sorted from mixed cultures at day 6 after infection. Data refer to *Mettl3* transcript levels normalized to those of the housekeeping gene *Rplp0* and represented as relative to those measured in the Ly5.1$^+$ populations of the control co-culture. Columns indicate the mean *Mettl3* transcript of three technical replicates, ± SD. Data shown are representative of a single experiment.

3.6.3. METTL3 knockdown modestly impairs surface CD40 levels in mCD40L/IL-21-stimulated iGB cells

To examine the effects of METTL3 knockdown on the repertoire of immunomodulatory receptors, expressed on the surface of mCD40L/IL-21-stimulated iGB cells, we performed a comprehensive immunophenotypic screening using a flow cytometric approach.

We then focused our attention on iGB cells retrieved at day-6 after infection, corresponding to two days of mCD40L + IL-21 stimulation. As shown in Figures 41a, intracellular flow cytometric analyses revealed a reproducible downregulation of the METTL3 protein in both *Mettl3*-hypomorphic cultures analyzed after two days of mCD40L + IL-21 stimulation. *Mettl3*-mutant iGB cells retained normal levels of surface CD19 and completed IgG1 isotyping switching comparably well, when compared to their *Mettl3*-proficient counterparts (Figure 41a). Moreover, *Mettl3*-mutant iGB cells displayed a mild, yet reproducible, downregulation of surface CD40 levels (Figure 41b), whereas CD95/Fas and CD86 levels were modestly upregulated (Figure 41c-d), when compared to control iGB cells. No differences were observed in surface CD80 levels between control and *Mettl3*-hypomorphic mCD40L + IL-21-stimulated B cells (Figure 41a).
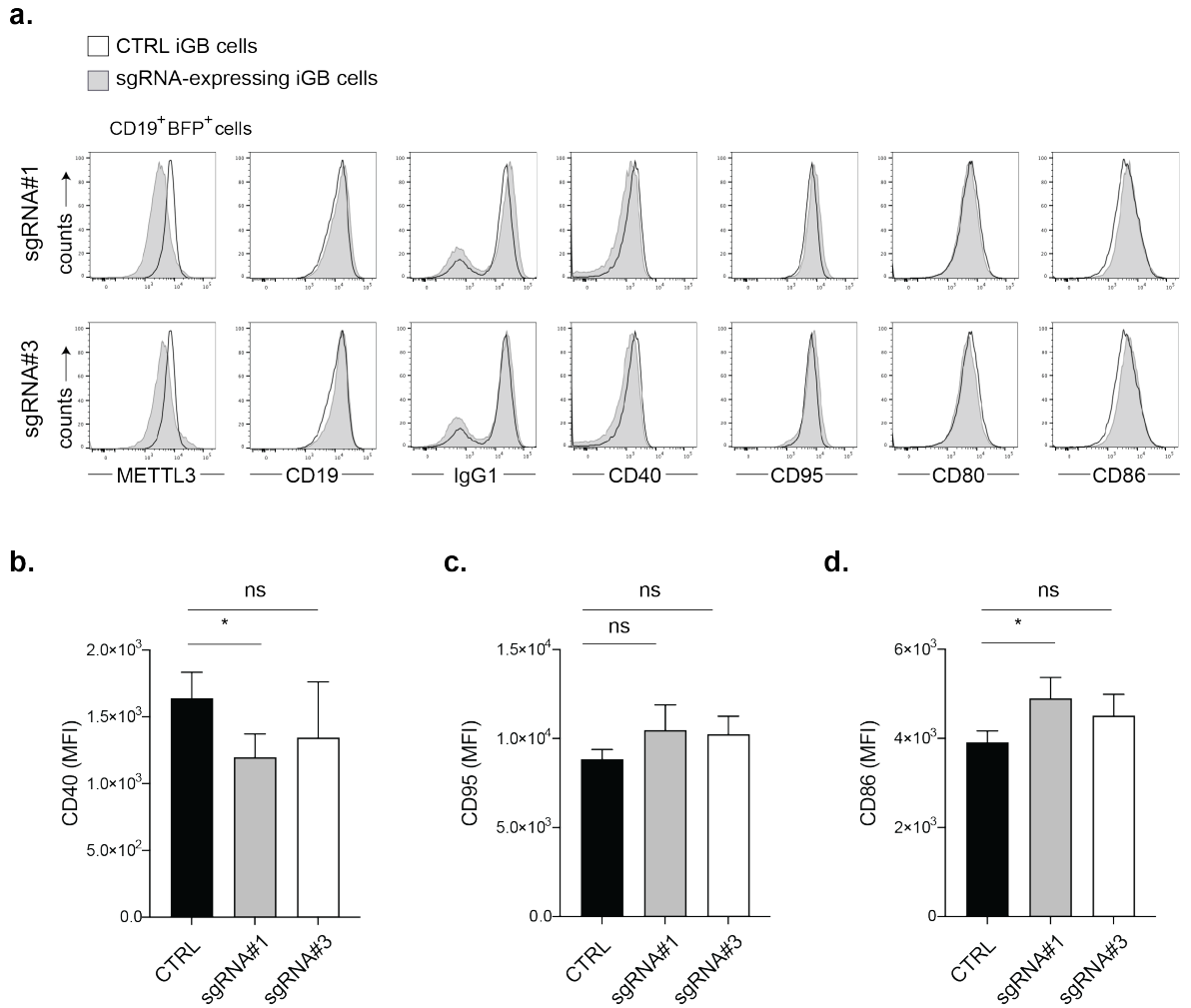
Figure 41. Immunophenotypic characterization of *Mettl3*-mutant iGB cells 6 days after infection.

a. Immunophenotypic characterization of *Mettl3*-mutant iGB cultures (filled grey line), infected with retroviral particles expressing either sgRNA#1 (top) or sgRNA#3 (bottom), at day 6 after infection. Comparison of *Mettl3*-deleted cells with their proficient counterparts (CTRL, black not filled) is shown. A representative case of at least 3 independent experiments is shown. **b.** Median fluorescence intensity (MFI) of CD40 expression measured by flow cytometry in pre-gated CD19$^+$ BFP$^+$ iGB cells from control (CTRL, black) and *Mettl3*-mutant cultures, expressing either sgRNA#1 (grey) or sgRNA#3 (white), at day 6 after infection. Columns indicate the mean (*n* = 3) values, ± SD. Unpaired student's *t*-test: sgRNA#1 vs CTRL: *P-value = 0.04; sgRNA#3 vs CTRL: ns *P*-value = 0.33. **c.** Median fluorescence intensity (MFI) of CD95 expression measured by flow cytometry in pre-gated CD19$^+$ BFP$^+$ iGB cells from control (CTRL, black) and *Mettl3*-mutant cultures, expressing either sgRNA#1 (grey) or sgRNA#3 (white), at day 6 after infection. Columns indicate the mean (*n* = 3) values, ± SD. Unpaired student's *t*-test: sgRNA#1 vs CTRL: ns *P*-value = 0.13; sgRNA#3 vs CTRL: ns *P*-value = 0.1. **d.** Median fluorescence intensity (MFI) of CD86 expression measured by flow cytometry in pre-gated CD19$^+$ BFP$^+$ iGB cells from control (CTRL, black) and *Mettl3*-mutant cultures, expressing either sgRNA#1 (grey) or sgRNA#3 (white), at day 6 after infection. Columns indicate the mean (*n* = 3) values, ± SD. Unpaired student's *t*-test: sgRNA#1 vs CTRL: *P-value = 0.03; sgRNA#3 vs CTRL: ns *P*-value = 0.13.

3.6.4. *Mettl3*-mutant iGB cells show normal frequencies of IRF4^{hi} CD138^{+} plasmablasts on day 8

We have shown that METTL3 knockdown causes an initial delay in the mitogenic response of primary B cells to mCD40L + IL-21 stimulation. Such growth retardation may negatively impinge on the generation of terminally differentiated PBs. Indeed, the latter process is strictly dependent on the execution by mCD40L/IL-21-stimulated B cells, of a defined number of cell divisions, which are needed to epigenetically derepress the expression of the PC master regulator *Prdm1*/BLIMP1 (Scharer et al. 2018).

To assess the effects of METTL3 knockdown on PC differentiation, we measured, by flow cytometry, the frequencies of IRF4^{hi} CD138^{+} PBs present in day-8 iGB cultures. As shown in Figure 42a, the proportion of PBs was comparable between *Mettl3*-proficient and -mutant cultures. However, when we measured the fraction of IRF4^{hi} cells that succeeded in differentiating into CD138^{+} PBs, we observed a tendency of *Mettl3*-mutant iGB cultures in performing less efficiently this transition, although it was not statistically significant (Figure 42b). Indeed, whereas in control cultures roughly one every four IRF4^{hi} B cells became an IRF4^{hi} CD138^{+} PB, the conversion rate in *Mettl3*-mutant cultures was lower, correspondingly approximately to one every five cells (Figure 42b).

These results point, once more, to a defect in the initial proliferative response of *Mettl3*-hypomorphic B cells to CD40L + IL-21 stimulation, which impairs the timely transition of IRF4^{hi} activated B cells into the pool of terminally differentiated IRF4^{hi} CD138^{+} PBs. Such defect gets gradually compensated over time, as the frequency and output of IRF4^{hi} CD138^{+} PBs returned comparable between *Mettl3*-proficient and -hypomorphic cultures at day-11 of the iGB culture (Figure 42a).
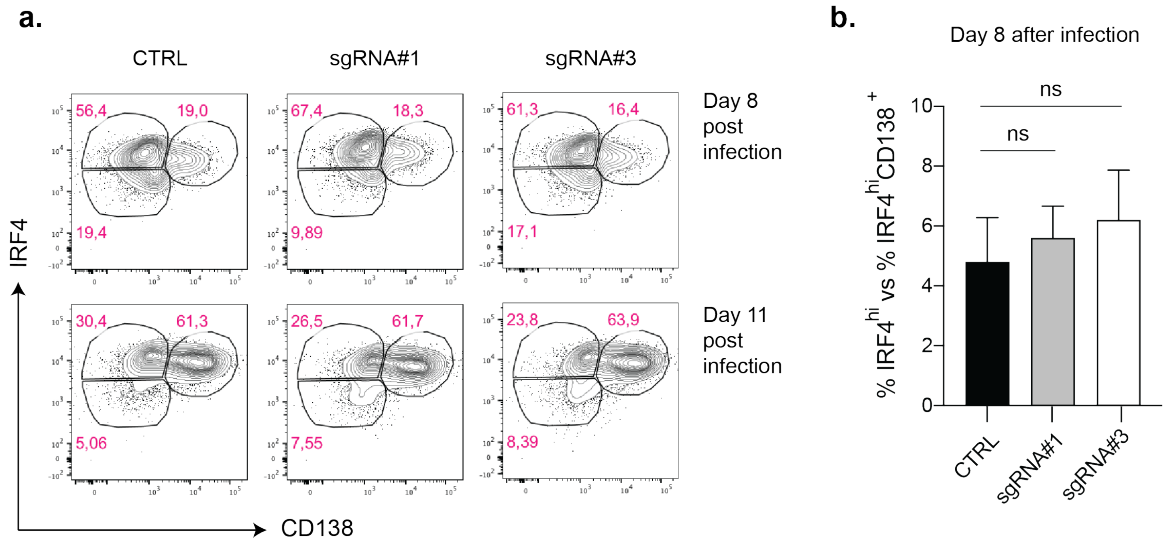
Figure 42. Terminal differentiation into IRF4^hi CD138+ plasmablasts in *Mettl3*-mutant iGB cells.

a. Flow cytometric analysis of IRF4 and CD138 markers in *Mettl3*-proficient (CTRL) and -mutant cultures, expressing either sgRNA#1 or sgRNA#3, at day 8 and 11 after infection. Cells were pre-gated on CD19+ BFP+ cells. Numbers refer to the frequency of cells present within the gate. A representative case of 4 independent experiments is shown. **b.** Efficiency of IRF4^hi cells to upregulate the PC marker CD138 at day 8 after infection, in control and mutant cultures (expressing either sgRNA#1 or sgRNA#3), measured as the ratio between the frequency of IRF4^hi cells and that of IRF4^hiCD138+ PBs. Columns indicate the mean ($n = 4$) values, ± SD. Unpaired student's *t*-test: sgRNA#1 vs CTRL: ns P-value = 0.41; sgRNA#3 vs CTRL: ns P-value = 0.25.

3.7. Effect of METTL3 knockdown on the gene expression profile of mCD40L/IL21-activated iGB cells

We have shown that METTL3 knockdown causes a significant growth retardation in the first two days of stimulation with mCD40L and IL-21. This initial growth delay contributed to retard and, possibly, impair the PC differentiation program, as suggested by the smaller fraction of IRF4^{hi} activated B cells which converted into terminally differentiated CD138^{+} PBs by day-8 of the iGB culture. Such defect was ultimately corrected at day-11, when the frequency of IRF4^{hi}CD138^{-} pPBs and IRF4^{hi} CD138^{+} PBs returned comparable between *Mettl3*-proficient and -mutant iGB cultures. These results predict a functional disturbance imposed by *Mettl3* downregulation during the first 48 hours of stimulation on the capacity of iGB cells to optimally execute the PC differentiation program at later timepoints.

To investigate the molecular bases of the weakened/delayed activation of *Mettl3*-mutant iGB cells in response to mCD40L + IL-21 stimulation, we performed whole transcriptome analyses, through RNA-sequencing, comparing control to sgRNA#1-expressing *Mettl3*-mutant iGB cells. Differentially expressed genes were selected based on fold-changes of $\geq$ + 1.5 (or $\leq$ - 1.5), and adjusted *p*-value $\leq$ 0.05. We profiled control and *Mettl3*-mutant iGB cells respectively at 2- (i.e. day-6 after infection) and 4- (day-8 after infection) days of activation with mCD40L + IL-21. Bioinformatic analysis of RNA-sequencing data revealed, at day-6 after infection, 151 downregulated and 168 upregulated genes in *Mettl3*-mutant iGB cells, when compared to their *Mettl3*-proficient counterparts (Appendix, Table 19, 20). Strikingly, the transcriptomes of *Mettl3*-mutant and -proficient iGB cells were largely comparable when analyzed two days later, at day-8 after infection. In line with these observations, Principal Component Analysis (PCA), performed on the top 500 variable genes among samples analyzed at day 6, showed a separation between knockdown and control samples, except for one experiment (exp-2) where, indeed, differences in B cell proliferation between mutant and control cells were milder than the other two conditions (data not shown) (Figure 43a). By contrast, PCA analysis performed on samples at day 8, did not allow to clearly separate knockdown from control samples (Figure 43b).

a.

Day 6 after infection (48 hours after mCD40L + IL-21 stimulation)
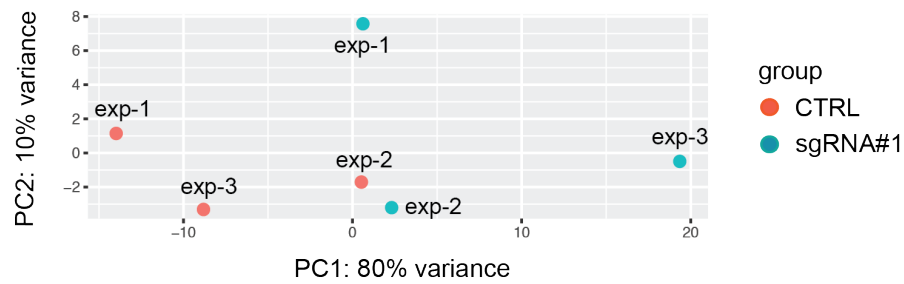
b.

Day 8 after infection (96 hours after mCD40L + IL-21 stimulation)
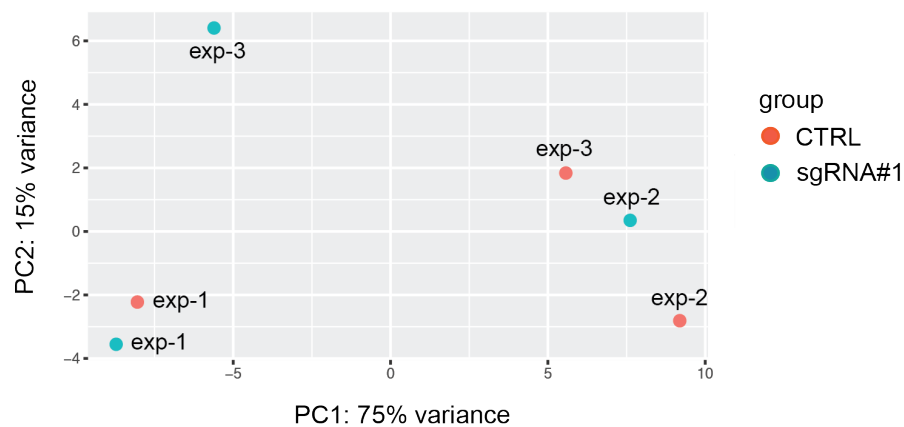
Figure 43. Principal component analysis for RNA-seq data of control and *Mettl3*-mutant iGB cells.

Two-dimensional principal component plots of Principal Component Analysis (PCA) for RNA-seq data of *Mettl3*-proficient (CTRL) and sgRNA#1-expressing *Mettl3*-mutant cultures, from three independent experiments, analyzed after 2 days (day 6 after infection) (**a**) or 4 days (day 8 after infection) (**b**) of mCD40L + IL-21 stimulation. The first principal component is shown for the X axis and the second principal component is shown for the Y axis. The value after the principal component identifier displays the proportion of variance explained by this particular principal component. In red: control cells (CTRL); in blue: *Mettl3*-mutant cells (sgRNA#1).

3.7.1. METTL3 knockdown blunts initial induction of master regulators of PC differentiation in response to mCD40L + IL-21 stimulation

Transcriptomic profiling of iGB cells 48 hours after the initial mCD40L + IL-21 stimulation, revealed a significant reduction in *Mettl3*-mutant iGB cells of a subset of genes, which plays a critical role in triggering terminal B cell differentiation. Specifically, *Mettl3*-mutant iGB cells showed reduced transcript levels of the transcription factors *Irf4*, *Prdm1* and *Pou2af1*, when compared to *Mettl3*-proficient counterparts. In particular, *Prdm1* and *Pou2af1* were among the 50 mostly downregulated transcripts in *Mettl3*-mutant iGB cells, two days after mCD40L + IL-21 stimulation (Figure 44).
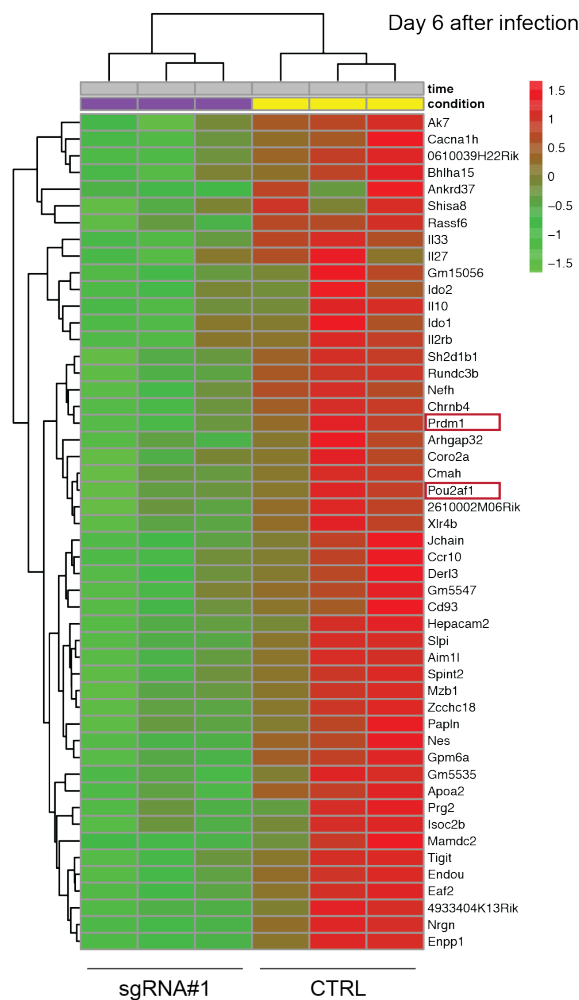
Figure 44. Downregulated genes in *Mettl3*-mutant iGB cells after 2 days of mCD40L + IL-21 stimulation.

Unsupervised hierarchical clustering of samples according to the normalized expression value of the 50 mostly downregulated genes in *Mettl3*-mutant (sgRNA#1) iGB cells at day 6, when compared to *Mettl3*-proficient (CTRL) counterparts, assessed by RNA sequencing.

150

We validated RNA-seq data for the *Irf4* transcription factor, by performing immunoblotting analyses. As shown in Figure 45a-b, IRF4 protein levels were reduced by 50% in *Mettl3*-mutant iGB cultures which have been infected with retroviral particles expressing sgRNA#1 or sgRNA#3, two days after mCD40L + IL-21 stimulation (day-6 after the infection), that corresponds to a timepoint when the expression of the transcription factor gets dramatically upregulated in the control culture (compare IRF4 protein levels between day-4 and day-6 in control cells) (Figure 45a). *Mettl3*-proficient and -mutant iGB cultures, analyzed 96 hours after stimulation (day 8 after infection) revealed, instead, comparable IRF4 protein levels (Figure 45a-b). These data are in agreement with flow cytometric results shown in Figure 42a, which indicated that the overall fraction of IRF4^{hi} B cells was, by-and-large, similar between control and mutant cultures at day-8 after infection.
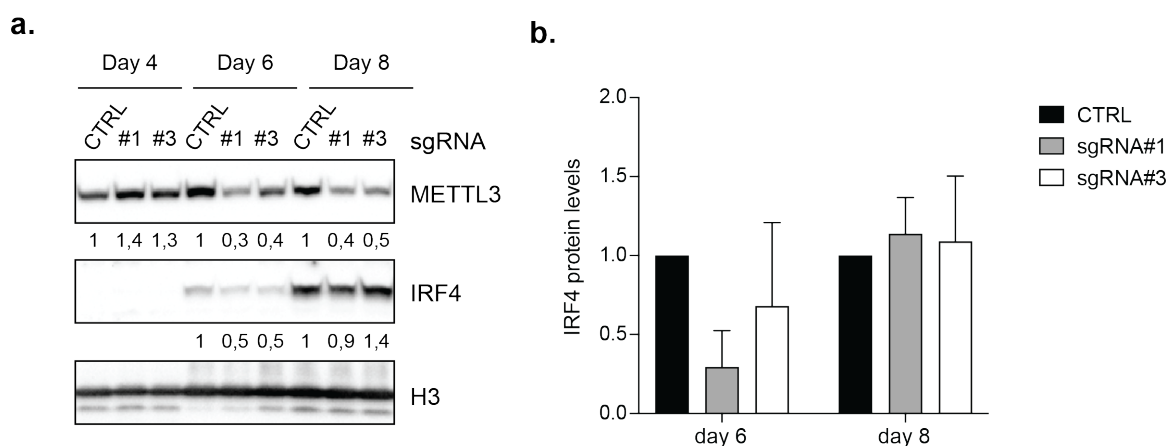
Figure 45. IRF4 expression in *Mettl3*-mutant iGB cells after 2 and 4 days of mCD40L + IL-21 stimulation.

a. Immunoblotting analysis for METTL3 and IRF4 protein levels in Cas9-expressing iGB cells infected either with the empty vector (CTRL), or with retroviral particles expressing one of the two sgRNAs targeting the *Mettl3* gene (sgRNA#1 or sgRNA#3), at day 4, 6 and 8 after infection, respectively. Numbers refer to METTL3 or IRF4 protein levels normalized to H3 housekeeping gene and shown as relative to those measured in control cells (CTRL) at the corresponding timepoint. A representative case of 3 independent experiments is shown. **b.** IRF4 protein levels measured by immunoblotting analysis in *Mettl3*-mutant iGB cultures expressing either sgRNA#1 (in grey) or sgRNA#3 (in white), at day 6 and 8 after infection, normalized to those of the housekeeping H3 and shown as relative to IRF4 protein levels measured in *Mettl3*-proficient cells (CTRL, in black) at the corresponding timepoint. Columns represent the mean (*n* = 3) values, ± SD.

Transcripts encoding for the PC master regulators IRF4 and BLIMP1 were also quantified in *Mettl3*-mutant iGB cells (Ly5.2$^+$) grown in co-cultures with their *Mettl3*-proficient counterparts (Ly5.1$^+$) (see paragraph 3.6.2). Specifically, quantitative RT-PCR analysis performed on cDNA prepared from FACS-sorted Ly5.2$^+$ and Ly5.1$^+$ iGB cells, 48 hours after mCD40L + IL-21 stimulation (day 6 after infection), revealed lower *Irf4* and *Prdm1* transcript levels in *Mettl3* mutant Ly5.2$^+$ B cells, when compared to Ly5.1$^+$ control counterparts (and to Ly5.2$^+$ B cells infected with empty vector; Figure 46). In the same experimental setting, transcripts for *Xbp1*, another key transcription factor required for PCs to sustain the high protein synthesis load, and positively controlled by BLIMP1 transcription factor, was found downregulated in *Mett3*-mutant iGB cells competing with their proficient counterparts in co-culture experiments (Figure 46). Most importantly, *Mettl3*-mutant iGB cells showed reduced transcript levels for the IRE1-excised version of the *Xbp1* transcript (*Xbp1s*), which encodes for the transcription-competent variant of *Xbp1* (Calfon et al. 2002).
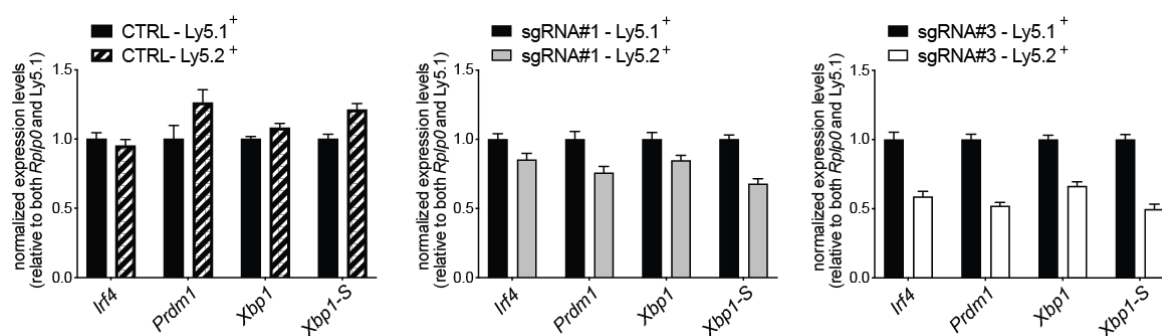
Figure 46. Expression of PC-associated genes in *Mettl3*-mutant iGB cells cultured in competition with wild-type cells.

Quantification of transcripts encoding for the indicated PC-associated transcription factors in sorted Ly5.1$^+$ and Ly5.2$^+$ iGB cells purified from control (CTRL) and *Mettl3*-mutant co-cultures (expressing either sgRNA#1 or sgRNA#3), after 2 days of mCD40L + IL-21 stimulation (day 6 after infection). Data refer to transcript levels of the indicated transcription factor after normalization to those of the housekeeping gene *Rplp0* and represented as relative to those measured in the corresponding population of control co-culture (Ly5.1$^+$). Columns indicate the mean of technical triplicates, ± SD. Data shown are representative of a single experiment.

The failure to optimally boost *Irf4* expression in *Mettl3*-hypomorphic iGB cells in response to mCD40L + IL-21 stimulation, may depend on impaired transcript stability as a result of reduced m^{6}A mRNA methylation. This hypothesis is supported by preliminary evidences obtained analyzing the repertoire of m^{6}A-marked mRNAs in MYC-transformed B cell lymphomas (see paragraph 3.9). Indeed, m^{6}A RNA immunoprecipitation assays, coupled to high-throughput sequencing, revealed focal deposition of m^{6}A within the 3' untranslated region (3' UTR) of *Irf4* transcripts in lymphoma cells (Figure 47).
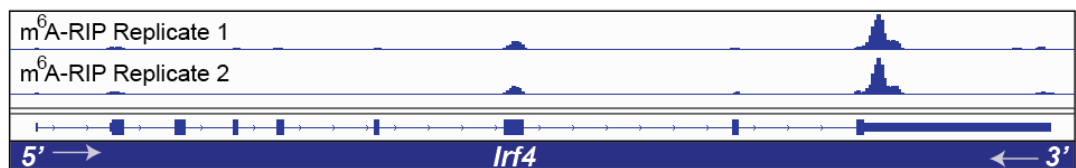
Figure 47. *Irf4* transcript is a target of m^{6}A modification in MYC-driven B cell lymphomas.

Genomic view with the Integrative Genomics Viewer (IGV), of the *Irf4* locus and m^{6}A-RNA immunoprecipitation signal assessed in two technical replicates of a λ-MYC lymphoma cell line.

3.7.2. METTL3 knockdown prevents optimal boosting of the translational machinery needed in PCs to sustain intense Ig synthesis

Gene Set Enrichment Analysis (GSEA) for gene sets of the MSigDB Hallmark collection, revealed a significant (adjusted *p*-value < 0.05) downregulation of transcripts belonging to mTORC1 signaling and to the unfolded protein response pathway in *Mettl3*-mutant iGB cells analyzed 48 hours after mCD40L + IL-21 stimulation, when compared to *Mettl3*-proficient cells (Figure 48). The downregulation of the latter pathways is extremely relevant, as mTORC1 signaling pathway is induced by T-cell help in LZ B cells upon positive selection, in order to sustain the anabolic program that supports cell proliferation in the DZ (Ersching et al. 2017). In addition, mTORC1 was recently shown to be employed by precursors of plasmablasts, to upregulate multiple components of the UPR before the transition into fully terminally differentiated PCs (Gaudette et al. 2020).
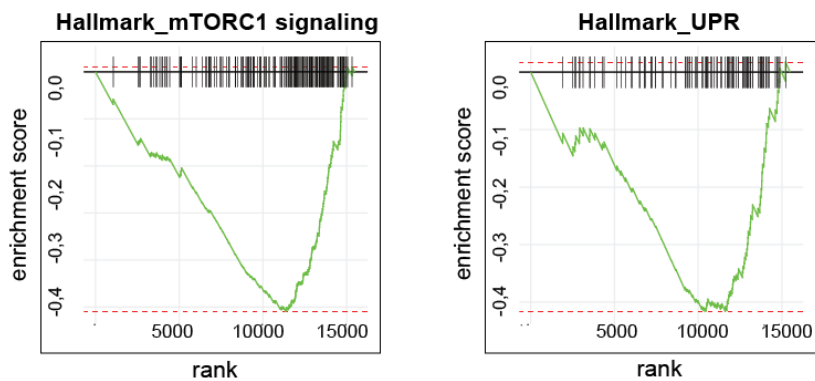
Figure 48. *Mettl3*-mutant iGB cells display downregulation of mTORC1 signaling and UPR pathways.

GSEA enrichment plots for gene signatures related to the downregulation of the mTORC1 signaling pathway (left, adjusted *p*-value = 0.02) and to the downregulation of the unfolded protein response (UPR) (right, adjusted *p*-value = 0.02) in *Mettl3*-mutant iGB cells at day 6 after infection, when compared to control iGB cells.

Transcripts downregulated in *Mettl3*-mutant iGB cells, belonging to the UPR gene ontology category, included mRNAs encoding for chaperones (*Hsp90b1* and *Mzb1)* and co-chaperones (*Dnajc3*), and for the endoplasmic-reticulum-associated protein degradation (ERAD) regulators *Edem1* and *Derl3*.

The latter proteins are strictly required in antibody-secreting cell precursors to optimize ER function and to prevent ER-stress resulting from heightened immunoglobulins synthesis. Taking together, these results establish for the first time an important contribution of *Mettl3* to the timely activation of the transcription factor network directing terminal B cell differentiation. METTL3 also contributes to enhance the protein synthesis machinery required for PCs to sustain intense Ig synthesis and secretion.

3.7.3. *Mettl3*-defective mCD40L/IL-21-activated iGB cells display blunted c-MYC transcriptional activity

GSEA performed on the list of differentially expressed transcripts between *Mettl3*-proficient and -hypomorphic iGB cells stimulated for 48 hours with mCD40L + IL-21, revealed a significant downregulation of MYC target gene signatures (Figure 49a). Specifically, out of 151 downregulated genes in *Mettl3*-mutant iGB cells, 66% (*n* = 100) represent previously described direct MYC targets (Figure 49b) (Sabo et al. 2014). On the contrary, only 32/168 (19%) upregulated genes in *Mettl3*-mutant iGB cells were under c-MYC control (Figure 49c). These data suggest that METTL3 positively regulates MYC-controlled gene expression in iGB cells stimulated with mCD40L + IL-21.
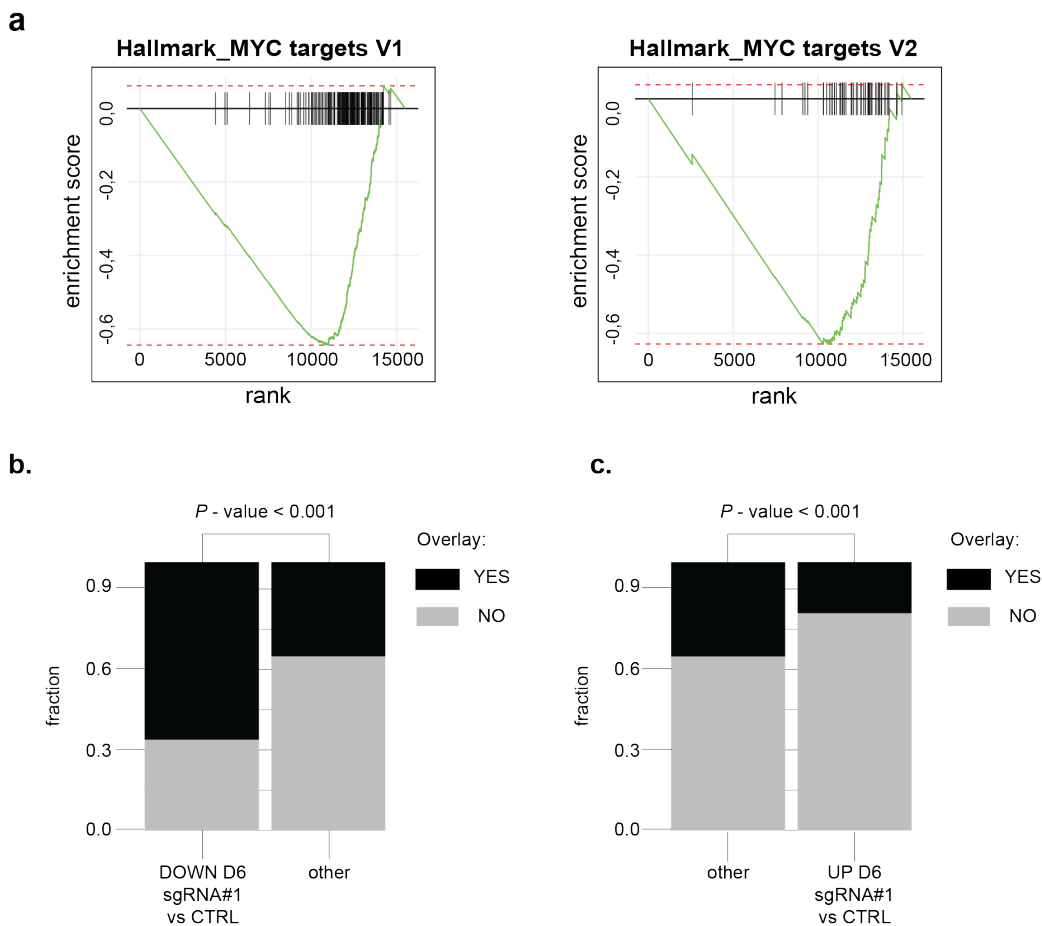
Figure 49. c-MYC target genes are downregulated in *Mettl3*-mutant cells at day 6 after infection.

a. GSEA enrichment plots for gene signatures related to the downregulation of c-MYC targets in *Mettl3*-mutant iGB cells at day 6 after infection, when compared to control cells. Left: MYC targets V1 gene set: adjusted *p*-value = 0.02. Right: MYC targets V2 gene set: adjusted *p*-value = 0.02. **b.** Columns showing the intersection of

156

known MYC target genes (in black) with the list of the downregulated genes in *Mettl3*-mutant iGB cells (left column, grey) and with all the other not differentially expressed genes (right column, grey), assessed by RNA-sequencing at day 6 after infection. A Chi-square test was applied in order to assess the significance of the enrichment for MYC targets between the two gene lists: ***P-value < 0.001. **c.** Columns showing the intersection of known MYC target genes (in black) with the list of the upregulated genes in *Mettl3*-mutant iGB cells (right column, grey) and with all the other not differentially expressed genes (left column, grey), assessed by RNA-sequencing at day 6 after infection. A Chi-square test was applied in order to assess the significance of the enrichment for MYC targets between the two gene lists: ***P-value < 0.001.

---

c-MYC exerts a positive control over cell-cycle progression by inducing the expression of members of the E2F transcription factor family, and thereby a large set of genes favoring the G_1-to-S transition of the cell-cycle (Sears, Ohtani, and Nevins 1997; Adams et al. 2000; Leung et al. 2008). Given the delay in the G_1-to-S transition observed in *Mettl3*-mutant iGB cells 48 hours after mCD40L + IL-21 stimulation, we asked whether the category of E2F target genes was enriched among those controlled by *Mettl3*. As shown in Figure 50, we observed a highly significant (adjusted p-value < 0.02) downregulation of E2F target genes in *Mettl3*-mutant iGB cells, when compared to their proficient counterparts.
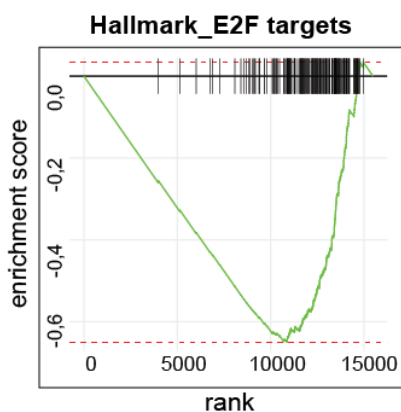
Figure 50. E2F target genes are downregulated in *Mettl3*-mutant iGB cells.

GSEA enrichment plots for gene signatures related to the downregulation of E2F targets in *Mettl3*-mutant iGB cells at day 6 after infection, when compared to control cells. Adjusted P-value < 0.02.

A number of recent reports have highlighted *c-Myc* transcript as direct target of m^{6}A mRNA methylation in different cell-types (Lee et al. 2019; Cheng et al. 2019; Yang et al. 2020). We confirmed these results in MYC-expressing transformed B cells, by performing m^{6}A RNA immunoprecipitation studies coupled to high-throughput sequencing. Specifically, as shown in Figure 51, peaks of m^{6}A deposition were identified in exon 2 and in the 3' UTR of the murine c-*Myc* transcript.
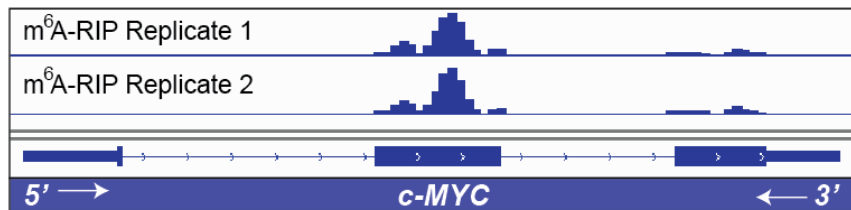
Figure 51. *c-Myc* transcript is a direct target of m^{6}A modification in MYC-driven B cell lymphomas.

IGV view of the m^{6}A-RNA immunoprecipitation signal assessed in two technical replicates of a representative λ-MYC lymphoma cell line in the genomic region of the *c-MYC* transgene.

To assess whether METTL3 knockdown exerted a detrimental effect on c-MYC protein levels in iGB cells, we performed immunoblotting analyses for the transcription factor. *Mettl3*-hypomorphic iGB cells stimulated for 48 hours with mCD40L + IL-21 showed a 40% reduction in c-MYC protein levels when compared to control B cells retrieved at the same timepoint (Figure 52a-b). By contrast, RNA-seq analyses excluded *c-Myc* from the list of differentially expressed genes at the same timepoint, between *Mettl3*-proficient and -mutant iGB cultures. Altogether, these results suggest that in B cells acutely responding to mCD40L + IL-21 stimulation, the m^{6}A methyltransferase complex positively controls *c-Myc* translation through m^{6}A deposition. Measurements of c-MYC protein levels in *Mettl3*-proficient and -mutant iGB cells after 4 days of mCD40L and IL-21 stimulation, presented an apparently paradoxical increase of c-MYC levels in the *Mettl3*-mutant cultures (Figure 52a-b).

However, these results are in line with cell-cycle distribution analyses obtained in iGB cells analyzed at the same timepoint, showing an increased fraction of cells in the S phase in both *Mettl3*-mutant cultures (Figure 36c). Indeed, after four days of mCD40L + IL-21 stimulation, whereas *Mettl3*-proficient iGB cultures largely arrested their growth, possibly due to reduced c-MYC expression (Figure 52a-b), *Mettl3*-mutant cultures progressively recuperated the initial growth impairment, thus sustaining further rounds of cell division. The latter behavior is compatible with ongoing *c-Myc* expression, which explains the higher levels of the transcription factor in *Mettl3*-mutant iGB cultures, when compared to controls at day-8 after infection.
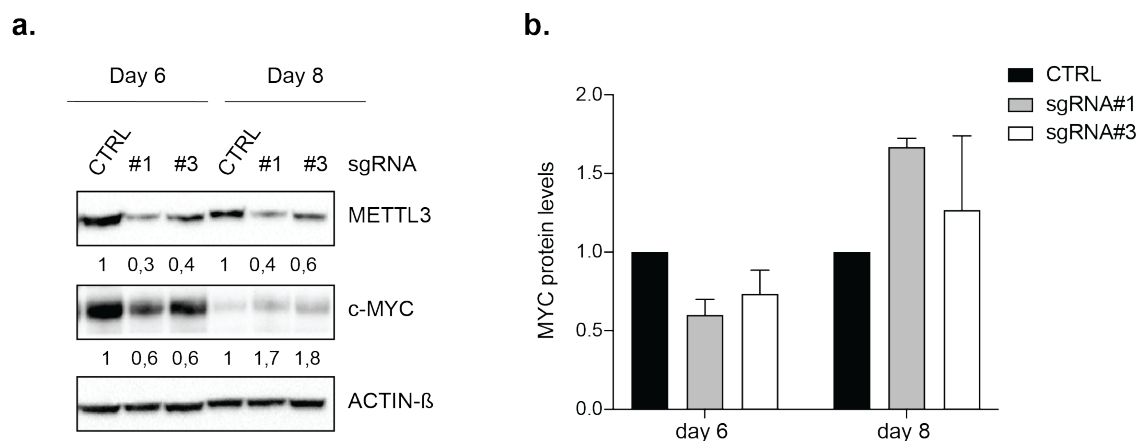
Figure 52. c-MYC protein levels are reduced in *Mettl3*-mutant iGB cells after 2 days of mCD40L + IL-21 stimulation.

a. Immunoblotting analysis for METTL3 and c-MYC protein levels in *Mettl3*-proficient (CTRL, infected with the EV) and *Mettl3*-mutant (expressing either sgRNA#1 or sgRNA#3) iGB cultures, analyzed 6 and 8 days after infection, respectively. Numbers refer to METTL3 or c-MYC protein levels normalized to the housekeeping ACTIN-β and shown as relative to those measured in control cells (CTRL) at the corresponding timepoint. A representative case of 3 independent experiments is shown. **b.** c-MYC protein levels in *Mettl3*-mutant iGB cells, expressing either sgRNA#1 (in grey) or sgRNA#3 (in white), measured at day-6 and -8 after infection, normalized to those of the housekeeping ACTIN-β and shown as relative to c-MYC protein levels measured in control cells (CTRL, in black) at the corresponding timepoint. Columns indicate the mean (n = 3) values, ± SD.

3.7.4. *Mettl3*-mutant and -proficient iGB cells show opposite transcriptome dynamics in the transition from 2-to-4 days of mCD40L + IL-21 stimulation

Bioinformatic analysis of RNA-sequencing data did not identify genes which were significantly differentially expressed between *Mettl3*-proficient and -hypomorphic iGB cells after 4 days of mCD40L + IL-21 stimulation (data not shown). Given the substantial differences in gene expression profile observed between *Mettl3*-proficient and -mutant iGB cells at the earlier timepoint (48 hours after stimulation), we hypothesized that the transition from day-2 to day-4 of stimulation followed different trajectories in the two types of iGB cultures. To this aim, we measured by RNA-sequencing the genes that were differentially expressed in the day-2-to-4 transition of mCD40L + IL-21 stimulation in *Mettl3*-proficient and -hypomorphic cultures. Bioinformatic analyses revealed that the number of differentially expressed genes (DEGs) was higher in *Mettl3*-mutant iGB cells, when compared to control cells. Specifically, *n* = 3531 and *n* = 3246 genes were found, respectively, down- and up-regulated in *Mettl3*-mutant iGB cells during this transition (Figure 53a-b). Instead, in *Mettl3*-proficient iGB cultures, we scored *n* = 2208 and *n* = 2383 genes which were, respectively, down- and up-regulated in the same time interval (Figure 53a-b).
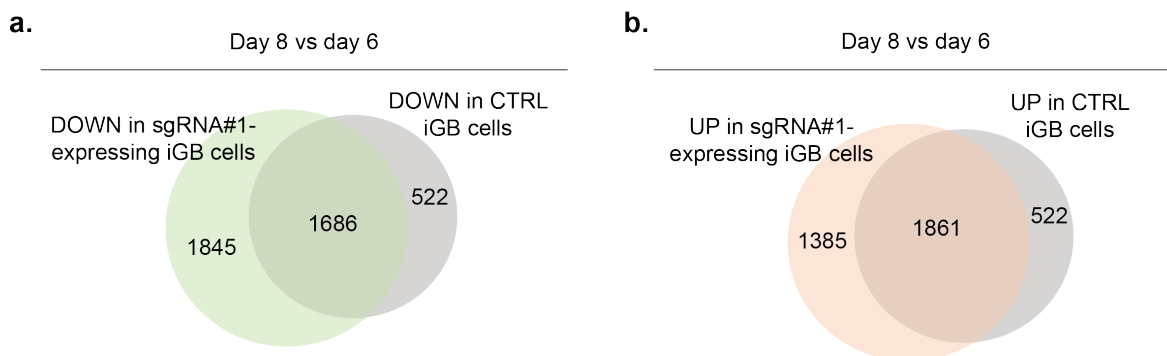
Figure 53. DEGs in control and *Mettl3*-mutant iGB cells in the transition from day-6 to day-8.

a. Venn diagram showing the overlap between the downregulated genes in *Mettl3*-mutant (green, sgRNA#1) and -proficient (grey, CTRL) iGB cells at day 8, when compared to day 6 after infection. **b.** Venn diagram showing the overlap between the upregulated genes in *Mettl3*-mutant (orange, sgRNA#1) and -proficient (grey, CTRL) iGB cells at day 8, when compared to day 6 after infection.

Intersections of the lists of the downregulated genes revealed $n = 1686$ genes which were shared between *Mettl3*-mutant and control iGB cultures (Figure 53a). Instead, $n = 1845$ and $n = 522$ genes were specifically downregulated in *Mettl3*-mutant and -proficient iGB cells, respectively (Figure 53a). Intersections of the lists of the upregulated genes revealed that $n = 1681$ genes were shared between *Mettl3*-mutant and control iGB cells, whereas $n = 1385$ and $n = 522$ genes were specifically upregulated in *Mettl3*-mutant and control iGB cultures, respectively (Figure 53b).

GSEA performed on the list of genes that were differentially expressed in iGB cells in the progression from day-2-to-4 of mCD40L + IL-21 stimulation, revealed striking differences between *Mettl3*-proficient and -hypomorphic iGB cells. Specifically, GSEA performed on DEGs of *Mettl3*-proficient cells, showed a significant downregulation of c-MYC and E2F targets and regulators of the G_2/M checkpoint (Figure 54a). In addition, we observed a significant upregulation of the IL-6/STAT3 signaling pathway, the interferon-γ and -α gene responses and IL-2/STAT5 signaling pathway (Figure 54a). These results are compatible with a culture that is undergoing growth arrest and, in a fraction of cells, executing an IL-6-dependent PC transcriptional program. Interestingly, GSEA performed on the list of DEGs in *Mettl3*-mutant iGB cultures, transiting from day-2 to day-4 of mCD40L + IL-21 stimulation, revealed a significantly positive enrichment for c-MYC and E2F targets, for the UPR and the mTORC1 signaling pathway (Figure 54b). These results confirm the delay imposed by METTL3 knockdown on the growth kinetics of iGB cells, which, in turn, has postponed the activation of the transcriptional programs induced in the early stages of PC differentiation. Importantly, as observed in control iGB cultures, *Mettl3*-mutant iGB cells, exposed for 4 days to mCD40L + IL-21 stimulation, upregulated the expression of genes involved in IL-6/STAT3 and IL-2/STAT5 signaling, together with genes activated by interferon type-I (IFN-α) and type-II (IFN-γ) (Figure 54b). Altogether, these results are suggestive of a delay imposed by METTL3 knockdown on the expansion of CD40L/IL-21-activated B cells, which in turn reduces the efficiency with which these cells upregulate key transcription factors for PC differentiation including IRF4, BLIMP1 and XBP1, as well as the capacity to expand their biosynthetic machinery that is required to become antibody-secreting PCs.
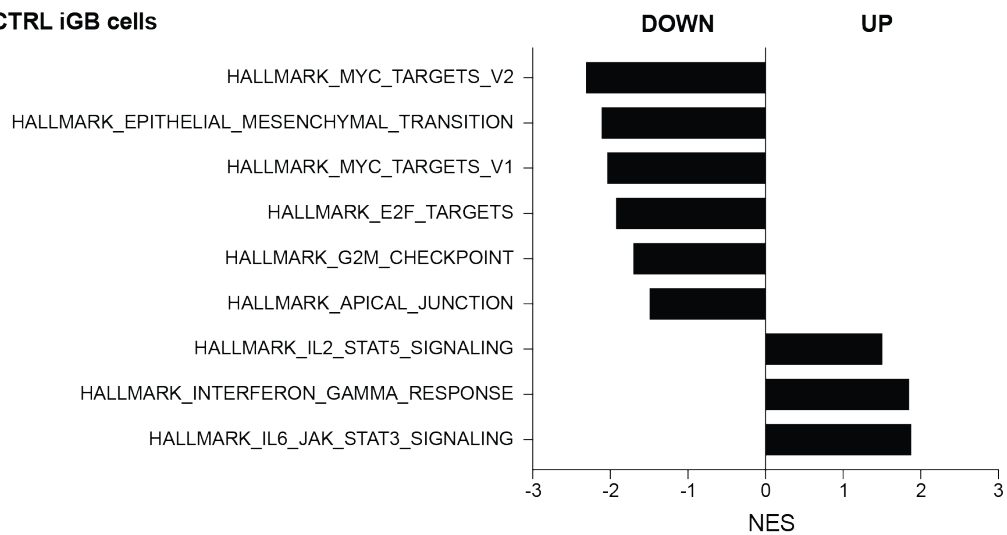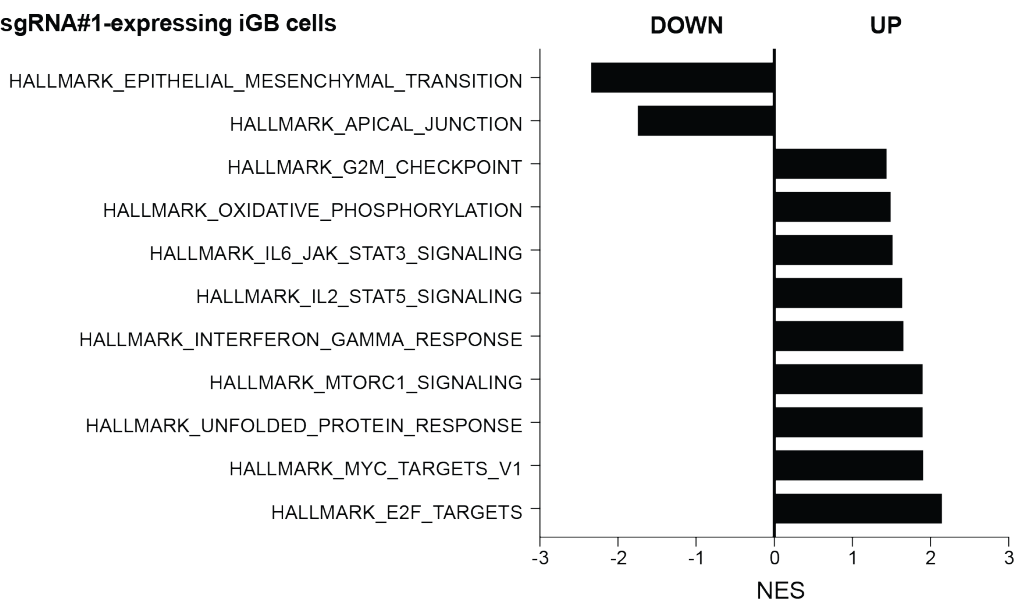
Figure 54. GSEA on DEGs in the transition from day 6 to 8, in control and *Mettl3*-mutant cells.

a. Bar plots showing the GSEA Normalized Enrichment Score (NES) for significantly enriched (adjusted *P*-value

< 0.05) gene sets of the Hallmark MSigDB Collection. The analysis was performed on the list of DEGs in control

iGB cells at day 8, when compared to day 6 after infection. **b.** Bar plots showing the GSEA Normalized

Enrichment Score (NES) for significantly enriched (adjusted *P*-value < 0.05) gene sets of the Hallmark MSigDB

Collection. The analysis was performed on the list of DEGs *Mettl3*-mutant iGB cells at day 8, when compared

to day 6 after infection.

3.8. Terminal differentiation favors the counter selection of *Mettl3*-mutant iGB cells

The observation that *Mettl3*-mutant iGB cells by-and-large normalize their gene expression profile, as compared to control iGB cells, after 4 days of mCD40L + IL-21 stimulation, is indicative either of the activation of compensatory mechanism(s), or of the preferential persistence in the culture, especially among terminally differentiated PBs, of cells that have (at least to a large extent) escaped *Mettl3* inactivation. To investigate the status of METTL3 in terminally differentiated PCs, we chose to extend *Mettl3*-proficient and -mutant cultures until day 13 after infection (corresponding to 9 days of mCD40L + IL-21 stimulation). At this timepoint, CD19$^+$CD138$^-$ activated B cells and CD19^{lo}CD138$^+$ PBs from the two iGB cultures were separately purified by FACS sorting and protein extracts subjected to immunoblotting analysis for METTL3 (Figure 55a). Strikingly, in both *Mettl3*-mutant cultures, CD19$^+$CD138$^-$ activated B cells were highly enriched for mutant cells, as confirmed by up to 80% downregulation of METTL3 protein levels (Figure 55b). By contrast, the fraction of CD19^{lo}CD138$^+$ PBs, showed a much weaker downregulation of the METTL3 protein, reaching at most 50% reduction (Figure 55b). Based on these results, we conclude that optimal levels of METTL3 expression are strictly required for the full execution of the PC differentiation program and/or for their long-term persistence.
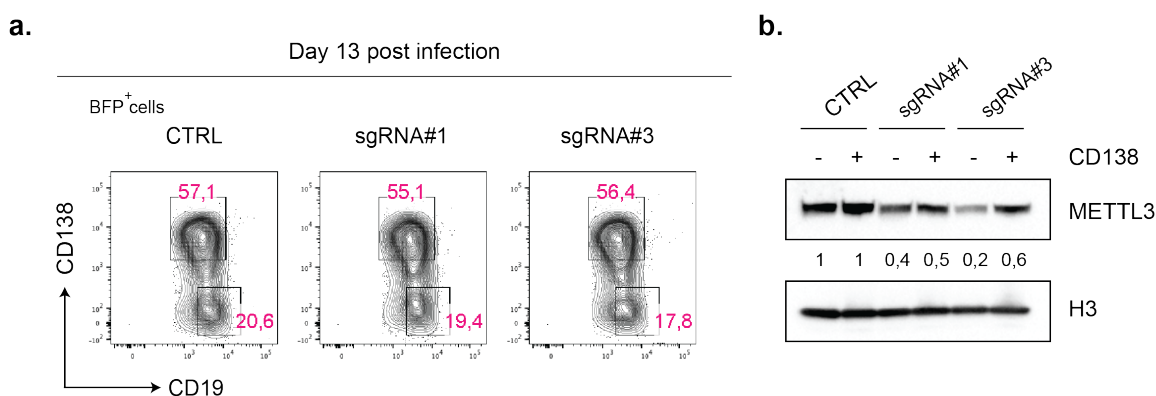
Figure 55. METTL3 expression in CD138$^+$ and CD138$^-$ cells sorted on day 13 after infection.

a. Gating strategy used to sort CD19$^+$CD138$^-$ and CD19^{lo}CD138$^+$ cells from *Mettl3*-proficient (CTRL) and *Mettl3*-mutant (expressing sgRNA#1 or sgRNA#3) iGB cultures, 13 days after infection. Cells were pre-gated on BFP$^+$ cells. **b.** Immunoblotting analysis for METTL3 protein levels in FACS-sorted CD19$^+$CD138$^-$ activated B cells and in CD19^{lo}CD138$^+$ plasmablasts, purified from control (CTRL) and *Mettl3*-mutant (expressing either sgRNA#1 or

#3) cultures, 13 days after infection. The same number of cells was loaded into each lane. Numbers refer to METTL3 protein levels normalized to those measured in the corresponding population of the CTRL culture. A representative case of 2 independent experiments is shown.

3.9. Identification of m^{6}A targets in MYC-expressing transformed B cells

3.9.1. METTL3 expression is induced during MYC-driven B cell lymphomagenesis

To obtain a transcriptome-wide map of m^{6}A mRNA targets in MYC-expressing B cells, we initially turned our attention to the λ-MYC mouse model of MYC-driven B cell lymphomas (Figure 56a). The choice of analyzing lymphoma cells was justified by the substantial number of starting cells (~ 1 x 10^9 cells) that is required to generate reproducible profiles of m^{6}A distribution on mRNA molecules, through anti-m^{6}A mRNA immunoprecipitation assays. Such numbers are difficult to achieve using the iGB cell culture system.

Moreover, in analogy to λ-MYC B cell lymphomas, iGB cells express c-MYC in response to mCD40L stimulation (Figure 56b), thereby possibly controlling the expression of a shared set of target genes, some of which, once transcribed, may also be subjected to m^{6}A methylation.

Primary λ-MYC lymphomas adapted to *in vitro* culture conditions have been successfully established in our laboratory (Varano et al. 2017). In the latter tumors, the expression of the *c-MYC* gene, cloned from a human Burkitt lymphoma line, is placed under the control of immunoglobulin lambda (λ) light chain regulatory sequences, thus ensuring constitutive expression of the proto-oncogene in IgM-expressing B cells (Figure 56a) (Kovalchuk et al. 2000).

Immunoblotting analysis for METTL3 and METTL14 revealed a progressive increase in the levels of both proteins transiting from naïve resting B cells, to λ-MYC pre-tumoral B cells, and ultimately to λ-MYC clonal lymphomas, thus suggesting that components of the m^{6}A methyltransferase complex are induced in the course of MYC-driven B cell malignant transformation (Figure 56c).
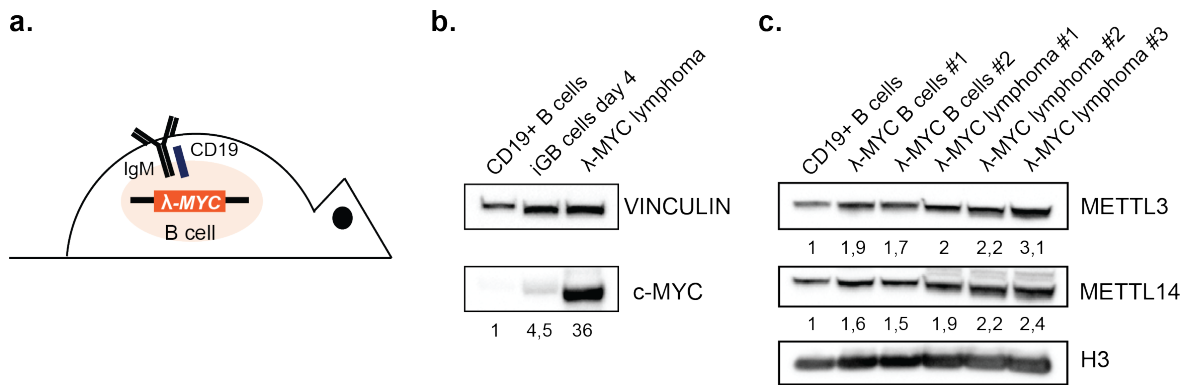
Figure 56. METTL3/METTL14 expression in MYC-driven B cell lymphomas.

a. Cartoon depicting the λ-MYC transgenic mouse model, where the human *c-MYC* proto-oncogene is placed under the control of immunoglobulin lambda (λ) light chain regulatory sequences, thus ensuring its constitutive expression selectively in B cells. **b.** Immunoblotting analysis of c-MYC protein levels respectively in C57BL/6J naïve B cells, in iGB cells activated for four days in the presence of mCD40L + IL-4 and in a representative λ-MYC lymphoma cell line. The same number of cells was loaded into each lane. Numbers refer to c-MYC protein levels shown as relative to those measured in C57BL/6J naïve B cells. **c.** Immunoblotting analysis of METTL3 and METTL14 protein levels in C57BL/6J naïve B cells, in naïve B cells isolated from two young λ-MYC transgenic mice, prior malignant transformation, and in three representative λ-MYC lymphoma cell lines established *ex vivo*. The same number of cells was loaded into each lane. Numbers refer to METTL3 or METTL14 protein levels shown as relative to those measured in C57BL/6J naïve CD19^{+} B cells.

3.9.2. m⁶A modification marks highly expressed genes in B cell lymphomas

To identify direct m^{6}A targets in MYC-driven B cell lymphomas, we purified in duplicate mRNA from *in vitro* cultured λ-MYC lymphoma B cells deriving from a representative established cell line (#2567), followed by immunoprecipitation of m^{6}A-marked transcripts, using an anti-m^{6}A-specific antibody. Libraries of reverse transcribed m^{6}A-marked transcripts were generated and subjected to next generation sequencing using an Illumina platform. Annealing of the NGS reads to the genome, followed by peak enrichment analysis using the MACS 2.0 algorithm, allowed us to identify, for each replicate, respectively $n = 2297$ and $n = 2184$ transcripts significantly (FDR, false discovery rate < 0.05) enriched in m^{6}A deposition. Importantly, 72%-to-75% ($n = 1654$) of the m^{6}A targets were shared between the two replicates, establishing high reproducibility of our m^{6}A RIP-seq protocol (Figure 57a). To test the reliability of the calls for m^{6}A-modified transcripts, we first analyzed the distribution of the peaks on the genome (Figure 57b-c). This analysis confirmed that, indeed, the majority of the peaks were distributed at promoters (37,32%) and on 3' untranslated regions (32,62%), whereas a very small percentage was distributed in regions downstream the gene (0,22%) or in distal intergenic regions (3,03%) (Figure 57b). Considering the target transcripts, the average distributions of the reads was found at the level of the transcription start site (TSS) and transcription end site (TES) (Figure 57c). These results are in agreement with a number of recent reports describing m^{6}A distribution patterns in different cell types (Dominissini et al. 2012; Linder et al. 2015).

In order to identify an m^{6}A consensus binding sites in target transcripts expressed in MYC-driven B cell lymphomas, we used the MEME-ChIP tool. In agreement with previous reports (Dominissini et al. 2012; Linder et al. 2015), we found the GGACA consensus sequence significantly enriched at sites of m^{6}A deposition (Figure 57d).

To explore the impact of m^{6}A methylation on the expression of the corresponding target transcript, we intersected the list of m^{6}A-marked transcripts with whole transcriptome data obtained from the same tumor, previously generated in our laboratory (Varano et al. 2017) (Figure 57e). This intersection revealed that the subset of transcripts marked by m^{6}A was significantly more expressed than the one that lacked the modification. (Figure 57e).

These results suggest that in our model of MYC-driven B cell lymphoma, m6A deposition increases the stability of the target transcripts.

a.

RIP1   RIP2

643   1654   530

b.

■ 37.32% Promoter
■ 4.23% 5' UTR
■ 32.62% 3' UTR
■ 3.54% 1st exon
■ 17.05% other exon
■ 0.61% 1st intron
■ 1.37% other intron
□ 0.22% downstream
■ 3.03% distal intergenic

c.

RIP1

RIP2

d.

Motif found

E-value 1.7e-0.24

e.

p=1.444503e−299
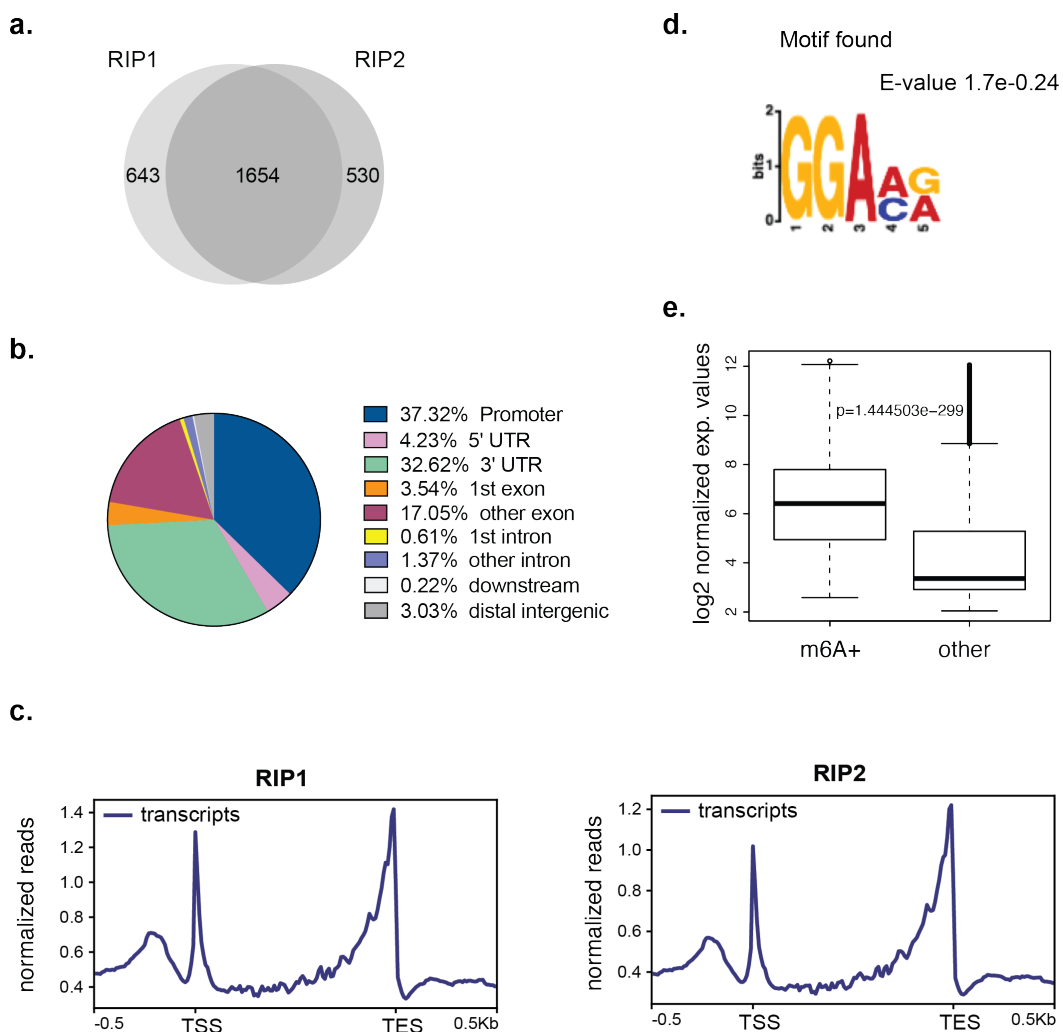
Figure 57. meRIP-seq in λ-MYC B-cell lymphomas.

a. Venn diagram showing the overlay of the m6A targets identified in two technical replicates of a representative λ-MYC B-cell lymphoma line, through meRIP-seq. **b.** Pie chart showing the distribution, with respect to the transcript features, of the m6A-called peaks, shared between the two technical replicates. **c.** Average distribution of the m6A reads within RefSeq transcripts, in the first (RIP1) and second (RIP2) technical replicate. **d.** Table showing the most common m6A consensus binding site, identified in peaks shared between the two technical replicates of meRIP-seq. E-value indicates the significance of the motif enrichment according to the DREME motif discovery software. **e.** Box plots showing the average distribution of the expression levels in the m6A targets (shared between the two m6A-RIP technical replicates) (left) and the genes which are not targeted by m6A (other), as assessed by Affymetrix GeneChip microarrays. An unpaired Student's *t*-test was applied to determine the significance in difference between the mean values of the two groups.

3.9.3. Transcripts marked by m⁶A in MYC-driven B cell lymphomas belong to cancer relevant pathways

To explore which biological processes are mostly regulated by m^{6}A mRNA methylation in MYC-driven B cell lymphomas, we performed gene ontology (GO) analysis on the subset of genes whose transcripts were marked by m^{6}A (Figure 58). This analysis showed a significant enrichment for genes under the control of c-MYC and E2F transcription factors, and other cell-cycle regulated genes (i.e. G2/M checkpoint and mitotic spindle assembly) (Figure 58). Moreover, several cancer-relevant gene categories (i.e. p53, PI3K/AKT/MTOR and Notch pathways) were significantly enriched among the targets of m^{6}A methylation in λ-MYC lymphoma B cells. Notably, several gene categories enriched for targets of m^{6}A in λ-MYC-lymphoma cells, were also over represented among the genes significantly down-regulated in *Mett3*-mutant iGB cells. These included the categories of MYC and E2F targets, the UPR and mTORC1 signaling-associated genes. Altogether, these results point to the existence of a possible set of cell-growth-relevant genes marked by m^{6}A, which are shared between MYC-transformed B cells and MYC-expressing iGB cells.
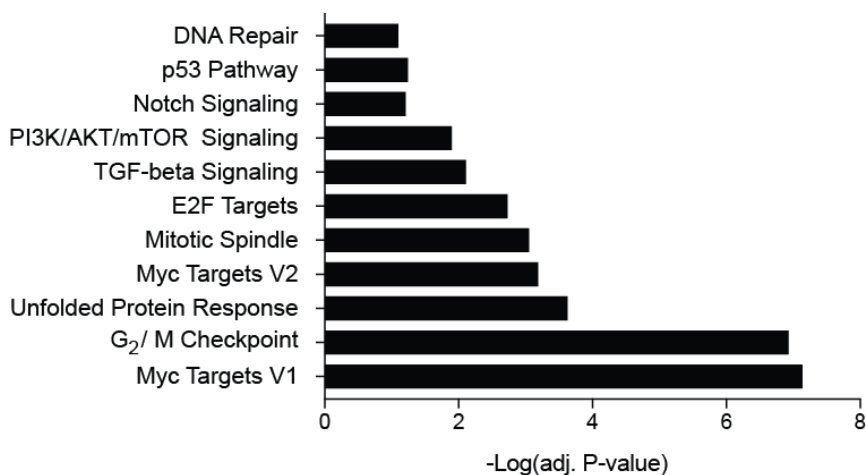
Figure 58. Gene ontology analysis of m⁶A targets identified in a representative λ-MYC B-cell lymphoma.

Gene ontology analysis was performed on the putative m^{6}A targets identified in both replicates by meRIP-seq. Barplots are showing the first 15 biological categories with an adjusted *p*-value < 0.05.

3.9.4. METTL3 knockdown affects the expression of selected m⁶A targets in iGB cells

To investigate whether DEGs between *Mettl3*-mutant and -control iGB cells, 2 days after mCD40L + IL-21 stimulation, consisted (at least in part) of m^{6}A targets, we intersected them with the list of m^{6}A targets identified in λ-MYC lymphomas. Specifically, for the list of m^{6}A direct targets, we considered the genes identified in at least one of the two replicates of meRIP-seq experiment (Figure 59). The cross-comparison revealed a total of 33 gene transcripts, which were significantly deregulated in iGB cells upon METTL3 knockdown and significantly enriched for m^{6}A deposition in λ-MYC lymphomas. Of these 33 transcripts, *n* = 12 and *n* = 21 corresponded to genes that were, respectively, up- and down-regulated in *Mettl3*-mutant CD40L/IL-21-stimulated iGB cells (Figure 59).
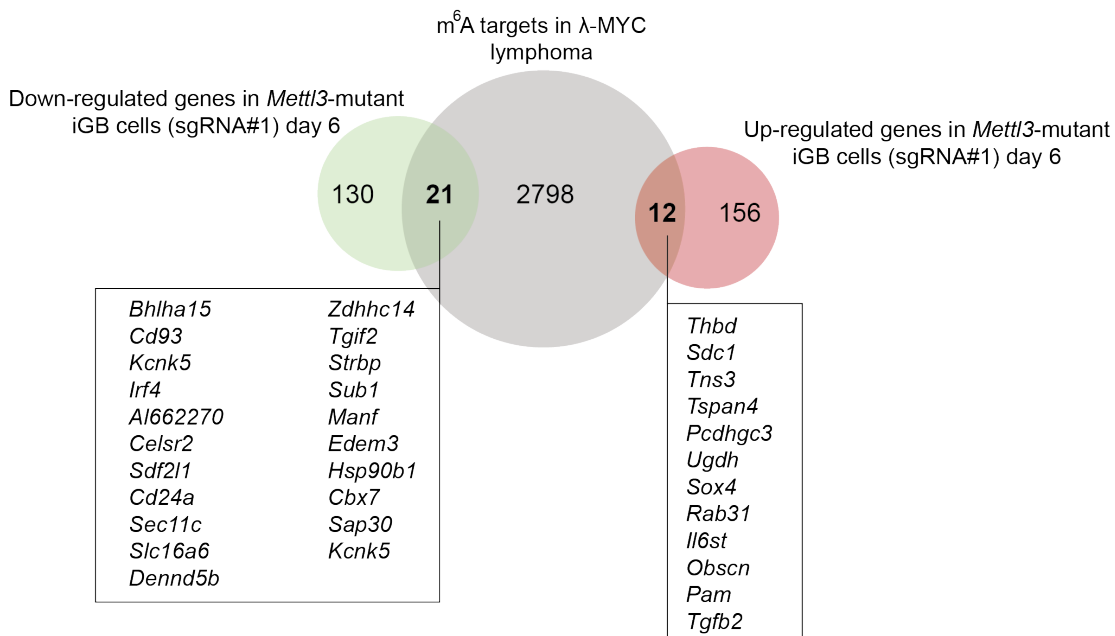
Figure 59. Intersection between the m⁶A targets identified in λ-MYC B cell lymphomas and the DEGs of *Mettl3*-mutant iGB cells at day 6.

Venn diagram showing the overlap between the m^{6}A targets (grey) and the genes which are down- (green) and up-regulated (red) in *Mettl3*-mutant iGB cells at day 6 after infection, when compared to control cells. The lists of down- (left) and up-regulated (right) genes in *Mettl3*-mutant iGB cells, whose transcripts are marked by m^{6}A in MYC B cell lymphomas, are shown in the two boxes.

Putative direct m^{6}A target transcripts that were downregulated in *Mettl3*-mutant iGB cells encoded for PC-associated factors, such as IRF4, proteins belonging to the UPR pathway, including EDEM3 and MANF, proteins involved in the mTORC1 signaling pathway, such as SDF2L1 and HSP90B1. In addition, there were genes encoding for chromatin remodelers, such as CBX7, a member of the Polycomb Repressive Complex 1 (PRC1), and SAP30, belonging to the histone deacetylase complex; genes encoding for proteins interacting with transcription factors, including SUB1 and TGIF2, and for surface markers, such as CD93 and CD24. This group also included genes encoding for solute transporters, such as SCL16A6 and MFSD2A proteins.

Instead, putative m^{6}A direct targets whose transcription was increased in *Mettl3*-mutant iGB cells at day 6 after infection included *Thbd* and *Pcdhgc3* genes, encoding for surface receptors; *Tns3* and *Tspan4*, encoding for proteins involved in the organization of the cytoskeleton; *Ugdh*, encoding for the enzyme that converts UDP-glucose into UDP-glucuronate, thereby involved in the biosynthesis of glycosaminoglycans; *Tgfb2*, encoding for the transforming growth factor beta-2 precursor 2; *Il6st*, encoding for the cytokine receptor complex associated to IL-6 signaling. Interestingly, this group also included the *Sdc1* gene, encoding for the PC-associated surface marker syndecan1/ CD138. However, when we measured CD138 expression by flow cytometry at day 6 after infection, we found comparable expression levels between *Mettl3*-mutant and control cultures, thus suggesting that CD138 expression may be subjected to additional post-transcriptional mechanisms of gene expression regulation (Figure 60).
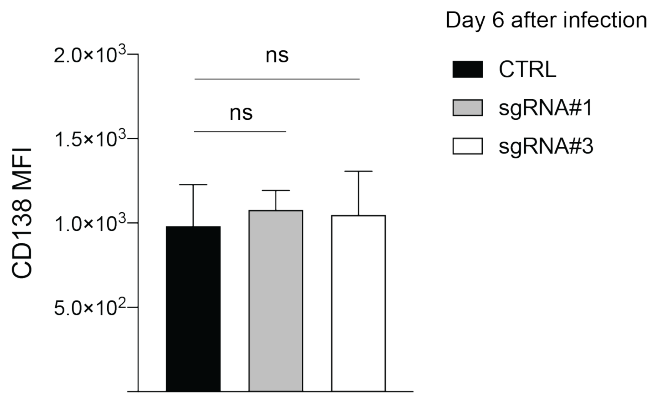
Figure 60. CD138 expression in *Mettl3*-mutant iGB cells at day 6 after infection.

Median fluorescence intensity (MFI) of CD138 expression in *Mettl3*-proficient (CTRL, black) and *Mettl3*-mutant iGB cells, expressing either sgRNA#1 (grey) or sgRNA#3 (white), measured by flow cytometry at day 6 after infection. Columns represent the mean (*n* = 4) values, ± SD. Unpaired student's *t*-test: sgRNA#1 vs CTRL: ns *P*-value = 0.5; sgRNA#3 vs CTRL: ns *P*-value = 0.7.

We then tested whether DEGs identified comparing *Mettl3*-proficient to -mutant iGB cells, after 48 hours of CD40L + IL-21 stimulation, were significantly enriched for genes marked by m^{6}A in λ-MYC lymphomas. As shown in Figure 61a-b, we failed to observe any significant enrichment for bona fide m^{6}A targets among the transcripts found up- or down-regulated in *Mettl3*-mutant iGB cultures.
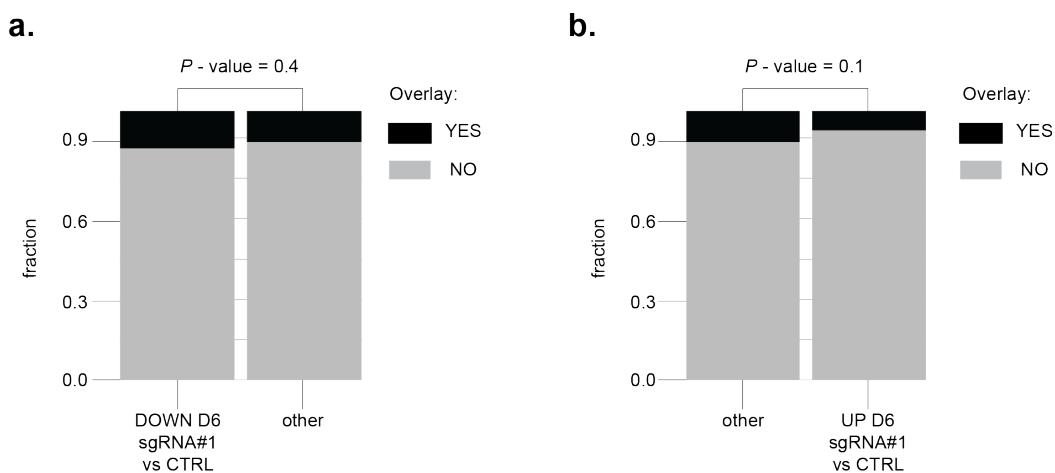
Figure 61. Intersection between m^{6}A targets of λ-MYC B cell lymphomas and genes showing normal or deregulated expression in *Mettl3*-mutant iGB cells.

a. Bar plots showing the intersection of m^{6}A direct targets identified in λ-MYC B cell lymphomas (in black) with the list of the downregulated genes in *Mettl3*-mutant iGB cells (left column, grey), and with all the other not

differentially expressed genes (right column, grey), assessed by RNA-sequencing at day 6 after infection. A Chi-square test was applied in order to assess the significance of the enrichment for MYC targets between the two gene lists: ns, P-value = 0.4. **b.** Bar plots showing the intersection of m^{6}A direct targets identified in λ-MYC B cell lymphomas (in black) with the list of the upregulated genes in *Mettl3*-mutant iGB cells (right column, grey), and with all the other not differentially expressed genes (left column, grey), assessed by RNA-sequencing at day 6 after infection. A Chi-square test was applied in order to assess the significance of the enrichment for MYC targets between the two gene lists: ns, P-value = 0.1.

With all the obvious intrinsic limitations of performing intersections between the repertoire of m^{6}A targets in MYC-expressing malignant B cells and genes modulated by METTL3 in CD40-activated iGB cells, the results so far obtained have identified a set of 33 candidate genes whose expression is directly influenced by METTL3 through deposition of m^{6}A on the corresponding transcripts. These preliminary analyses also suggest that in mCD40L/IL-21-activated iGB cells, METTL3 exerts on its putative mRNA targets opposite functions, stabilizing some, while facilitating the degradation of others. Finally, the evidence that only a restricted set of differentially expressed genes, identified in *Mettl3*-mutant activated B cells, is marked by m^{6}A in their malignant counterparts, points to m^{6}A methylation as a highly dynamic process which is strongly influenced by cell-intrinsic and extrinsic signals, including those associated with the transformation process.

3.10. Analysis of the effects of *Mettl3* gene disruption in an inducible murine hematopoietic progenitor cell differentiation model

3.10.1. Inducible HoxB8-ER-immortalized hematopoietic progenitor cells as a model system to monitor the early steps of hematopoiesis *in vitro*

To study the role of METTL3 in the early commitment of hematopoietic progenitors towards the myeloid and lymphoid lineage, we took advantage of a previously described *in vitro*-differentiation model, based on reversible immortalization of murine short-term HSCs (Redecke et al. 2013) (Figure 62a). In this protocol, bone marrow cell suspensions are activated *in vitro* for two days in the presence of IL-6, IL-3 and murine stem cell factor (mSCF), followed by cell transduction with retroviral particles expressing the transcription factor HoxB8 fused to the human estrogen receptor ligand-binding domain (ERHBD-HoxB8) (Figure 62a). After infection, cells are cultured in the presence of β-estradiol to ensure activation of HoxB8 transcriptional activity via shuffling of the transcription factor from the cytoplasm to the nucleus. Bone marrow cultures continuously exposed to the action of β-estradiol in the presence of Flt3L, establish, on average after two weeks, a homogeneous population of intensively proliferating hematopoietic progenitor cells. Flow cytometric analyses of the latter cells indicate expression of the c-Kit receptor, while they are negative for the stem cell-associated protein Sca-1, together with lineage cell-associated markers (Figure 62b). Upon β-estradiol removal, HoxB8-immortalized hematopoietic progenitor cells (hereafter called H8-HPCs) progressively revert to a population of resting cells, which can be instructed to differentiate towards individual blood cell-types upon exposure to specific cocktails of soluble differentiation factors (Figure 62a). For example, it is reported that continuous exposure of β-estradiol-deprived H8-HPCs to soluble IL-7 drives their commitment to the B-lymphoid lineage (Figure 62a) (Redecke et al. 2013).
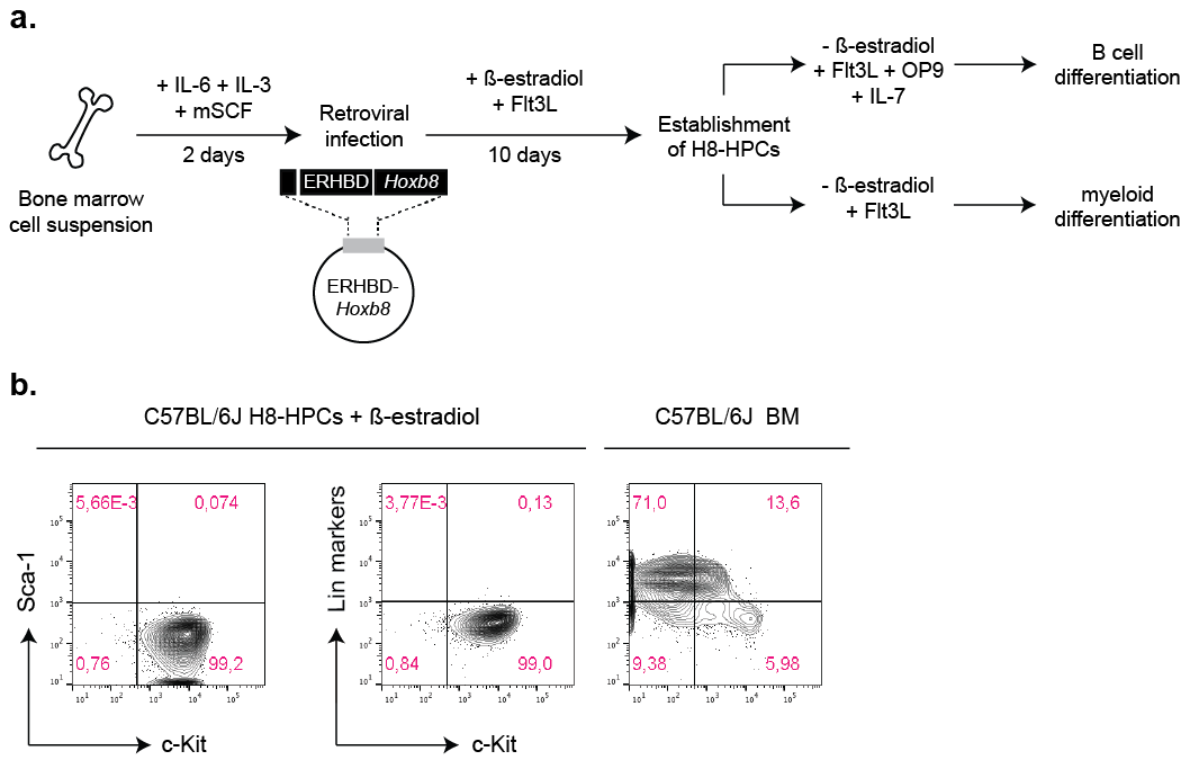
a. Schematic representation of the protocol employed to immortalize *in vitro* hematopoietic progenitor cells from bone marrow cell suspensions. Bone marrow cells are activated for two days in the presence of IL-6, IL-3 and mSCF and then transduced with a retrovirus expressing the HoxB8 transcription factor, fused together with the estrogen recognition human binding domain (ERHBD). Culturing of the infected cells in the presence of Flt3L and β-estradiol for about 10 days will lead to the establishment of HoxB8-immortalized hematopoietic progenitor cells (H8-HPCs). The latter cells can be now triggered to differentiate either into B cells, when cultured without β-estradiol on OP9 cells and in the presence of IL-7 and Flt3L, or into myeloid cells, when cultured without β-estradiol and in the presence of Flt3L. **b.** On the left: flow cytometric analysis of Sca-1 and c-Kit expression measured in H8-HPCs. On the right: flow cytometric analysis of lineage markers and c-Kit expression measured in H8-HPCs and in bone marrow (BM) cells. The latter cells were used as positive controls for lineage markers. A representative case of 3 independent experiments is shown.

3.10.2. Expression of m⁶A regulators in uncommitted H8-HPCs

We measured by quantitative RT-PCR (qRT-PCR) analysis the expression of *Mettl3* and *Mettl14* genes encoding for the subunits of the m⁶A methyltransferase complex and of the *Fto* and *Alkbh5* genes, encoding for the m⁶A demethylases, in proliferating uncommitted H8-HPCs, established from wild-type C57BL/6J mice and cultured in the presence of β-estradiol. As shown in Figure 63a, undifferentiated H8-HPCs expressed all four genes, with *Mettl3* and *Fto* displaying the highest and the lowest expression, respectively. However, when we attempted to measure the corresponding protein levels, we failed to detect immunoreactive bands for METTL3 and FTO in immunoblotting analyses on lysates produced from either bulk or cloned H8-HPCs (Figure 63b). These results suggest that H8-HPCs express extremely low levels of key enzymes controlling m⁶A homeostasis.
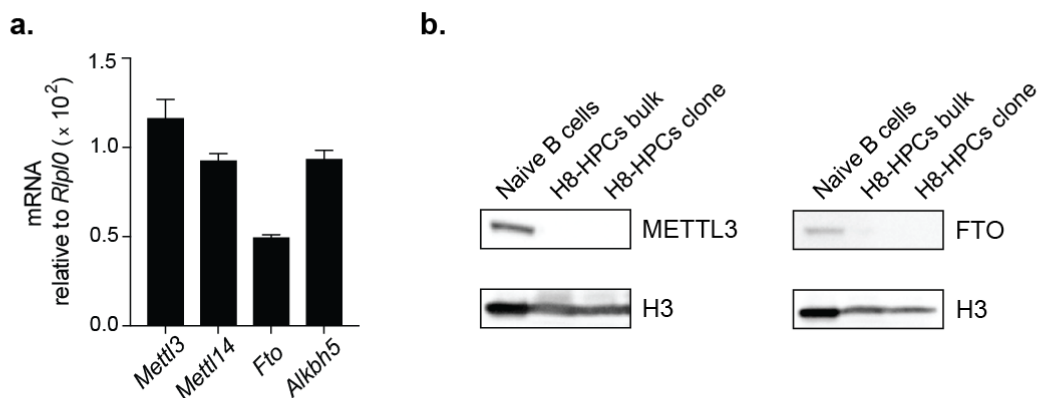
Figure 63. Expression of m⁶A players in HoxB8-immortalized HPCs.

a. Quantification of *Mettl3*, *Mettl14*, *Fto* and *Alkbh5* transcript levels, measured in immortalized H8-HPCs, cultured in the presence of β-estradiol. Data refer to transcript levels normalized to those of the housekeeping gene *Rplp0*. Columns indicate the mean of technical triplicates, ± SD. **b.** Immunoblotting analysis of METTL3 and FTO protein levels in naïve B cells isolated from the spleen of a C57BL/6J mouse, in the bulk of H8-HPCs established from C57BL/6J bone marrow cell suspension and in one clone obtained from the previous bulk by limiting dilution. The same number of cells was loaded into each lane. A representative case of 3 independent experiments is shown.

3.10.3. METTL3 is induced in H8-HPCs undergoing B cell differentiation *in vitro*

Upon β-estradiol withdrawal, IL-7 plus Flt3L stimulation will induce, in a fraction of H8-HPCs, the upregulation of the panB-cell marker B220 and, most importantly, the induction of the master regulator of B cell differentiation and identity *Pax5*. The latter will, in turn, guide the differentiation of H8-HPCs into CD19$^+$ progenitor B cells, which appear in the culture roughly 10 days after continuous treatment with IL-7 + Flt3L (Figure 64).
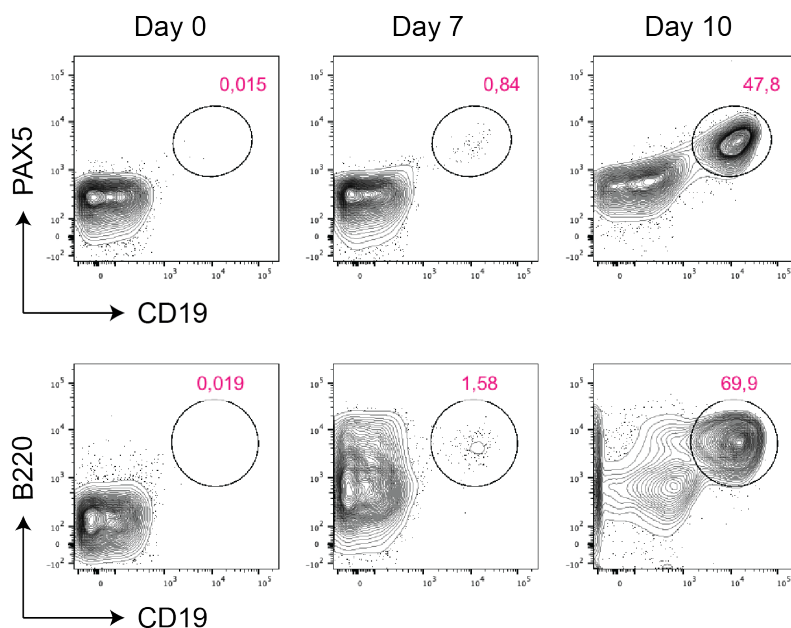
Figure 64. *In vitro* B cell differentiation of HoxB8-immortalized HPCs.

Flow cytometric analysis of B cell markers expression in H8-HPCs undergoing B cell differentiation *in vitro*. Expression of the B-cell transcription factor PAX5 and of the B-cell surface markers B220 and CD19 was assessed in H8-HPCs cultured in the presence of β-estradiol (day 0) and after 7 and 10 days of Flt3L + IL-7 stimulation, in the absence of β-estradiol. Numbers refer to percentage of cells within the gate.

To study the dynamics of METTL3 expression during the phase of IL-7-driven B cell commitment of H8-HPCs, we FACS-sorted B220$^+$CD19$^-$ pro-B cell precursors and their B220$^+$CD19$^+$ pro-B cell derivatives on day-8 and -10 of the culture, respectively. Protein extracts retrieved from these cells were subjected to immunoblotting analysis to monitor the status of METTL3 and METTL14 expression (Figure 65a). This analysis revealed that, compared to uncommitted H8-HPCs, pro-B cell precursors showed a strong induction in METTL3 and METTL14 expression, which further increased in pro-B cells (Figure 65a).

However, despite H8-HPCs managed to differentiate into B220$^+$CD19$^+$ pro-B cells after 10 days of IL-7 stimulation, the yield of B cells obtained using this *in-vitro*-B-cell differentiation system was sub-optimal, due to the spontaneous differentiation into other non-B-cell-lineages, displayed by other cells in the culture upon β-estradiol withdrawal (Figure 65b). Indeed, by day-10 of IL-7 + Fl3tL stimulation, at most 50% of the cells expressed the B cell marker and PAX5-target CD19. (Figure 65b).

a.

b.
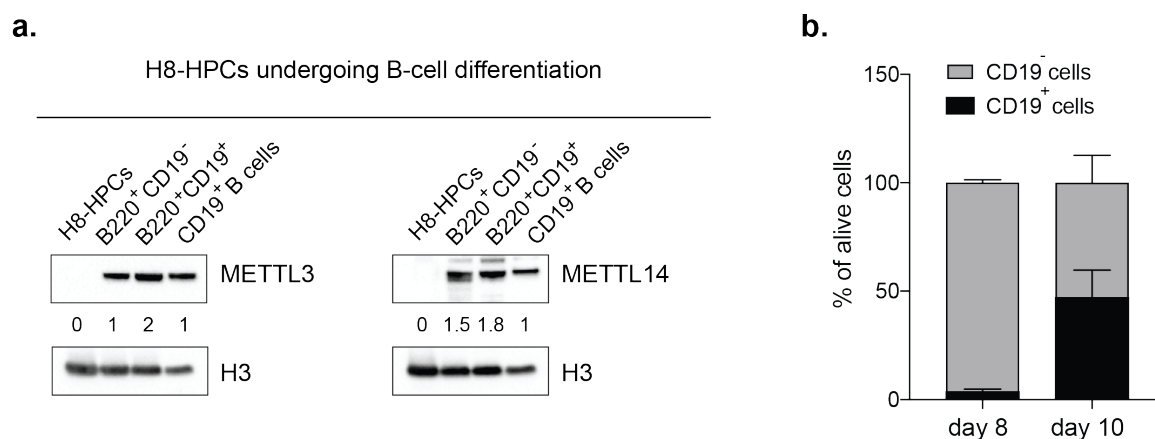
Figure 65. METTL3 and METTL14 expression in H8-HPCs undergoing B cell differentiation *in vitro*.

a. Immunoblotting analysis for METTL3 and METTL14 protein levels measured in H8-HPCs cultured in the presence of β-estradiol, and in FACS-sorted B220$^+$CD19$^-$ and in B220$^+$CD19$^+$ cells, purified on day 8 and 10, respectively, from the bulk of H8-HPCs undergoing B cell differentiation *in vitro*. Each lane contains the same number of cells. Numbers refer to METTL3 or METTL14 protein levels shown as relative to those measured in naïve CD19$^+$ B cells, isolated from the spleen of a C57BL/6J mouse. Data are representative of a single experiment. **b.** Frequency of CD19$^+$ and CD19$^-$ cells relative to the total number of H8-HPCs in the culture, measured on day 8 and 10 after Flt3L + IL-7 stimulation and β-estradiol withdrawal. Columns represent the mean (*n* = 3) values, ± SD.

3.10.4. HoxB8 extinction triggers spontaneous differentiation of H8-HPCs into *Mettl3*-expressing CD11b⁺ myeloid cells

Contrary to the partial conversion of H8-HPCs to committed B cell progenitors, in agreement with previous reports (Redecke et al. 2013), we observed a striking spontaneous propensity of H8-HPCs to differentiate into myeloid-lineage cells. Specifically, upon removal of β-estradiol, H8-HPCs, cultured only in the presence of Fl3tL, gave rise, after seven days, to a homogenous population of cells expressing the myeloid marker CD11b (Figure 66a). Immunoblotting analyses revealed that METTL3 protein levels became detectable after five days of estrogen removal, and progressively incremented until day-7 of the culture (Figure 66b). Altogether, these data indicate that commitment of H8-HPCs into either the myeloid or lymphoid lineage is accompanied by a strong induction of METTL3 expression.
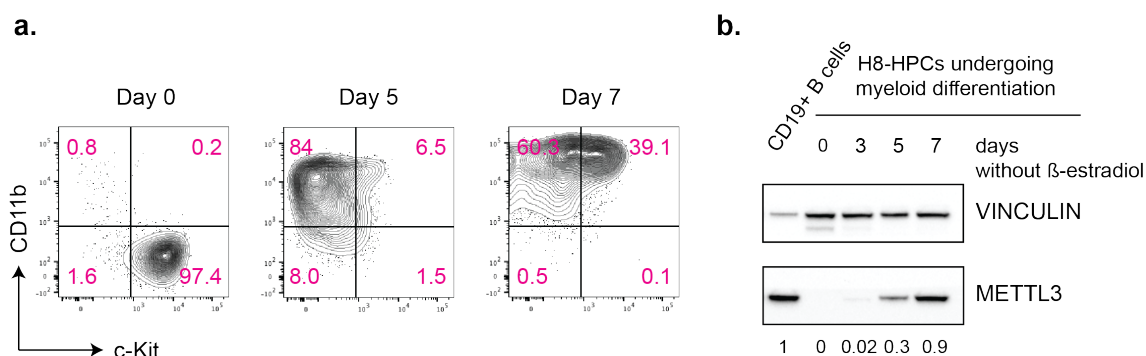
Figure 66. METTL3 expression in H8-HPCs undergoing myeloid differentiation *in vitro*.

a. Flow cytometric analysis of CD11b and c-Kit expression levels in H8-HPCs cultured in the presence of β-estradiol (day 0) and after 5 and 7 days from β-estradiol withdrawal, respectively. Numbers refer to the frequency of cells within the corresponding quadrant. A representative case of 3 independent experiments is shown. **b.** Immunoblotting analysis for METTL3 protein levels in H8-HPCs cultured in the presence of β-estradiol (day 0) and in H8-HPCs after 3, 5 and 7 days from β-estradiol withdrawal, respectively. Each lane contains the same number of cells. Numbers refer to METTL3 protein levels shown as relative to those measured in naïve CD19⁺ B cells isolated from the spleen of a C57BL/6J mouse. A representative case of 2 independent experiments is shown.

3.10.5. Generation of *Mettl3*-mutant C9-H8-HPCs

To explore the role of METTL3 function in both undifferentiated and lineage-committed H8-HPCs, we employed CRISPR/Cas9 technology to disrupt the *Mettl3* gene in these cells. For this, we isolated BM cell suspensions from a Rosa26-Cas9iGFP transgenic mouse and activated cells *in vitro* with IL-6, IL-3 and mSCF for two days (Figure 67a). Activated BM cells were subsequently infected with HoxB8-ER expressing retroviruses and allowed to grow for 10 days in the presence of β-estradiol and Flt3L. Ultimately, we generated a homogenously growing population of immortalized H8-HPCs, constitutively expressing the Cas9 nuclease (hereafter called C9-H8-HPCs) (Figure 67a). Immunophenotypic analysis of C9-H8-HPCs, confirmed expression of the c-Kit marker, while they were negative for both Sca-1 and lineage markers (Ter119, CD3, CD11b and B220; Figure 67b).
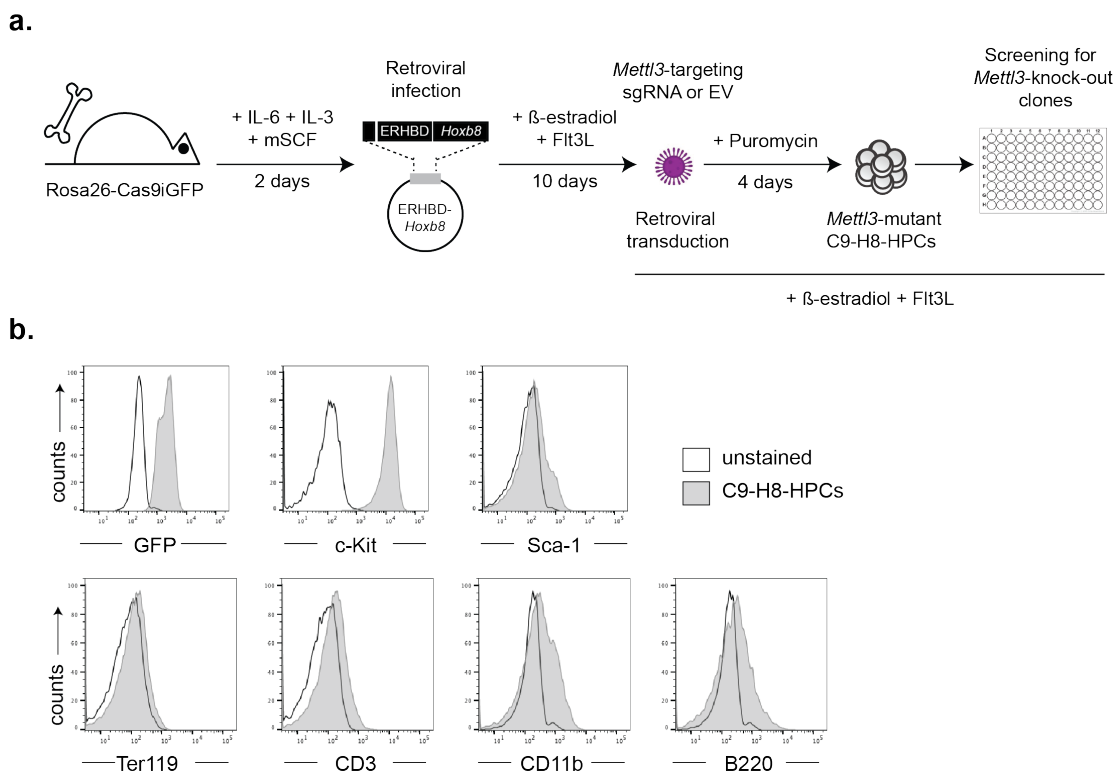
Figure 67. Generation of Cas9-expressing *Mettl3*-mutant H8-HPCs.

a. Schematic representation of the protocol used to generate *Mettl3*-mutant HoxB8-immortalized hematopoietic progenitor clones through CRISPR/Cas9 technology *in vitro*. BM cells isolated from a Rosa26-Cas9iGFP mouse are activated *in vitro* for two days in the presence of IL-6, IL-3 and mSCF. After that, activated BM cells are infected with retroviral particles expressing the transcription factor HoxB8, fused to the human estrogen receptor

ligand-binding domain (ERHBD-HoxB8). Infected cells are then cultured in the presence of β-estradiol and Flt3L in order to establish a homogeneous population of Cas9-expressing immortalized hematopoietic progenitor cells (named C9-H8-HPCs). Next, C9-H8-HPCs are infected either with the empty vector, expressing the BFP and the puromycin resistance genes, or with retroviral particles expressing also one of the two sgRNAs targeting the *Mettl3* gene (sgRNA#1 or sgRNA#3). The infected bulks are then subjected to puromycin selection in order to kill all the not infected cells. Finally, infected cells are subjected to limiting dilution assays in order to establish *Mettl3*-mutant HPC clones. **b.** Flow cytometric analysis of GFP, c-Kit, Sca-1 (top) and lineage markers expression, including Ter119, CD3, CD11b and B220 (bottom) measured in the bulk of Cas9-expressing H8-HPCs (grey, filled). Expression levels are compared to those measured in the unstained control (black, not filled). A representative case of at least 3 independent experiments is shown.

The bulk culture of C9-H8-HPCs was further infected either with an empty retroviral vector expressing the BFP gene and the puromycin resistance gene, or with retroviral particles expressing also either one of the two sgRNAs targeting the *Mettl3* gene, previously used in the iGB experiments (Figure 68a). After four days of puromycin selection, flow cytometric analysis confirmed that the three infected C9-H8-HPCs bulks were successfully expressing the BFP fluorescent protein (Figure 68a). Importantly, both C9-H8-HPCs bulks infected with viruses expressing the sgRNAs, showed evidence of disruption of the *Mettl3* gene, as revealed by T7 endonuclease surveyor assays performed on PCR amplicons covering the exon targeted by the Cas9 (Figure 68b). To assess the nature of the mutations introduced through Cas9 gene editing at the *Mettl3* locus, PCR amplicons, covering the targeted region of the gene, were cloned and subjected to Sanger sequencing. This analysis revealed that sgRNA #1 and #3 achieved, respectively, 75% and 90% targeting efficiency. Analysis of the reading frame indicated that infection with retroviruses expressing sgRNA #1 and #3 led, in 50% and 63% of the cases, to out-of-frame mutations, respectively (Figure 68c-d).
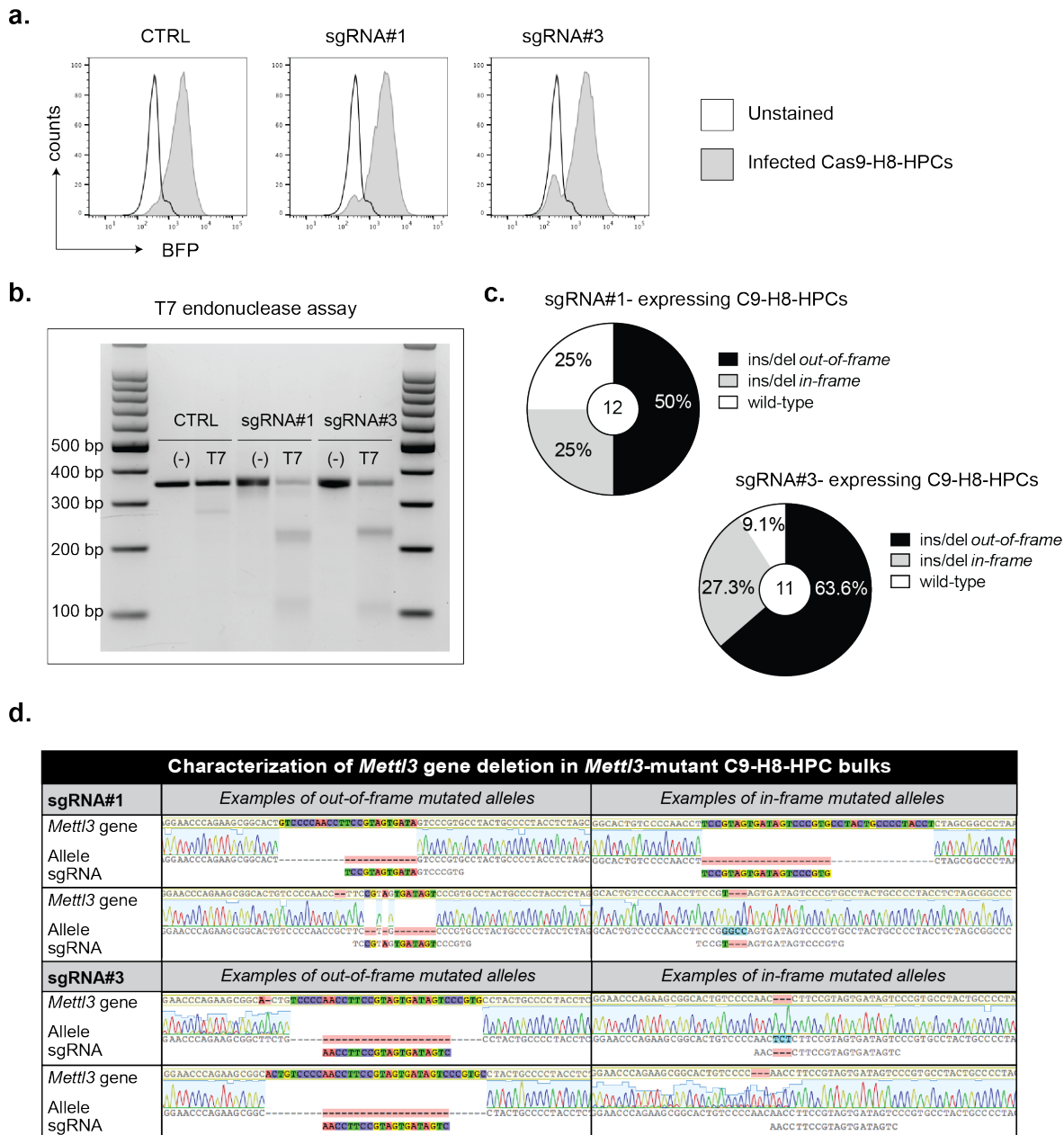
Figure 68. Assessment of *Mettl3* gene disruption in C9-H8-HPCs.

a. Flow cytometric analysis of BFP reporter expression in the bulks of C9-H8-HPCs (grey, filled) infected either with the empty vector (CTRL), or with retroviral particles expressing one of the two sgRNAs targeting the *Mettl3* gene (sgRNA#1 or sgRNA#3), respectively, performed after 4 days of puromycin selection. BFP expression levels are compared to those measured in the unstained control (black, not filled). **b.** Agarose gel electrophoretic analysis of T7 digested PCR products, covering the *Mettl3*-targeted region, amplified from the bulks of C9-H8-HPCs, infected either with the empty vector (CTRL), or with retroviral particles expressing one of the two sgRNAs targeting the *Mettl3* gene (sgRNA#1 or sgRNA#3). In the presence of heteroduplexes, T7 enzyme will cut the amplicon at the site of mismatch, leading to the formation of two smaller fragments. Aliquots of PCR products which were not digested with T7 (-) acted as negative controls. A representative case of 3 independent experiments is shown. **c.** Pie chart showing the frequencies of wild-type (in white) and of mutant alleles carrying

182

out-of-frame (black) or in-frame (grey) mutations at the *Mettl3* locus, amplified from *Mettl3*-mutant C9-H8-HPCs and analyzed by Sanger sequencing. For *Mettl3*-mutant C9-H8-HPCs bulk expressing the sgRNA#1, 12 alleles were characterized. For *Mettl3*-mutant C9-H8-HPCs bulk expressing the sgRNA#3, 11 alleles were characterized. **d.** Examples of Sanger sequencing results of two alleles carrying out-of-frame mutations (on the left) and two alleles carrying in-frame mutations (on the right) at the *Mettl3* locus, amplified from C9-H8-HPCs bulks expressing the sgRNA#1 (top) or the sgRNA#3 (bottom).

To assess whether *Mettl3* gene mutations, obtained using either sgRNA #1 or #3, affected the growth of undifferentiated C9-H8-HPCs, we compared their growth to bulk *Mettl3*-proficient control cultures, that had been infected with the empty vector. As shown in Figure 69, growth curves of the three cultures were largely comparable, indicating that *Mettl3* gene disruption is compatible with continuous growth of HoxB8-expressing HPCs.
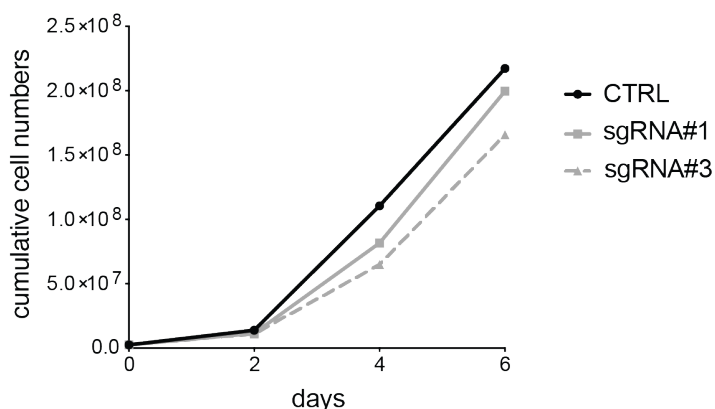
Figure 69. *Mettl3* gene deletion does not affect the growth of H8-HPCs.

Cumulative growth curve of C9-H8-HPCs infected either with the empty vector (CTRL, in black) or with one of the two sgRNAs targeting the *Mettl3* gene (sgRNA#1 in grey; sgRNA#3 in grey, dashed line), respectively. A representative case of 3 independent experiments is shown.

3.10.6. Generation of *Mettl3*-mutant C9-H8-HPCs clones

One of the strengths of H8-HPC cultures, is the possibility to derive clones using the limiting dilution method. To identify C9-H8-HPCs homogenously lacking *Mettl3* expression, we established clones from bulk-cultures that were infected either with the empty vector (acting as control) or with viruses expressing sgRNA #1 or #3. We established $n = 6$ clones from *Mettl3*-proficient C9-H8-HPC bulk cultures, and $n = 7$ (sgRNA #1) and $n = 5$ (sgRNA # 3) clones from the *Mettl3*-mutant counterparts. To assess the status of the *Mettl3* gene in the isolated clones, we extracted DNA from each of them and amplified by PCR the region of the *Mettl3* gene surrounding the Cas9-targeted sequence. PCR fragments were cloned and subjected to Sanger sequencing. As expected, we obtained only two alleles for each clone. Despite over 90% of the alleles found in the independent clones carried insertion or deletions, we observed a striking under-representation among *Mettl3*-mutant clones of those carrying bi-allelic out-of-frame mutations (Figure 70a). Indeed, among the clones carrying mutant alleles on both chromosomes ($n = 11$), only 9% ($n = 1$) carried bi-allelic frameshift mutations. Although the data so far collected were generated on a limited number of clones, the results point to an essential role played by METTL3 for the self-renewal and/or persistence of uncommitted H8-HPCs. To support this scenario, we asked whether loss/haploinsufficiency of *Mettl3* could negatively influence the maintenance of the uncommitted phenotype. To this end, we analyzed *Mettl3*-control and -mutant (either heterozygous or homozygous) C9-H8-HPC clones growing under β-estradiol, for the expression of the myeloid marker CD11b. Interestingly, we observed that *Mettl3*-mutant clones spontaneously expressed CD11b more often (4/11) than their control counterparts (1/6) (Figure 70b). These results suggest a higher susceptibility of *Mettl3*-mutant (i.e. carrying either one or two *Mettl3* inactive alleles) C9-H8-HPCs to lose their multipotent state, and possibly spontaneously drift towards the myeloid lineage. In this regard, flow cytometric analyses hypothesize a *Mettl3* gene dosage effect, with the *Mettl3* homozygous mutant clone expressing higher levels of surface CD11b than its heterozygous counterparts (Figure 70c).
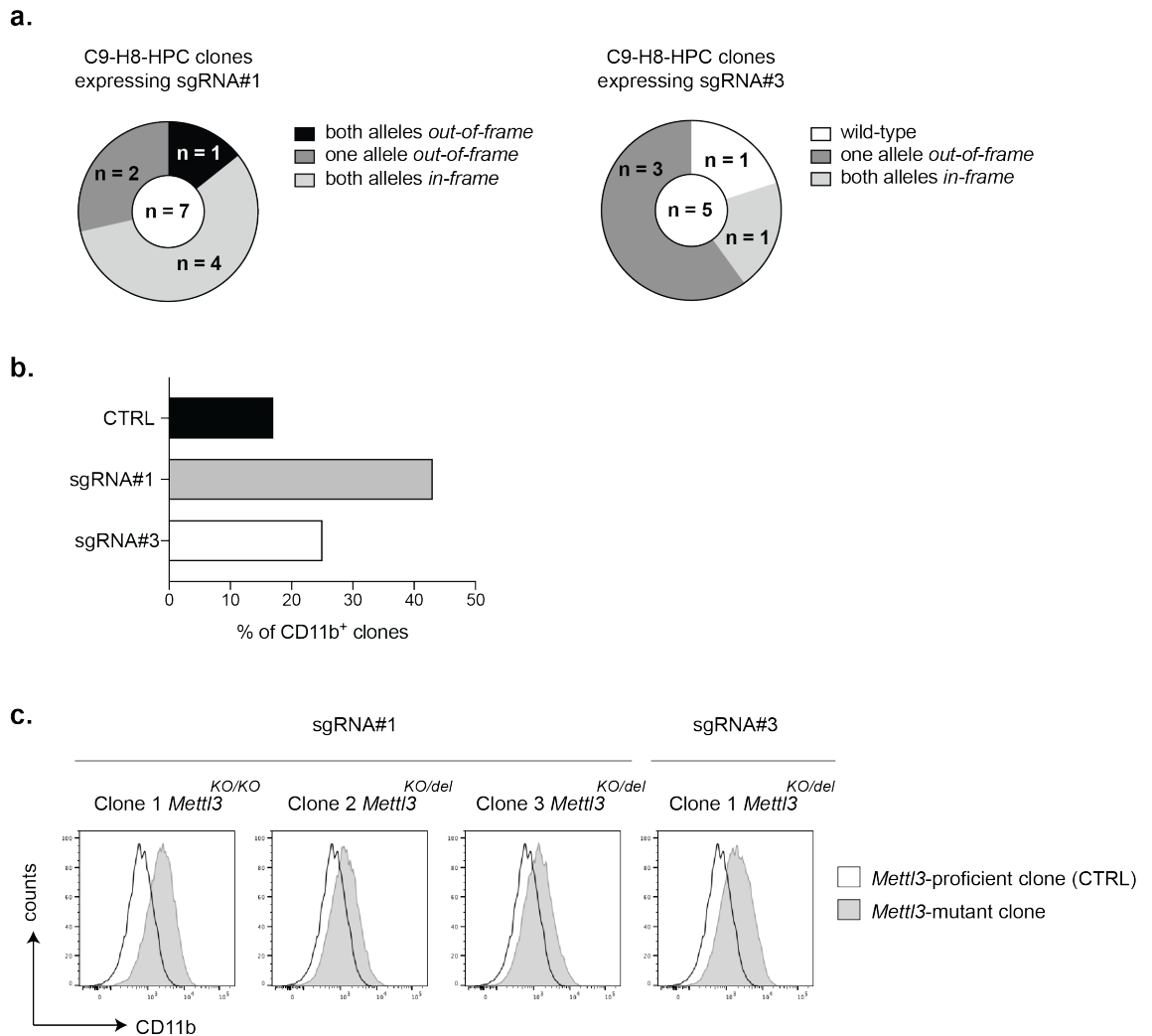
Figure 70. *Mettl3*-mutant H8-HPC clones spontaneously upregulate CD11b expression.

a. Pie chart representation showing the genetic status of the two *Mettl3* alleles of *Mettl3*-mutant C9-H8-HPC clones, obtained from the bulks infected with retroviral particles expressing either the sgRNA#1 (left) or the sgRNA#3 (right). For sgRNA#1-expressing C9-H8-HPCs bulk, 7 clones were analyzed. For sgRNA#3-expressing C9-H8-HPCs bulk, 5 clones were analyzed. Data shown are representative of a single experiment. **b.** Frequency of CD11b$^+$ clones obtained from the bulk of *Mettl3*-proficient C9-H8-HPCs (CTRL, in black) and from the two *Mettl3*-mutant bulks, expressing either the sgRNA#1 (in grey) or the sgRNA#3 (in white), respectively. **c.** Flow cytometric analysis of CD11b expression levels, measured in CD11b$^+$ *Mettl3*-mutant clones (grey, filled) and compared to those measured in the sole CD11b$^+$ clone obtained from the control bulk (CTRL, in black, not filled). The genetic status of the two *Mettl3* alleles for each mutant clone is indicated above each FACS plot. *KO*: allele bearing an out-of-frame mutation; *del* = allele bearing an in-frame mutation. Data shown are representative of a single experiment.

185

3.10.7. METTL3 controls CD11b expression in H8-HPCs undergoing myeloid differentiation

Given the high frequency of *Mettl3*-mutant H8-HPCs clones spontaneously expressing the myeloid marker CD11b under culture conditions otherwise supporting multipotency, we hypothesized that such property could accelerate/facilitate myeloid differentiation of the mutant cells upon β-estradiol removal. To test this hypothesis, bulk cultures of *Mettl3*-proficient (infected with the empty vector), and *Mettl3*-mutant (expressing either sgRNA#1 or sgRNA#3) C9-H8-HPCs, were deprived of β-estradiol and cultured in the presence of Flt3L. Puromycin was also added to the culture medium, in order to kill cells which may have silenced the retrovirus. In accordance with what we saw in individual clones, *Mettl3*-mutant bulk C9-H8-HPCs cultures (especially those infected with sgRNA#1) revealed a higher fraction of CD11b$^+$ cells already prior to estrogen removal, possibly representing mutant cells (Figure 71a). Five days after β-estradiol removal, we observed a larger proportion of cells expressing high CD11b levels in bulk *Mettl3*-mutant C9-H8-HPCs cultures. Finally, 7 days after β-estradiol removal, whereas all *Mettl3*-mutant C9-H8-HPCs expressed homogenously high CD11b levels, control cultures contained a distinct (and substantial) proportion of cells that expressed still low-intermediate levels of the myeloid marker (Figure 71a). These results are in support of a role for METTL3 in preventing differentiation of hematopoietic progenitor cells into CD11b-expressing myeloid cells. This conclusion is supported by immunoblotting analysis for METTL3 performed on protein extracts isolated from control and *Mettl3*-mutant cultures respectively at day-0, -5 and -7 after estrogen withdrawal (Figure 71b). Quantification of the data indicated that METTL3 protein levels in bulk *Mettl3*-mutant C9-H8-HPC cultures were substantially lower than in the control counterparts (Figure 71b). Importantly, the time-dependent increase in the fraction of CD11b^{hi} myeloid cells, seen in *Mettl3*-mutant C9-H8-HPC cultures, correlated with a progressive decrease in METTL3 protein levels (Figure 71b). These results further confirm a scenario whereby METTL3 activity in hematopoietic progenitor cells sustains the multipotent state of these cells, in particular by preventing spontaneous differentiation into CD11b-expressing myeloid cells.

a.

- ß-estradiol + Flt3L + Puromycin

b.

- ß-estradiol + Flt3L + Puromycin
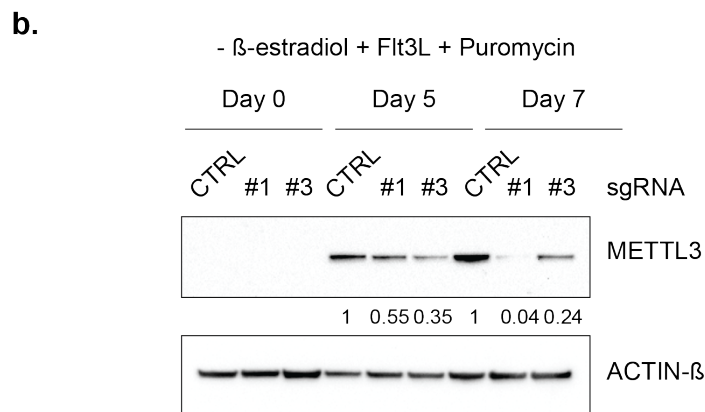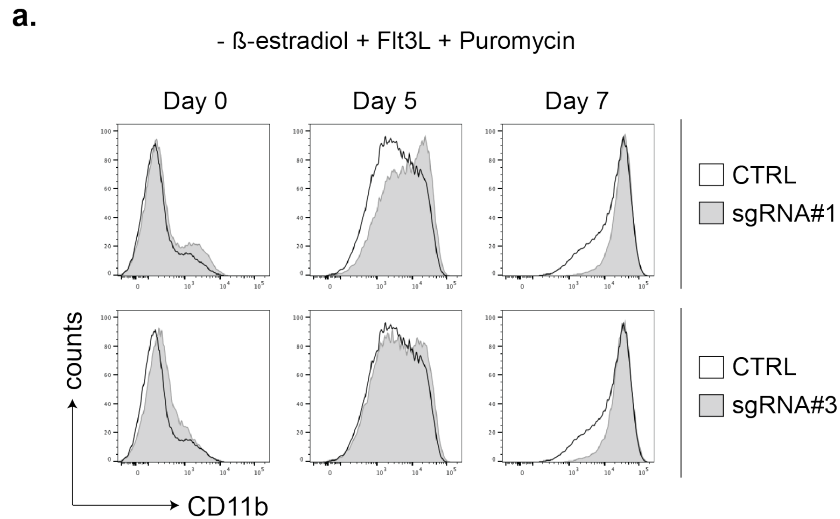
Figure 71. *Mettl3*-**mutant C9-H8-HPCs display anticipated myeloid differentiation** *in vitro***.**

a. Flow cytometric analysis of CD11b expression levels in *Mettl3*-mutant C9-H8-HPCs bulks (grey filled), expressing either sgRNA#1 (top) or sgRNA#3 (bottom), undergoing myeloid differentiation *in vitro*. Comparison with CD11b expression levels measured in *Mettl3*-proficient C9-H8-HPC bulks (CTRL, black not filled) at the corresponding timepoint is shown. CD11b expression levels were measured before β-estradiol removal (day 0), and after 5 and 7 days from β-estradiol withdrawal, in the presence of Flt3L and puromycin. A representative case of 2 independent experiments is shown. **b.** Immunoblotting analysis for METTL3 protein levels in *Mettl3*-proficient (CTRL) and -mutant (expressing either sgRNA#1 or sgRNA#3) C9-H8-HPC bulks undergoing myeloid differentiation *in vitro*. METTL3 expression was measured before β-estradiol removal (day 0), and after 5 and 7 days from β-estradiol withdrawal, in the presence of Flt3L and puromycin. The same number of cells was loaded into each lane. Numbers refer to METTL3 levels shown as relative to those measured in CTRL cells at the corresponding timepoint. A representative case of 2 independent experiments is shown.

4. Discussion

This study has addressed the role of METTL3, the catalytic subunit of the m^6A methyltransferase complex, in B cells undergoing CD40 activation and IL-21-induced terminal differentiation *in vitro*. We showed that *Mettl3* is expressed throughout B-cell development, both in progenitor and mature B cell subsets; most importantly, we could show that *Mettl3* expression is retained in B cells that have been recruited into the GCs of secondary lymphoid organs during T-cell dependent immune responses. Given the established role of m^6A mRNA modification in modulating cytokine responses in immune cells (Li, Tong, et al. 2017), as well as in promoting transcriptome switching during cell fate transitions (Batista et al. 2014), we focused our investigations on the role of m^6A selectively in the last stage of B cell development, which takes place in the GC reaction and that ultimately leads to the transition of antigen-specific GC B cells into terminally differentiated antibody-secreting PCs. By taking advantage of the *in vitro*-induced germinal center B (iGB) cell culture system, established by Nojima and colleagues (Nojima et al. 2011), we had the opportunity to study the contribution of METTL3/m^6A methylation in B-cell responses to T-cell-derived signals, including CD40L and IL-21, at a resolution which would not be possible to achieve *in vivo*. In agreements with previous studies, we demonstrated that culturing naïve resting B cells onto 40LB cells, constitutively expressing membrane-bound CD40-ligand and BAFF, in the presence of IL-4 for four days, led to a potent proliferative response of B cells, which upregulated the expression of the costimulatory molecules CD80, CD86 and MHC-II and of the pro-apoptotic receptor CD95/Fas. In addition, B cells also induced the expression of AID, a hallmark of GC B cells, leading to the appearance of a fraction of IgG1-expressing B cells on day 4 of the culture, as a result of AID-dependent Ig class switch recombination *in vitro*. Replacement of IL-4 with IL-21 on day-4 of the iGB culture, together with continuous CD40 stimulation, favored the upregulation of the PC-associated transcription factor IRF4, leading to the appearance, on day-8 of the culture, of IRF4^{hi}CD138$^+$ plasmablasts, which downregulated the expression of B-cell specific markers, including CD19.

In addition, we showed that, in concomitance with PC differentiation and, hence, exit from cell-cycle, iGB cells downregulate CD40 receptor and other genes controlled by CD40 signaling, including CD95/Fas receptor. The latter dynamics indicate that the iGB cell culture system recapitulates the complexity of B-cell responses featured by GC LZ B cells upon interaction with Tfh cells, thus representing a suitable model where to study determinants of GC B cell positive selection during the GC reaction at high resolution.

4.1. Opposite regulation of CD40L and IL-21 stimulation on *Mettl3* expression in iGB cells

To investigate the role of METTL3/m^{6}A methylation in GC-like B cells receiving Tfh-derived signals, we first measured the expression of the main subunits of the methyltransferase complex and m^{6}A levels on total RNA in iGB cells over time. *In vitro* stimulation of naïve B cells for four days with IL-4 and mCD40L, was accompanied by induction of both *Mettl3* and *Mettl14* expression, resulting in a transient increase of total m^{6}A levels from day 0 to day 4 of the culture. During the last four days, IL-21 + mCD40L stimulation initially contributed to further sustain METTL3 upregulation, and triggered a robust proliferative response.

On the other hand, continuous IL-21 + mCD40L stimulation progressively led to the downregulation of METTL3 expression, both in CD19$^+$CD138$^{lo/mid}$ activated B cells and in CD19^{lo}CD138$^+$ PBs, resulting in reduced m^{6}A-marked RNA on day 8 of the culture.

To understand the individual contribution of IL-21 and mCD40L in the modulation of *Mettl3* expression, B cells, which had been previously stimulated for four days in the presence of IL-4 + mCD40L, were further stimulated with IL-21 and mCD40L, provided either in combination or in a separate fashion. We demonstrated that IL-21 and mCD40L play antagonistic roles in modulating *Mettl3* expression, as B cells stimulated either with only IL-21 or mCD40L, showed reduced and increased METTL3 levels, respectively. Moreover, B cells stimulated with only one of the two signals were not able to proliferate efficiently, indicating that, similarly to what observed in the GC reaction *in vivo* (Luo, Weisel, and Shlomchik 2018), T-cell derived signals synergize and cooperate together, in order to guarantee the most potent proliferative burst of GC B cells.

We then showed that the vigorous expansion induced by the combination of mCD40L + IL-21, was initially accompanied with the upregulation of *Mettl3* expression thanks to CD40 signaling, that counteracted the negative regulation exerted by IL-21 on the expression of the *Mettl3* gene; on the other hand, upon exhaustion of iGB proliferative burst, as a result of IL-21-induced terminal differentiation, and in concomitance with the downregulation of the CD40 receptor, IL-21-driven signals contributed to the silencing of *Mettl3* expression. The latter dynamics suggest a scenario whereby GC B cells receiving T-cell help in the LZ, may upregulate components of the m^6A methyltransferase complex to undergo m^6A methylation events in response to CD40 stimulation. By contrast, IL-21-directed terminal differentiation of GC LZ B cells into PCs and exit from cell-cycle associate with a progressive silencing of *Mettl3* expression.

4.2. Experimental design to optimize *Mettl3* gene disruption in primary B cells

To address the role of the m^6A methyltransferase METTL3 in iGB cells, we optimized a CRISPR/Cas9-based gene editing protocol which has been recently described by the Rajewsky group, to genetically manipulate Cas9-expressing iGB cells *in vitro* (Chu, Graf, et al. 2016). Specifically, we demonstrated that B cell activation through membrane-bound CD40L allows to achieve higher B cell infection efficiency, when compared to B cell activation through soluble α-CD40. Our data are in line with the knowledge that trimeric mCD40L is able to trigger a more vigorous response, than soluble agonistic α-CD40 stimulation (Elmetwali et al. 2020). We also demonstrated that deprivation of IL-4 from the step of B cell activation, prevented IgG1 isotype switching, without affecting efficiency of Cas9-mediated gene editing, thus ensuring the possibility to study the effects of candidate genes on early B cell activation steps and isotype switching guided by IL-4, starting from the early days of the iGB culture. To improve Cas9-directed gene editing efficiency, we established clonal variants of the neuroblastoma cell line NG108-15, constitutively expressing intermediate levels of the Cas9 nuclease. Such clonal variants combine high transfection efficiency with the possibility to rapidly establish the targeting efficiency of independent sgRNAs against the gene of interest.

With this approach, we selected the two most efficient sgRNAs targeting the murine *Mettl3* gene, which were used in all the experiments described in this work. The extremely high efficiency (over 90%) of gene mutations scored at the *Mettl3* locus using either iGB cells or HoxB8-immortalized HPCs, confirms the usefulness of the Cas9-expressing NG108-15 in experimentally validating sgRNAs, previously chosen based on widely used algorithms.

4.3. Effects of *Mettl3* gene deletion in mCD40L/IL-21-stimulated iGB cells

4.3.1. *Mettl3* gene disruption in iGB cultures selects *Mettl3*-hypomorphic B cells

By applying our optimized version of the CRISPR/Cas9-based protocol, we reproducibly achieved 90% of infection efficiency of iGB cells infected either with empty or sgRNA-expressing retroviral particles. The comparison of iGB cultures infected with either control or two independent *Mettl3*-directed sgRNAs revealed comparable frequency of cells expressing the BFP reporter gene. These results are compatible with at least three independent scenarios: 1) *Mettl3* loss does not affect iGB cell survival, proliferation and terminal differentiation; 2) *Mettl3* gene targeting ensures iGB cells to survive, proliferate and become PCs strictly under conditions of *Mettl3* haploinsufficiency and 3) *Mettl3* gene disruption exerts limited effects on iGB cell biology because of the long half-life of residual METTL3 protein and/or of the limited turnover of m^{6}A marked mRNAs crucial for B cell survival, proliferation and terminal differentiation. T7 endonuclease assays performed on DNA from day-8 iGB cultures, confirmed high efficiency of Cas9 targeting of the *Mettl3* locus using either of the two selected sgRNAs, thus confirming the persistence of *Mettl3*-mutant cells until late timepoints of the culture. Importantly, an in-depth analysis of *Mettl3*-mutant alleles that were PCR amplified and sequenced from such cultures, indicated a high frequency (56%) of alleles bearing in-frame mutations. The latter results strongly hint to the selection throughout the iGB culture for B cells responding to mCD40L + IL-21 thanks to the expression of METTL3 protein variants that retain (at least partially) catalytic activity. Instead, the slow kinetics of METTL3 downregulation, which was detected at the earliest at day-6 of the iGB culture, prevented us to draw any conclusion on the contribution of METTL3 to mCD40L/IL-4-induced IgG1 switching, which takes place in the first four days

of the culture. The extent of METTL3 downregulation neither increased nor decreased in the day-6-to-day-8 time-interval, which accompanies a critical developmental switch that turns a proliferating iGB culture into one that undergoes terminal differentiation or senescence. This result points to the dependence of terminally differentiating B cells on (at least low levels of) functional METTL3 protein. In support of this result, we observed that CD138-expressing PBs purified at day-13 of the iGB culture largely consisted of *Mettl3*-proficient cells, while their CD19$^+$CD138$^-$ progenitors expressed strikingly lower METTL3 levels.

4.3.2. *Mettl3* expression is crucial for optimal proliferation of CD40-activated iGBs

A reproducible and significant delay in the growth of iGB cells disrupted for *Mettl3* gene integrity was scored between day-4 and day-8 of the culture. A close monitoring of the growth behavior of *Mettl3*-mutant iGB cells in the latter time-interval revealed that the contraction in B cell expansion was primarily restricted to the first 48 hours following mCD40L + IL-21 stimulation. This was confirmed by cell-cycle distribution analysis, revealing a distinct delay in the G$_1$-to-S transition in *Mettl3*-mutant iGB cultures, together with an increased fraction of cells displaying a sub-G1 content of DNA, likely representing cells undergoing programmed cell death.

To investigate the molecular bases for the initial delay in the proliferative response of *Mettl3*-hypomorphic iGB cells, we turned to whole transcriptomics analyses. These analyses identified the c-MYC transcription factor as a likely molecular determinant for the delayed growth of *Mettl3*-mutant B cells. Indeed, genes downregulated in *Mettl3*-hypomorphic cultures, as compared to controls, were significantly enriched ($p < 0.001$) for bona-fide MYC targets in B cells (n = 100 of the n = 151 downregulated genes in *Mettl3*-mutant cultures) (Sabo et al. 2014). On the contrary, only 32 of the 168 upregulated genes in *Mettl3*-mutant cultures, as compared to controls, where bound by MYC protein.

These results are supportive of a model whereby m^{6}A methylation positively regulates stability and/or translation of c-MYC-target genes and/or the *c-Myc* transcript.

In support of the latter hypothesis, we showed that *Mettl3*-mutant cells displayed a reproducible downregulation of c-MYC protein levels 48 hours after mCD40L + IL-21 stimulation, whereas *c-Myc* steady-state transcript levels did not significantly change. The latter result is in agreement with previous studies on GC LZ B cells, showing upregulation of c-MYC protein levels in response to CD40 engagement, while *c-Myc* transcripts remained unperturbed (Calado et al. 2012).

A further evidence for a positive role exerted by m^{6}A methylation in B cells on *c-Myc* regulation has come from an in-depth characterization of the m^{6}A mRNA methylome profile, which we established for the first time for a primary murine MYC-driven lymphoma established in our lab from the lymphoma-prone λ-MYC mouse strain (Kovalchuk et al. 2000; Varano et al. 2017). Indeed, in these malignant B cells, the *c-Myc* transcript was directly targeted by the m^{6}A methylation machinery. Our results are in line with several previous studies reporting m^{6}A methylation of *c-Myc* transcripts in different cell types, which positively correlated with expression of the corresponding protein (Cheng et al. 2019; Lee et al. 2019; Yang et al. 2020). In addition, the m^{6}A methylome of λ-MYC lymphoma cells was significantly (adjusted *p*-value < 0.05) enriched for transcripts encoded by previously described MYC target genes. These included transcripts encoding for proteins involved in ribosome biogenesis (*Rcl1*, *Mrto4*, *Utp20*, *Rrp12*, *Nip7*, *Wdr43*), ribosomal proteins (*Rps10*, *Rps2*, *Rplp0*, *Npm1*), components of the translational machinery (*Eif3b*, *Eif1ax*, *Pabpc1*), regulators of DNA and RNA polymerase (*Ran*, *Pcna*, *Nolc1*) and RNA binding proteins (*Hnrpu*, *Hnrnpa3*, *Hnrnpa2b1*, *Hnrnpd*). This result indicates that m^{6}A methylation extends its control to a broader c-MYC-centered transcriptional network. Notably, we show that m^{6}A-marked transcripts in MYC transformed B cells display higher expression when compared to mRNAs lacking m^{6}A methylation, thus suggesting that in MYC-expressing B cells, m^{6}A deposition sustains the expression of targets of the transcription factor.

The delayed growth suffered by *Mettl3*-mutant B cells in the first 48 hours of mCD40L + IL-21 stimulation could be explained by the reduced expression of genes promoting G$_1$-to-S cell-cycle progression. Indeed, among the downregulated genes in *Mettl3*-mutant iGB cells, we found a significant (adjusted *p*-value = 0.02) enrichment for targets of E2F transcription

factor family members, which are key controllers of the G_1-to-S transition of the cell-cycle (Sears, Ohtani, and Nevins 1997; Adams et al. 2000; Leung et al. 2008).

Interestingly, transcripts of genes controlled by E2F transcription factors were also significantly (adjusted p-value < 0.05) enriched among m^6A targets in MYC-expressing B cell lymphomas. These results highlight a MYC-E2F gene regulatory axis whose control on cell-cycle progression is supported by m^6A deposition on the corresponding transcripts, enhancing their expression. We then hypothesized that weakening of the initial proliferative response of iGB cells to mCD40L + IL-21 stimulation may exert a detrimental effect on the competitive fitness of these cells. In support of this hypothesis, we observed a reproducible counterselection of *Mettl3*-hypomorphic B cells when placed in competition with their proficient counterparts at 1:1 ratio, in iGB mixed cultures. These results are of potential relevance in the context of the events occurring in antigen-selected GC LZ B cells following the first interaction with Tfh cells. Indeed, based on our results, we hypothesize that the METTL3/METTL14 complex, and the m^6A regulatory axis as a whole, represent crucial regulators of the strength of signals emanating from the CD40 receptor (and possibly the BCR), which ultimately determines the proliferative potential (and thereby their fitness) of antigen-selected GC B cells, once they are recruited back to the DZ area of the GC (Gitlin et al. 2015; Mesin, Ersching, and Victora 2016).

Supporting evidences for an important role of the m^6A methylation axis in the control of B cell proliferation, comes from recent work by Zheng and colleagues, who studied the effects of conditional inactivation of METTL14 in B cell progenitors (Zheng et al. 2020). In this study, inactivation of *Mettl14* by means of the *Mb1-cre* transgene, which is active starting in pro-B cells, caused a significant block in early B cell lymphopoiesis (Zheng et al. 2020). Upon *in vitro* IL-7 stimulation, *Mettl14*-deficient pro-B cells showed reduced proliferation, when compared to control cells, despite comparable activation of the IL-7/STAT5-signaling cascade. As possible molecular determinant responsible for the reduced proliferation of the *Mettl14*-defective progenitor B cells, authors identified Cyclin D3 (*Ccnd3*), whose transcript was significantly reduced in mutant cells. It is worth mentioning that within B-lineage cells, progenitor B cells share the expression of *Ccnd3* with GC B cells (Peled et al. 2010; Cato

et al. 2011). Thus, it will be relevant to determine whether interference with the m^{6}A regulatory-axis affects DZ GC B cell proliferation by limiting *Ccnd3* expression.

4.3.3. *Mettl3*-hypomorphic iGB cells recover over time from the proliferative defect

The initial impairment in the proliferative burst suffered by *Mettl3*-mutant cells, was progressively corrected in the subsequent 48 hours of the culture, as *Mettl3*-proficient and -hypomorphic B cells showed similar doubling time by 96 hours of mCD40L + IL-21 stimulation. The latter result is compatible with different kinetics of *Mettl3*-proficient and -hypomorphic iGB cultures. Indeed, by four days of mCD40L + IL-21 stimulation, whereas control iGB cells are rapidly extinguishing their proliferative potential, the *Mettl3*-hypomorphic counterparts, which are lagging behind, continue to respond to CD40 engagement to fulfill the number of cell divisions required to epigenetically activate the transcriptional program leading to cell-cycle arrest and terminal differentiation (Scharer et al. 2018). In agreement with the temporal desynchronization of *Mettl3*-proficient and -mutant iGB cultures, we observed a higher fraction of actively dividing cells in *Mettl3*-mutant iGB cultures after 4 days of mCD40L + IL-21 stimulation, which correlated with increased expression of the c-MYC protein and its associated gene signatures, when compared to controls.

4.3.4. Reduced *Mettl3* expression in mCD40L-activated B cells delays the onset of IL-21-induced terminal differentiation

Differentiation of GC B cells into PCs strictly depends on the concerted induction of a set of transcription factors, including BLIMP1 (encoded by the *Prdm1* gene), IRF4, XBP1 and OBF1, which are under reciprocal transcriptional regulation (Nutt, Hodgkin, et al. 2015; Muto et al. 2010; Klein et al. 2006). Transcriptome coupled to immunoblotting analyses revealed that expression of the major TFs controlling B cell terminal differentiation was negatively influenced by METTL3 knockdown in the first 48 hours of mCD40L + IL-21 stimulation. Indeed, we observed reduced *Prdm1* transcript levels in recently activated *Mettl3*-mutant iGB cultures.

It has been proposed that fine tuning of IRF4 protein levels critically regulates B cells at different stages of the GC response. Indeed, whereas low IRF4 protein levels in GC B cell precursors facilitate their entry into the GC, possibly sustaining the expression of the DZ GC B cell master regulator *Bcl6* and *Pou2af1*, increased expression of the transcription factor in a selected subset of LZ B cells shifts its binding to interferon response regulatory elements within the promoter of the PC determinant *Prdm1,* thereby triggering terminal differentiation (Ochiai et al. 2013; Sciammas et al. 2006). In agreement with these data, reduced levels of *Prdm1* in *Mettl3*-mutant iGB cells were accompanied by reduced *Irf4* expression, determined both at the transcript and protein level. Notably, in MYC-expressing λ-MYC lymphoma B cells, *Irf4* transcripts were significantly enriched for m^{6}A deposition. Should this result be confirmed in future experiments in wild-type MYC-expressing CD40-activated B cells, the results establish a positive regulation imposed by m^{6}A deposition on *Irf4* steady state transcript levels.

Within the first 48 hours of mCD40L and IL-21 stimulation, *Mettl3*-hypomorphic B cells showed impaired upregulation of *Pou2af1*/OBF1, a coactivator of the OCT2 transcription factor. Expression of *Pou2af1* gene was shown to be required for transcriptional activation of the *Prdm1* locus and for optimal induction of terminal B cell differentiation in response to CD40L/IL-4 stimulation (Corcoran et al. 2005; Schubart et al. 1996). In accordance with what previously shown in *Pou2af1*-deficient CD40-activated B cells (Corcoran et al. 2005; Schubart et al. 1996), *Mettl3*-mutant iGB cells displayed reduced expression of the PC-associated gene *J chain*, encoding for a mediator of polymeric IgM and IgA transport.

Alongside with reduced *Prdm1* expression, we observed weaker induction in the first 48 hours of mCD40L + IL-21 stimulation of *Mettl3*-hypomorphic iGB cultures, of the PC transcription factor XBP1, which is under BLIMP1 positive control (Shaffer et al. 2004). Most importantly, *Mettl3*-mutant B cells expressed lower levels of the *Xbp1* mRNA isoform (*Xbp1S*) generated by IRE1-mediated cleavage of the 3' end of the transcript, which confers transcriptional activity to the protein (Calfon et al. 2002). In PCs, XBP1 controls the expression of a selected set of genes involved in the UPR, which is strictly required in these cells to ensure the high synthesis rate of properly folded immunoglobulin heavy and light

chains polypeptides (Reimold et al. 2001). Coherently with reduced XBP1 expression, UPR gene expression signature was significantly (adjusted p-value = 0.02) downregulated in *Mettl3*-mutant iGB cells, when compared to control cells, 48 hours after mCD40L and IL-21 stimulation. Altogether, these results are consistent with a scenario whereby within the first 48 hours of mCD40L + IL-21 stimulation, METTL3 plays a crucial role in orchestrating the initial activation of the transcriptional network, which will be crucial after several further rounds of cell divisions, to commit B cells to the PC fate. Whether direct control over *Irf4* expression through m^6A methylation of its transcripts represents the key molecular event through which *Mettl3* controls the onset of the PC-associated transcriptional program in mCD40L/IL-21 stimulated B cells represents an attractive hypothesis that awaits dedicated future validation experiments.

A complementary mechanism through which METTL3 could facilitate the activation of the PC transcriptional network from the early stages of mCD40L + IL-21 stimulation is linked to its positive influence on cell-cycle progression. Indeed, activation of BLIMP1 expression is strictly linked to cell-division based epigenetic erasure of repressive chromatin marks at the promoter of the *Prdm1* gene (Caganova et al. 2013; Beguelin et al. 2013; Scharer et al. 2018). Hence, METTL3 knockdown could delay (yet not prevent) the onset of PC differentiation by negatively impacting on the length of the cell-cycle, as indicated by the prolonged doubling time of mutant iGB cells, when compared to controls, in the first 48 hours of mCD40L + IL-21 stimulation. Compatible with the proposed scenario, we report a reproducible delay of *Mettl3*-hypomorphic mCD40L + IL-21-activated B cells at day-6/8 of the culture, to transit from CD19$^+$IRF4^{hi}CD138$^-$ PB precursors to CD19^{lo}IRF4^{hi}CD138$^+$ terminally differentiated PBs. In this context, it is worth pointing out that it took *Mettl3*-hypomorphic iGB cultures three further days to normalize the differences with *Mettl3*-proficient cultures of the frequency of terminally differentiated IRF4^{hi}CD138$^+$ PBs.

4.4. METTL3 is required for the persistence of *in vitro*-generated terminally differentiated plasmablasts

The data discussed so far point to a crucial role exerted by optimal METTL3 levels in the commitment of mCD40L/IL-21-stimulated B cells to the PC lineage. We next asked, whether METTL3 had any impact on the persistence of newly generated short-lived PBs generated *in vitro* in response to mCD40L + IL-21 stimulation. Despite the observed effect of IL-21 signaling to reduce METTL3 protein levels in latest stages of the iGB culture, multiple evidences point to an important contribution of *Mettl3* to the persistence of terminally differentiated PBs. First, genotyping analysis of *Mettl3* mutant alleles in the bulk of B cells retrieved after 96 hours of mCD40L + IL-21 stimulation revealed over 50% of the sequences carrying in-frame deletions. This result suggests that the bulk population of activated B cells has been selected for the expression of *Mettl3* variants retaining (at least some degree of) enzymatic function. Indeed, *Mettl3* gene deletions targeted the *N*-terminus of the protein, which is predicted to interact with WTAP, the regulatory subunit involved in the recruitment of the methyltransferase complex to the target mRNAs (Ping et al. 2014).

Second, immunoblotting analyses performed on purified CD19^{+}CD138^{-} activated B cells and on their CD138^{+} PB derivatives showed a striking difference in the levels of METTL3 expression. Whereas CD138^{-} activated B cells displayed 60-to-80% reduction of METTL3 protein levels, those that successfully differentiated into CD138-expressing PBs expressed higher levels of METTL3 protein, showing only a 40% reduction, when compared to control terminally differentiated cells. This result indicates that the transition from a PB precursor to a fully differentiated PB requires the full complement of METTL3 molecules, yet at reduced levels. The strong counter selection of *Mettl3*-defective PBs and precursors is supported by the substantial normalization of the gene expression profile of bulk *Mettl3* gene-edited B cells retrieved after 96 hours of mCD40L and IL-21 stimulation. In an analogous fashion, in preliminary data obtained from a first quantitative proteome analysis, we obtained only limited information on the impact of *Mettl3* gene inactivation on the repertoire of proteins expressed by late stages iGB cultures (collected after 96 hours of mCD40L and IL-21 stimulation, data not shown).

4.5. METTL3 function in positively selected GC LZ B cells: lessons from *Mettl3-mutant iGB cultures*

Engagement of antigen-selected GC LZ B cells through the CD40 receptor, as a result of the establishment of an immune synapse with Tfh cells, represents a central moment in the GC response. Indeed, B cells receiving signals through CD40 and the BCR are committed to return to the DZ where they execute further rounds of Ig somatic hypermutations to further increase affinity of their BCR for cognate antigen. In this context, recent reports have highlighted the importance of the signal strength received through the BCR/CD40 axis to determine the competitive fitness of different LZ B cells destined to return to the DZ area for further rounds of cell division (Calado et al. 2012; Luo, Weisel, and Shlomchik 2018). Among the key determinants controlling the fitness of individual positively-selected B cells is the transcription factor c-MYC, whose expression is transiently induced and stabilized in response to CD40 and BCR engagement (Calado et al. 2012; Luo, Weisel, and Shlomchik 2018). The reduction in c-MYC protein (but not transcript) levels, detected in *Mettl3*-hypomorphic iGB cultures, transiently activated for 48 hours through the CD40 receptor in the presence of IL-21, identifies the METTL3/METTL14 complex as a new positive regulator of c-MYC protein levels in LZ B cells that have recently interacted with Tfh cells.

The identification, for the first time in MYC-expressing malignant mature B cells, of m^6A deposition on *c-Myc* transcripts is compatible with the view whereby the METTL3/METTL14 axis directly, positively regulates c-MYC protein levels in positively selected LZ B cells upon engagement of the CD40 (and possibly BCR) receptor.

Similar conclusions were recently reached by the Shulman group in a pre-print article deposited in bioRxiv.org (Grenov et al., 2020). In this article, authors report the effects of conditional inactivation of *Mettl3* in GC B cells using the *Aicda*-cre transgene. After normal nucleation of GCs, mice with GC B cell-specific inactivation of *Mettl3* showed reduced fraction of GC B cells by day-14 after immunization with the T-cell dependent antigen NP-KLH (keyhole limpet hemocyanin). Even in this case, the phenotype correlated with reduced *c-Myc* expression, combined with the downregulation of MYC- and E2F-target genes.

Mechanistically, Grenov and colleagues have proposed that m⁶A methylation enhances in GC B cells *c-Myc* transcript stability, thanks to its binding to the RNA-binding protein IGF2BP3, whose expression is induced upon CD40 engagement.

The finding that a substantial set of downregulated genes in *Mettl3*-hypomorphic iGB cells, were direct c-MYC targets and also marked by m⁶A in MYC-transformed B cells, extends the control imposed by m⁶A methylation to a broader network of c-MYC regulated genes, including genes controlling cell-cycle progression, such as E2F-controlled genes.

Furthermore, we detected a mild, yet reproducible, acute reduction in surface CD40 levels expressed by *Mettl3*-mutant iGB cells within the first 48 hours of mCD40L and IL-21 stimulation, thus suggesting a positive contribution of METTL3 to optimal CD40 expression in activated iGB cells. This scenario is in agreement with recent work by Wang et al, which have identified, in dendritic cells, METTL3 and the m⁶A reader YTHDF1, as positive regulators of *Cd40* mRNA translation through m⁶A deposition (Wang et al. 2019). Importantly, the mild downregulation of CD40 may contribute to acutely limit the extent of c-MYC upregulation in *Mettl3*-mutant iGB cells responding to mCD40L. These results predict a negative impact imposed by sub-optimal METTL3 functionality on the competitive fitness of antigen-selected GC LZ B cells. To test the latter hypothesis, we performed co-culture experiments, mixing at 1:1 ratio *Mettl3*-proficient and -hypomorphic iGB cells, while responding to mCD40L and IL-21 stimulation. Strikingly, under these experimental conditions, iGB cells showing over 50% reduction of *Mettl3* transcript levels, were rapidly counter selected by their proficient counterparts.

Recent studies have highlighted the importance of mTORC1 in supporting the anabolic demands of recently CD40-activated GC LZ B cells, to sustain further rounds of cell division in the DZ area of the GC reaction (Ersching et al. 2017). Importantly, the strength of co-stimulatory signals, received by antigen-selected GC B cells from Tfh cells through mCD40L, positively determines the number of cell divisions which the same cells will carry out in the DZ area (Gitlin et al. 2015). In this context, it was proposed that the amplitude of mTORC1 activation in GC LZ B cells, as reflection of the strength of costimulatory signals received from Tfh cells, defines the proliferative potential and, hence, the fitness of GC B

cells, possibly also through a direct regulation of c-MYC translation (Yang et al. 2016; West, Stoneley, and Willis 1998; Verbist et al. 2016). Notably, *Mettl3*-hypomorphic iGB cells, stimulated for 48 hours with mCD40L + IL-21, showed reduced transcript levels of genes associated with mTORC1 signaling pathway (adjusted *p*-value = 0.02). In support of this result, transcripts belonging to mTORC1 signaling pathway showed significant enrichment for m^{6}A deposition in MYC-expressing B cell lymphomas (adjusted *p*-value < 0.05).

In summary, by analyzing *Mettl3*-hypomorphic iGB cells, we have identified for the first time, molecular determinants (c-MYC, E2F-controlled cell-cycle genes) and signaling pathways (mTORC1) under control of m^{6}A mRNA methylation, which are predicted to critically influence the fitness of antigen-selected GC LZ B cells, following establishment of the immune synapse with Tfh cells (Figure 72). The rapid disappearance of CD40-activated *Mettl3*-mutant iGB cells, when placed in competition with their proficient counterparts, highlights the advantage of using the iGB culture system to specifically capture molecular insights of GC B cells selection processes taking place in the LZ area, which would otherwise be difficult to monitor *in vivo* in such a highly selective environment. Furthermore, genetic tools to study the *in vivo* function of genes of interest, restricted to antigen-selected GC LZ B cells, remain unavailable, whereas data reached with pan-GC-B-cell-induced gene inactivation risk to be misinterpreted, given the highly dynamic environment of the GC reaction.
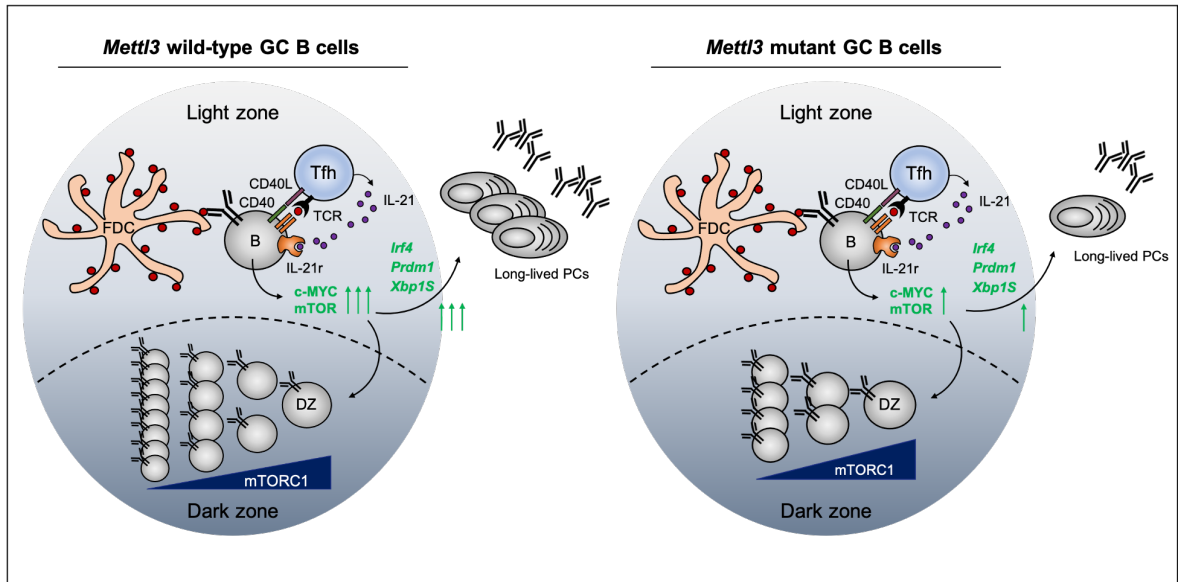
Figure 72. Proposed model for METTL3 functions in antigen-selected germinal center B cells.

Cartoon describing the proposed functions of METTL3 in germinal center (GC) B cells, receiving T-cell help in the light zone (LZ). In wild-type LZ GC B cells (right panel), METTL3 may sustain c-MYC expression, induced upon the concerted action of BCR and CD40 signaling pathways, thus favoring the survival of B cells expressing high-affinity BCRs. METTL3 may also promote terminal differentiation of positively selected LZ B cells into PCs, by triggering the induction of key PC-associated transcription factors, including *Irf4*, *Prdm1* and *Xbp1S*. Finally, by positively sustaining the activation of mTOR kinase in LZ B cells upon CD40 engagement, METTL3 may be crucial to ensure the anabolic support that is required by B cells to undergo a certain number of cell divisions, once re-entered in the DZ. Upon METTL3 downregulation (left panel), proliferation and survival of high-affinity LZ B cells are negatively affected, due to impaired c-MYC expression. The reduced proliferation, together with a possible negative effect of reduced m^6A methylation on the stability and/or translation of key PC-associated transcripts, including *Irf4*, *Prdm1* and *Xbp1S*, also impairs the induction of the PC transcriptional program, thus preventing B cell terminal differentiation into PCs. Finally, METTL3 downregulation may negatively affect clonal selection in the DZ, due to the limited activation of mTORC1 signaling pathway received in the LZ, which will, in turn, reduce the number of cell divisions to which B cells will undergo once re-entered in the DZ.

4.6. METTL3 sustains multipotency of murine hematopoietic progenitor cells

During my graduate studies, I extended my interest in understanding the function of METTL3 in early multipotential hematopoietic progenitor cells (HPCs). The choice to study this type of cells came from the interest to closely monitor the impact of *Mettl3* dysfunction on important lineage commitment decisions, which take place in the early stages of hematopoiesis. For this, I turned my attention to an *in vitro* inducible HPC differentiation system, based on the ability of a single transcriptional factor, HoxB8, to immortalize primary murine HPCs (Redecke et al. 2013). Importantly, reversibility of the system, achieved through the expression in murine HPCs of a β-estradiol-inducible HoxB8-ER fusion protein, allowed a stage- and time-controlled monitoring of the effects of *Mettl3* gene disruption on the growth of these cells (also called H8-HPCs), as well as on their capacity to give rise to different blood lineages cell-types upon removal of the estrogen (Redecke et al. 2013).

The possibility to clone conditionally immortalized HPCs using a limiting dilution protocol, provided us with the possibility to follow the effects of *Mettl3* inactivation in a clonal fashion. To perform *Mettl3* gene targeting in HPCs, we immortalized constitutively-expressing Cas9 primary bone marrow cells from Rosa26-Cas9iGFP mice, with an HoxB8-ERHBD retroviral vector, which was followed by a second round of infections with retroviruses expressing the same *Mettl3*-targeting sgRNAs used for the study of iGB cells.

In immortalized H8-HPCs, *Mettl3* expression was confirmed at the transcript level, whereas, at the protein level, it remained below the limit of detection by immunoblotting analyses. These results are in agreement with recent reports showing low expression levels of METTL3 in the earliest hematopoietic progenitors (Weng et al. 2018).

Upon commitment of H8-HPCs to B-lineage cells, in response to IL-7, we report a strong induction of METTL3 and METTL14 protein expression. In a similar fashion, METTL3 was also strongly upregulated in H8-HPCs triggered to differentiate into myeloid-type CD11b-expressing cells. Altogether, these results indicate that commitment of HPCs to multiple blood cell lineage types is accompanied with a remarkable increase in the expression of the essential catalytic subunits of the m^6A methyltransferase complex, pointing to an important role played by m^6A mRNA methylation in early hematopoiesis.

To study the importance of METTL3/m^{6}A methylation for the maintenance of multipotent HPCs, we disrupted the *Mettl3* gene in Cas9-expressing H8-HPCs, grown in the presence of β-estradiol. T7 endonuclease assays, coupled with Sanger sequencing of the *Mettl3* gene, using as template genomic DNA extracted from bulk sgRNA-expressing C9-H8-HPC cultures, revealed between 50% and 63% (depending on the sgRNA used) of *Mettl3* alleles carrying inactivating, frameshift mutations. Notably, when similar analyses were extended to individual C9-H8-HPC clones, obtained by limiting dilution of *Mettl3* sgRNA-expressing bulk cultures, we scored a low number of clones carrying bi-allelic *Mettl3* loss-of-function alleles. Together with the low-level expression of METTL3 protein recorded in HPCs, these results establish the strict dependence on full METTL3 catalytic activity for the continued growth of these cells. Future investigations will be needed to establish whether METTL3 activity controls self-renewal rather than long-term survival of these cells.

Immunophenotypic analyses of *Mettl3*-mutant C9-H8-HPCs pointed to another possible function of *Mettl3* in these cells. Indeed, flow cytometric analyses of *Mettl3*-mutant cells from bulk cultures grown in the presence of β-estradiol to prevent their differentiation, indicated a higher fraction, compared to control cultures, of cells spontaneously expressing the myeloid marker CD11b. In support of this result, isolation of independent *Mettl3*-mutant clones from mutant bulk cultures, identified a higher fraction of them spontaneously and homogeneously upregulating the myeloid-associated CD11b marker, as compared to *Mettl3*-proficient H8-HPC clones, established from the control culture infected with the empty vector. Finally, we observed a gene-dosage effect, whereby *Mettl3* homozygous mutant clones expressed higher levels of surface CD11b than their heterozygous counterparts. Altogether, these results are compatible with a scenario whereby METTL3 prevents premature expression of myeloid-associated markers in multipotent HPCs.

Motivated by these observations, we explored the possibility that METTL3 expression in HPCs could prevent their differentiation into myeloid lineage cells. To address this point, we released *Mettl3*-mutant HPC bulk cultures from β-estradiol exposure, to inhibit HoxB8 activity, and monitored the Flt3L-induced differentiation of cells into the myeloid lineage.

Notably, flow cytometric analysis revealed a temporal anticipation in the induction of the myeloid marker CD11b in *Mettl3*-mutant cultures, as compared to their *Mettl3*-proficient counterparts. Strikingly, time-dependent increase in the fraction of CD11b^{hi}-expressing myeloid cells, correlated with a progressive decrease in METTL3 protein levels measured in *Mettl3*-mutant C9-H8-HPC cultures. This result suggests a progressive selection in HPC cultures committed to the myeloid lineage for *Mettl3* knock-out cells.

Although preliminary, our data are in agreement with two studies, which identified, through knockdown experiments, METTL3 and METTL14 as negative regulators of *in vitro* myeloid differentiation of human CD34$^+$ hematopoietic cells (Weng et al. 2018; Vu et al. 2017). Other reports have assigned a different role to METTL3/METTL14 in HSCs and progenitors. Using the *Mx1*-cre transgene to achieve conditional inactivation of *Mettl3* or *Mettl14* starting from long-term HSCs, different reports have described an expansion of the HSC pool, which was accompanied by defects in HSCs differentiation (Yao et al. 2018; Lee et al. 2019; Cheng et al. 2019). Our results are only in apparent contrast with those described above. Indeed, timing of *Mettl3* inactivation may lead to different (possibly opposite) effects when triggered in different consecutive stages of early hematopoiesis.

Specifically, whereas METTL3/METTL14 appear crucial to facilitate the transition from long-lived HSCs to multipotent hematopoietic progenitors, the subsequent differentiation of these cells to committed myeloid (and possibly lymphoid) progenitors appears to be restrained by the same m^{6}A methyltransferase complex. Whether such restriction is linked to the positive control exerted by METTL3/METTL14 on the proliferation of the multipotent hematopoietic progenitors and/or on the negative regulation on the expression of lineage-commitment transcription factors awaits future dedicated investigations.

4.7. Future goals

This study has laid the groundwork for a better understanding of the role of METTL3/m^{6}A methylation in B cells responding to proliferative and terminal differentiation cues, after having received T-cell help. The findings are relevant for deciphering the importance of *Mettl3* and, more in general, of m^{6}A mRNA methylation in the GC reaction. In particular, our results are instrumental to understand the role of m^{6}A methylation in a highly selected subset of GC B cells, namely those that succeeded in receiving key proliferation and terminal differentiation signals, through the engagement of CD40 and IL-21 receptors, as a result of antigen presentation to Tfh cells. Data presented in this thesis will benefit from a selected set of validation experiments to strengthen its conclusions. Specifically:

1) <u>Characterization of the m^{6}A methylome of wild-type iGB cells.</u> To obtain a better understanding of the direct versus indirect effects of *Mettl3* inactivation in mCD40L/IL-21-stimulated iGB cells, it is mandatory to obtain a full m^{6}A methylome of these cells. This analysis was initially postponed, as the amount of mRNA (~ 5 µg) required for meRIP assays exceeded our capacity of iGB expansion. Recently, we have optimized the meRIP protocol and we will attempt to perform similar assays on mCD40L/IL-21-stimulated iGB cells.

2) <u>Higher resolution assessment of the molecular networks and pathways activated in *Mettl3*-defective mCD40L/IL-21 activated B cells</u>. The significant counterselection of iGB cells carrying loss-of-function mutations throughout the four days of mCD40L + IL-21 stimulation has impeded a comprehensive capture of the molecular defects suffered by these cells. Future investigations will be dedicated to the isolation of pure populations of *Mettl3*-defective mCD40L/IL-21-stimulated iGB cells. To achieve this goal, we will proceed in the following order:

   a. RNA-seq analyses revealed reduced levels in *Mettl3*-mutant iGB cultures of transcripts encoding for CD24 and CD93 surface markers. Should these data be confirmed also at the protein level by flow cytometry, we will exploit

this information to purify by FACS sorting CD24^{lo}CD93^{lo} iGB cells and test by immunoblotting analysis whether the latter subset represents bona-fide *Mettl3* knock-out cells. Should this turn out to be the case, we will first closely monitor the dynamics of appearance and disappearance of these cells throughout the thirteen days of an iGB culture. Next, we will extract from the CD24^{lo}CD93^{lo} *Mettl3* knock-out iGB subset, total RNA and proteins to repeat whole transcriptome and perform quantitative proteome analyses 48 hours after mCD40L + IL-21 stimulation. Finally, we will closely monitor the growth and PC differentiation potential of CD24^{lo}CD93^{lo} *Mettl3* knock-out cells kept in isolation (after their separation from their *Mettl3*-proficient counterparts).

b. Should we fail to identify surface biomarkers of *Mettl3* inactivation, we will attempt an alternative strategy of gene knock-out. Specifically, we will design two sgRNAs flanking the targeted exon (exon 2) of the *Mettl3* gene and try to co-express them in Cas9-expressing iGB cells. The goal of this approach would be to achieve the entire deletion of the second exon, thus preventing cells from expressing any METTL3 protein.

3) <u>Analysis of the anabolic response of iGB cells upon *Mettl3* inactivation.</u> The reduced expression of genes involved in the amino-acid sensitive mTORC1 pathway in *Mettl3*-hypomorphic iGB cultures, stimulated for 48 hours with mCD40L + IL-21, predicts an impaired neo-synthesis of polypeptides. We will analyze in closer details the activation of the mTOR pathway, by measuring expression levels and phosphorylation of a critical downstream effector, such as the S6 kinase (Laplante and Sabatini 2012). To confirm the detrimental impact of METTL3 knockdown on protein synthesis, following a previously published protocol (Schmidt et al. 2009), we will briefly treat mCD40L-activated *Mettl3*-mutant and control cultures with high concentration of puromycin which, once incorporated in nascent proteins, will block further elongation of the polypeptide chain during mRNA translation. Flow cytometric assessment of puromycin incorporation into nascent polypeptides by means of a

fluorescent-labeled anti-puromycin antibody will determine the impact of METTL3 knockdown on protein biosynthesis.

4) <u>METTL3 and PC differentiation.</u> The reduced *Irf4* expression, both at the transcript and protein level, displayed by *Mettl3*-hypomorphic iGB cells stimulated for 48 hours with mCD40L + IL-21, coupled to preliminary evidences showing deposition of m^{6}A on *Irf4* transcripts in MYC-expressing B cell lymphomas, identifies METTL3 as a positive regulator of a crucial determinant of PC differentiation and maintenance. m^{6}A-RIP-qPCR assays will confirm whether *Irf4* is a direct target of m^{6}A methylation in iGB cells. Similar experiments will be repeated for the other transcription factors implicated in B cell terminal differentiation (*Prdm1*, *Pou2af1* and *Xbp1S*) which were found to be downregulated in *Mettl3*-mutant iGB cells, 48 hours after mCD40L + IL-21 stimulation. The isolation of *Mettl3*-full knockout iGB cells, through the strategies depicted in point #2, will allow us to quantitively measure expression of PC-relevant transcription factors *Irf4*, *Prdm1*, *Pou2af1* and *Xbp1S*, respectively at early (48 hours of mCD40L + IL-21 stimulation) and late (96 and 144 hours of mCD40L + IL-21 stimulation) timepoints of IL-21-driven PC differentiation.

5) <u>Rescue of proliferative and differentiation defects of *Mettl3*-mutant iGB cells by incremented MYC expression</u>. One of the main conclusions raised by our investigations is the positive regulation imposed by the METTL3/m^{6}A methylation-axis on CD40-triggered iGB cell proliferation. We hypothesize that such control is greatly contributed by improved *c-Myc* translation. Reduced c-MYC expression in *Mettl3*-hypomorphic iGB cells may also indirectly interfere with IL-21-driven PC differentiation, by delaying DNA replication and thereby cell-division-dependent de-repression of the PC master regulator BLIMP1. To establish whether reduction in c-MYC protein levels was alone responsible for the growth and developmental defects seen in *Mettl3*-mutant iGB cultures, we will inactivate the *Mettl3* gene in pre-tumoral B cells isolated from Rosa26-Cas9iGFP; λ-MYC transgenic mice.

Indeed, the analysis of λ-MYC-complemented *Mettl3*-mutant iGB cells will reveal whether heightened c-MYC expression is able to restore acute mitogenic response to mCD40L + IL-21 stimulation and the yield of *Mettl3*-defective CD19^{lo}IRF4^{hi}CD138^{+} PBs at day-13 of the culture. Importantly, should c-MYC complementation restore the main proliferative and fitness defects seen in *Mettl3*-mutant iGB cultures, we expect to identify a significantly higher fraction of iGB cells that carry *Mettl3* loss-of-function mutations in late-stage cultures.

Adams, M. R., R. Sears, F. Nuckolls, G. Leone, and J. R. Nevins. 2000. 'Complex transcriptional regulatory mechanisms control expression of the E2F3 locus', *Mol Cell Biol*, 20: 3633-9.

Alinikula, J., K. P. Nera, S. Junttila, and O. Lassila. 2011. 'Alternate pathways for Bcl6-mediated regulation of B cell to plasma cell differentiation', *Eur J Immunol*, 41: 2404-13.

Allen, C. D., K. M. Ansel, C. Low, R. Lesley, H. Tamamura, N. Fujii, and J. G. Cyster. 2004. 'Germinal center dark and light zone organization is mediated by CXCR4 and CXCR5', *Nat Immunol*, 5: 943-52.

Allen, C. D., T. Okada, and J. G. Cyster. 2007. 'Germinal-center organization and cellular dynamics', *Immunity*, 27: 190-202.

Allman, D., A. Jain, A. Dent, R. R. Maile, T. Selvaggi, M. R. Kehry, and L. M. Staudt. 1996. 'BCL-6 expression during B-cell activation', *Blood*, 87: 5257-68.

Allman, D., R. C. Lindsley, W. DeMuth, K. Rudd, S. A. Shinton, and R. R. Hardy. 2001. 'Resolution of three nonproliferative immature splenic B cell subsets reveals multiple selection points during peripheral B cell maturation', *J Immunol*, 167: 6834-40.

Angelin-Duclos, C., G. Cattoretti, K. I. Lin, and K. Calame. 2000. 'Commitment of B lymphocytes to a plasma cell fate is associated with Blimp-1 expression in vivo', *J Immunol*, 165: 5462-71.

Asao, H., C. Okuyama, S. Kumaki, N. Ishii, S. Tsuchiya, D. Foster, and K. Sugamura. 2001. 'Cutting edge: the common gamma-chain is an indispensable subunit of the IL-21 receptor complex', *J Immunol*, 167: 1-5.

Banchereau, J., B. Dubois, J. Fayette, N. Burdin, F. Briere, P. Miossec, M. C. Rissoan, C. van Kooten, and C. Caux. 1995. 'Functional CD40 antigen on B cells, dendritic cells and fibroblasts', *Adv Exp Med Biol*, 378: 79-83.

Barbieri, I., K. Tzelepis, L. Pandolfini, J. Shi, G. Millan-Zambrano, S. C. Robson, D. Aspris, V. Migliori, A. J. Bannister, N. Han, E. De Braekeleer, H. Ponstingl, A. Hendrick, C. R. Vakoc, G. S. Vassiliou, and T. Kouzarides. 2017. 'Promoter-bound METTL3 maintains myeloid leukaemia by m(6)A-dependent translation control', *Nature*, 552: 126-31.

Barreto, V., B. Reina-San-Martin, A. R. Ramiro, K. M. McBride, and M. C. Nussenzweig. 2003. 'C-terminal deletion of AID uncouples class switch recombination from somatic hypermutation and gene conversion', *Mol Cell*, 12: 501-8.

Basso, K., and R. Dalla-Favera. 2010. 'BCL6: master regulator of the germinal center reaction and key oncogene in B cell lymphomagenesis', *Adv Immunol*, 105: 193-210.

Batista, P. J., B. Molinie, J. Wang, K. Qu, J. Zhang, L. Li, D. M. Bouley, E. Lujan, B. Haddad, K. Daneshvar, A. C. Carter, R. A. Flynn, C. Zhou, K. S. Lim, P. Dedon, M. Wernig, A. C. Mullen, Y. Xing, C. C. Giallourakis, and H. Y. Chang. 2014. 'm(6)A RNA modification controls cell fate transition in mammalian embryonic stem cells', *Cell Stem Cell*, 15: 707-19.

Baxendale, A. J., C. W. Dawson, S. E. Stewart, V. Mudaliar, G. Reynolds, J. Gordon, P. G. Murray, L. S. Young, and A. G. Eliopoulos. 2005. 'Constitutive activation of the CD40 pathway promotes cell transformation and neoplastic growth', *Oncogene*, 24: 7913-23.

Beguelin, W., R. Popovic, M. Teater, Y. Jiang, K. L. Bunting, M. Rosen, H. Shen, S. N. Yang, L. Wang, T. Ezponda, E. Martinez-Garcia, H. Zhang, Y. Zheng, S. K. Verma, M. T. McCabe, H. M. Ott, G. S. Van Aller, R. G. Kruger, Y. Liu, C. F. McHugh, D. W. Scott, Y. R. Chung, N. Kelleher, R. Shaknovich, C. L. Creasy, R. D. Gascoyne, K. K. Wong, L. Cerchietti, R. L. Levine, O. Abdel-Wahab, J. D. Licht, O. Elemento, and A. M. Melnick. 2013. 'EZH2 is required for germinal center formation and somatic EZH2 mutations promote lymphoid transformation', *Cancer Cell*, 23: 677-92.

Begum, N. A., K. Kinoshita, N. Kakazu, M. Muramatsu, H. Nagaoka, R. Shinkura, D. Biniszkiewicz, L. A. Boyer, R. Jaenisch, and T. Honjo. 2004. 'Uracil DNA glycosylase activity is dispensable for immunoglobulin class switch', *Science*, 305: 1160-3.

Ben-Sasson, S. Z., G. Le Gros, D. H. Conrad, F. D. Finkelman, and W. E. Paul. 1990. 'IL-4 production by T cells from naive donors. IL-2 is required for IL-4 production', *J Immunol*, 145: 1127-36.

Benson, M. J., S. R. Dillon, E. Castigli, R. S. Geha, S. Xu, K. P. Lam, and R. J. Noelle. 2008. 'Cutting edge: the dependence of plasma cells and independence of memory B cells on BAFF and APRIL', *J Immunol*, 180: 3655-9.

Berberich, I., G. L. Shu, and E. A. Clark. 1994. 'Cross-linking CD40 on B cells rapidly activates nuclear factor-kappa B', *J Immunol*, 153: 4357-66.

Berek, C., A. Berger, and M. Apel. 1991. 'Maturation of the immune response in germinal centers', *Cell*, 67: 1121-9.

Berek, C., and C. Milstein. 1987. 'Mutation drift and repertoire shift in the maturation of the immune response', *Immunol Rev*, 96: 23-41.

Berger, S. L., T. Kouzarides, R. Shiekhattar, and A. Shilatifard. 2009. 'An operational definition of epigenetics', *Genes Dev*, 23: 781-3.

Bertero, A., S. Brown, P. Madrigal, A. Osnato, D. Ortmann, L. Yiangou, J. Kadiwala, N. C. Hubner, I. R. de Los Mozos, C. Sadee, A. S. Lenaerts, S. Nakanoh, R. Grandy, E. Farnell, J. Ule, H. G. Stunnenberg, S. Mendjan, and L. Vallier. 2018. 'The SMAD2/3 interactome reveals that TGFbeta controls m(6)A mRNA methylation in pluripotency', *Nature*, 555: 256-59.

Bishop, G. A., C. R. Moore, P. Xie, L. L. Stunz, and Z. J. Kraus. 2007. 'TRAF proteins in CD40 signaling', *Adv Exp Med Biol*, 597: 131-51.

Bonizzi, G., M. Bebien, D. C. Otero, K. E. Johnson-Vroom, Y. Cao, D. Vu, A. G. Jegga, B. J. Aronow, G. Ghosh, R. C. Rickert, and M. Karin. 2004. 'Activation of IKKalpha target genes depends on recognition of specific kappaB binding sites by RelB:p52 dimers', *EMBO J*, 23: 4202-10.

Bonizzi, G., and M. Karin. 2004. 'The two NF-kappaB activation pathways and their role in innate and adaptive immunity', *Trends Immunol*, 25: 280-8.

Bouchard, C., K. Thieke, A. Maier, R. Saffrich, J. Hanley-Hyde, W. Ansorge, S. Reed, P. Sicinski, J. Bartek, and M. Eilers. 1999. 'Direct induction of cyclin D2 by Myc contributes to cell cycle progression and sequestration of p27', *EMBO J*, 18: 5321-33.

Bourgeois, C., B. Rocha, and C. Tanchot. 2002. 'A role for CD40 expression on CD8+ T cells in the generation of CD8+ T cell memory', *Science*, 297: 2060-3.

Breiling, A., and F. Lyko. 2015. 'Epigenetic regulatory functions of DNA modifications: 5-methylcytosine and beyond', *Epigenetics Chromatin*, 8: 24.

Bujnicki, J. M., M. Feder, M. Radlinska, and R. M. Blumenthal. 2002. 'Structure prediction and phylogenetic analysis of a functionally diverse family of proteins homologous to the MT-A70 subunit of the human mRNA:m(6)A methyltransferase', *J Mol Evol*, 55: 431-44.

Busslinger, M. 2004. 'Transcriptional control of early B cell development', *Annu Rev Immunol*, 22: 55-79.

Caganova, M., C. Carrisi, G. Varano, F. Mainoldi, F. Zanardi, P. L. Germain, L. George, F. Alberghini, L. Ferrarini, A. K. Talukder, M. Ponzoni, G. Testa, T. Nojima, C. Doglioni, D. Kitamura, K. M. Toellner, I. H. Su, and S. Casola. 2013. 'Germinal center dysregulation by histone methyltransferase EZH2 promotes lymphomagenesis', *J Clin Invest*, 123: 5009-22.

Calado, D. P., Y. Sasaki, S. A. Godinho, A. Pellerin, K. Kochert, B. P. Sleckman, I. M. de Alboran, M. Janz, S. Rodig, and K. Rajewsky. 2012. 'The cell-cycle regulator c-Myc is essential for the formation and maintenance of germinal centers', *Nat Immunol*, 13: 1092-100.

Calfon, M., H. Zeng, F. Urano, J. H. Till, S. R. Hubbard, H. P. Harding, S. G. Clark, and D. Ron. 2002. 'IRE1 couples endoplasmic reticulum load to secretory capacity by processing the XBP-1 mRNA', *Nature*, 415: 92-6.

Carbone, E., G. Ruggiero, G. Terrazzano, C. Palomba, C. Manzo, S. Fontana, H. Spits, K. Karre, and S. Zappacosta. 1997. 'A new mechanism of NK cell cytotoxicity activation: the CD40-CD40 ligand interaction', *J Exp Med*, 185: 2053-60.

Casola, S., K. L. Otipoby, M. Alimzhanov, S. Humme, N. Uyttersprot, J. L. Kutok, M. C. Carroll, and K. Rajewsky. 2004. 'B cell receptor signal strength determines B cell fate', *Nat Immunol*, 5: 317-27.

Cassese, G., S. Arce, A. E. Hauser, K. Lehnert, B. Moewes, M. Mostarac, G. Muehlinghaus, M. Szyska, A. Radbruch, and R. A. Manz. 2003. 'Plasma cell survival is mediated by synergistic effects of cytokines and adhesion-dependent signals', *J Immunol*, 171: 1684-90.

Castro-Dopico, T., and M. R. Clatworthy. 2019. 'IgG and Fcgamma Receptors in Intestinal Immunity and Inflammation', *Front Immunol*, 10: 805.

Cato, M. H., S. K. Chintalapati, I. W. Yau, S. A. Omori, and R. C. Rickert. 2011. 'Cyclin D3 is selectively required for proliferative expansion of germinal center B cells', *Mol Cell Biol*, 31: 127-37.

Cattoretti, G., C. C. Chang, K. Cechova, J. Zhang, B. H. Ye, B. Falini, D. C. Louie, K. Offit, R. S. Chaganti, and R. Dalla-Favera. 1995. 'BCL-6 protein is expressed in germinal-center B cells', *Blood*, 86: 45-53.

Cattoretti, G., L. Pasqualucci, G. Ballon, W. Tam, S. V. Nandula, Q. Shen, T. Mo, V. V. Murty, and R. Dalla-Favera. 2005. 'Deregulated BCL6 expression recapitulates the pathogenesis of human diffuse large B cell lymphomas in mice', *Cancer Cell*, 7: 445-55.

Cattoretti, G., R. Shaknovich, P. M. Smith, H. M. Jack, V. V. Murty, and B. Alobeid. 2006. 'Stages of germinal center transit are defined by B cell transcription factor coexpression and relative abundance', *J Immunol*, 177: 6930-9.

Challa, A., A. G. Eliopoulos, M. J. Holder, A. S. Burguete, J. D. Pound, A. Chamba, G. Grafton, R. J. Armitage, C. D. Gregory, H. Martinez-Valdez, L. Young, and J. Gordon. 2002. 'Population depletion activates autonomous CD154-dependent survival in biopsylike Burkitt lymphoma cells', *Blood*, 99: 3411-8.

Chan, T. D., K. Wood, J. R. Hermes, D. Butt, C. J. Jolly, A. Basten, and R. Brink. 2012. 'Elimination of germinal-center-derived self-reactive B cells is governed by the location and concentration of self-antigen', *Immunity*, 37: 893-904.

Chasman, D., K. Cepek, P. A. Sharp, and C. O. Pabo. 1999. 'Crystal structure of an OCA-B peptide bound to an Oct-1 POU domain/octamer DNA complex: specific recognition of a protein-DNA interface', *Genes Dev*, 13: 2650-7.

Chaudhuri, J., C. Khuong, and F. W. Alt. 2004. 'Replication protein A interacts with AID to promote deamination of somatic hypermutation targets', *Nature*, 430: 992-8.

Chen, M., L. Wei, C. T. Law, F. H. Tsang, J. Shen, C. L. Cheng, L. H. Tsang, D. W. Ho, D. K. Chiu, J. M. Lee, C. C. Wong, I. O. Ng, and C. M. Wong. 2018. 'RNA N6-methyladenosine methyltransferase-like 3 promotes liver cancer progression through YTHDF2-dependent posttranscriptional silencing of SOCS2', *Hepatology*, 67: 2254-70.

Cheng, Y., H. Luo, F. Izzo, B. F. Pickering, D. Nguyen, R. Myers, A. Schurer, S. Gourkanti, J. C. Bruning, L. P. Vu, S. R. Jaffrey, D. A. Landau, and M. G. Kharas. 2019. 'm(6)A RNA Methylation Maintains Hematopoietic Stem Cell Identity and Symmetric Commitment', *Cell Rep*, 28: 1703-16 e6.

Choe, J., S. Lin, W. Zhang, Q. Liu, L. Wang, J. Ramirez-Moya, P. Du, W. Kim, S. Tang, P. Sliz, P. Santisteban, R. E. George, W. G. Richards, K. K. Wong, N. Locker, F. J. Slack, and R. I. Gregory. 2018. 'mRNA circularization by METTL3-eIF3h enhances translation and promotes oncogenesis', *Nature*, 561: 556-60.

Chtanova, T., S. G. Tangye, R. Newton, N. Frank, M. R. Hodge, M. S. Rolph, and C. R. Mackay. 2004. 'T follicular helper cells express a distinctive transcriptional profile, reflecting their role as non-Th1/Th2 effector cells that provide help for B cells', *J Immunol*, 173: 68-78.

Chu, V. T., R. Graf, T. Wirtz, T. Weber, J. Favret, X. Li, K. Petsch, N. T. Tran, M. H. Sieweke, C. Berek, R. Kuhn, and K. Rajewsky. 2016. 'Efficient CRISPR-mediated mutagenesis in primary immune cells using CrispRGold and a C57BL/6 Cas9 transgenic mouse line', *Proc Natl Acad Sci U S A*, 113: 12514-19.

Chu, V. T., T. Weber, R. Graf, T. Sommermann, K. Petsch, U. Sack, P. Volchkov, K. Rajewsky, and R. Kuhn. 2016. 'Efficient generation of Rosa26 knock-in mice using CRISPR/Cas9 in C57BL/6 zygotes', *BMC Biotechnol*, 16: 4.

Ci, W., J. M. Polo, L. Cerchietti, R. Shaknovich, L. Wang, S. N. Yang, K. Ye, P. Farinha, D. E. Horsman, R. D. Gascoyne, O. Elemento, and A. Melnick. 2009. 'The BCL6 transcriptional program features repression of multiple oncogenes in primary B cells and is deregulated in DLBCL', *Blood*, 113: 5536-48.

Cobaleda, C., A. Schebesta, A. Delogu, and M. Busslinger. 2007. 'Pax5: the guardian of B cell identity and function', *Nat Immunol*, 8: 463-70.

Conacci-Sorrell, M., L. McFerrin, and R. N. Eisenman. 2014. 'An overview of MYC and its interactome', *Cold Spring Harb Perspect Med*, 4: a014357.

Coope, H. J., P. G. Atkinson, B. Huhse, M. Belich, J. Janzen, M. J. Holman, G. G. Klaus, L. H. Johnston, and S. C. Ley. 2002. 'CD40 regulates the processing of NF-kappaB2 p100 to p52', *EMBO J*, 21: 5375-85.

Corcoran, L. M., J. Hasbold, W. Dietrich, E. Hawkins, A. Kallies, S. L. Nutt, D. M. Tarlinton, P. Matthias, and P. D. Hodgkin. 2005. 'Differential requirement for OBF-1 during antibody-secreting cell differentiation', *J Exp Med*, 201: 1385-96.

Corcoran, L. M., and M. Karvelas. 1994. 'Oct-2 is required early in T cell-independent B cell activation for G1 progression and for proliferation', *Immunity*, 1: 635-45.

Corcoran, L. M., M. Karvelas, G. J. Nossal, Z. S. Ye, T. Jacks, and D. Baltimore. 1993. 'Oct-2, although not required for early B-cell development, is critical for later B-cell maturation and for postnatal survival', *Genes Dev*, 7: 570-82.

Dal Porto, J. M., S. B. Gauld, K. T. Merrell, D. Mills, A. E. Pugh-Bernard, and J. Cambier. 2004. 'B cell antigen receptor signaling 101', *Mol Immunol*, 41: 599-613.

de Alboran, I. M., R. C. O'Hagan, F. Gartner, B. Malynn, L. Davidson, R. Rickert, K. Rajewsky, R. A. DePinho, and F. W. Alt. 2001. 'Analysis of C-MYC function in normal cells via conditional gene-targeted mutation', *Immunity*, 14: 45-55.

De Silva, N. S., and U. Klein. 2015. 'Dynamics of B cells in germinal centres', *Nat Rev Immunol*, 15: 137-48.

DeFranco, A. L. 1997. 'The complexity of signaling pathways activated by the BCR', *Curr Opin Immunol*, 9: 296-308.

Delogu, A., A. Schebesta, Q. Sun, K. Aschenbrenner, T. Perlot, and M. Busslinger. 2006. 'Gene repression by Pax5 in B cells is essential for blood cell homeostasis and is reversed in plasma cells', *Immunity*, 24: 269-81.

Derudder, E., E. Dejardin, L. L. Pritchard, D. R. Green, M. Korner, and V. Baud. 2003. 'RelB/p50 dimers are differentially regulated by tumor necrosis factor-alpha and lymphotoxin-beta receptor activation: critical roles for p100', *J Biol Chem*, 278: 23278-84.

Di Noia, J. M., and M. S. Neuberger. 2007. 'Molecular mechanisms of antibody somatic hypermutation', *Annu Rev Biochem*, 76: 1-22.

Dobin, A., and T. R. Gingeras. 2015. 'Mapping RNA-seq Reads with STAR', *Curr Protoc Bioinformatics*, 51: 11 14 1-11 14 19.

Dominguez-Sola, D., J. Kung, A. B. Holmes, V. A. Wells, T. Mo, K. Basso, and R. Dalla-Favera. 2015. 'The FOXO1 Transcription Factor Instructs the Germinal Center Dark Zone Program', *Immunity*, 43: 1064-74.

Dominguez-Sola, D., G. D. Victora, C. Y. Ying, R. T. Phan, M. Saito, M. C. Nussenzweig, and R. Dalla-Favera. 2012. 'The proto-oncogene MYC is required for selection in the germinal center and cyclic reentry', *Nat Immunol*, 13: 1083-91.

Dominissini, D., S. Moshitch-Moshkovitz, M. Salmon-Divon, N. Amariglio, and G. Rechavi. 2013. 'Transcriptome-wide mapping of N(6)-methyladenosine by m(6)A-seq based on immunocapturing and massively parallel sequencing', *Nat Protoc*, 8: 176-89.

Dominissini, D., S. Moshitch-Moshkovitz, S. Schwartz, M. Salmon-Divon, L. Ungar, S. Osenberg, K. Cesarkas, J. Jacob-Hirsch, N. Amariglio, M. Kupiec, R. Sorek, and G. Rechavi. 2012. 'Topology of the human and mouse m6A RNA methylomes revealed by m6A-seq', *Nature*, 485: 201-6.

Eijkelenboom, A., and B. M. Burgering. 2013. 'FOXOs: signalling integrators for homeostasis maintenance', *Nat Rev Mol Cell Biol*, 14: 83-97.

Elgueta, R., M. J. Benson, V. C. de Vries, A. Wasiuk, Y. Guo, and R. J. Noelle. 2009. 'Molecular mechanism and function of CD40/CD40L engagement in the immune system', *Immunol Rev*, 229: 152-72.

Elmetwali, T., A. Salman, W. Wei, S. A. Hussain, L. S. Young, and D. H. Palmer. 2020. 'CD40L membrane retention enhances the immunostimulatory effects of CD40 ligation', *Sci Rep*, 10: 342.

Engel, M., C. Eggert, P. M. Kaplick, M. Eder, S. Roh, L. Tietze, C. Namendorf, J. Arloth, P. Weber, M. Rex-Haffner, S. Geula, M. Jakovcevski, J. H. Hanna, D. Leshkowitz, M. Uhr, C. T. Wotjak, M. V. Schmidt, J. M. Deussing, E. B. Binder, and A. Chen. 2018. 'The Role of m(6)A/m-RNA Methylation in Stress Response Regulation', *Neuron*, 99: 389-403 e9.

Ersching, J., A. Efeyan, L. Mesin, J. T. Jacobsen, G. Pasqual, B. C. Grabiner, D. Dominguez-Sola, D. M. Sabatini, and G. D. Victora. 2017. 'Germinal Center Selection and Affinity Maturation Require Dynamic Regulation of mTORC1 Kinase', *Immunity*, 46: 1045-58 e6.

Fasnacht, N., H. Y. Huang, U. Koch, S. Favre, F. Auderset, Q. Chai, L. Onder, S. Kallert, D. D. Pinschewer, H. R. MacDonald, F. Tacchini-Cottier, B. Ludewig, S. A. Luther, and F. Radtke. 2014. 'Specific fibroblastic niches in secondary lymphoid organs orchestrate distinct Notch-regulated immune responses', *J Exp Med*, 211: 2265-79.

Feinberg, A. P. 2018. 'The Key Role of Epigenetics in Human Disease Prevention and Mitigation', *N Engl J Med*, 378: 1323-34.

Feng, J., H. Wang, D. M. Shin, M. Masiuk, C. F. Qi, and H. C. Morse, 3rd. 2011. 'IFN regulatory factor 8 restricts the size of the marginal zone and follicular B cell pools', *J Immunol*, 186: 1458-66.

Finkelman, F. D., J. Holmes, I. M. Katona, J. F. Urban, Jr., M. P. Beckmann, L. S. Park, K. A. Schooley, R. L. Coffman, T. R. Mosmann, and W. E. Paul. 1990. 'Lymphokine control of in vivo immunoglobulin isotype selection', *Annu Rev Immunol*, 8: 303-33.

Frayling, T. M., N. J. Timpson, M. N. Weedon, E. Zeggini, R. M. Freathy, C. M. Lindgren, J. R. Perry, K. S. Elliott, H. Lango, N. W. Rayner, B. Shields, L. W. Harries, J. C. Barrett, S. Ellard, C. J. Groves, B. Knight, A. M. Patch, A. R. Ness, S. Ebrahim, D. A. Lawlor, S. M. Ring, Y. Ben-Shlomo, M. R. Jarvelin, U. Sovio, A. J. Bennett, D. Melzer, L. Ferrucci, R. J. Loos, I. Barroso, N. J. Wareham, F. Karpe, K. R. Owen, L. R. Cardon, M. Walker, G. A. Hitman, C. N. Palmer, A. S. Doney, A. D. Morris, G. D. Smith, A. T. Hattersley, and M. I. McCarthy. 2007. 'A common variant in the FTO gene is associated with body mass index and predisposes to childhood and adult obesity', *Science*, 316: 889-94.

Frye, M., B. T. Harada, M. Behm, and C. He. 2018. 'RNA modifications modulate gene expression during development', *Science*, 361: 1346-49.

Furman, R. R., Z. Asgary, J. O. Mascarenhas, H. C. Liou, and E. J. Schattner. 2000. 'Modulation of NF-kappa B activity and apoptosis in chronic lymphocytic leukemia B cells', *J Immunol*, 164: 2200-6.

Garcia-Campos, M. A., S. Edelheit, U. Toth, M. Safra, R. Shachar, S. Viukov, R. Winkler, R. Nir, L. Lasman, A. Brandis, J. H. Hanna, W. Rossmanith, and S. Schwartz. 2019. 'Deciphering the "m(6)A Code" via Antibody-Independent Quantitative Profiling', *Cell*, 178: 731-47 e16.

Gass, J. N., N. M. Gifford, and J. W. Brewer. 2002. 'Activation of an unfolded protein response during differentiation of antibody-secreting B cells', *J Biol Chem*, 277: 49047-54.

Gaudette, B. T., D. D. Jones, A. Bortnick, Y. Argon, and D. Allman. 2020. 'mTORC1 coordinates an immediate unfolded protein response-related transcriptome in activated B cells preceding antibody secretion', *Nat Commun*, 11: 723.

Geula, S., S. Moshitch-Moshkovitz, D. Dominissini, A. A. Mansour, N. Kol, M. Salmon-Divon, V. Hershkovitz, E. Peer, N. Mor, Y. S. Manor, M. S. Ben-Haim, E. Eyal, S. Yunger, Y. Pinto, D. A. Jaitin, S. Viukov, Y. Rais, V. Krupalnik, E. Chomsky, M. Zerbib, I. Maza, Y. Rechavi, R. Massarwa, S. Hanna, I. Amit, E. Y. Levanon, N. Amariglio, N. Stern-Ginossar, N. Novershtern, G. Rechavi, and J. H. Hanna. 2015. 'Stem cells. m6A mRNA methylation facilitates resolution of naive pluripotency toward differentiation', *Science*, 347: 1002-6.

Gitlin, A. D., C. T. Mayer, T. Y. Oliveira, Z. Shulman, M. J. Jones, A. Koren, and M. C. Nussenzweig. 2015. 'HUMORAL IMMUNITY. T cell help controls the speed of the cell cycle in germinal center B cells', *Science*, 349: 643-6.

Goldberg, A. D., C. D. Allis, and E. Bernstein. 2007. 'Epigenetics: a landscape takes shape', *Cell*, 128: 635-8.

Good, K. L., V. L. Bryant, and S. G. Tangye. 2006. 'Kinetics of human B cell behavior and amplification of proliferative responses following stimulation with IL-21', *J Immunol*, 177: 5236-47.

Gstaiger, M., L. Knoepfel, O. Georgiev, W. Schaffner, and C. M. Hovens. 1995. 'A B-cell coactivator of octamer-binding transcription factors', *Nature*, 373: 360-2.

Guikema, J. E., E. K. Linehan, D. Tsuchimoto, Y. Nakabeppu, P. R. Strauss, J. Stavnezer, and C. E. Schrader. 2007. 'APE1- and APE2-dependent DNA breaks in immunoglobulin class switch recombination', *J Exp Med*, 204: 3017-26.

Hampel, F., S. Ehrenberg, C. Hojer, A. Draeseke, G. Marschall-Schroter, R. Kuhn, B. Mack, O. Gires, C. J. Vahl, M. Schmidt-Supprian, L. J. Strobl, and U. Zimber-Strobl. 2011. 'CD19-independent instruction of murine marginal zone B-cell development by constitutive Notch2 signaling', *Blood*, 118: 6321-31.

Han, D., J. Liu, C. Chen, L. Dong, Y. Liu, R. Chang, X. Huang, Y. Liu, J. Wang, U. Dougherty, M. B. Bissonnette, B. Shen, R. R. Weichselbaum, M. M. Xu, and C. He. 2019. 'Anti-tumour immunity controlled through mRNA m(6)A methylation and YTHDF1 in dendritic cells', *Nature*, 566: 270-74.

Hao, Z., and K. Rajewsky. 2001. 'Homeostasis of peripheral B cells in the absence of B cell influx from the bone marrow', *J Exp Med*, 194: 1151-64.

Hess, J., P. J. Nielsen, K. D. Fischer, H. Bujard, and T. Wirth. 2001. 'The B lymphocyte-specific coactivator BOB.1/OBF.1 is required at multiple stages of B-cell development', *Mol Cell Biol*, 21: 1531-9.

Hodson, D. J., A. L. Shaffer, W. Xiao, G. W. Wright, R. Schmitz, J. D. Phelan, Y. Yang, D. E. Webster, L. Rui, H. Kohlhammer, M. Nakagawa, T. A. Waldmann, and L. M. Staudt. 2016. 'Regulation of normal B-cell differentiation and malignant B-cell survival by OCT2', *Proc Natl Acad Sci U S A*, 113: E2039-46.

Homig-Holzel, C., C. Hojer, J. Rastelli, S. Casola, L. J. Strobl, W. Muller, L. Quintanilla-Martinez, A. Gewies, J. Ruland, K. Rajewsky, and U. Zimber-Strobl. 2008. 'Constitutive CD40 signaling in B cells selectively activates the noncanonical NF-kappaB pathway and promotes lymphomagenesis', *J Exp Med*, 205: 1317-29.

Hou, J., U. Schindler, W. J. Henzel, T. C. Ho, M. Brasseur, and S. L. McKnight. 1994. 'An interleukin-4-induced transcription factor: IL-4 Stat', *Science*, 265: 1701-6.

Hsu, P. J., and C. He. 2019. 'High-Resolution Mapping of N (6)-Methyladenosine Using m(6)A Crosslinking Immunoprecipitation Sequencing (m(6)A-CLIP-Seq)', *Methods Mol Biol*, 1870: 69-79.

Hsu, P. J., Y. Zhu, H. Ma, Y. Guo, X. Shi, Y. Liu, M. Qi, Z. Lu, H. Shi, J. Wang, Y. Cheng, G. Luo, Q. Dai, M. Liu, X. Guo, J. Sha, B. Shen, and C. He. 2017. 'Ythdc2 is an N(6)-methyladenosine binding protein that regulates mammalian spermatogenesis', *Cell Res*, 27: 1115-27.

Huang, H., H. Weng, K. Zhou, T. Wu, B. S. Zhao, M. Sun, Z. Chen, X. Deng, G. Xiao, F. Auer, L. Klemm, H. Wu, Z. Zuo, X. Qin, Y. Dong, Y. Zhou, H. Qin, S. Tao, J. Du, J. Liu, Z. Lu, H. Yin, A. Mesquita, C. L. Yuan, Y. C. Hu, W. Sun, R. Su, L. Dong, C. Shen, C. Li, Y. Qing, X. Jiang, X. Wu, M. Sun, J. L. Guan, L. Qu, M. Wei, M. Muschen, G. Huang, C. He, J. Yang, and J. Chen. 2019. 'Histone H3 trimethylation at lysine 36 guides m(6)A RNA modification co-transcriptionally', *Nature*, 567: 414-19.

Inoue, T., R. Shinnakasu, W. Ise, C. Kawai, T. Egawa, and T. Kurosaki. 2017. 'The transcription factor Foxo1 controls germinal center B cell proliferation in response to T cell help', *J Exp Med*, 214: 1181-98.

Inoue, T., R. Shinnakasu, C. Kawai, W. Ise, E. Kawakami, N. Sax, T. Oki, T. Kitamura, K. Yamashita, H. Fukuyama, and T. Kurosaki. 2021. 'Exit from germinal center to become quiescent memory B cells depends on metabolic reprograming and provision of a survival signal', *J Exp Med*, 218.

Jacob, J., G. Kelsoe, K. Rajewsky, and U. Weiss. 1991. 'Intraclonal generation of antibody mutants in germinal centres', *Nature*, 354: 389-92.

Jia, G., Y. Fu, X. Zhao, Q. Dai, G. Zheng, Y. Yang, C. Yi, T. Lindahl, T. Pan, Y. G. Yang, and C. He. 2011. 'N6-methyladenosine in nuclear RNA is a major substrate of the obesity-associated FTO', *Nat Chem Biol*, 7: 885-7.

Jiao, Y., J. Zhang, L. Lu, J. Xu, and L. Qin. 2016. 'The Fto Gene Regulates the Proliferation and Differentiation of Pre-Adipocytes in Vitro', *Nutrients*, 8: 102.

Jin, H., R. Carrio, A. Yu, and T. R. Malek. 2004. 'Distinct activation signals determine whether IL-21 induces B cell costimulation, growth arrest, or Bim-dependent apoptosis', *J Immunol*, 173: 657-65.

Jones, D. D., B. T. Gaudette, J. R. Wilmore, I. Chernova, A. Bortnick, B. M. Weiss, and D. Allman. 2016. 'mTOR has distinct functions in generating versus sustaining humoral immunity', *J Clin Invest*, 126: 4250-61.

Jones, P. A. 2012. 'Functions of DNA methylation: islands, start sites, gene bodies and beyond', *Nat Rev Genet*, 13: 484-92.

Kabashima, K., N. M. Haynes, Y. Xu, S. L. Nutt, M. L. Allende, R. L. Proia, and J. G. Cyster. 2006. 'Plasma cell S1P1 expression determines secondary lymphoid organ retention versus bone marrow tropism', *J Exp Med*, 203: 2683-90.

Kallies, A., J. Hasbold, D. M. Tarlinton, W. Dietrich, L. M. Corcoran, P. D. Hodgkin, and S. L. Nutt. 2004. 'Plasma cell ontogeny defined by quantitative changes in blimp-1 expression', *J Exp Med*, 200: 967-77.

Kariko, K., M. Buckstein, H. Ni, and D. Weissman. 2005. 'Suppression of RNA recognition by Toll-like receptors: the impact of nucleoside modification and the evolutionary origin of RNA', *Immunity*, 23: 165-75.

Karthiya, R., and P. Khandelia. 2020. 'm6A RNA Methylation: Ramifications for Gene Expression and Human Health', *Mol Biotechnol*, 62: 467-84.

Kawabe, T., T. Naka, K. Yoshida, T. Tanaka, H. Fujiwara, S. Suematsu, N. Yoshida, T. Kishimoto, and H. Kikutani. 1994. 'The immune responses in CD40-deficient mice: impaired immunoglobulin class switching and germinal center formation', *Immunity*, 1: 167-78.

Kawano, M. M., K. Mihara, N. Huang, T. Tsujimoto, and A. Kuramoto. 1995. 'Differentiation of early plasma cells on bone marrow stromal cells requires interleukin-6 for escaping from apoptosis', *Blood*, 85: 487-94.

Keating, R., T. Hertz, M. Wehenkel, T. L. Harris, B. A. Edwards, J. L. McClaren, S. A. Brown, S. Surman, Z. S. Wilson, P. Bradley, J. Hurwitz, H. Chi, P. C. Doherty, P. G. Thomas, and M. A. McGargill. 2013. 'The kinase mTOR modulates the antibody response to provide cross-protective immunity to lethal infection with influenza virus', *Nat Immunol*, 14: 1266-76.

Kennedy, D. E., M. K. Okoreeh, M. Maienschein-Cline, J. Ai, M. Veselits, K. C. McLean, Y. Dhungana, H. Wang, J. Peng, H. Chi, M. Mandal, and M. R. Clark. 2020. 'Novel specialized cell state and spatial compartments within the germinal center', *Nat Immunol*, 21: 660-70.

Kim, U., X. F. Qin, S. Gong, S. Stevens, Y. Luo, M. Nussenzweig, and R. G. Roeder. 1996. 'The B-cell-specific transcription coactivator OCA-B/OBF-1/Bob-1 is essential for normal production of immunoglobulin isotypes', *Nature*, 383: 542-7.

Klein, U., S. Casola, G. Cattoretti, Q. Shen, M. Lia, T. Mo, T. Ludwig, K. Rajewsky, and R. Dalla-Favera. 2006. 'Transcription factor IRF4 controls plasma cell differentiation and class-switch recombination', *Nat Immunol*, 7: 773-82.

Klein, U., and R. Dalla-Favera. 2008. 'Germinal centres: role in B-cell physiology and malignancy', *Nat Rev Immunol*, 8: 22-33.

Klein, U., Y. Tu, G. A. Stolovitzky, J. L. Keller, J. Haddad, Jr., V. Miljkovic, G. Cattoretti, A. Califano, and R. Dalla-Favera. 2003a. 'Gene expression dynamics during germinal center transit in B cells', *Ann N Y Acad Sci*, 987: 166-72.

———. 2003b. 'Transcriptional analysis of the B cell germinal center reaction', *Proc Natl Acad Sci U S A*, 100: 2639-44.

Kondo, M., I. L. Weissman, and K. Akashi. 1997. 'Identification of clonogenic common lymphoid progenitors in mouse bone marrow', *Cell*, 91: 661-72.

Kosco-Vilbois, M. H., and D. Scheidegger. 1995. 'Follicular dendritic cells induce B cell activation', *Adv Exp Med Biol*, 378: 301-4.

Kovalchuk, A. L., C. F. Qi, T. A. Torrey, L. Taddesse-Heath, L. Feigenbaum, S. S. Park, A. Gerbitz, G. Klobeck, K. Hoertnagel, A. Polack, G. W. Bornkamm, S. Janz, and H. C. Morse, 3rd. 2000. 'Burkitt lymphoma in the mouse', *J Exp Med*, 192: 1183-90.

Kuhn, R., K. Rajewsky, and W. Muller. 1991. 'Generation and analysis of interleukin-4 deficient mice', *Science*, 254: 707-10.

Kuleshov, M. V., M. R. Jones, A. D. Rouillard, N. F. Fernandez, Q. Duan, Z. Wang, S. Koplev, S. L. Jenkins, K. M. Jagodnik, A. Lachmann, M. G. McDermott, C. D. Monteiro, G. W. Gundersen, and A. Ma'ayan. 2016. 'Enrichr: a comprehensive gene set enrichment analysis web server 2016 update', *Nucleic Acids Res*, 44: W90-7.

Kuppers, R. 2005. 'Mechanisms of B-cell lymphoma pathogenesis', *Nat Rev Cancer*, 5: 251-62.

Kuppers, R., U. Klein, M. L. Hansmann, and K. Rajewsky. 1999. 'Cellular origin of human B-cell lymphomas', *N Engl J Med*, 341: 1520-9.

Kurdistani, S. K. 2007. 'Histone modifications as markers of cancer prognosis: a cellular view', *Br J Cancer*, 97: 1-5.

Kurosaki, T. 1999. 'Genetic analysis of B cell antigen receptor signaling', *Annu Rev Immunol*, 17: 555-92.

Kurosaki, T., and M. Kurosaki. 1997. 'Transphosphorylation of Bruton's tyrosine kinase on tyrosine 551 is critical for B cell antigen receptor function', *J Biol Chem*, 272: 15595-8.

Kwon, H., D. Thierry-Mieg, J. Thierry-Mieg, H. P. Kim, J. Oh, C. Tunyaplin, S. Carotta, C. E. Donovan, M. L. Goldman, P. Tailor, K. Ozato, D. E. Levy, S. L. Nutt, K. Calame, and W. J. Leonard. 2009. 'Analysis of interleukin-21-induced Prdm1 gene regulation reveals functional cooperation of STAT3 and IRF4 transcription factors', *Immunity*, 31: 941-52.

Kwon, K., C. Hutter, Q. Sun, I. Bilic, C. Cobaleda, S. Malin, and M. Busslinger. 2008. 'Instructive role of the transcription factor E2A in early B lymphopoiesis and germinal center B cell development', *Immunity*, 28: 751-62.

Laplante, M., and D. M. Sabatini. 2012. 'mTOR signaling in growth control and disease', *Cell*, 149: 274-93.

Lasman, L., V. Krupalnik, S. Viukov, N. Mor, A. Aguilera-Castrejon, D. Schneir, J. Bayerl, O. Mizrahi, S. Peles, S. Tawil, S. Sathe, A. Nachshon, T. Shani, M. Zerbib, I. Kilimnik, S. Aigner, A. Shankar, J. R. Mueller, S. Schwartz, N. Stern-Ginossar, G. W. Yeo, S. Geula, N. Novershtern, and J. H. Hanna. 2020. 'Context-dependent functional compensation between Ythdf m(6)A reader proteins', *Genes Dev*, 34: 1373-91.

Lawrence, M., S. Daujat, and R. Schneider. 2016. 'Lateral Thinking: How Histone Modifications Regulate Gene Expression', *Trends Genet*, 32: 42-56.

Lee, H., S. Bao, Y. Qian, S. Geula, J. Leslie, C. Zhang, J. H. Hanna, and L. Ding. 2019. 'Stage-specific requirement for Mettl3-dependent m(6)A mRNA methylation during haematopoietic stem cell differentiation', *Nat Cell Biol*, 21: 700-09.

Leonard, W. J. 2001. 'Cytokines and immunodeficiency diseases', *Nat Rev Immunol*, 1: 200-8.

Lesbirel, S., N. Viphakone, M. Parker, J. Parker, C. Heath, I. Sudbery, and S. A. Wilson. 2018. 'The m(6)A-methylase complex recruits TREX and regulates mRNA export', *Sci Rep*, 8: 13827.

Leung, J. Y., G. L. Ehmann, P. H. Giangrande, and J. R. Nevins. 2008. 'A role for Myc in facilitating transcription activation by E2F1', *Oncogene*, 27: 4172-9.

Li, A., Y. S. Chen, X. L. Ping, X. Yang, W. Xiao, Y. Yang, H. Y. Sun, Q. Zhu, P. Baidya, X. Wang, D. P. Bhattarai, Y. L. Zhao, B. F. Sun, and Y. G. Yang. 2017. 'Cytoplasmic m(6)A reader YTHDF3 promotes mRNA translation', *Cell Res*, 27: 444-47.

Li, H. B., J. Tong, S. Zhu, P. J. Batista, E. E. Duffy, J. Zhao, W. Bailis, G. Cao, L. Kroehling, Y. Chen, G. Wang, J. P. Broughton, Y. G. Chen, Y. Kluger, M. D. Simon, H. Y. Chang, Z. Yin, and R. A. Flavell. 2017. 'm(6)A mRNA methylation controls T cell homeostasis by targeting the IL-7/STAT5/SOCS pathways', *Nature*, 548: 338-42.

Li, Z., P. Qian, W. Shao, H. Shi, X. C. He, M. Gogol, Z. Yu, Y. Wang, M. Qi, Y. Zhu, J. M. Perry, K. Zhang, F. Tao, K. Zhou, D. Hu, Y. Han, C. Zhao, R. Alexander, H. Xu, S. Chen, A. Peak, K. Hall, M. Peterson, A. Perera, J. S. Haug, T. Parmely, H. Li, B. Shen, J. Zeitlinger, C. He, and L. Li. 2018. 'Suppression of m(6)A reader Ythdf2 promotes hematopoietic stem cell expansion', *Cell Res*, 28: 904-17.

Li, Z., H. Weng, R. Su, X. Weng, Z. Zuo, C. Li, H. Huang, S. Nachtergaele, L. Dong, C. Hu, X. Qin, L. Tang, Y. Wang, G. M. Hong, H. Huang, X. Wang, P. Chen, S. Gurbuxani, S. Arnovitz, Y. Li, S. Li, J. Strong, M. B. Neilly, R. A. Larson, X. Jiang, P. Zhang, J. Jin, C. He, and J. Chen. 2017. 'FTO Plays an Oncogenic Role in Acute Myeloid Leukemia as a N(6)-Methyladenosine RNA Demethylase', *Cancer Cell*, 31: 127-41.

Liang, P. I., C. F. Li, L. T. Chen, D. P. Sun, T. J. Chen, C. H. Hsing, H. P. Hsu, and C. Y. Lin. 2014. 'BCL6 overexpression is associated with decreased p19 ARF expression and confers an independent prognosticator in gallbladder carcinoma', *Tumour Biol*, 35: 1417-26.

Lin, S., J. Choe, P. Du, R. Triboulet, and R. I. Gregory. 2016. 'The m(6)A Methyltransferase METTL3 Promotes Translation in Human Cancer Cells', *Mol Cell*, 62: 335-45.

Linder, B., A. V. Grozhik, A. O. Olarerin-George, C. Meydan, C. E. Mason, and S. R. Jaffrey. 2015. 'Single-nucleotide-resolution mapping of m6A and m6Am throughout the transcriptome', *Nat Methods*, 12: 767-72.

Liu, J., X. Dou, C. Chen, C. Chen, C. Liu, M. M. Xu, S. Zhao, B. Shen, Y. Gao, D. Han, and C. He. 2020. 'N (6)-methyladenosine of chromosome-associated regulatory RNA regulates chromatin state and transcription', *Science*, 367: 580-86.

Liu, J., K. Li, J. Cai, M. Zhang, X. Zhang, X. Xiong, H. Meng, X. Xu, Z. Huang, J. Peng, J. Fan, and C. Yi. 2020. 'Landscape and Regulation of m(6)A and m(6)Am Methylome across Human and Mouse Tissues', *Mol Cell*, 77: 426-40 e6.

Liu, J., D. Ren, Z. Du, H. Wang, H. Zhang, and Y. Jin. 2018. 'm(6)A demethylase FTO facilitates tumor progression in lung squamous cell carcinoma by regulating MZF1 expression', *Biochem Biophys Res Commun*, 502: 456-64.

Liu, J., Y. Yue, D. Han, X. Wang, Y. Fu, L. Zhang, G. Jia, M. Yu, Z. Lu, X. Deng, Q. Dai, W. Chen, and C. He. 2014. 'A METTL3-METTL14 complex mediates mammalian nuclear RNA N6-adenosine methylation', *Nat Chem Biol*, 10: 93-5.

Liu, S. Y., Y. Feng, J. J. Wu, M. L. Zou, Z. L. Sun, X. Li, and F. L. Yuan. 2020. 'm(6) A facilitates YTHDF-independent phase separation', *J Cell Mol Med*, 24: 2070-72.

Loder, F., B. Mutschler, R. J. Ray, C. J. Paige, P. Sideras, R. Torres, M. C. Lamers, and R. Carsetti. 1999. 'B cell development in the spleen takes place in discrete steps and is determined by the quality of B cell receptor-derived signals', *J Exp Med*, 190: 75-89.

Love, M. I., W. Huber, and S. Anders. 2014. 'Moderated estimation of fold change and dispersion for RNA-seq data with DESeq2', *Genome Biol*, 15: 550.

Lu, M., Z. Zhang, M. Xue, B. S. Zhao, O. Harder, A. Li, X. Liang, T. Z. Gao, Y. Xu, J. Zhou, Z. Feng, S. Niewiesk, M. E. Peeples, C. He, and J. Li. 2020. 'N(6)-methyladenosine modification enables viral RNA to escape recognition by RNA sensor RIG-I', *Nat Microbiol*, 5: 584-98.

Luo, W., F. Weisel, and M. J. Shlomchik. 2018. 'B Cell Receptor and CD40 Signaling Are Rewired for Synergistic Induction of the c-Myc Transcription Factor in Germinal Center B Cells', *Immunity*, 48: 313-26 e5.

Luo, Y., H. Fujii, T. Gerster, and R. G. Roeder. 1992. 'A novel B cell-derived coactivator potentiates the activation of immunoglobulin promoters by octamer-binding transcription factors', *Cell*, 71: 231-41.

Luo, Y., and R. G. Roeder. 1995. 'Cloning, functional characterization, and mechanism of action of the B-cell-specific transcriptional coactivator OCA-B', *Mol Cell Biol*, 15: 4115-24.

Lv, J., Y. Zhang, S. Gao, C. Zhang, Y. Chen, W. Li, Y. G. Yang, Q. Zhou, and F. Liu. 2018. 'Endothelial-specific m(6)A modulates mouse hematopoietic stem and progenitor cell development via Notch signaling', *Cell Res*, 28: 249-52.

Ma, H., X. Wang, J. Cai, Q. Dai, S. K. Natchiar, R. Lv, K. Chen, Z. Lu, H. Chen, Y. G. Shi, F. Lan, J. Fan, B. P. Klaholz, T. Pan, Y. Shi, and C. He. 2019. 'N(6-)Methyladenosine methyltransferase ZCCHC4 mediates ribosomal RNA methylation', *Nat Chem Biol*, 15: 88-94.

Machanick, P., and T. L. Bailey. 2011. 'MEME-ChIP: motif analysis of large DNA datasets', *Bioinformatics*, 27: 1696-7.

Mackay, F., and J. L. Browning. 2002. 'BAFF: a fundamental survival factor for B cells', *Nat Rev Immunol*, 2: 465-75.

Mauer, J., X. Luo, A. Blanjoie, X. Jiao, A. V. Grozhik, D. P. Patil, B. Linder, B. F. Pickering, J. J. Vasseur, Q. Chen, S. S. Gross, O. Elemento, F. Debart, M. Kiledjian, and S. R. Jaffrey. 2017. 'Reversible methylation of m(6)Am in the 5' cap controls mRNA stability', *Nature*, 541: 371-75.

Mauer, J., M. Sindelar, V. Despic, T. Guez, B. R. Hawley, J. J. Vasseur, A. Rentmeister, S. S. Gross, L. Pellizzoni, F. Debart, H. Goodarzi, and S. R. Jaffrey. 2019. 'FTO controls reversible m(6)Am RNA methylation during snRNA biogenesis', *Nat Chem Biol*, 15: 340-47.

Mayer, C. T., J. P. Nieke, A. Gazumyan, M. Cipolla, Q. Wang, T. Y. Oliveira, V. Ramos, S. Monette, Q. Z. Li, M. E. Gershwin, H. Kashkar, and M. C. Nussenzweig. 2020. 'An apoptosis-dependent checkpoint for autoimmunity in memory B and plasma cells', *Proc Natl Acad Sci U S A*, 117: 24957-63.

McBlane, J. F., D. C. van Gent, D. A. Ramsden, C. Romeo, C. A. Cuomo, M. Gellert, and M. A. Oettinger. 1995. 'Cleavage at a V(D)J recombination signal requires only RAG1 and RAG2 proteins and occurs in two steps', *Cell*, 83: 387-95.

McDonnell, T. J., and S. J. Korsmeyer. 1991. 'Progression from lymphoid hyperplasia to high-grade malignant lymphoma in mice transgenic for the t(14; 18)', *Nature*, 349: 254-6.

McKean, D., K. Huppi, M. Bell, L. Staudt, W. Gerhard, and M. Weigert. 1984. 'Generation of antibody diversity in the immune response of BALB/c mice to influenza virus hemagglutinin', *Proc Natl Acad Sci U S A*, 81: 3180-4.

Mesin, L., J. Ersching, and G. D. Victora. 2016. 'Germinal Center B Cell Dynamics', *Immunity*, 45: 471-82.

Meyer, K. D., D. P. Patil, J. Zhou, A. Zinoviev, M. A. Skabkin, O. Elemento, T. V. Pestova, S. B. Qian, and S. R. Jaffrey. 2015. '5' UTR m(6)A Promotes Cap-Independent Translation', *Cell*, 163: 999-1010.

Muramatsu, M., K. Kinoshita, S. Fagarasan, S. Yamada, Y. Shinkai, and T. Honjo. 2000. 'Class switch recombination and hypermutation require activation-induced cytidine deaminase (AID), a potential RNA editing enzyme', *Cell*, 102: 553-63.

Muto, A., K. Ochiai, Y. Kimura, A. Itoh-Nakadai, K. L. Calame, D. Ikebe, S. Tashiro, and K. Igarashi. 2010. 'Bach2 represses plasma cell gene regulatory network in B cells to promote antibody class switch', *EMBO J*, 29: 4048-61.

Muto, A., S. Tashiro, O. Nakajima, H. Hoshino, S. Takahashi, E. Sakoda, D. Ikebe, M. Yamamoto, and K. Igarashi. 2004. 'The transcriptional programme of antibody class switching involves the repressor Bach2', *Nature*, 429: 566-71.

Nambu, Y., M. Sugai, H. Gonda, C. G. Lee, T. Katakai, Y. Agata, Y. Yokota, and A. Shimizu. 2003. 'Transcription-coupled events associating with immunoglobulin switch region chromatin', *Science*, 302: 2137-40.

Nebbioso, A., F. P. Tambaro, C. Dell'Aversana, and L. Altucci. 2018. 'Cancer epigenetics: Moving forward', *PLoS Genet*, 14: e1007362.

Nielsen, P. J., O. Georgiev, B. Lorenz, and W. Schaffner. 1996. 'B lymphocytes are impaired in mice lacking the transcriptional co-activator Bob1/OCA-B/OBF1', *Eur J Immunol*, 26: 3214-8.

Niu, H., B. H. Ye, and R. Dalla-Favera. 1998. 'Antigen receptor signaling induces MAP kinase-mediated phosphorylation and degradation of the BCL-6 transcription factor', *Genes Dev*, 12: 1953-61.

Nojima, T., K. Haniuda, T. Moutai, M. Matsudaira, S. Mizokawa, I. Shiratori, T. Azuma, and D. Kitamura. 2011. 'In-vitro derived germinal centre B cells differentially generate memory B or plasma cells in vivo', *Nat Commun*, 2: 465.

Nutt, S. L., B. Heavey, A. G. Rolink, and M. Busslinger. 2015. 'Pillars Article: Commitment to the B-lymphoid lineage depends on the transcription factor Pax5. Nature. 1999. 401: 556-562', *J Immunol*, 195: 766-72.

Nutt, S. L., P. D. Hodgkin, D. M. Tarlinton, and L. M. Corcoran. 2015. 'The generation of antibody-secreting plasma cells', *Nat Rev Immunol*, 15: 160-71.

Ochiai, K., Y. Katoh, T. Ikura, Y. Hoshikawa, T. Noda, H. Karasuyama, S. Tashiro, A. Muto, and K. Igarashi. 2006. 'Plasmacytic transcription factor Blimp-1 is repressed by Bach2 in B cells', *J Biol Chem*, 281: 38226-34.

Ochiai, K., M. Maienschein-Cline, G. Simonetti, J. Chen, R. Rosenthal, R. Brink, A. S. Chong, U. Klein, A. R. Dinner, H. Singh, and R. Sciammas. 2013. 'Transcriptional regulation of germinal center B and plasma cell fates by dynamical control of IRF4', *Immunity*, 38: 918-29.

Pan, T. 2018. 'Modifications and functional genomics of human transfer RNA', *Cell Res*, 28: 395-404.

Park, O. H., H. Ha, Y. Lee, S. H. Boo, D. H. Kwon, H. K. Song, and Y. K. Kim. 2019. 'Endoribonucleolytic Cleavage of m(6)A-Containing RNAs by RNase P/MRP Complex', *Mol Cell*, 74: 494-507 e8.

Park, S. R., H. Zan, Z. Pal, J. Zhang, A. Al-Qahtani, E. J. Pone, Z. Xu, T. Mai, and P. Casali. 2009. 'HoxC4 binds to the promoter of the cytidine deaminase AID gene to induce AID expression, class-switch DNA recombination and somatic hypermutation', *Nat Immunol*, 10: 540-50.

Pasqualucci, L. 2019. 'Molecular pathogenesis of germinal center-derived B cell lymphomas', *Immunol Rev*, 288: 240-61.

Patil, D. P., C. K. Chen, B. F. Pickering, A. Chow, C. Jackson, M. Guttman, and S. R. Jaffrey. 2016. 'm(6)A RNA methylation promotes XIST-mediated transcriptional repression', *Nature*, 537: 369-73.

Peled, J. U., J. J. Yu, J. Venkatesh, E. Bi, B. B. Ding, M. Krupski-Downs, R. Shaknovich, P. Sicinski, B. Diamond, M. D. Scharff, and B. H. Ye. 2010. 'Requirement for cyclin D3 in germinal center formation and function', *Cell Res*, 20: 631-46.

Pendleton, K. E., B. Chen, K. Liu, O. V. Hunter, Y. Xie, B. P. Tu, and N. K. Conrad. 2017. 'The U6 snRNA m(6)A Methyltransferase METTL16 Regulates SAM Synthetase Intron Retention', *Cell*, 169: 824-35 e14.

Peperzak, V., I. Vikstrom, J. Walker, S. P. Glaser, M. LePage, C. M. Coquery, L. D. Erickson, K. Fairfax, F. Mackay, A. Strasser, S. L. Nutt, and D. M. Tarlinton. 2013. 'Mcl-1 is essential for the survival of plasma cells', *Nat Immunol*, 14: 290-7.

Pereira, J. P., L. M. Kelly, and J. G. Cyster. 2010. 'Finding the right niche: B-cell migration in the early phases of T-dependent antibody responses', *Int Immunol*, 22: 413-9.

Perez-Roger, I., S. H. Kim, B. Griffiths, A. Sewing, and H. Land. 1999. 'Cyclins D1 and D2 mediate myc-induced proliferation via sequestration of p27(Kip1) and p21(Cip1)', *EMBO J*, 18: 5310-20.

Phan, R. T., and R. Dalla-Favera. 2004. 'The BCL6 proto-oncogene suppresses p53 expression in germinal-centre B cells', *Nature*, 432: 635-9.

Phan, R. T., M. Saito, K. Basso, H. Niu, and R. Dalla-Favera. 2005. 'BCL6 interacts with the transcription factor Miz-1 to suppress the cyclin-dependent kinase inhibitor p21 and cell cycle arrest in germinal center B cells', *Nat Immunol*, 6: 1054-60.

Phan, R. T., M. Saito, Y. Kitagawa, A. R. Means, and R. Dalla-Favera. 2007. 'Genotoxic stress regulates expression of the proto-oncogene Bcl6 in germinal center B cells', *Nat Immunol*, 8: 1132-9.

Pillai, S., and A. Cariappa. 2009. 'The follicular versus marginal zone B lymphocyte cell fate decision', *Nat Rev Immunol*, 9: 767-77.

Ping, X. L., B. F. Sun, L. Wang, W. Xiao, X. Yang, W. J. Wang, S. Adhikari, Y. Shi, Y. Lv, Y. S. Chen, X. Zhao, A. Li, Y. Yang, U. Dahal, X. M. Lou, X. Liu, J. Huang, W. P. Yuan, X. F. Zhu, T. Cheng, Y. L. Zhao, X. Wang, J. M. Rendtlew Danielsen, F. Liu, and Y. G. Yang. 2014. 'Mammalian WTAP is a regulatory subunit of the RNA N6-methyladenosine methyltransferase', *Cell Res*, 24: 177-89.

Rada, C., J. M. Di Noia, and M. S. Neuberger. 2004. 'Mismatch recognition and uracil excision provide complementary paths to both Ig switching and the A/T-focused phase of somatic mutation', *Mol Cell*, 16: 163-71.

Ramirez, F., D. P. Ryan, B. Gruning, V. Bhardwaj, F. Kilpert, A. S. Richter, S. Heyne, F. Dundar, and T. Manke. 2016. 'deepTools2: a next generation web server for deep-sequencing data analysis', *Nucleic Acids Res*, 44: W160-5.

Ranuncolo, S. M., J. M. Polo, J. Dierov, M. Singer, T. Kuo, J. Greally, R. Green, M. Carroll, and A. Melnick. 2007. 'Bcl-6 mediates the germinal center B cell phenotype and lymphomagenesis through transcriptional repression of the DNA-damage sensor ATR', *Nat Immunol*, 8: 705-14.

Ranuncolo, S. M., J. M. Polo, and A. Melnick. 2008. 'BCL6 represses CHEK1 and suppresses DNA damage pathways in normal and malignant B-cells', *Blood Cells Mol Dis*, 41: 95-9.

Raybuck, A. L., S. H. Cho, J. Li, M. C. Rogers, K. Lee, C. L. Williams, M. Shlomchik, J. W. Thomas, J. Chen, J. V. Williams, and M. R. Boothby. 2018. 'B Cell-Intrinsic mTORC1 Promotes Germinal Center-Defining Transcription Factor Gene Expression, Somatic Hypermutation, and Memory B Cell Generation in Humoral Immunity', *J Immunol*, 200: 2627-39.

Redecke, V., R. Wu, J. Zhou, D. Finkelstein, V. Chaturvedi, A. A. High, and H. Hacker. 2013. 'Hematopoietic progenitor cell lines with myeloid and lymphoid potential', *Nat Methods*, 10: 795-803.

Reimold, A. M., N. N. Iwakoshi, J. Manis, P. Vallabhajosyula, E. Szomolanyi-Tsuda, E. M. Gravallese, D. Friend, M. J. Grusby, F. Alt, and L. H. Glimcher. 2001. 'Plasma cell differentiation requires the transcription factor XBP-1', *Nature*, 412: 300-7.

Reimold, A. M., P. D. Ponath, Y. S. Li, R. R. Hardy, C. S. David, J. L. Strominger, and L. H. Glimcher. 1996. 'Transcription factor B cell lineage-specific activator protein regulates the gene for human X-box binding protein 1', *J Exp Med*, 183: 393-401.

Reth, M. 1989. 'Antigen receptor tail clue', *Nature*, 338: 383-4.

Reth, M., and J. Wienands. 1997. 'Initiation and processing of signals from the B cell antigen receptor', *Annu Rev Immunol*, 15: 453-79.

Ries, R. J., S. Zaccara, P. Klein, A. Olarerin-George, S. Namkoong, B. F. Pickering, D. P. Patil, H. Kwak, J. H. Lee, and S. R. Jaffrey. 2019. 'm(6)A enhances the phase separation potential of mRNA', *Nature*, 571: 424-28.

Roco, J. A., L. Mesin, S. C. Binder, C. Nefzger, P. Gonzalez-Figueroa, P. F. Canete, J. Ellyard, Q. Shen, P. A. Robert, J. Cappello, H. Vohra, Y. Zhang, C. R. Nowosad, A. Schiepers, L. M. Corcoran, K. M. Toellner, J. M. Polo, M. Meyer-Hermann, G. D. Victora, and C. G. Vinuesa. 2019. 'Class-Switch Recombination Occurs Infrequently in Germinal Centers', *Immunity*, 51: 337-50 e7.

Roundtree, I. A., and C. He. 2016. 'RNA epigenetics--chemical messages for posttranscriptional gene regulation', *Curr Opin Chem Biol*, 30: 46-51.

Roundtree, I. A., G. Z. Luo, Z. Zhang, X. Wang, T. Zhou, Y. Cui, J. Sha, X. Huang, L. Guerrero, P. Xie, E. He, B. Shen, and C. He. 2017. 'YTHDC1 mediates nuclear export of N(6)-methyladenosine methylated mRNAs', *Elife*, 6.

Sabo, A., T. R. Kress, M. Pelizzola, S. de Pretis, M. M. Gorski, A. Tesi, M. J. Morelli, P. Bora, M. Doni, A. Verrecchia, C. Tonelli, G. Faga, V. Bianchi, A. Ronchi, D. Low, H. Muller, E. Guccione, S. Campaner, and B. Amati. 2014. 'Selective transcriptional regulation by Myc in cellular growth control and lymphomagenesis', *Nature*, 511: 488-92.

Saito, M., J. Gao, K. Basso, Y. Kitagawa, P. M. Smith, G. Bhagat, A. Pernis, L. Pasqualucci, and R. Dalla-Favera. 2007. 'A signaling pathway mediating downregulation of BCL6 in germinal center B cells is blocked by BCL6 gene alterations in B cell lymphoma', *Cancer Cell*, 12: 280-92.

Saito, M., U. Novak, E. Piovan, K. Basso, P. Sumazin, C. Schneider, M. Crespo, Q. Shen, G. Bhagat, A. Califano, A. Chadburn, L. Pasqualucci, and R. Dalla-Favera. 2009. 'BCL6 suppression of BCL2 via Miz1 and its disruption in diffuse large B cell lymphoma', *Proc Natl Acad Sci U S A*, 106: 11294-9.

Samardzic, T., D. Marinkovic, P. J. Nielsen, L. Nitschke, and T. Wirth. 2002. 'BOB.1/OBF.1 deficiency affects marginal-zone B-cell compartment', *Mol Cell Biol*, 22: 8320-31.

Sander, S., V. T. Chu, T. Yasuda, A. Franklin, R. Graf, D. P. Calado, S. Li, K. Imami, M. Selbach, M. Di Virgilio, L. Bullinger, and K. Rajewsky. 2015. 'PI3 Kinase and FOXO1 Transcription Factor Activity Differentially Control B Cells in the Germinal Center Light and Dark Zones', *Immunity*, 43: 1075-86.

Sauter, P., and P. Matthias. 1998. 'Coactivator OBF-1 makes selective contacts with both the POU-specific domain and the POU homeodomain and acts as a molecular clamp on DNA', *Mol Cell Biol*, 18: 7397-409.

Saxton, R. A., and D. M. Sabatini. 2017. 'mTOR Signaling in Growth, Metabolism, and Disease', *Cell*, 168: 960-76.

Scharer, C. D., B. G. Barwick, M. Guo, A. P. R. Bally, and J. M. Boss. 2018. 'Plasma cell differentiation is controlled by multiple cell division-coupled epigenetic programs', *Nat Commun*, 9: 1698.

Schatz, D. G. 1997. 'V(D)J recombination moves in vitro', *Semin Immunol*, 9: 149-59.

Schebesta, A., S. McManus, G. Salvagiotto, A. Delogu, G. A. Busslinger, and M. Busslinger. 2007. 'Transcription factor Pax5 activates the chromatin of key genes involved in B cell signaling, adhesion, migration, and immune function', *Immunity*, 27: 49-63.

Schindler, C., D. E. Levy, and T. Decker. 2007. 'JAK-STAT signaling: from interferons to cytokines', *J Biol Chem*, 282: 20059-63.

Schmidt, E. K., G. Clavarino, M. Ceppi, and P. Pierre. 2009. 'SUnSET, a nonradioactive method to monitor protein synthesis', *Nat Methods*, 6: 275-7.

Schubart, D. B., A. Rolink, M. H. Kosco-Vilbois, F. Botteri, and P. Matthias. 1996. 'B-cell-specific coactivator OBF-1/OCA-B/Bob1 required for immune response and germinal centre formation', *Nature*, 383: 538-42.

Schubart, K., S. Massa, D. Schubart, L. M. Corcoran, A. G. Rolink, and P. Matthias. 2001. 'B cell development and immunoglobulin gene transcription in the absence of Oct-2 and OBF-1', *Nat Immunol*, 2: 69-74.

Schwickert, T. A., R. L. Lindquist, G. Shakhar, G. Livshits, D. Skokos, M. H. Kosco-Vilbois, M. L. Dustin, and M. C. Nussenzweig. 2007. 'In vivo imaging of germinal centres reveals a dynamic open structure', *Nature*, 446: 83-7.

Sciammas, R., A. L. Shaffer, J. H. Schatz, H. Zhao, L. M. Staudt, and H. Singh. 2006. 'Graded expression of interferon regulatory factor-4 coordinates isotype switching with plasma cell differentiation', *Immunity*, 25: 225-36.

Sears, R., K. Ohtani, and J. R. Nevins. 1997. 'Identification of positively and negatively acting elements regulating expression of the E2F2 gene in response to cell growth signals', *Mol Cell Biol*, 17: 5227-35.

Sendinc, E., D. Valle-Garcia, A. Dhall, H. Chen, T. Henriques, J. Navarrete-Perea, W. Sheng, S. P. Gygi, K. Adelman, and Y. Shi. 2019. 'PCIF1 Catalyzes m6Am mRNA Methylation to Regulate Gene Expression', *Mol Cell*, 75: 620-30 e9.

Shaffer, A. L., K. I. Lin, T. C. Kuo, X. Yu, E. M. Hurt, A. Rosenwald, J. M. Giltnane, L. Yang, H. Zhao, K. Calame, and L. M. Staudt. 2002. 'Blimp-1 orchestrates plasma cell differentiation by extinguishing the mature B cell gene expression program', *Immunity*, 17: 51-62.

Shaffer, A. L., M. Shapiro-Shelef, N. N. Iwakoshi, A. H. Lee, S. B. Qian, H. Zhao, X. Yu, L. Yang, B. K. Tan, A. Rosenwald, E. M. Hurt, E. Petroulakis, N. Sonenberg, J. W. Yewdell, K. Calame, L. H. Glimcher, and L. M. Staudt. 2004. 'XBP1, downstream of Blimp-1, expands the secretory apparatus and other organelles, and increases protein synthesis in plasma cell differentiation', *Immunity*, 21: 81-93.

Shaffer, A. L., X. Yu, Y. He, J. Boldrick, E. P. Chan, and L. M. Staudt. 2000. 'BCL-6 represses genes that function in lymphocyte differentiation, inflammation, and cell cycle control', *Immunity*, 13: 199-212.

Shi, H., X. Wang, Z. Lu, B. S. Zhao, H. Ma, P. J. Hsu, C. Liu, and C. He. 2017. 'YTHDF3 facilitates translation and decay of N(6)-methyladenosine-modified RNA', *Cell Res*, 27: 315-28.

Shi, H., J. Wei, and C. He. 2019. 'Where, When, and How: Context-Dependent Functions of RNA Methylation Writers, Readers, and Erasers', *Mol Cell*, 74: 640-50.

Shinkura, R., S. Ito, N. A. Begum, H. Nagaoka, M. Muramatsu, K. Kinoshita, Y. Sakakibara, H. Hijikata, and T. Honjo. 2004. 'Separate domains of AID are required for somatic hypermutation and class-switch recombination', *Nat Immunol*, 5: 707-12.

Shulman, Z., A. D. Gitlin, J. S. Weinstein, B. Lainez, E. Esplugues, R. A. Flavell, J. E. Craft, and M. C. Nussenzweig. 2014. 'Dynamic signaling by T follicular helper cells during germinal center B cell selection', *Science*, 345: 1058-62.

Shulman, Z., and N. Stern-Ginossar. 2020. 'The RNA modification N(6)-methyladenosine as a novel regulator of the immune system', *Nat Immunol*, 21: 501-12.

Sledz, P., and M. Jinek. 2016. 'Structural insights into the molecular mechanism of the m(6)A writer complex', *Elife*, 5.

Sloan, K. E., A. S. Warda, S. Sharma, K. D. Entian, D. L. J. Lafontaine, and M. T. Bohnsack. 2017. 'Tuning the ribosome: The influence of rRNA modification on eukaryotic ribosome biogenesis and function', *RNA Biol*, 14: 1138-52.

Slobodin, B., R. Han, V. Calderone, Jafo Vrielink, F. Loayza-Puch, R. Elkon, and R. Agami. 2017. 'Transcription Impacts the Efficiency of mRNA Translation via Co-transcriptional N6-adenosine Methylation', *Cell*, 169: 326-37 e12.

Smith, K. G., T. D. Hewitson, G. J. Nossal, and D. M. Tarlinton. 1996. 'The phenotype and fate of the antibody-forming cells of the splenic foci', *Eur J Immunol*, 26: 444-8.

Smith, K. G., U. Weiss, K. Rajewsky, G. J. Nossal, and D. M. Tarlinton. 1994. 'Bcl-2 increases memory B cell recruitment but does not perturb selection in germinal centers', *Immunity*, 1: 803-13.

Staudt, L. M., R. G. Clerc, H. Singh, J. H. LeBowitz, P. A. Sharp, and D. Baltimore. 1988. 'Cloning of a lymphoid-specific cDNA encoding a protein binding the regulatory octamer DNA motif', *Science*, 241: 577-80.

Stavnezer, J. 1996. 'Immunoglobulin class switching', *Curr Opin Immunol*, 8: 199-205.

Stavnezer, J., J. E. Guikema, and C. E. Schrader. 2008. 'Mechanism and regulation of class switch recombination', *Annu Rev Immunol*, 26: 261-92.

Strubin, M., J. W. Newell, and P. Matthias. 1995. 'OBF-1, a novel B cell-specific coactivator that stimulates immunoglobulin promoter activity through association with octamer-binding proteins', *Cell*, 80: 497-506.

Ta, V. T., H. Nagaoka, N. Catalan, A. Durandy, A. Fischer, K. Imai, S. Nonoyama, J. Tashiro, M. Ikegawa, S. Ito, K. Kinoshita, M. Muramatsu, and T. Honjo. 2003. 'AID mutant analyses indicate requirement for class-switch-specific cofactors', *Nat Immunol*, 4: 843-8.

Tang, C., R. Klukovich, H. Peng, Z. Wang, T. Yu, Y. Zhang, H. Zheng, A. Klungland, and W. Yan. 2018. 'ALKBH5-dependent m6A demethylation controls splicing and stability of long 3'-UTR mRNAs in male germ cells', *Proc Natl Acad Sci U S A*, 115: E325-E33.

Tang, X., S. Liu, D. Chen, Z. Zhao, and J. Zhou. 2019. 'The role of the fat mass and obesity-associated protein in the proliferation of pancreatic cancer cells', *Oncol Lett*, 17: 2473-78.

Tellier, J., W. Shi, M. Minnich, Y. Liao, S. Crawford, G. K. Smyth, A. Kallies, M. Busslinger, and S. L. Nutt. 2016. 'Blimp-1 controls plasma cell function through the regulation of immunoglobulin secretion and the unfolded protein response', *Nat Immunol*, 17: 323-30.

Thalhammer, A., Z. Bencokova, R. Poole, C. Loenarz, J. Adam, L. O'Flaherty, J. Schodel, D. Mole, K. Giaslakiotis, C. J. Schofield, E. M. Hammond, P. J. Ratcliffe, and P. J. Pollard. 2011. 'Human AlkB homologue 5 is a nuclear 2-oxoglutarate dependent oxygenase and a direct target of hypoxia-inducible factor 1alpha (HIF-1alpha)', *PLoS One*, 6: e16210.

Tonegawa, S. 1983. 'Somatic generation of antibody diversity', *Nature*, 302: 575-81.

Tong, J., G. Cao, T. Zhang, E. Sefik, M. C. Amezcua Vesely, J. P. Broughton, S. Zhu, H. Li, B. Li, L. Chen, H. Y. Chang, B. Su, R. A. Flavell, and H. B. Li. 2018. 'm(6)A mRNA methylation sustains Treg suppressive functions', *Cell Res*, 28: 253-56.

Vallabhapurapu, S., A. Matsuzawa, W. Zhang, P. H. Tseng, J. J. Keats, H. Wang, D. A. Vignali, P. L. Bergsagel, and M. Karin. 2008. 'Nonredundant and complementary functions of TRAF2 and TRAF3 in a ubiquitination cascade that activates NIK-dependent alternative NF-kappaB signaling', *Nat Immunol*, 9: 1364-70.

van Tran, N., F. G. M. Ernst, B. R. Hawley, C. Zorbas, N. Ulryck, P. Hackert, K. E. Bohnsack, M. T. Bohnsack, S. R. Jaffrey, M. Graille, and D. L. J. Lafontaine. 2019. 'The human 18S rRNA m6A methyltransferase METTL5 is stabilized by TRMT112', *Nucleic Acids Res*, 47: 7719-33.

Varano, G., S. Raffel, M. Sormani, F. Zanardi, S. Lonardi, C. Zasada, L. Perucho, V. Petrocelli, A. Haake, A. K. Lee, M. Bugatti, U. Paul, E. Van Anken, L. Pasqualucci, R. Rabadan, R. Siebert, S. Kempa, M. Ponzoni, F. Facchetti, K. Rajewsky, and S. Casola. 2017. 'The B-cell receptor controls fitness of MYC-driven lymphoma cells via GSK3beta inhibition', *Nature*, 546: 302-06.

Verbist, K. C., C. S. Guy, S. Milasta, S. Liedmann, M. M. Kaminski, R. Wang, and D. R. Green. 2016. 'Metabolic maintenance of cell asymmetry following division in activated T lymphocytes', *Nature*, 532: 389-93.

Victora, G. D., D. Dominguez-Sola, A. B. Holmes, S. Deroubaix, R. Dalla-Favera, and M. C. Nussenzweig. 2012. 'Identification of human germinal center light and dark zone cells and their relationship to human B-cell lymphomas', *Blood*, 120: 2240-8.

Victora, G. D., and M. C. Nussenzweig. 2012. 'Germinal centers', *Annu Rev Immunol*, 30: 429-57.

Victora, G. D., T. A. Schwickert, D. R. Fooksman, A. O. Kamphorst, M. Meyer-Hermann, M. L. Dustin, and M. C. Nussenzweig. 2010. 'Germinal center dynamics revealed by multiphoton microscopy with a photoactivatable fluorescent reporter', *Cell*, 143: 592-605.

Vu, L. P., B. F. Pickering, Y. Cheng, S. Zaccara, D. Nguyen, G. Minuesa, T. Chou, A. Chow, Y. Saletore, M. MacKay, J. Schulman, C. Famulare, M. Patel, V. M. Klimek, F. E. Garrett-Bakelman, A. Melnick, M. Carroll, C. E. Mason, S. R. Jaffrey, and M. G. Kharas. 2017. 'The N(6)-methyladenosine (m(6)A)-forming enzyme METTL3 controls myeloid differentiation of normal hematopoietic and leukemia cells', *Nat Med*, 23: 1369-76.

Wang, C. Y., S. S. Shie, I. C. Hsieh, M. L. Tsai, and M. S. Wen. 2015. 'FTO modulates circadian rhythms and inhibits the CLOCK-BMAL1-induced transcription', *Biochem Biophys Res Commun*, 464: 826-32.

Wang, C. Y., S. S. Shie, M. S. Wen, K. C. Hung, I. C. Hsieh, T. S. Yeh, and D. Wu. 2015. 'Loss of FTO in adipose tissue decreases Angptl4 translation and alters triglyceride metabolism', *Sci Signal*, 8: ra127.

Wang, H., X. Hu, M. Huang, J. Liu, Y. Gu, L. Ma, Q. Zhou, and X. Cao. 2019. 'Mettl3-mediated mRNA m(6)A methylation promotes dendritic cell activation', *Nat Commun*, 10: 1898.

Wang, H., H. Zuo, J. Liu, F. Wen, Y. Gao, X. Zhu, B. Liu, F. Xiao, W. Wang, G. Huang, B. Shen, and Z. Ju. 2018. 'Loss of YTHDF2-mediated m(6)A-dependent mRNA clearance facilitates hematopoietic stem cell regeneration', *Cell Res*, 28: 1035-38.

Wang, X., J. Feng, Y. Xue, Z. Guan, D. Zhang, Z. Liu, Z. Gong, Q. Wang, J. Huang, C. Tang, T. Zou, and P. Yin. 2016. 'Structural basis of N(6)-adenosine methylation by the METTL3-METTL14 complex', *Nature*, 534: 575-8.

Wang, X., Z. Lu, A. Gomez, G. C. Hon, Y. Yue, D. Han, Y. Fu, M. Parisien, Q. Dai, G. Jia, B. Ren, T. Pan, and C. He. 2014. 'N6-methyladenosine-dependent regulation of messenger RNA stability', *Nature*, 505: 117-20.

Wang, X., B. S. Zhao, I. A. Roundtree, Z. Lu, D. Han, H. Ma, X. Weng, K. Chen, H. Shi, and C. He. 2015. 'N(6)-methyladenosine Modulates Messenger RNA Translation Efficiency', *Cell*, 161: 1388-99.

Wei, J., F. Liu, Z. Lu, Q. Fei, Y. Ai, P. C. He, H. Shi, X. Cui, R. Su, A. Klungland, G. Jia, J. Chen, and C. He. 2018. 'Differential m(6)A, m(6)Am, and m(1)A Demethylation Mediated by FTO in the Cell Nucleus and Cytoplasm', *Mol Cell*, 71: 973-85 e5.

Wen, J., R. Lv, H. Ma, H. Shen, C. He, J. Wang, F. Jiao, H. Liu, P. Yang, L. Tan, F. Lan, Y. G. Shi, C. He, Y. Shi, and J. Diao. 2018. 'Zc3h13 Regulates Nuclear RNA m(6)A Methylation and Mouse Embryonic Stem Cell Self-Renewal', *Mol Cell*, 69: 1028-38 e6.

Weng, H., H. Huang, H. Wu, X. Qin, B. S. Zhao, L. Dong, H. Shi, J. Skibbe, C. Shen, C. Hu, Y. Sheng, Y. Wang, M. Wunderlich, B. Zhang, L. C. Dore, R. Su, X. Deng, K. Ferchen, C. Li, M. Sun, Z. Lu, X. Jiang, G. Marcucci, J. C. Mulloy, J. Yang, Z. Qian, M. Wei, C. He, and J. Chen. 2018. 'METTL14 Inhibits Hematopoietic Stem/Progenitor Differentiation and Promotes Leukemogenesis via mRNA m(6)A Modification', *Cell Stem Cell*, 22: 191-205 e9.

West, M. J., M. Stoneley, and A. E. Willis. 1998. 'Translational induction of the c-myc oncogene via activation of the FRAP/TOR signalling pathway', *Oncogene*, 17: 769-80.

Wu, J., and Z. J. Chen. 2014. 'Innate immune sensing and signaling of cytosolic nucleic acids', *Annu Rev Immunol*, 32: 461-88.

Xu, J., T. M. Foy, J. D. Laman, E. A. Elliott, J. J. Dunn, T. J. Waldschmidt, J. Elsemore, R. J. Noelle, and R. A. Flavell. 1994. 'Mice deficient for the CD40 ligand', *Immunity*, 1: 423-31.

Xu, Z., E. J. Pone, A. Al-Qahtani, S. R. Park, H. Zan, and P. Casali. 2007. 'Regulation of aicda expression and AID activity: relevance to somatic hypermutation and class switch DNA recombination', *Crit Rev Immunol*, 27: 367-97.

Yang, D. D., Z. H. Chen, K. Yu, J. H. Lu, Q. N. Wu, Y. Wang, H. Q. Ju, R. H. Xu, Z. X. Liu, and Z. L. Zeng. 2020. 'METTL3 Promotes the Progression of Gastric Cancer via Targeting the MYC Pathway', *Front Oncol*, 10: 115.

Yang, D., J. Qiao, G. Wang, Y. Lan, G. Li, X. Guo, J. Xi, D. Ye, S. Zhu, W. Chen, W. Jia, Y. Leng, X. Wan, and J. Kang. 2018. 'N6-Methyladenosine modification of lincRNA 1281 is critically required for mESC differentiation potential', *Nucleic Acids Res*, 46: 3906-20.

Yang, J., X. Lin, Y. Pan, J. Wang, P. Chen, H. Huang, H. H. Xue, J. Gao, and X. P. Zhong. 2016. 'Critical roles of mTOR Complex 1 and 2 for T follicular helper cell differentiation and germinal center responses', *Elife*, 5.

Yao, Q. J., L. Sang, M. Lin, X. Yin, W. Dong, Y. Gong, and B. O. Zhou. 2018. 'Mettl3-Mettl14 methyltransferase complex regulates the quiescence of adult hematopoietic stem cells', *Cell Res*, 28: 952-54.

Yau, I. W., M. H. Cato, J. Jellusova, T. Hurtado de Mendoza, R. Brink, and R. C. Rickert. 2013. 'Censoring of self-reactive B cells by follicular dendritic cell-displayed self-antigen', *J Immunol*, 191: 1082-90.

Ye, B. H., G. Cattoretti, Q. Shen, J. Zhang, N. Hawe, R. de Waard, C. Leung, M. Nouri-Shirazi, A. Orazi, R. S. Chaganti, P. Rothman, A. M. Stall, P. P. Pandolfi, and R. Dalla-Favera. 1997. 'The BCL-6 proto-oncogene controls germinal-centre formation and Th2-type inflammation', *Nat Genet*, 16: 161-70.

Yoshida, H., T. Okada, K. Haze, H. Yanagi, T. Yura, M. Negishi, and K. Mori. 2000. 'ATF6 activated by proteolysis binds in the presence of NF-Y (CBF) directly to the cis-acting element responsible for the mammalian unfolded protein response', *Mol Cell Biol*, 20: 6755-67.

Yu, G., L. G. Wang, and Q. Y. He. 2015. 'ChIPseeker: an R/Bioconductor package for ChIP peak annotation, comparison and visualization', *Bioinformatics*, 31: 2382-3.

Yu, J., Y. Li, T. Wang, and X. Zhong. 2018. 'Modification of N6-methyladenosine RNA methylation on heat shock protein expression', *PLoS One*, 13: e0198604.

Yue, Y., J. Liu, X. Cui, J. Cao, G. Luo, Z. Zhang, T. Cheng, M. Gao, X. Shu, H. Ma, F. Wang, X. Wang, B. Shen, Y. Wang, X. Feng, C. He, and J. Liu. 2018. 'VIRMA mediates preferential m(6)A mRNA methylation in 3'UTR and near stop codon and associates with alternative polyadenylation', *Cell Discov*, 4: 10.

Yusuf, I., X. Zhu, M. G. Kharas, J. Chen, and D. A. Fruman. 2004. 'Optimal B-cell proliferation requires phosphoinositide 3-kinase-dependent inactivation of FOXO transcription factors', *Blood*, 104: 784-7.

Zaccara, S., and S. R. Jaffrey. 2020. 'A Unified Model for the Function of YTHDF Proteins in Regulating m(6)A-Modified mRNA', *Cell*, 181: 1582-95 e18.

Zaccara, S., R. J. Ries, and S. R. Jaffrey. 2019. 'Reading, writing and erasing mRNA methylation', *Nat Rev Mol Cell Biol*, 20: 608-24.

Zarnegar, B. J., Y. Wang, D. J. Mahoney, P. W. Dempsey, H. H. Cheung, J. He, T. Shiba, X. Yang, W. C. Yeh, T. W. Mak, R. G. Korneluk, and G. Cheng. 2008. 'Noncanonical NF-kappaB activation requires coordinated assembly of a regulatory complex of the adaptors cIAP1, cIAP2, TRAF2 and TRAF3 and the kinase NIK', *Nat Immunol*, 9: 1371-8.

Zhang, C., D. Samanta, H. Lu, J. W. Bullen, H. Zhang, I. Chen, X. He, and G. L. Semenza. 2016. 'Hypoxia induces the breast cancer stem cell phenotype by HIF-dependent and ALKBH5-mediated m(6)A-demethylation of NANOG mRNA', *Proc Natl Acad Sci U S A*, 113: E2047-56.

Zhang, C., W. I. Zhi, H. Lu, D. Samanta, I. Chen, E. Gabrielson, and G. L. Semenza. 2016. 'Hypoxia-inducible factors regulate pluripotency factor expression by ZNF217- and ALKBH5-mediated modulation of RNA methylation in breast cancer cells', *Oncotarget*, 7: 64527-42.

Zhang, Y., L. Garcia-Ibanez, and K. M. Toellner. 2016. 'Regulation of germinal center B-cell differentiation', *Immunol Rev*, 270: 8-19.

Zhang, Y., T. Liu, C. A. Meyer, J. Eeckhoute, D. S. Johnson, B. E. Bernstein, C. Nusbaum, R. M. Myers, M. Brown, W. Li, and X. S. Liu. 2008. 'Model-based analysis of ChIP-Seq (MACS)', *Genome Biol*, 9: R137.

Zhang, Z., L. Q. Chen, Y. L. Zhao, C. G. Yang, I. A. Roundtree, Z. Zhang, J. Ren, W. Xie, C. He, and G. Z. Luo. 2019. 'Single-base mapping of m(6)A by an antibody-independent method', *Sci Adv*, 5: eaax0250.

Zheng, G., J. A. Dahl, Y. Niu, P. Fedorcsak, C. M. Huang, C. J. Li, C. B. Vagbo, Y. Shi, W. L. Wang, S. H. Song, Z. Lu, R. P. Bosmans, Q. Dai, Y. J. Hao, X. Yang, W. M. Zhao, W. M. Tong, X. J. Wang, F. Bogdan, K. Furu, Y. Fu, G. Jia, X. Zhao, J. Liu, H. E. Krokan, A. Klungland, Y. G. Yang, and C. He. 2013. 'ALKBH5 is a mammalian RNA demethylase that impacts RNA metabolism and mouse fertility', *Mol Cell*, 49: 18-29.

Zheng, Z., L. Zhang, X. L. Cui, X. Yu, P. J. Hsu, R. Lyu, H. Tan, M. Mandal, M. Zhang, H. L. Sun, A. Sanchez Castillo, J. Peng, M. R. Clark, C. He, and H. Huang. 2020. 'Control of Early B Cell Development by the RNA N(6)-Methyladenosine Methylation', *Cell Rep*, 31: 107819.

Zhong, L., D. Liao, M. Zhang, C. Zeng, X. Li, R. Zhang, H. Ma, and T. Kang. 2019. 'YTHDF2 suppresses cell proliferation and growth via destabilizing the EGFR mRNA in hepatocellular carcinoma', *Cancer Lett*, 442: 252-61.

Zhou, J., J. Wan, X. E. Shu, Y. Mao, X. M. Liu, X. Yuan, X. Zhang, M. E. Hess, J. C. Bruning, and S. B. Qian. 2018. 'N(6)-Methyladenosine Guides mRNA Alternative Translation during Integrated Stress Response', *Mol Cell*, 69: 636-47 e7.

Zotos, D., J. M. Coquet, Y. Zhang, A. Light, K. D'Costa, A. Kallies, L. M. Corcoran, D. I. Godfrey, K. M. Toellner, M. J. Smyth, S. L. Nutt, and D. M. Tarlinton. 2010. 'IL-21 regulates germinal center B cell differentiation and proliferation through a B cell-intrinsic mechanism', *J Exp Med*, 207: 365-78.

Zotos, D., and D. M. Tarlinton. 2012. 'Determining germinal centre B cell fate', *Trends Immunol*, 33: 281-8.

Table 19. List of the downregulated genes in *Mettl3*-mutant iGB cells after 2 days of mCD40L + IL-21 stimulation.

	Gene	log2FoldChange	adjusted *p*-value
1	*Enpp1*	-1.86E+00	4.61E-04
2	*Gm5535*	-3.05E+00	5.57E-04
3	*Chrnb4*	-2.19E+00	5.57E-04
4	*Slpi*	-2.15E+00	5.57E-04
5	*Endou*	-1.95E+00	5.57E-04
6	*Cntnap1*	-1.36E+00	5.57E-04
7	*Prdm1*	-2.01E+00	8.99E-04
8	*Eaf2*	-1.78E+00	1.00E-03
9	*Jchain*	-2.19E+00	1.12E-03
10	*Pfkp*	-1.46E+00	1.32E-03
11	*Sdf2l1*	-1.44E+00	1.32E-03
12	*Sap30*	-1.14E+00	1.32E-03
13	*Rundc3b*	-1.62E+00	2.75E-03
14	*Gpm6a*	-1.60E+00	4.33E-03
15	*Irf4*	-1.54E+00	5.42E-03
16	*4933404K13Rik*	-1.96E+00	6.83E-03
17	*Rassf6*	-1.68E+00	6.83E-03
18	*Pdia6*	-1.19E+00	6.83E-03
19	*Creld2*	-1.05E+00	6.83E-03
20	*Impdh1*	-8.96E-01	6.83E-03
21	*Nampt*	-8.62E-01	7.45E-03
22	*Tigit*	-1.60E+00	9.43E-03
23	*Mzb1*	-1.75E+00	9.57E-03
24	*Sh2d1b1*	-1.76E+00	9.58E-03
25	*Nefh*	-1.58E+00	9.58E-03
26	*Arhgap32*	-2.26E+00	1.08E-02
27	*Ankrd37*	-2.08E+00	1.09E-02
28	*Cacna1h*	-2.13E+00	1.30E-02
29	*Edem1*	-1.14E+00	1.30E-02
30	*Derl3*	-1.82E+00	1.32E-02
31	*Spint2*	-1.80E+00	1.33E-02
32	*Ccr10*	-2.02E+00	1.64E-02
33	*0610039H22Rik*	-2.40E+00	1.68E-02
34	*Nes*	-1.62E+00	1.68E-02
35	*Hapln1*	-1.45E+00	1.68E-02
36	*Tox*	-1.51E+00	1.72E-02
37	*Slc35f2*	-1.51E+00	1.85E-02
38	*Klhdc2*	-1.29E+00	1.85E-02

39	Zcchc18	-1.61E+00	1.96E-02
40	Cth	-1.14E+00	2.09E-02
41	Ak7	-2.03E+00	2.13E-02
42	Bhlha15	-1.86E+00	2.23E-02
43	Hyou1	-9.06E-01	2.23E-02
44	2610002M06Rik	-1.59E+00	2.24E-02
45	Manf	-9.42E-01	2.25E-02
46	Il33	-2.43E+00	2.37E-02
47	Phf10	-7.93E-01	2.37E-02
48	Pole2	-1.32E+00	2.59E-02
49	Cd93	-1.65E+00	2.59E-02
50	Egr3	-1.42E+00	2.72E-02
51	Cmah	-1.67E+00	2.76E-02
52	Gm5547	-1.76E+00	2.83E-02
53	Pou2af1	-1.58E+00	2.89E-02
54	Kcnk5	-1.57E+00	2.89E-02
55	Sec11c	-1.35E+00	2.89E-02
56	Cpox	-8.50E-01	2.89E-02
57	Hepacam2	-1.76E+00	2.94E-02
58	Alpl	-1.42E+00	2.94E-02
59	Prg2	-1.90E+00	3.02E-02
60	Zdhhc14	-1.22E+00	3.02E-02
61	Gca	-1.47E+00	3.31E-02
62	Cd24a	-1.40E+00	3.33E-02
63	Erp44	-1.06E+00	3.36E-02
64	Coro2a	-1.66E+00	3.36E-02
65	Aim1l	-1.63E+00	3.36E-02
66	Papln	-1.62E+00	3.36E-02
67	Dhdh	-1.45E+00	3.36E-02
68	Slc7a3	-1.40E+00	3.36E-02
69	Mfsd2a	-1.34E+00	3.36E-02
70	Nfkbid	-1.31E+00	3.36E-02
71	Ada	-1.22E+00	3.36E-02
72	Uchl5	-1.19E+00	3.36E-02
73	Strbp	-1.05E+00	3.36E-02
74	Fkbp2	-9.40E-01	3.36E-02
75	2510002D24Rik	-8.68E-01	3.36E-02
76	Edem3	-7.94E-01	3.36E-02
77	Mamdc2	-2.00E+00	3.37E-02
78	Usp44	-1.45E+00	3.42E-02
79	Nrgn	-2.19E+00	3.45E-02
80	Isoc2b	-1.85E+00	3.62E-02
81	Dna2	-1.43E+00	3.62E-02
82	Rbm47	-1.36E+00	3.62E-02
83	Nle1	-1.23E+00	3.62E-02
84	Ppa1	-1.21E+00	3.62E-02

85	Sumf2	-1.08E+00	3.62E-02
86	Rap1a	-1.05E+00	3.62E-02
87	Pold2	-1.01E+00	3.62E-02
88	Abcb6	-1.01E+00	3.62E-02
89	Ecsit	-9.58E-01	3.62E-02
90	Cbx7	-7.74E-01	3.62E-02
91	Il2rb	-1.64E+00	3.71E-02
92	Trp53i11	-1.54E+00	3.78E-02
93	Cacna1s	-1.53E+00	3.78E-02
94	Tgif2	-1.20E+00	3.78E-02
95	Chd1l	-1.09E+00	3.78E-02
96	Spcs3	-1.04E+00	3.84E-02
97	Ido1	-1.94E+00	3.87E-02
98	AI662270	-1.53E+00	3.87E-02
99	Sub1	-1.04E+00	3.87E-02
100	Gatm	-1.50E+00	3.87E-02
101	Hsp90b1	-7.91E-01	3.87E-02
102	Xlr4b	-1.57E+00	3.95E-02
103	Ripk3	-1.39E+00	4.05E-02
104	Cyb5a	-1.15E+00	4.05E-02
105	Mycbp	-6.94E-01	4.05E-02
106	Dnajc3	-9.17E-01	4.14E-02
107	Syce2	-1.46E+00	4.15E-02
108	Isyna1	-1.42E+00	4.16E-02
109	Cep76	-1.04E+00	4.16E-02
110	Aldh9a1	-9.44E-01	4.16E-02
111	Usp45	-5.91E-01	4.16E-02
112	St14	-1.39E+00	4.20E-02
113	Entpd5	-7.99E-01	4.24E-02
114	Alcam	-1.11E+00	4.28E-02
115	Galk1	-9.04E-01	4.28E-02
116	Rpn1	-7.20E-01	4.31E-02
117	Gm15056	-1.92E+00	4.34E-02
118	Shisa8	-1.75E+00	4.40E-02
119	Sms	-8.99E-01	4.40E-02
120	Icam2	-1.47E+00	4.41E-02
121	Dad1	-7.32E-01	4.41E-02
122	Ido2	-1.83E+00	4.42E-02
123	Rapgef5	-1.46E+00	4.43E-02
124	Prps1	-1.07E+00	4.53E-02
125	Arhgap19	-1.29E+00	4.60E-02
126	Gpr55	-1.52E+00	4.66E-02
127	Tmem180	-1.17E+00	4.66E-02
128	Myl4	-1.29E+00	4.69E-02
129	Tdp1	-1.17E+00	4.69E-02
130	Cars2	-7.64E-01	4.69E-02

131	*Tg*	-1.54E+00	4.72E-02
132	*Hopx*	-1.46E+00	4.72E-02
133	*Tnfrsf13c*	-1.42E+00	4.72E-02
134	*Chchd10*	-1.42E+00	4.72E-02
135	*Ero1lb*	-1.21E+00	4.72E-02
136	*Qrsl1*	-1.11E+00	4.72E-02
137	*Timm21*	-1.10E+00	4.72E-02
138	*Rnaseh2b*	-1.04E+00	4.72E-02
139	*Parp2*	-7.88E-01	4.72E-02
140	*Celsr2*	-1.45E+00	4.79E-02
141	*Dennd5b*	-1.24E+00	4.79E-02
142	*Ccdc115*	-9.13E-01	4.79E-02
143	*Armcx6*	-1.33E+00	4.80E-02
144	*Ctage5*	-8.51E-01	4.82E-02
145	*Apoa2*	-1.98E+00	4.88E-02
146	*Il27*	-1.75E+00	4.88E-02
147	*Il10*	-1.68E+00	4.88E-02
148	*Mad2l2*	-7.30E-01	4.88E-02
149	*Slc16a6*	-1.29E+00	4.89E-02
150	*Ostc*	-8.07E-01	4.92E-02
151	*Gtf2a1*	-6.69E-01	4.95E-02

Table 20. List of the upregulated genes in *Mettl3*-mutant iGB cells after 2 days of mCD40L + IL-21 stimulation.

	Gene	log2FoldChange	adjusted *p*-value
1	Thbd	1.14E+00	5.57E-04
2	Lrig1	1.03E+00	5.57E-04
3	Ppap2b	1.38E+00	1.32E-03
4	Ctsl	9.68E-01	1.32E-03
5	Osmr	1.02E+00	1.65E-03
6	Pdgfra	1.33E+00	3.25E-03
7	Arrdc4	1.00E+00	4.46E-03
8	Htra1	9.76E-01	4.46E-03
9	Vegfc	1.08E+00	4.46E-03
10	Grem1	1.44E+00	6.83E-03
11	C3	1.24E+00	6.83E-03
12	Lbp	1.13E+00	7.73E-03
13	Pcdh7	1.09E+00	8.44E-03
14	Rab27b	9.78E-01	8.44E-03
15	Scara5	9.51E-01	9.25E-03
16	Sdc1	8.20E-01	9.58E-03
17	Angptl2	8.94E-01	1.08E-02
18	Trem2	1.68E+00	1.33E-02
19	Nupr1	7.81E-01	1.33E-02
20	Unc5b	7.07E-01	1.37E-02
21	Ank	1.02E+00	1.42E-02
22	Oaf	8.44E-01	1.61E-02
23	Il1rn	1.51E+00	1.68E-02
24	Mira	1.32E+00	1.68E-02
25	Spon2	1.83E+00	1.72E-02
26	Fn1	1.09E+00	1.72E-02
27	Lox	1.03E+00	1.96E-02
28	Lpin3	1.03E+00	1.96E-02
29	Mmp19	1.20E+00	1.97E-02
30	2610305D13Rik	1.03E+00	2.17E-02
31	Ugt1a6a	1.22E+00	2.23E-02
32	Cd300lb	1.00E+00	2.25E-02
33	Ly6c1	1.20E+00	2.30E-02
34	Prss23	1.17E+00	2.59E-02
35	Sod3	9.74E-01	2.59E-02
36	Antxr2	8.65E-01	2.76E-02
37	Ptprk	8.02E-01	2.76E-02
38	Ttyh2	8.62E-01	2.77E-02
39	Cpne8	9.32E-01	2.83E-02
40	Slit2	1.12E+00	2.86E-02
41	Shc2	1.15E+00	2.86E-02
42	Havcr2	1.00E+00	2.89E-02
43	Layn	9.81E-01	2.89E-02
44	Cpe	9.62E-01	2.89E-02
45	Apobr	7.90E-01	2.89E-02
46	Tns3	7.75E-01	2.89E-02
47	Loxl1	1.03E+00	2.94E-02
48	Rin2	8.34E-01	2.94E-02

49	*P3h4*	8.23E-01	2.94E-02
50	*Fgfr1*	8.18E-01	2.94E-02
51	*Dcn*	1.55E+00	2.94E-02
52	*Gstt1*	9.79E-01	2.94E-02
53	*Dpt*	1.86E+00	3.02E-02
54	*Cd63*	8.92E-01	3.24E-02
55	*Dmkn*	1.17E+00	3.31E-02
56	*Dclk1*	1.14E+00	3.31E-02
57	*Aebp1*	1.09E+00	3.31E-02
58	*Hoxd8*	1.06E+00	3.31E-02
59	*Tnc*	9.81E-01	3.31E-02
60	*Fgf7*	9.37E-01	3.31E-02
61	*Plekhf1*	8.94E-01	3.31E-02
62	*Plat*	8.91E-01	3.36E-02
63	*S100a4*	8.26E-01	3.36E-02
64	*Npr3*	1.18E+00	3.36E-02
65	*Aldh3a1*	9.51E-01	3.36E-02
66	*Maged2*	9.39E-01	3.36E-02
67	*Efemp2*	8.70E-01	3.36E-02
68	*Gpc1*	8.39E-01	3.36E-02
69	*Tspan4*	7.58E-01	3.36E-02
70	*Tcn2*	7.23E-01	3.36E-02
71	*Ext1*	6.16E-01	3.36E-02
72	*Ptges*	7.70E-01	3.37E-02
73	*Rab7b*	9.72E-01	3.51E-02
74	*Enpp2*	1.62E+00	3.62E-02
75	*Rnf150*	1.27E+00	3.62E-02
76	*Pcdhgc3*	1.14E+00	3.62E-02
77	*Tmem119*	1.09E+00	3.62E-02
78	*Nnmt*	9.85E-01	3.62E-02
79	*Igfbp4*	9.43E-01	3.62E-02
80	*Slc41a2*	9.26E-01	3.62E-02
81	*Ppic*	8.38E-01	3.62E-02
82	*Ugdh*	7.47E-01	3.62E-02
83	*Fhdc1*	7.29E-01	3.62E-02
84	*Cp*	1.59E+00	3.71E-02
85	*Rassf8*	1.01E+00	3.78E-02
86	*Eva1b*	8.90E-01	3.78E-02
87	*Col4a2*	8.35E-01	3.78E-02
88	*Tpbg*	8.09E-01	3.78E-02
89	*Fbln2*	6.93E-01	3.78E-02
90	*Sox4*	1.00E+00	3.84E-02
91	*Pcolce*	1.02E+00	3.87E-02
92	*Pttg1ip*	7.07E-01	3.87E-02
93	*Rab31*	6.91E-01	3.87E-02
94	*Colec12*	9.44E-01	3.87E-02
95	*Gprc5b*	8.66E-01	3.87E-02
96	*Thbs2*	1.50E+00	3.95E-02
97	*Vcan*	1.15E+00	3.95E-02
98	*Xpnpep2*	1.12E+00	3.96E-02
99	*Angptl7*	1.70E+00	4.04E-02
100	*Col1a2*	9.68E-01	4.04E-02
101	*Aif1l*	8.28E-01	4.04E-02

102	Six1	1.11E+00	4.05E-02
103	Srxn1	7.23E-01	4.05E-02
104	Parvb	6.99E-01	4.05E-02
105	Zfp334	1.04E+00	4.14E-02
106	Col3a1	1.68E+00	4.16E-02
107	S100b	1.31E+00	4.16E-02
108	S1pr3	1.22E+00	4.16E-02
109	Sbsn	1.01E+00	4.16E-02
110	Krt13	9.72E-01	4.16E-02
111	Gorab	9.25E-01	4.16E-02
112	Plod1	7.29E-01	4.16E-02
113	Lgals3	7.61E-01	4.20E-02
114	Cbr3	7.48E-01	4.20E-02
115	Pla2g5	8.40E-01	4.23E-02
116	Plxnd1	6.88E-01	4.28E-02
117	Fnip2	1.31E+00	4.28E-02
118	Il6st	8.62E-01	4.28E-02
119	Gdnf	1.02E+00	4.32E-02
120	Pla1a	9.51E-01	4.32E-02
121	App	7.55E-01	4.38E-02
122	Gda	2.78E+00	4.41E-02
123	Tgfbr3	1.14E+00	4.41E-02
124	Thsd7a	1.00E+00	4.41E-02
125	Ltbr	8.61E-01	4.41E-02
126	Plin2	8.45E-01	4.41E-02
127	Col4a1	7.78E-01	4.41E-02
128	Micall2	7.71E-01	4.41E-02
129	St3gal4	7.61E-01	4.41E-02
130	Mrc2	1.01E+00	4.41E-02
131	Aqp1	6.13E-01	4.41E-02
132	Hdgfrp3	8.55E-01	4.42E-02
133	Isg15	9.42E-01	4.42E-02
134	Col8a1	8.64E-01	4.42E-02
135	Obscn	1.33E+00	4.43E-02
136	Trim2	8.75E-01	4.43E-02
137	Sparc	8.59E-01	4.43E-02
138	Mfge8	8.05E-01	4.43E-02
139	Lamb1	7.08E-01	4.51E-02
140	Ecm1	7.66E-01	4.65E-02
141	Cped1	1.41E+00	4.65E-02
142	Gm8909	8.98E-01	4.65E-02
143	Masp1	1.41E+00	4.66E-02
144	Ldb2	1.33E+00	4.66E-02
145	Tnfrsf23	8.22E-01	4.66E-02
146	Ccdc109b	8.06E-01	4.66E-02
147	Lgi4	1.50E+00	4.69E-02
148	Rnd3	1.02E+00	4.72E-02
149	Tmem158	1.01E+00	4.72E-02
150	Cxx1c	9.20E-01	4.72E-02
151	Cdsn	9.10E-01	4.72E-02
152	Pam	8.91E-01	4.72E-02
153	Tmem140	7.87E-01	4.72E-02
154	AI607873	1.52E+00	4.76E-02

155	*Lxn*	6.41E-01	4.79E-02
156	*Sla2*	9.31E-01	4.80E-02
157	*Raph1*	8.07E-01	4.82E-02
158	*Ghr*	1.07E+00	4.88E-02
159	*Xlr*	8.34E-01	4.88E-02
160	*Sgms2*	1.04E+00	4.91E-02
161	*Sestd1*	7.71E-01	4.92E-02
162	*Pltp*	7.69E-01	4.93E-02
163	*Serpinb9b*	6.71E-01	4.93E-02
164	*Iglon5*	8.68E-01	4.93E-02
165	*Tgfb2*	1.23E+00	4.95E-02
166	*Sorbs2*	9.55E-01	4.95E-02
167	*Slurp1*	9.81E-01	4.96E-02
168	*Cpt1a*	6.82E-01	4.98E-02

Acknowledgements